Net Percolation as a Function of Topographic Variation in a Reclamation Cover over a Saline-Sodic Overburden Dump

A Thesis Submitted to the College of Graduate Studies and Research in Partial Fulfillment of the Degree of Master of Science in the Department of Civil Engineering, University of Saskatchewan, Saskatoon, Canada

By

Joel Neil Hilderman

PERMISSION TO USE

In presenting this thesis in partial fulfillment of the requirements for a Postgraduate degree from the University of Saskatchewan, I agree that the Libraries of this University may make it freely available for inspection. I further agree that permission for the copying of this thesis in any manner, in whole or in part, for scholarly purposes may be granted by the professor or professors who supervised my thesis work or, in their absence, by the head of the Department or the Dean of the College in which my thesis work was done. It is understood that any copying or publication or use of this thesis or parts thereof for financial gain shall not be allowed without my written permission. It is also understood that due recognition shall be given to me and to the University of Saskatchewan in any scholarly use which may be made of any material in my thesis.

Requests for permission to copy or to make other use of material in this thesis in whole or part should be addressed to:

Head of the Department of Civil Engineering
University of Saskatchewan
57 Campus Drive
Saskatoon, Saskatchewan S7N 5A9
Canada

OR

Dean of the College of Graduate Studies and Research
University of Saskatchewan
107 Administration Place
Saskatoon, Saskatchewan S7N 5A2
Canada

ABSTRACT

Surface mining of oil sands in northern Alberta requires stripping of saline-sodic shale overburden, which is typically placed in large upland overburden dumps. Due to the chemical nature of this shale, engineered soil covers must be constructed over the shale to support the growth of forest vegetation. A research site on South Bison Hill (SBH), a shale overburden dump at the Syncrude Canada Ltd. Mildred Lake Mine, has been used by researchers over the past decade to study the performance of a reclamation cover.

This study was undertaken to improve the understanding of salt and moisture dynamics in the cover-shale system. In particular, the objective of this study was to develop an estimate of the net percolation rate through the cover soil and into the shale overburden. Stable isotope (δ^2H and $\delta^{18}O$) measurements obtained from the pore water of soil samples were used to develop stable isotope profiles at various sampling locations along the slope and plateau of the SBH. Simulated profiles were then generated using 2D, finite element numerical modelling software and compared to the measured profiles. Model parameters were obtained from testing and the work of previous researchers. The model results revealed that the net percolation is greatest (32-50 mm/yr) for the plateau and mid-slope bench sample locations. Net percolation rates for sample locations on the slope were lower at 0-12 mm/yr.

The results from the stable isotope modelling were utilized in a SO_4^{2-} transport model to ascertain if calculated net percolation rates could explain measured salinity profiles. This modelling exercise revealed that calculated SO_4^{2-} profiles are highly dependent on the assumed SO_4^{2-} production rates in the shale, which is primarily attributed to pyrite oxidation. The model results showed the isotope-based net percolation rates could explain the measured SO_4^{2-}profiles for a reasonable range SO_4^{2-} production rates. The SO_4^{2-} production rates calculated in the model were greatest for the plateau and mid-slope bench locations and lesser for the sloped locations. The model also showed that the mass of SO_4^{2-} removed by interflow was minimal compared to the mass generated by pyrite oxidation and that net percolation is the dominant flushing mechanism at net percolation rates of 8 mm/yr or more.

ACKNOWLEDGEMENTS

There are many organizations and individuals whose assistance has been instrumental in the completion of this study. Generous financial support has been provided by the Canadian Oil Sands Network for Research and Development (CONRAD), Syncrude Canada Ltd., the National Science and Engineering Research Council of Canada (NSERC), the University of Saskatchewan, Klohn Crippen Berger, Manulife Financial, Mr. George Carter, Dr. K.K. Wong, Dr. Del Fredlund, Dr. J.D. Mollard, and the family of the late Mr. Russell Haid.

Sincere thanks to Dr. Lee Barbour for his expert guidance in this endeavour. Dr. Barbour's intellect and grounded focus have been inspiring. I also wish to thank Dr. Jim Hendry for sharing his wisdom in the areas of geochemistry and stable isotopes.

I owe a debt of gratitude to those who have provided me with field and laboratory assistance including Sean Shaw, Virginia Chostner, Doug Fisher, Alex Kozlow, Mike McCallister, Tom McCallister, and Jeremy Ledding. Julie Zettyl was a tremendous help both in the field and as site visit coordinator. I wish to thank the staff at Syncrude Canada Ltd. including Lori Cyprien, Marty Yarmuch, Audrey Lanoue, Rob Vassov, Chris Beierling, and especially Leah Timmons for her enthusiastic assistance in the field. Perhaps the greatest asset to me during this project was Sophie Kessler who not only provided a great deal of field support but also acted as the SBH resident expert. She has my sincere appreciation and my utmost respect for her determination and work ethic. I would also like to thank Chris Kelln for answering a barrage of fine detail questions that tested his memory and patience.

Most importantly, I wish to thank my wife, Olivia, and our children, Caley, Mya, and Cain, for their love, sacrifice, interest, and encouragement during these past two years. I have been blessed with much in my life, for which I am grateful, but my family is truly the greatest of these gifts and will always be the centre of my world.

TABLE OF CONTENTS

LIST OF FIGURES

LIST OF TABLES

1. INTRODUCTION

The surface mining of oil sands in northern Alberta has disturbed over 60,000 ha of land (Alberta Energy 2009) including muskeg and boreal forest habitat and will continue to expand as new mines come online and current operators increase their production capacities. This land disturbance can take the forms of end-pit lakes, fine tailings ponds, coarse tailings sand piles, or overburden dumps. Each of these landscapes presents unique challenges that must be addressed by mine operators to reclaim the lands to self-sustained ecosystems.

1.1 Description of the Problem

The extraction of bitumen or heavy oil from the Athabasca oil sands region of northern Alberta (Figure 1.1) is accomplished by one of two methods: in-situ recovery or surface mining, depending on the depth of the ore body. In-situ recovery methods are similar to conventional oil wells except that they generally use steam to assist the viscous bitumen in flowing to the recovery well. Surface mining is accomplished by stripping overburden to gain access to the underlying oil sands.

The energy required to generate steam for in-situ recovery is currently provided by natural gas which results in a higher cost per barrel for in-situ bitumen recovery (NEB 2006). In-situ methods recover approximately 20% of the bitumen in the reservoir (Alberta ERCB 2009). In contrast, the costs of surface mining tend to be considerably lower and the recovery rate is estimated at 82% of the mined ore body (Alberta ERCB 2009). While it is estimated that only 3% of the oil sands areas in Alberta are surface mineable (Alberta Energy 2009), the favourable economic factors have led to a faster rate of expansion of oil sands mines than in-situ operations.

Both in-situ and surface mine recovery of bitumen have negative environmental impacts. The primary environmental concerns with in-situ recovery are the use of large volumes of fresh water, the release of greenhouse gases from the burning of natural gas to

generate steam, and the fragmentation of forests by pipelines (Jordaan et al. 2009). The environmental impacts of surface mining of oil sands are more obvious and include the mined out pits, tailings ponds and overburden dumps that disturb natural habitat. This land disturbance and the associated reclamation requirements are a concern to regulators, oil sands mine operators, and the general public.

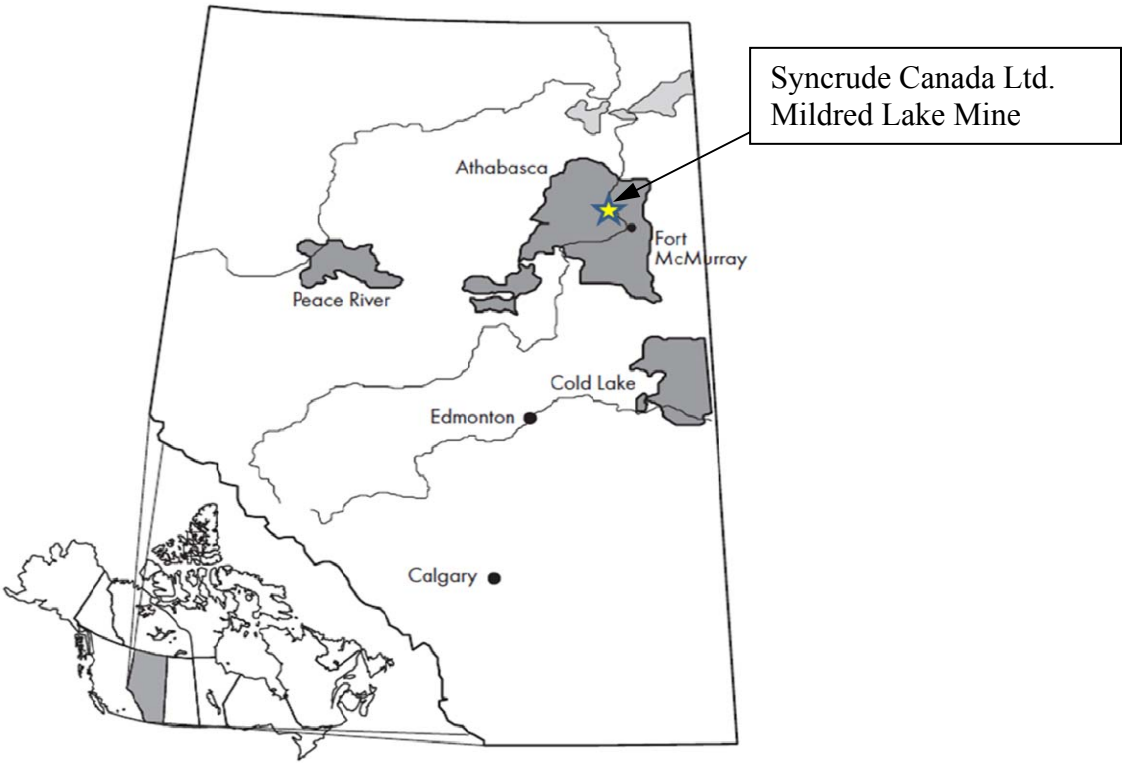

Figure 1.1: Oil sands regions of Alberta. (Modified from NEB 2004)

Approximately 480,000 ha of the Athabasca region are underlain by surface mineable oil sands deposits where the overburden thickness is 65 m or less (Alberta ERCB 2009). At Syncrude Canada Limited's (SCL) Mildred Lake Mine, the overburden is predominantly Cretaceous clay shale that is both saline and sodic (Lord and Isaac 1989, Wall 2005). This saline-sodic overburden is backfilled into mined-out pits; however bulking of the overburden material upon excavation and constraints in operation material handling result in the volumes of overburden being greater than the available pit space. Consequently, much of the shale overburden is placed in upland overburden dumps.

Upon closure of the SCL Mildred Lake Mine, it is estimated that approximately 7000 ha or roughly 1/3 of the total reclaimed landscape will comprise reworked saline-sodic overburden as the primary substrate (Kelln et al. 2008). Given the total area of potentially surface mineable oil sands deposits across the oil sands region and the volume of overlying shale, it is reasonable to expect there will be a demand for understanding the impacts of salt transport in reclaimed saline-sodic mine overburden dumps.

The Cretaceous clay shale of the Athabasca region is part of the Clearwater formation. These sediments were deposited in a marine environment and naturally contain high concentrations of soluble salts, especially sodium and sulphate (Lord and Isaac 1989). The elevated salinity creates adverse conditions for vegetation growth; thus, a soil cover must be placed over the shale to permit vegetative growth and allow the landscape to be reclaimed. However, experience has shown that salts from the underlying shale can be transported into the cover soil by various processes which may lead to saline/sodic conditions that could jeopardize the long-term success of the reclaimed landscape (Kessler 2007, Merrill et al. 1983, Moran et al. 1990).

Mine operators and provincial regulators both seek a cover prescription that will support a self-sustaining reclaimed ecosystem while minimizing construction costs. The minimum soil cover thickness over shale overburden dumps required of operators in the Athabasca Oil Sands region has recently increased. Beginning in 1984, oil sands mine operators were required by Alberta Environment to cap saline overburden dumps with a minimum of 1.0 m of suitable soil for reclamation purposes (Macyk and Drozdowski 2008). This was the capping requirement applied to the SW 30 Hills Overburden Dump at the Mildred Lake Mine (Boese 2003). Current operating permits issued to SCL for more recent overburden dumps require a minimum cover thickness of 130 - 150 cm over saline-sodic shale overburden (Alberta Environment 2007; clauses 6.1.32, 6.1.33 and 6.1.34). Provincial regulators have increased the cover thickness requirement due to concerns with the documented ingress of salt into the reclamation covers from field

trials. For example, the work of Kessler (2007, 2010) showed that within four years of cover placement the bottom 15 cm of a cover soil was degraded by salt ingress.

The instrumented watershed that was investigated for this research program has been a source of data for numerous studies over the past decade (Boese 2003; Shurniak 2003; Meiers et al. 2003; Wall 2005; Kessler 2007, Kessler et al. 2010, Kelln et al. 2007, 2008, 2009; Lazorko 2008; Chapman 2008). The following studies were of particular relevance to the work described in this thesis. Kessler (2007) studied the upward transport of salts into the reclamation cover. Kelln et al. (2007, 2008, and 2009) demonstrated the importance of soil structure and topography in the infiltration and redistribution of pore water within the cover soil. Wall (2005) characterized and quantified the various geochemical reactions associated with pyrite oxidation that produce salts in the reworked shale.

In 2006, the Canadian Oil Sands Network for Research and Development (CONRAD) commissioned a technology transfer document to synthesize the reclamation research findings from the SCL instrumented overburden dump as well as an instrumented tailings sand storage structure. This document, produced by Barbour et al. (2006), highlighted the importance of two mechanisms, net percolation and down-slope interflow, in countering the upward diffusion of salts from the underlying saline-sodic shale into the reclamation cover. The authors describe how the contribution of net percolation to salt flushing is more critical in areas of reduced slope, such as the plateaus of upland structures, where slopes are insufficient to allow interflow. Therefore, to improve the overall understanding of salt and moisture dynamics, a more reliable estimate of net percolation of precipitation water through the cover and into the underlying shale is required. Filling the knowledge gaps for this instrumented study site will assist operators and regulators in implementing sustainable reclamation design guidelines.

1.2 Site Description

The study site is located at the SCL Mildred Lake oil sands mine, approximately 40 km north of Fort McMurray, Alberta in the Athabasca oil sands region (Figure 1.1). The area is part of the Central Mixedwood natural subregion of Alberta (Natural Regions Committee 2006) which is characterized by upland forests of mixed coniferous and deciduous trees and expansive low-lying wetlands. The climate in this region is sub-humid continental under the Koppen Classification (McKnight and Hess 2005). Historical climate data collected from Fort McMurray between 1971 and 2000 reveal a mean annual temperature of 0.7°C with mean monthly temperatures ranging from -19°C in January to 17°C in July (Environment Canada 2011). The Fort McMurray area has an average annual precipitation of 456 mm with 342 mm occurring as rain and 136 mm (water equivalent) as snow (Environment Canada 2011). The mean annual gross evaporation at Fort McMurray was 458 mm between 1971 and 2000 (Agriculture and Agri-Food Canada 2002). Actual evapotranspiration for the study site is 346 mm/yr on average (Elshorbagy et al. 2005), or roughly equivalent to the average annual rain fall.

The research in this study was focused on an instrumented watershed on a reclaimed saline-sodic shale overburden dump at the SCL Mildred Lake oil sands mine. Figure 1.2 shows an aerial photograph of the Mildred Lake Mine footprint with the South Bison Hill Overburden Dump (SBH) located at the southern perimeter.

The SBH is one of six upland overburden dumps constructed in the South Hills area of Mildred Lake Mine (Chapman 2008). It was constructed over the course of two decades with the last lift of overburden placed in 1996 (Kessler 2007). Final grading of the dump was undertaken sometime between 1996 and early 1999. In the winter of 1999, the reclamation cover soil was placed on three research plots along the north facing slope of the SBH (Boese 2003). Each of these 1 ha plots are 50 m wide by 200 m long in the direction of the slope. The three plots, designated D1, D2, and D3, were each constructed with a different cover prescription to study the effect of cover thickness on reclamation success. Figure 1.3 shows the layout of the research plots on SBH and Figure 1.4 illustrates the three cover prescriptions. The three research plots were seeded

with barley in June 1999 to reduce erosion. Alternating rows of white spruce and aspen seedlings were planted in the fall of 1999.

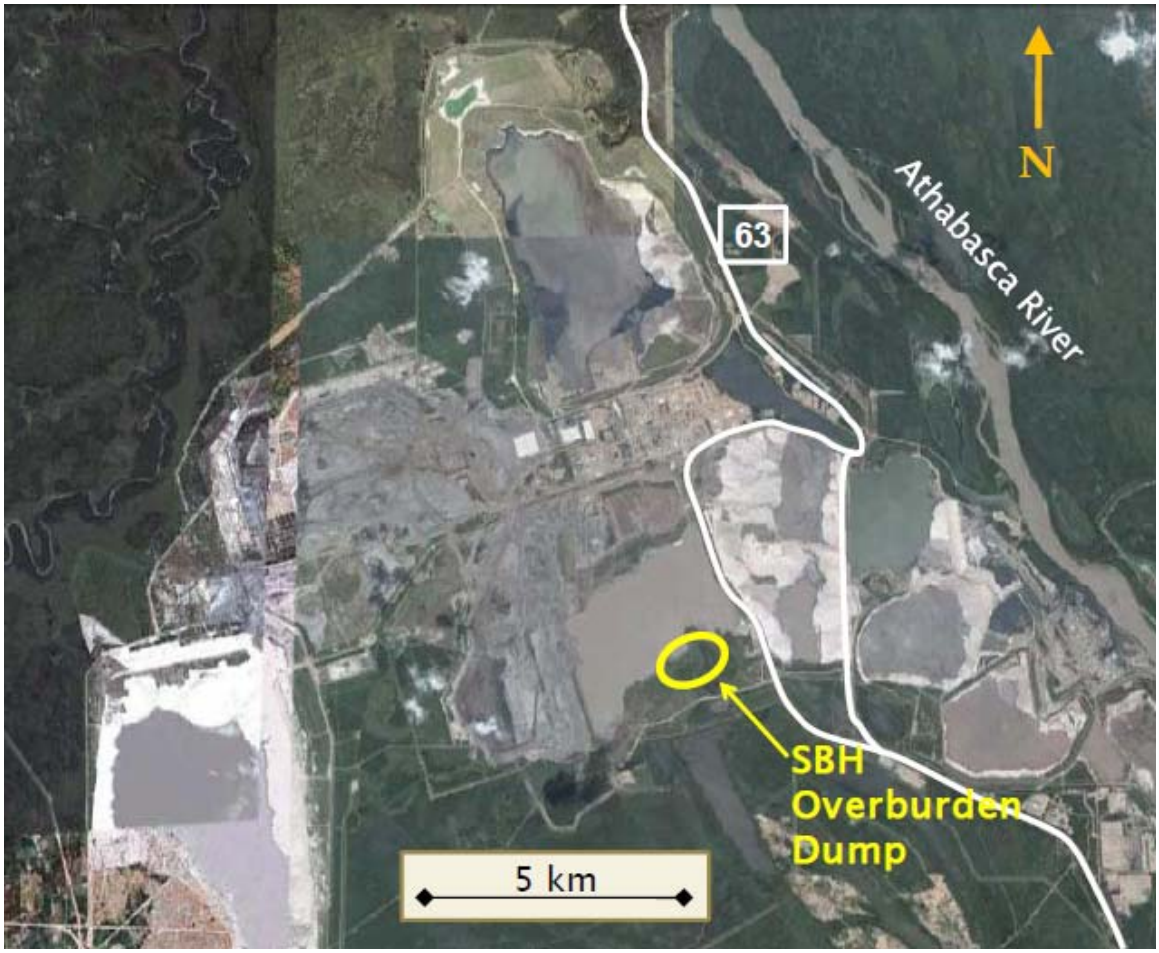

Figure 1.2: Aerial photograph of Mildred Lake Mine.
(Image from Google 2009)

Previous research showed that the thinner D1 and D2 covers do not provide sufficient water storage to meet vegetative demands (Shurniak 2003), and are more susceptible to degradation by salt ingress (Kessler 2007, Kessler et al. 2010). Therefore, this study focused on the D3 cover plot with the 100 cm thick cover.

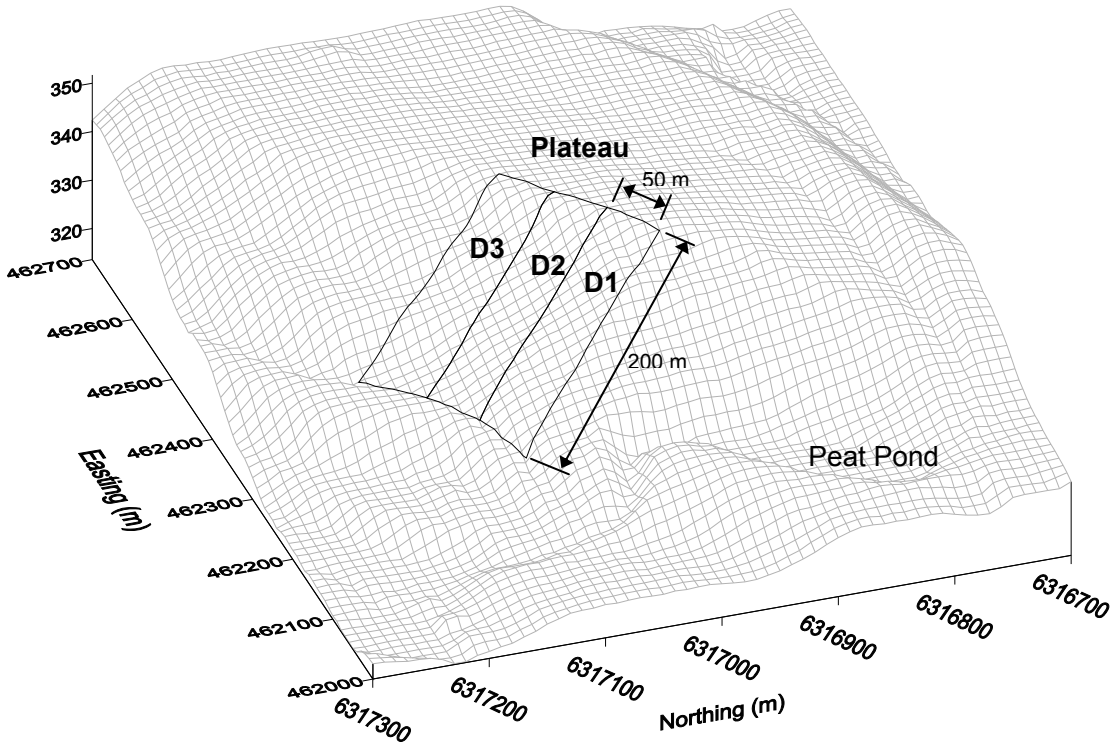

Figure 1.3: SBH instrumented watershed 3D surface model (looking NE).

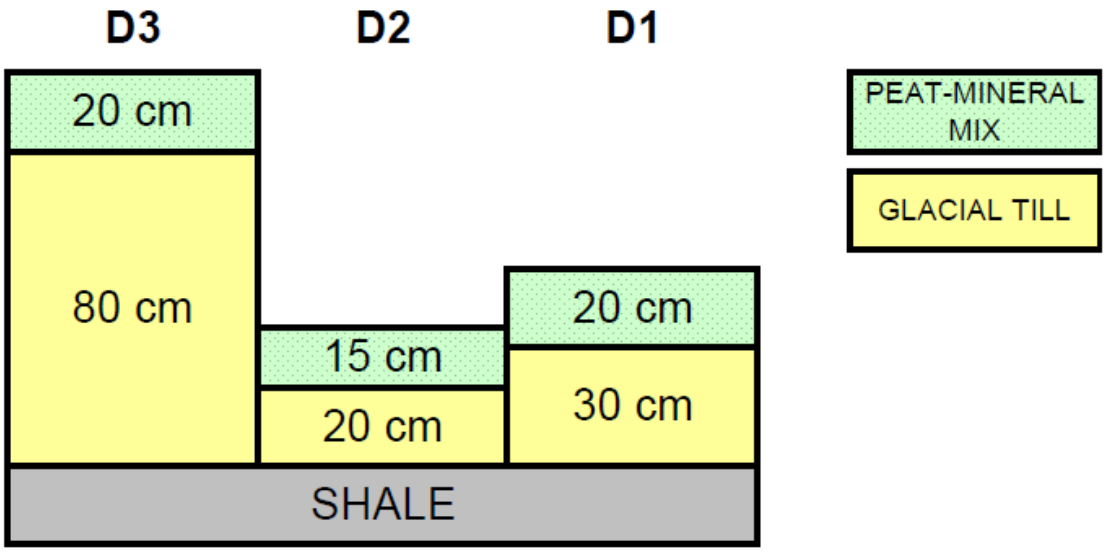

Figure 1.4: SBH research plot cover configurations. (After Shurniak 2003)

The plateau of the SBH dump was also important to this study as the relatively flat slope of the plateau affects the salt and water dynamics resulting in differences when compared to the cover plots on the slope. The cover prescription for the plateau was the same as the D3 cover plot (20 cm of peat mineral mix over 80 cm of clayey till secondary material); however, the plateau cover material was not placed until early 2001. It was seeded with barley in the summer of 2001 to reduce erosion and establish soil structure. White spruce and seedlings were planted in 2003 (Marty Yarmuch, SCL – personal communication, 18 May 2010). An aerial photograph of the SBH study site is shown in Figure 1.5. The photograph was taken in 2001, 3 years after tree planting on the slopes and immediately after tree planting on the plateau.

Instruments to measure soil and climatic conditions were installed in the slope and plateau locations by University of Saskatchewan (U of S) researchers between 1999 and 2005. The following instrumentation installed by Boese (2003) is of relevance to the current study:

- A mid-slope weather station installed in 1999 collects meteorological information including precipitation, air temperature, relative humidity, wind speed and direction;
- A mid-slope Bowen Ratio station installed in 1999 collected actual evapotranspiration data from 1999-2008;
- Three soil monitoring stations installed in 1999 at the mid-slope of each of the three cover plots collect soil moisture, soil temperature and soil suction data;
- A runoff collection and measurement system in the ditch at the toe of the cover slope was installed in 1999; and
- An interflow collection system at the toe of the cover slope was installed in 2000.

Figure 1.5: Aerial photograph of SBH study site looking east.
(Image source: Gord McKenna , formerly of SCL, 3 July 2001)

Other relevant monitoring instruments installed by researchers at the SBH study site include:

- A plateau weather and soil monitoring station installed by O'Kane Consultants Inc. (OKC) in June 2001 that collects the same information as described above for the sloping covers (O'Kane 2001);
- A network of monitoring wells along the toe of the slope installed in 2001 by Greg Meiers and in 2002 by Denise Chapman (Sophie Kessler, OKC, personal communication, 2009);
- A network of monitoring wells on the plateau installed in 2005 by Sophie Kessler (Sophie Kessler, OKC, personal communication, 2009); and,
- A dense network of monitoring wells in the lower slope portion of the D3 cover plot, installed by Chris Kelln in 2006 (Kelln et al. 2008).

1.3 Research Objectives

The long-term success of a reclaimed landscape over saline sodic overburden is dependent on the magnitude of salinization of the reclamation cover. The key processes that control salt ingress into the cover are upward diffusion of salts from the shale and flushing of salts from the cover by net percolation and interflow. This study had a global objective of developing an understanding of net percolation and salt redistribution within saline-sodic overburden dumps in relationship to topographic position (e.g. slope or plateau). This global objective necessitated the synthesis of data and discoveries from past research on this site. The specific objectives of this study were to:

1. Interpret profiles of stable isotopes of pore water at plateau and slope positions to estimate net percolation as a function of topographic variation; and,
2. Evaluate the influence of this net percolation on soil salinity profiles at plateau and slope positions.

These objectives were achieved through a two part research program that included a field component and a numerical modelling component. The field component included field measurements and the collection of soil and water samples for laboratory analysis. Numerical modelling was used to interpret the field data in light of the specific objectives described previously.

2. LITERATURE REVIEW

This chapter summarizes available background information on several concepts of importance to the current study. This background information has been retrieved from a variety of literary sources, including theses and journal articles focused directly on the SBH study site. The topics of discussion in this chapter include: the purposes of soil covers, the origin and transport of dissolved salts in the reclamation soil cover, and a general description of stable isotopes in water.

2.1 Soil Covers

The purpose of a soil cover will vary depending on the waste material being covered, the local climate, as well as the design objectives and regulatory requirements for the cover. Often soil covers are installed over acid producing mine waste to restrict the ingress of atmospheric oxygen. The oxidation of sulphide minerals in the mine waste can produce acid mine drainage, a severe environmental problem at some mines. Soil covers can also be designed to limit the infiltration of precipitation water into the waste material.

In recent years, scientists and engineers have utilized covers with capillary barrier effects to limit the infiltration of both oxygen and water (Aubertin et al. 1996, 2006; Bussiere et al. 1997, 2003; Khire et al. 2000; Morris and Stormont 1997; Nicholson et al. 1989; Ross 1990; Stormont and Anderson 1999; Yanful et al. 1993). These multilayered covers systems rely on the contrast in particle size between a finer textured layer overlying a coarser textured layer to create a 'capillary break'. The presence of the coarse textured layer limits the level of suction that can develop on the overlying finer textured layer. At these low suction levels the finer layer remains saturated, increasing the water stored within the profile and limiting the flux of oxygen across the cover.

If acid mine drainage is not a concern, mines might actually choose to use cover material that increases infiltration and limits runoff, thereby reducing erosion (McKenna 2002). Soil covers might also be constructed to prevent the escape of gases produced by the

waste material. In landfill applications, covers can be designed to trap, divert and capture greenhouse gases such as methane and carbon dioxide that are produced through the decomposition of biodegradable waste (Spokas et al. 2006). In general, the purpose of soil covers in the oil sands is to provide a suitable substrate for vegetative growth taking into consideration nutrient levels and plant available water holding capacity (Leskiw 1998).

The soil cover examined in this research project is a reclamation cover that is intended to support a boreal forest ecosystem equivalent to that which existed before the disturbance (Qualizza et al. 2004). In order to satisfy Alberta government regulations (Alberta Environment 2008), reclaimed landscapes will be required to support a land use that is equivalent to, but not necessarily identical to, that which existed prior to disturbance. Generally, on upland overburden dumps like the SBH, this is interpreted as a requirement for harvestable timber.

2.2 Origin of Soluble Salts

The oil sands mining process removes soil and rock from beneath the ground surface where it is was in a state of anoxic chemical equilibrium. In the Athabasca oil sands region of northeastern Alberta, the overburden material usually consists of peat overlying glacial deposits including till, glaciolacustrine clay and silt, or glaciofluvial sands and gravels. Beneath this lies the clay shale of the Clearwater formation which can vary in thickness from 0 to 65 m in the surface mineable area of the Athabasca oil sands (Alberta ERCB, 2009). The average thickness of Clearwater shale overburden at the SCL Mildred Lake Mine is 40-45 m (Isaac et al. 1982). The Clearwater formation overlies the Wabiskaw-McMurray formation which contains the bitumen-rich sand layers. The McMurray formation can also contain lean oil sands that yield insufficient bitumen for economical processing. These lean oil sands become mine waste and are typically disposed of in dumps along with the shale overburden.

The Clearwater shale of the Athabasca oil sands region was deposited in a marine environment between approximately 112 and 100 Ma during the Albian Age of the

Cretaceous Period (AEUB 2000; Ogg et al. 2008). The pore water contains high concentrations of dissolved solids, principally sodium and sulphate. Geochemical analysis of the shale suggests that sulphate is produced when sulphide minerals, especially pyrite are oxidized (Wall 2005). The acidity from this reaction is neutralized by the dissolution of carbonates, which releases Ca^{2+} and Mg^{2+} cations. These cations are preferentially adsorbed to the clay particle surfaces releasing additional Na^{+} into the pore water (Nichol et al. 2006).

2.3 Sodicity and Salinity Concerns

The success of a reclamation cover on an overburden dump hinges on the ability of the cover soil to provide sufficient plant-available water for vegetation establishment and conditions which allow continued growth in perpetuity (Power et al. 1979). Deficiencies in plant-available water can be caused by insufficient precipitation or insufficient infiltration and storage of water. The inability to store water may be due to cover texture (e.g. too coarse), thickness, compaction or clay dispersion and swelling (Potter et al. 1988, Simunek and Suarez 1997). Plant growth can be limited by compaction leading to restrictions in root propagation (Doll et al. 1983) or salinization of pore water inducing high osmotic pressures (Sandoval and Gould, 1978). The current study is primarily concerned with salinity and sodicity effects on the cover soil.

Salinity in soils is not necessarily harmful to vegetation as long as osmotic pressures do not restrict water uptake. Non-sodic, saline clay soils are generally flocculated, which maintains pore space for water storage, infiltration and root penetration. However, if the concentration of soluble salts in the pore water exceeds the tolerance of a plant, the associated osmotic stress makes it difficult for the plant roots to extract water from the soil. Soils are considered saline when the electrical conductivity (EC) of a saturated paste soil sample exceeds 4 dS/cm (USDA 1954); however, deleterious effects on vegetation can occur at EC values as low as 2 dS/cm (Leskiw 1998).

Sodic soils contain a higher proportion of exchangeable Na^{+} ions than other cations, regardless of the overall salt concentrations. The primary concern with sodicity is that,

when sodic soils are exposed to fresh water, the diffuse double layer of clay particles expands resulting in swelling of the clay and the potential for dispersion of clay aggregates (Simunek and Suarez 1997). These processes reduce pore space, thus decreasing water storage capacity and the hydraulic conductivity of the soil. The loss of soil structure due to clay swelling also makes it more difficult for plant roots to penetrate through the soil.

Sodicity of a soil is measured by the exchangeable sodium percentage (ESP) or, more commonly, by the simpler measurement of sodium adsorption ratio (SAR). ESP and SAR are defined as follows:

$$ESP = (Na^{+} / CEC) \times 100 \quad [2.1]$$

$$SAR = Na^{+} / \sqrt{(Ca^{2+} + Mg^{2+}) / 2} \quad [2.2]$$

Where Na^{+}, Ca^{2+} and Mg^{2+} are the measured exchangeable sodium, calcium and magnesium, respectively, and CEC is the cation exchange capacity.

The measurements of ESP and SAR have been correlated (USDA 1954) allowing researchers to measure the SAR and calculate the ESP. By definition, a sodic soil has an ESP > 15 (USDA 1954) which is approximately equal to a SAR value of 13; however, dispersion of clay particles has been noted to occur at a SAR value of 12 (Power et al. 1978). Consequently, a SAR value greater than 12 is considered an indication of sodicity problems in soils (Alberta Agriculture 1987).

Kessler (2007) reported electrical conductivity values from saturated paste extracts averaging 10 dS/cm for shale samples from the SBH study site. This level of salinity far exceeds the allowable EC range of 0 – 2 dS/cm for optimum vegetation growing conditions in a cover soil (Leskiw 1998). However, soil salinity in a reclamation cover is only critical when the high concentrations of salts migrate into the root zone of the cover. Kessler's research showed that a substantial amount of salt had migrated into the soil cover with EC values exceeding acceptable levels in the bottom 0.15 m of the cover. The potential impact of this salinity is greater for thinner covers where the root zone is

closer to the soil-shale interface and Kessler concluded that the overall quality of the thicker 1 m soil cover was acceptable for vegetation growth.

Kessler reported average SAR values of 17 from saturated paste extracts of shale samples from the SBH study site, which exceeds the allowable level of 12. Similar to salinity levels, Kessler demonstrated that SAR values in the soil cover decrease with distance above the shale interface. Again, this pattern allowed the thicker 1 m soil cover to achieve overall acceptable SAR levels in the cover, while the thinner covers were less amenable to vegetative growth.

2.4 Salt Transport Mechanisms

Several mechanisms can be responsible for the transport of dissolved salts into the cover soil. The dominant salt transport mechanism will vary depending on the properties of the cover soil and waste material, the thickness of the cover soil, the topography, the climate, and the vegetation (Moran et al. 1990).

Merrill et al. (1983) cited molecular diffusion and evapotranspiration-induced advection as the two primary mechanisms causing upward salt migration into soil covers over saline-sodic mine spoil. Molecular diffusion is the transport of a solute within a solution by random molecular movement driven by concentration gradients (Crank 1956). Molecular diffusion is often the dominant process in systems with low hydraulic conductivity (Shackelford and Daniel 1991). A large salt concentration gradient is created between the low concentration cover material and the high concentration shale overburden immediately after cover placement (Kessler 2007). This gradient drives dissolved salts up into the till cover. If pyrite oxidation is occurring in the shale, the concentration of salts in the upper oxidized shale will also increase beyond that of the lower unoxidized shale. This results in an additional downward concentration gradient that drives salts deeper into the shale. This double front concentration gradient is illustrated in Figure 2.1.

Merrill et al. (1983) determined from laboratory tests and field studies that diffusion was the dominant process driving salt upward into fine-grained soil covers placed over saline coal mine spoil. However, the authors stipulated that the net upward flux of salts by diffusion can only occur if the hydraulic conductivity of the underlying mine spoil is very low as in a dispersed clay. Otherwise, downward infiltration of precipitation would counteract the upward diffusion of salts. The field data from the study by Merrill et al. were collected from a research site in North Dakota where the climate is continental semi-arid with a mean annual precipitation <380 mm (Merrill et al. 1983).

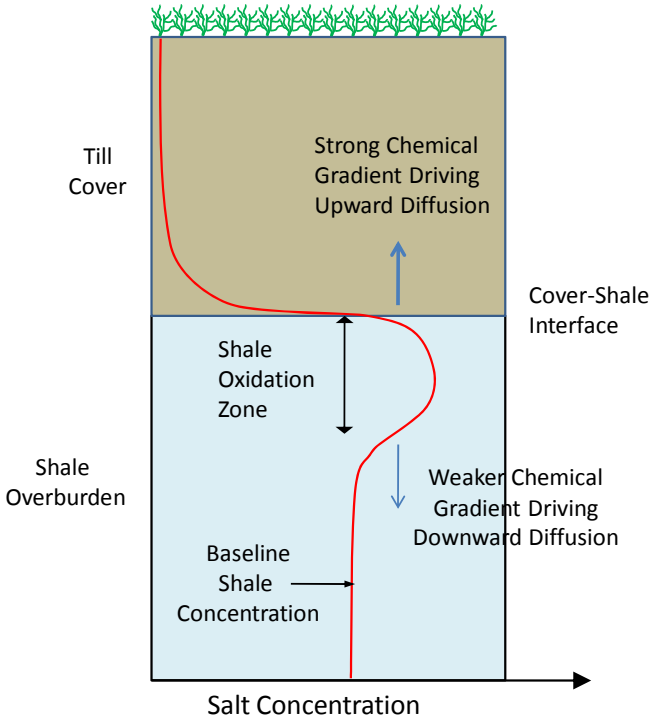

Figure 2.1: Double front salinity profile.

In a similar study, Bailey (2001) suggested that diffusion was the primary mechanism responsible for salt transport into soil covers over coal mine spoil. The soil cover in Bailey's study was constructed of silty clay and clay loam and the study site was located in central Alberta.

While diffusion can be the dominant process in fine grained soils, in most contaminant transport analyses, advective transport is the mechanism of greatest interest because it has the potential to move more contaminant mass over greater distances. Upward

advective transport could occur as a result of groundwater discharge towards the soil surface or as an upward water movement in response to evapotranspiration. However, soil covers are often elevated and in topographic positions of groundwater recharge. Consequently, advection is generally a transient process created by periods of infiltration and drainage (e.g. snow melt and rainfall) alternating with periods of evaporation or evapotranspiration during the summer months.

In contrast to the results of Merrill et al. (1983) and Bailey (2001), numerous documented studies showed that evapotranspiration-induced advection is the dominant method of upward salt transport (Talsma 1981, Fullerton and Pawluk 1987, Moran et al. 1980). Researchers studying loamy soils in Australia concluded that, except under unusually low evaporation rates (i.e., < 32 mm/yr), upward advection of salts is dominant over molecular diffusion (Talsma 1981). Researchers at various sites in North America have come to similar conclusions for both undisturbed sites and reclaimed soils. Fullerton and Pawluk (1987), studying uncultivated pasture land in east-central Alberta with glacial till origin soils, reported that the upper soil horizon was becoming increasingly salinized through the process of capillary movement and evaporation. Moran et al. (1990) studied reclaimed landscapes over saline-sodic coal-mining spoil and also concluded that salinization of the soil is primarily due to evapotranspiration induced upward advection. Moran et al. also stated that for salinization to occur, the rate of evapotranspiration has to exceed the rate of precipitation and that the groundwater table must be within a critical level of surface. For salinization of the soil surface, this critical depth was reported as 0.6 m below ground surface.

The potential for evapotranspiration induced advective salt transport has led to recommendations from the Alberta Land Conservation and Reclamation Council's Reclamation Research Technical Advisory Committee that reclaimed landscapes should be designed to minimize ponded water (Moran et al. 1990). Temporary or permanently ponded water in depressions will lead to the development of a persistent water table close to the ground surface allowing upward transport of salts from the water table via evapotranspiration (Moran et al. 1990). Design recommendations also include the

sloping of uplands at 1.5 to 3% and creating rolling hills in lowland areas with grades of 3 to 5% to limit the extent of ponded water (Pauls 1988).

Rehm et al. (1982) describe a third mechanism that could potentially cause upward salt migration. The downward advance of frost through soil has been shown to draw moisture from below the frost front up into the frozen soil zone. If the cover thicknesses was less than the annual-frost penetration depth, this bulk movement of moisture could potentially result in upward salt movement. The thickest cover prescription for the SBH is 1m; far less than the 1.6 and >1.7 m of frost penetration documented by Boese (2003) for the SBH over the winters of 1999/2000 and 2000/2001, respectively. Therefore, the SBH cover could be affected by advective salt transport induced by a freezing front.

There are also processes that counteract the upward diffusive and advective transport into the cover. The net percolation of water from the base of the cover into the shale can result in salts being flushed downwards into the waste. A second counteracting process in the SBH cover system is lateral subsurface "interflow" (Kelln et al. 2008). Interflow is gravity driven flow of water that becomes perched along the interface of the cover soil and underlying shale overburden. It is caused by the development of a transient water table that develops on the lower hydraulic conductivity shale (Kelln et al. 2007). This lateral flow of groundwater can carry with it salts that have accumulated above the cover-shale interface.

2.5 Estimating Salt Transport Rates and Mechanisms for the SBH Site

The numerous salt transport mechanisms and seemingly conflicting results from studies on soil cover systems highlights the need to characterize the predominant mechanisms for salt transport at specific covers such as the SBH study site. The results from one reclamation area can be translated to other areas but only insofar as the variables, including soil properties, topography, climate, and vegetation, stay reasonably consistent.

The characterization of salt and moisture dynamics within the SBH study site began in 1999 during construction of the soil cover, when extensive soil and climate monitoring instrumentation was installed (Boese 2003). Subsequent researchers from the U of S have installed additional instrumentation and undertaken soil and water sampling programs to develop a better understanding of the water and salt transport regime at the SBH site (Meiers et al. 2003, Wall 2005, Kessler 2007, Chapman 2008, Kelln 2008).

Kessler (2007) collected soil samples from the cover and shale overburden to map the salinity profiles at the SBH study site four years after construction. Holes were drilled at approximately 20 m spacing along three transects. The three parallel transects ran up the slope of the cover, each transect located in a different cover plot (i.e. different cover prescription).

Kessler (2007) used laboratory diffusion experiments and Fick's Second Law to calculate an effective diffusion coefficient for total salt transport between the shale and the cover soil. The mean value of the coefficient of diffusion was determined to be $6x10^{-11}$ m²/s at a gravimetric water content of 20% (approximately 30% volumetric water content). Using this experimentally determined diffusion coefficient and Fick's Second Law, Kessler developed theoretical salinity profiles for the SBH soil cover system. These calculated salinity profiles were found to have a similar pattern to measured field profiles. This led Kessler to conclude that salt transport from the shale into the cover during the first few years after placement (approximately 4 years) was dominated by diffusion. However, using a similar methodology, in a study several years later, Kelln et al. (2008) found that diffusion alone could not explain soil salinity profiles and suggested that evapotranspiration-induced advection was also pulling salts upward into the cover soil.

In Kessler's study it was assumed that downward percolation of precipitation at the SBH site is negligible given the low hydraulic conductivity of the shale overburden (in the order of 10^{-8} m/s) as measured by Meiers (2002). The validity of this assumption seems to be strengthened by single ring infiltrometer testing performed by SCL in 1998 on the

shale surface prior to cover placement (SCL unpublished data). In 15 of 19 tests, the rate of infiltration was not measurable and assumed to be zero. These tests experienced some initial infiltration which tailed off to zero after 2-20 minutes. It is believed that this was due in part to the effect of fresh infiltrating water causing the shale to disperse and swell. No tests were conducted using saline water. However, it should also be noted that four of the 19 infiltrometer tests conducted showed very high infiltration rates presumably due to the presence of secondary structure in the shale.

Kessler (2007) suggested that lateral relocation of salts within the cover soil by interflow must be negligible based on the lack of a relationship between slope location and salinity in the cover. That is, the salt concentrations were not found to be greater in the lower slope locations as one would expect if interflow was the dominant mechanism of salt transport

Contrary to the conclusions of Kessler, Kelln et al. (2008) found that the accumulation of salts in the cover was being attenuated by deep percolation and by lateral subsurface "interflow" along the interface of the shale and soil cover. Kelln et al. simulated downslope interflow using a 2D finite element seepage model, considering the fractured till cover soil as an equivalent porous medium with a composite porosity soil-water characteristic curve. Predicted volumes of lateral subsurface flow were compared to those captured in the interflow collection system and found to be similar. The net percolation rate for the model was selected based on the assumption that there was a seasonally developed shallow water table, along with assumed values of hydraulic conductivity and gradient. A more accurate estimation of this net percolation rate is required to improve the numerical model developed by Kelln et al. (2008).

2.6 Stable Isotopes of Water as Tracers

2.6.1 Problems with Salt Ions as Tracers

Using salt profiles to characterize the salt and moisture dynamics in a cover soil system can be complicated by the non-conservative nature of the salt ions. Sodium is the salt ion of greatest concern because of its detrimental effects on soil properties. It also happens

to be the cation of greatest concentration in the shale overburden. However, Na^+ is not a conservative ion in that it can be adsorbed and desorbed by clay particles. As described in Section 2.3, the clay particles in the shale contain substantial amounts of adsorbed Na^+ which is released when dissolved Ca^{2+} and Mg^{2+} are preferentially adsorbed. Conversely, when the dissolved Na^+ is transported into the cover, where initial pore water concentrations are relatively low, it may be adsorbed by clay particles (Nichol et al. 2006).

Sulphate is the other major ion of concern as it is present in higher concentrations than any other ion. However, SO_4^{2-} transport is only marginally easier to model than Na^+. While SO_4^{2-} is rarely adsorbed by clay particles, except under low pH conditions (Drever 1988), it is produced by the oxidation of pyrite. This adds an additional level of uncertainty to contaminant transport models because the model now requires an estimate of the initial pyrite concentrations available for oxidation, the depth of oxidation which will deepen as the pyrite is depleted, and the oxidation rate which decreases as the oxidation zone becomes deeper. Elevated SO_4^{2-} pore-fluid concentrations can also lead to precipitation of gypsum (Hendry et al. 1986, Mermut and Arshad 1987). This further complicates the geochemistry as precipitation and dissolution of gypsum will alter the SO_4^{2-} concentrations in the pore water.

Chloride is considered to be the most conservative salt ion as it is not a significant component of rock minerals, is not adsorbed by clay particles, and maintains a high solubility in water (Feth 1981). However, in many soils, including the SBH cover system, Cl^- is present only at low concentrations at which analytical precision and various sources of error can have a significant impact on the salinity profile.

2.6.2 Stable isotopes of water

The inherent challenges associated with using salt ions as tracers to characterize hydrogeological regimes have led researchers to search for alternative conservative tracers. Stable isotope analysis of soil pore water has been used by researchers to estimate groundwater flow rates and determine the mechanisms responsible for solute

transport (Hendry and Wassenaar 1999, 2004; Hendry et al. 2004; Desaulniers et al 1986; Simpkins and Bradbury 1992; Remenda et al. 1996).

Isotopes are atoms of the same element that differ only in the number of neutrons in the nucleus. In other words, isotopes of an element have different atomic masses but the same atomic number. Most elements have one isotope that is far more abundant than the others. Generally the rarer isotopes will have an excess of neutrons. When describing isotopes, the elemental symbol is given along with the associated atomic mass. For example, the most abundant isotope of oxygen, ^{16}O, has an atomic mass of 16, while the next most common isotope of oxygen, ^{18}O, has an atomic mass of 18.

Stable isotopes are naturally occurring and are not subject to radioactive decay. The two primary stable isotopes of water are deuterium (^{2}H) and oxygen-18 (^{18}O). These stable isotopes are ideal tracers of water because they form part of water molecules that have essentially the same chemical properties as non-isotopic water molecules (Gat et al. 2001). Stable isotopes of water are conservative tracers in that they are not significantly affected by geochemical reactions at normal near-surface groundwater temperatures (Lawrence and Taylor 1972, Dowuona et al. 1993, Remenda et al. 1996) and do not experience attenuation during transport. Stable isotopic profiles, therefore, can provide a better calibration tool for the 1D numerical transport model than dissolved ion profiles.

2.6.3 Stable Isotope Measurements

The abundance of a stable isotope is generally not stated as an absolute concentration but instead is presented as the relative difference between a sample and the internationally accepted standard for the isotope in question. For example, stable isotopes of water are compared to Vienna Standard Mean Ocean Water (VSMOW). The relative difference is signified by the 'δ' symbol and is presented in units of per mil (‰). The 'δ' value is defined as follows (Fritz and Fontes 1980, Gat et al. 2001):

$$\delta = \left(\frac{R_{sample} - R_{s\tan dard}}{R_{s\tan dard}} \right) x1000\,‰ \qquad [2.3]$$

where R is the ratio of the abundance of the rare isotope to the dominant isotope. For example, with oxygen-18 this ratio is $^{18}O/^{16}O$.

One of the primary reasons for using δ-notation in describing stable isotope concentrations is that the rare stable isotopes are often present in such low concentrations that many significant figures would have to be presented, particularly when dealing with isotopic fractionation (see Section 2.6.4) (Domenico and Schwartz 1998). In addition, measurement of stable isotopes is often conducted using mass spectrometers that are capable of measuring relative abundances to a very high degree of precision but not absolute concentrations (Gat et al. 2001). In recent years, improvements in technology have allowed absolute concentration measurements of stable isotopes in water (Lis et al. 2007) but the use of δ-notation persists.

2.6.4 Isotopic Fractionation and the Meteoric Water Line

While isotopes of an element are nearly chemically identical, there are slight, but measurable, variations in the behaviour of the individual atoms caused by mass differences (Fritz and Fontes 1980). These mass differences translate to inequalities in the motion or velocity of the individual atoms or molecules containing the isotopes (Rose 1995). The increased mobility of lighter isotopes makes those atoms and molecules more likely to break their chemical bonds or change phases (Gat et al. 2001, Gat 1996). This results in measurable differences in isotopic ratios between chemical species and physical phases and is known as "fractionation".

There are numerous fractionation processes that can affect δ^2H and $\delta^{18}O$ distributions. In geological settings, fractionation can occur through isotopic exchange between water and minerals in the soil or as a result of chemical reactions. Isotopic exchange between water and minerals can be significant at high temperatures and pressures such as those in deep geothermal systems (Domenico and Schwartz 1998). At normal shallow groundwater temperatures and pressures, and over geologically short time periods, the stable isotopes in water will not experience any significant exchange with minerals in

the soil (Lawrence and Taylor 1972, Yeh and Epstein 1978). Chemical reactions such as precipitation, dissolution, reduction and oxidation can involve hydrogen and oxygen atoms from water. A relevant example of this is the oxidation of pyrite minerals in the shale overburden as described in Section 2.3. Hendry et al. (1989) found that the primary source of oxygen in SO_4^{2-}, produced from the oxidation of reduced sulphur, is the water itself. Any chemical reactions involving ^{2}H and ^{18}O from water are sure to experience fractionation effects. These fractionation effects would likely result in an observable difference between the stable isotope ratio in the water and that of the chemical compound. However, as Savin (1980) points out, the isotopic signature of the liquid water will rarely be affected by geochemical reactions or water-mineral exchange because of the massive amount of hydrogen and oxygen in the water relative to the chemical compound or exchanging surface.

It is noted by Gat et al. (2001) that diffusion is also a fractionating process. This would seem to be of critical importance in the context of this study where stable isotopes are being used to characterize water and salt dynamics, including the process of diffusion. However, fractionation by diffusion only applies if the isotope of interest is diffusing through a fluid of different molecules than the isotope. Therefore, in hydrogeologic settings, fractionation by diffusion would be important if the stable isotopes being analyzed were not part of the water itself but were instead isotopes of a solute diffusing through the pore water. A further example where fractionation by diffusion could be significant is water vapour diffusing through air (Gat et al. 2001). This example might have relevance in unsaturated soil environments. However, if one is studying the diffusion of ^{2}H or ^{18}O through water and it is the concentration gradient of the stable isotope that is causing the diffusion, then fractionation by diffusion does not apply.

The principles laid out by Gat et al. (2001) do imply, however, that the diffusion coefficient of ^{18}O will be slightly lower than that of ^{2}H, and both of these will be slightly lower than the "true" self diffusion coefficient of water, because of slightly different molecular weights. However, it should be noted that it would be impossible to measure

the true self diffusion coefficient of water without the use of stable isotopes (Shackelford and Daniel 1991) and therefore it is of limited use in contaminant transport studies.

It would appear that concentrations of ^{2}H and ^{18}O in atmospheric, surface and near-surface groundwater are largely unaffected by chemical, biological and mixing fractionation processes. However, the stable isotope concentrations of these waters are affected by changes in the physical state of the water. For example, the processes of evaporation, condensation, freezing, thawing and sublimation are all important fractionation processes. When evaporation occurs in the oceans, a greater fraction of lighter isotopes will make the phase transition from liquid to vapour. Therefore, water vapour in the atmosphere will be more depleted in ^{2}H and ^{18}O than ocean water. Conversely, when the water vapour condenses to form rain drops, it is the heavier, slower moving water molecules that are more likely to drop to the lower energy liquid phase. Therefore, each rain drop will be more enriched in ^{2}H and ^{18}O than the water vapour from which it was formed. This process is known as "Rayleigh fractionation" or "Rayleigh distillation" (Rose 1995).

Globally, the majority of water vapour in the atmosphere evaporates from ocean waters with the warm equatorial ocean regions contributing the most evaporation (Rose 1995). As air masses cool they are unable to hold as much moisture and more vapour will condense and fall as rain or snow, resulting in progressively depleted $\delta^{2}H$ and $\delta^{18}O$ levels in the remaining water vapour. This cooling of air masses can be caused by movement of oceanic air masses inland (continental effect), away from the equator towards the poles (latitude effect), and movement to higher elevations (altitude effect) (Gat 1996). In addition, for a given location, seasonal variations are observed in the $\delta^{2}H$ and $\delta^{18}O$ values of water vapour or precipitation. Colder temperatures will result in more depleted isotopic levels.

The progressive isotopic depletion of water present in air as vapour, and the concomitant enrichment of precipitation affect both $\delta^{2}H$ and $\delta^{18}O$ values in a similar and predictable manner. This was initially observed by Craig (1961) who plotted $\delta^{2}H$ and $\delta^{18}O$ values

from many global freshwater sources and found that the points plot along a straight line known as the Global Meteoric Water Line (GMWL) as illustrated in Figure 2.2. The equation of this line has since been refined by Gat (1980) and is approximately:

$$\delta^2H = 8.17\ \delta^{18}O + 10.56‰ \qquad [2.4]$$

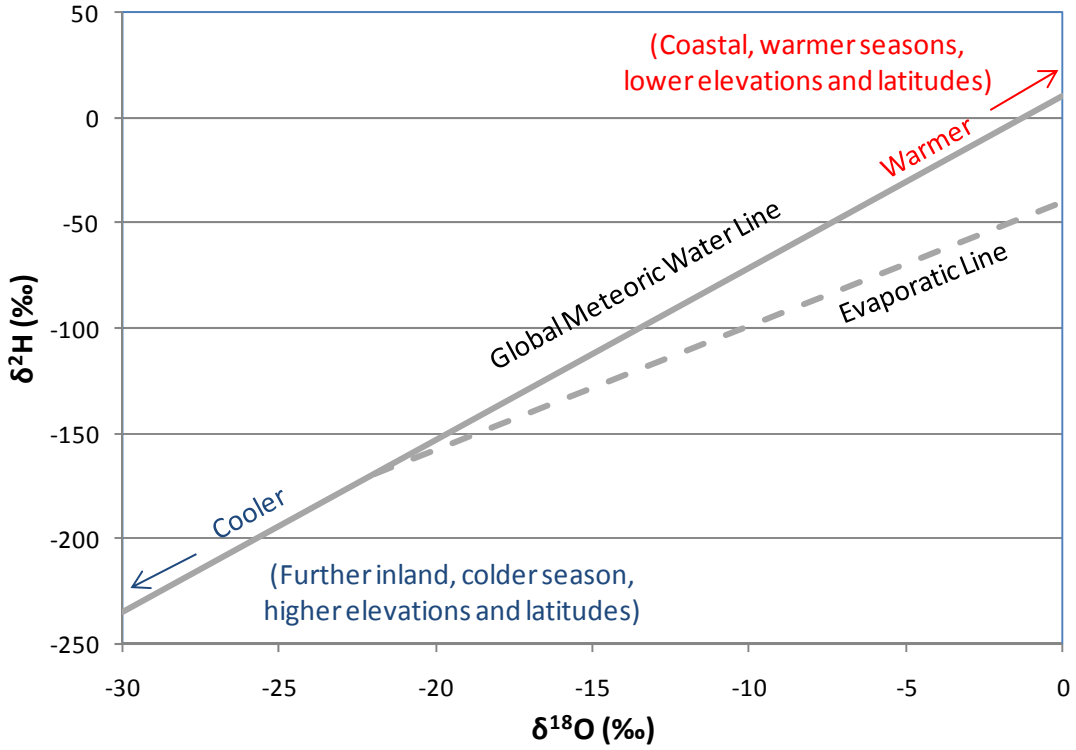

Figure 2.2: Meteoric water line explanation.

While progressive isotopic depletion of meteoric water originating from the ocean plots along a straight line, water that falls as precipitation and is then re-evaporated before mixing in the ocean will diverge from the meteoric water line, along what is known as an "evaporatic line" (Rose 1995). This is illustrated in Figure 2.2 as a dashed line. The importance of this distinguishing signature is that it can help describe the history of surface and groundwater.

Often, researchers will plot the meteoric water line for a particular location, referred to as the "Local Meteoric Water Line" (LMWL). These LMWLs are intended to characterize consistent deviations from the global MWL. For example, if a location

receives a large proportion of precipitation originating from inland seas or lakes, the LWML may have a shallower slope. However, Gat (1996) questions the meaning of such lines, stating that weather patterns are often inconsistent and the source of water in the air mass delivering precipitation can vary.

The discussion of meteoric water fractionation generally centres on condensation and evaporation, or in other words, the liquid and gaseous states of water. However, fractionation occurs whenever water changes from one physical state to another and in Canada, freezing and thawing will also be important fractionation processes. As described above, when the water is moving from a lower energy state to a higher energy state the water will tend to become more depleted in heavier stable isotopes. If the water is moving to a lower energy state, it will tend to become more enriched. This trend applies equally to processes involving frozen water (i.e. ice and snow), as shown in Figure 2.3.

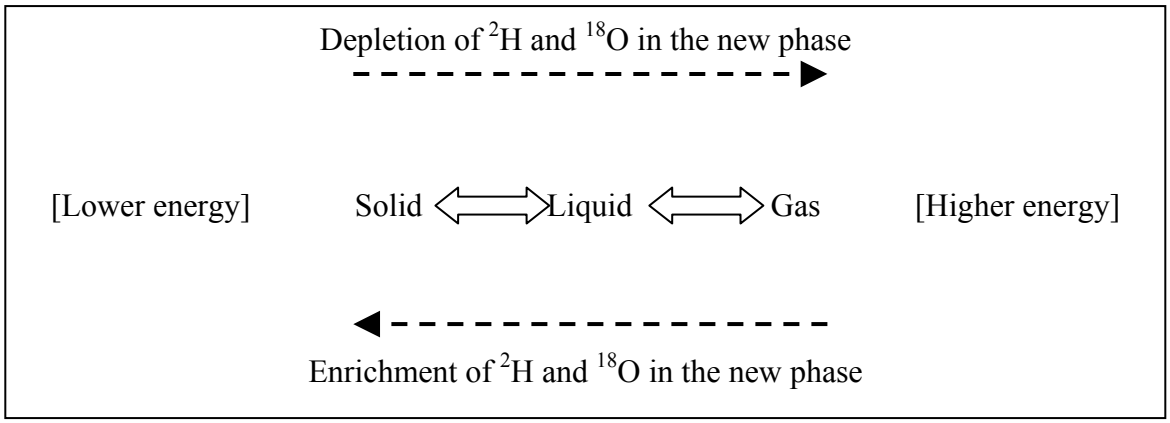

Figure 2.3: Fractionation due to changes in physical state.

Figure 2.3 illustrates that sublimation (solid to gas) and melting (solid to liquid) of ice or snow will result in depletion of ^{2}H and ^{18}O in the new phase of water, and a corresponding enrichment in the remaining frozen water (Taylor et al. 2002, Moser and Stichler 1980). Conversely, ice will be more enriched in ^{2}H and ^{18}O than the source of water from which it was formed, if the volume of the liquid water reservoir is much greater than that of the forming ice (Friedman et al. 1964).

An important consideration when dealing with these fractionation processes is that of mixing. The higher the energy state of a physical phase, the higher the velocity of the individual molecules and, thus, the faster that fractionation effects will spread through a given volume. This can have implications on fractionation effects involving snow and ice and is further discussed in Section 4.1.3.

3. METHODOLOGY

This chapter presents the methodology used to conduct the research for this study. The steps are presented in approximately the order that they were performed beginning with field work; including field measurements, water sample collection, and soil sample collection. The laboratory testing procedures are described next followed by a discussion of the numerical model inputs and procedures.

3.1 Sampling and Measurements

The SBH site has been the focus of numerous research projects over the past decade and as such, a great wealth of data exists for the site. A major component of the current proposed research project was to sort through the existing data and to determine the relevance and application of this data to this study. Existing data files current to January 2009 were catalogued to expedite the process of incorporating relevant data into the current research project.

Many of the sampling and measurement protocols followed in 2009 were originally established during previous studies at the SBH site (Kelln 2008, Kessler 2007, Boese 2003). The locations of the instruments and sampling locations described in this chapter are illustrated in Figure 3.1.

3.1.1 Interflow Monitoring

The spring season is a period of particular importance for the SBH site. As temperatures increase, snow melt and ground thaw contribute to net percolation and the creation of interflow. Net percolation and interflow are the only mechanisms that can flush soluble salts from the soil cover. It is anticipated that interflow will only provide a potential mechanism for salt flushing over the slopes, and therefore, it is of particular importance to characterize net percolation with respect to topographic position.

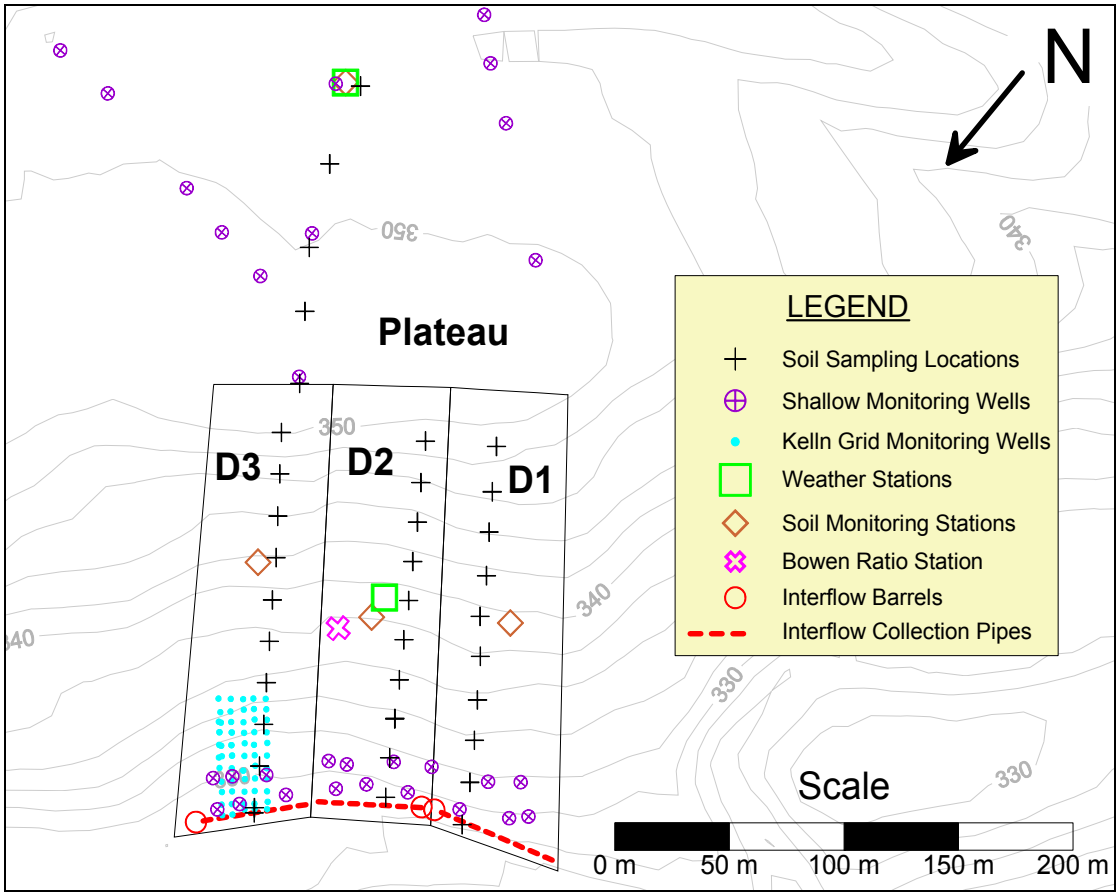

Figure 3.1: SBH instrumentation layout.

An interflow collection system was installed in the summer of 2000 by researchers from the U of S and SCL. The detailed installation procedure and components of the system are described in Boese (2003). A trench was excavated at the toe of the slope across each of the three cover plots (D1, D2 and D3). The downstream side of the trench was lined with a geomembrane and a 150 mm diameter, perforated, flexible polyethylene pipe (weeping tile) was placed at the bottom of the trench. A sufficient amount of sand backfill was placed to completely encapsulate the weeping tile followed by replacement of the excavated cover soil back into the trench. The geomembrane intercepts any lateral groundwater flow passing through the till cover soil and directs it into the weeping tile. The weeping tiles are sloped towards one of three buried collection barrels; one for each cover plot. The collection barrels consist of 45 gallon PVC drums with steel wall braces to prevent collapse. A cross-sectional sketch of the interflow collection system is shown in Figure 3.2.

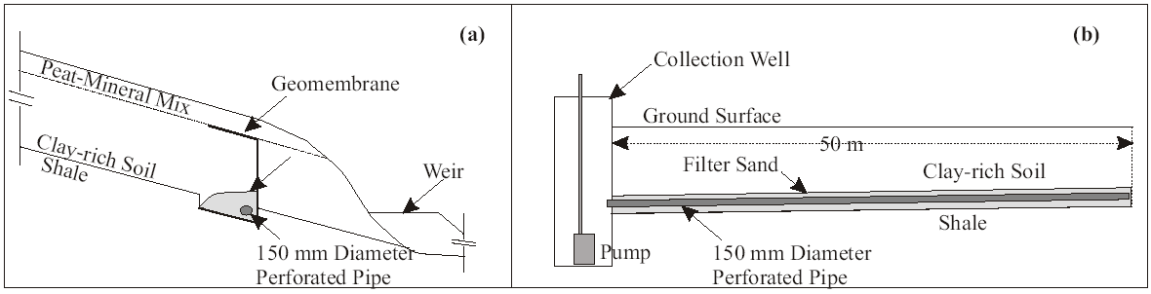

Figure 3.2: Cross-sectional views of interflow collection system
(a) North-south profile. (b) East-west profile. (from Kelln et al. 2009)

Interflow monitoring consisted of recording the cumulative interflow from each of the three cover plots as well as collecting water samples for chemistry and stable isotope analysis. During the years 2000 to 2008, the collection barrels have been alternately equipped with a float-switch activated submersible pump and flow meter or have been manually pumped with a portable electric submersible pump. The automated pump systems are powered by a 12 Volt marine battery connected to a solar panel battery charger. An in-line turbine-style flowmeter is attached to the discharge pipe to measure cumulative flow from the system. Figure 3.3 shows a photograph of the automated pump setup. Flow measurement during manual pumping was accomplished using a bucket and stopwatch.

Interflow pumping is initiated each spring once the ice has melted sufficiently from the water surface in the interflow barrel to allow the pump to pass through to the bottom of the barrel. Even if the pump can be lowered into the collection barrel, flow of water from the weeping tile will be impeded until the majority of ice within the collection pipe and cover soil has thawed. In 2009, some minor pumping using the smaller portable submersible pump was initiated on April 30; however, it was observed that recharge was slow indicating ice restrictions in the system. Automated pump systems were installed in the D1 and D3 interflow collection barrels on May 11 once the ice in the barrels had thawed sufficiently. The D2 interflow barrel was not equipped with an automatic pump system but was emptied regularly using the portable pump.

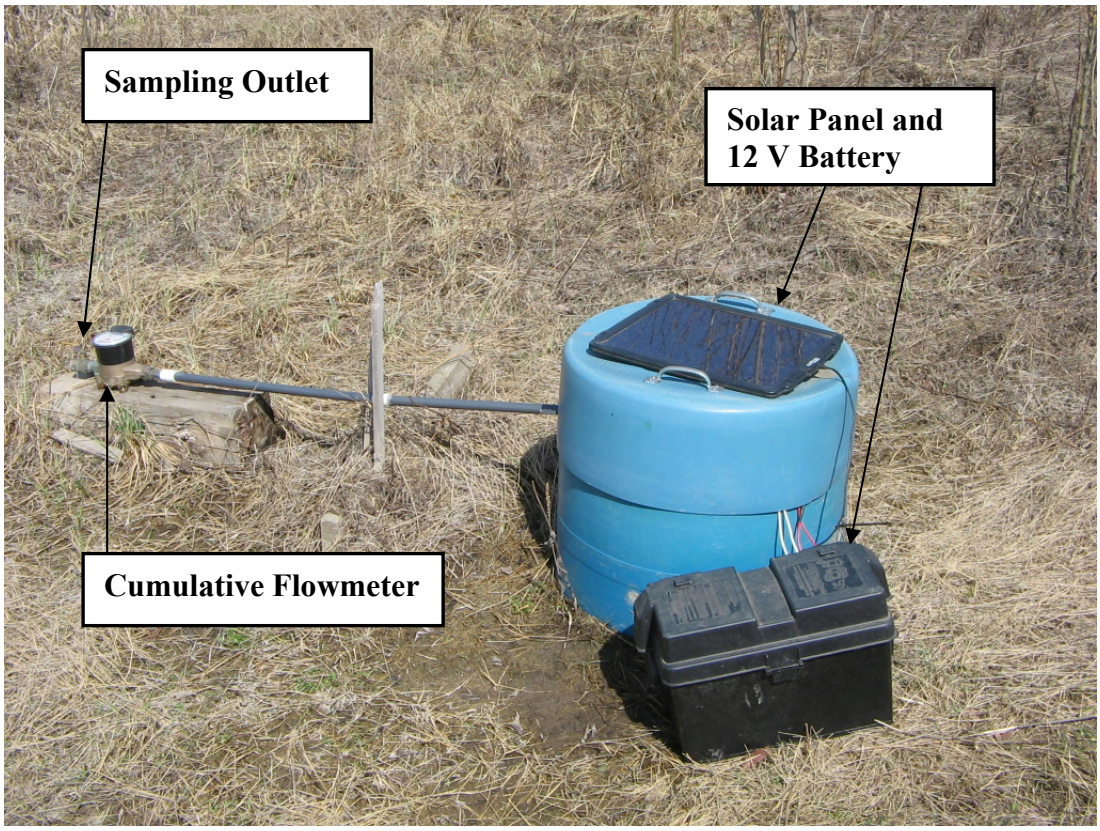

Figure 3.3: Automated interflow pumping system with metered outflow pipe.

Interflow water samples were collected approximately daily from the start of interflow (May 11) until the end of May. OKC collected interflow water samples approximately once per week through June and July, until interflow ceased completely on July 24. Water samples were collected in two parts: i) approximately 500 ml of water was collected for chemical analysis, and ii) approximately 60 ml of water collected for stable isotope analysis. Samples were collected in polyethylene bottles at the discharge pipe outlets.

3.1.2 Groundwater Monitoring

In addition to monitoring interflow volumes and chemistry, an effort was made to monitor the height of the perched groundwater table throughout the 2009 growing season and to sample the groundwater for chemistry and stable isotope analyses.

The height of the perched groundwater table was measured using a network of shallow monitoring wells across the three cover plots and on the plateau of the SBH site. These monitoring wells were installed between 2001 and 2006 by various researchers from the U of S. The locations of these monitoring wells are shown in the instrumentation map in Figure 3.1. The monitoring wells are concentrated near the toe of the slope where the perched water table is most persistent. An especially high density of monitoring wells was installed in the D3 cover in 2006 (Kelln et al. 2008). The monitoring wells on the plateau were installed along three transects as shown in Figure 3.1.

The monitoring wells were constructed using 50 mm diameter PVC pipe that was hand slotted over the bottom 0.3 m of the pipe. A solid PVC cap was fixed to the bottom of the pipe. The monitoring wells were installed with the shale-till interface at approximately the midpoint of the slotted section and the top of the pipe was cut so that the stick-up was approximately 0.3 m above ground surface.

Measurements of the depth to water were taken with an electronic water level meter that was also capable of measuring electrical conductivity (EC) of the water. Water level and EC measurements were taken approximately daily during the month of May in 2009. OKC continued to take water level and EC readings 2-3 times per week in June with an additional two sets of measurements in July and a final round of measurements in September.

Groundwater samples were collected from the same network of monitoring wells throughout the 2009 season. Three complete rounds of groundwater samples were collected in May, each spaced approximately two weeks apart. OKC collected an additional round of groundwater samples in early August; however, only the monitoring wells which could yield sufficient water were sampled. A final round of groundwater sampling was planned for late fall as some previous years had experienced replenished perched water table levels from late fall rains. However, in 2009 the monitoring wells remained dry throughout the fall and this final round of samples could not be collected.

The groundwater samples were collected using a hand-powered suction pump as shown in Figure 3.4. The sampling apparatus comprised a 250 ml glass Erlenmeyer flask sealed with a rubber stopper. The rubber stopper had an intake and outtake port to which 6 mm ID polyethylene tubing was connected. The intake tubing was lowered all the way down the monitoring well. The outtake tubing was connected to the suction pump which extracted air from the flask. The lower air pressure in the flask created a head gradient that would pull fluid through the intake tube into the flask. Prior to use, the inside of the flask and the outside of the polyethylene tubing to be lowered into the monitoring well were rinsed with distilled water. The first 30 ml of water sample collected were considered to be rinse water and were used to flush the previous sample water from the tubing and to rinse the flask. Water samples were then collected in the following amounts: i) approximately 200 ml of sample for water chemistry analysis, and ii) approximately 30 ml for isotope analysis. Samples were collected in polyethylene bottles and stored in coolers until they could be refrigerated at the end of the day.

Figure 3.4: Water sample extraction from monitoring wells.

3.1.3 Snow Survey and Sample Collection

An annual snow survey has been conducted at the SBH site each year since 2000. The data from the snow surveys provide an estimate of the snow water equivalent for the snow pack. The snow survey cannot account for snow melted during mid-winter warm spells, nor can it account for sublimation over the winter. The snow survey involves measuring the depth and density of snow at a regular spacing along transects that run up each of the three cover plots and across the plateau. The surveys are usually conducted in late winter just prior to snow melt. Depending on the year, the snow survey has been conducted by researchers from the University of Alberta, the University of Saskatchewan, or OKC Consultants and sometimes with assistance from SCL employees. The 2009 snow survey was led by OKC on 30 March 2009.

During the 2009 snow survey a total of 14 snow samples were collected for stable isotope analysis; eight from the plateau and six from the D3 cover. These samples were taken from cores through the full depth of the snow pack and, therefore, represent the average stable isotope signature of the snowpack prior to snowmelt. Snow samples were stored in sealed plastic freezer bags and allowed to melt in the airtight bags in a refrigerator. Approximately 10 ml of water from each the melted snow samples was then poured into polyethylene bottles and shipped to the laboratory for stable isotope testing.

3.1.4 Precipitation Collection

On 11 May 2009 a simple precipitation collection device was installed at the SBH for the purpose of collecting rainwater to be analyzed for stable isotopes. The collection device consisted of a plastic funnel set approximately 1.5 m above ground surface and affixed to a metal rod driven into the ground, as shown in Figure 3.5. The precipitation collection device was located at the toe of the D3 slope as shown in Figure 3.6. Sample bottles were threaded into the device to allow easy exchange. Samples were generally collected less than 24 hours after precipitation events to minimize evaporation effects on the sample, as described in Section 2.6.4. Precipitation samples were collected after every rain event during the May field program. OKC assumed responsibility for precipitation collection from June to September, sampling after every rain event.

Figure 3.5: Precipitation sampling device.

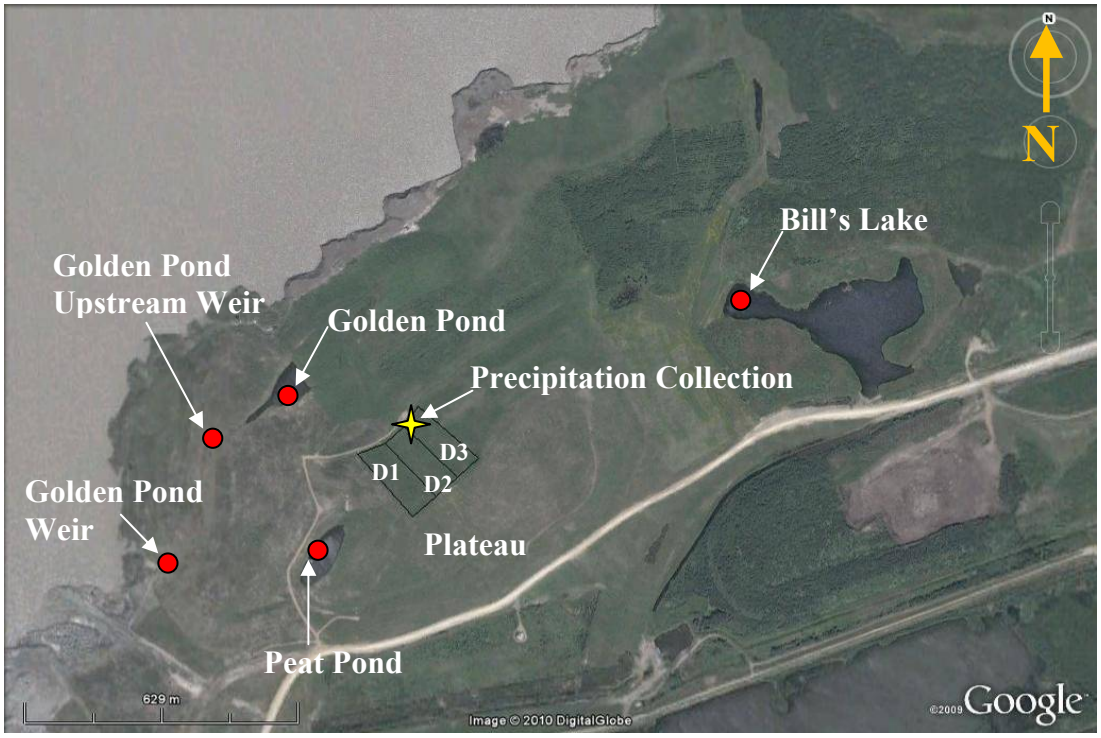

Figure 3.6: SBH surface water and precipitation sample collection points from 2008. Shaded circles indicate surface water sampling locations.
Star indicates precipitation collection location. (Image from Google 2009).

3.1.5 Surface Water Collection

A total of 10 surface water samples were collected from the SBH over the month of May 2008. These samples were collected for stable isotope analysis to compare to the groundwater and interflow samples with an objective of demonstrating a difference in evaporative effects (as discussed in Section 2.6.4). The samples were collected from five locations across the site: Bill's Lake, Peat Pond, Golden Pond and two weirs on the drainage ditch downstream of Golden Pond. These locations are illustrated in Figure 3.6.

3.1.6 Soil Sample Collection

Soil samples for salinity analysis were collected from the three cover plots in August 2008 and from the plateau in May 2009. Holes were drilled using a Dutch hand auger, as shown in Figure 3.7, with soil samples collected over 0.1 m depth intervals. The holes were drilled through the cover and at least 0.3 m into the shale. The drill holes on the slope were located along three transects extending up the slope, one transect per each of the cover plots, with approximately 20 m spacing between holes. The plateau drill holes were located on a single transect extending from the slope crest to the centre of the plateau. The sample locations and sampling intervals were selected to correspond as closely as possible to previous soil sampling performed by Sophie Kessler on the cover slopes in 2002 (Kessler 2007) and on the plateau in 2004 (unpublished data). Hole locations were targeted using handheld GPS devices or, whenever possible, were located next to existing instrumentation that marked the location of previous sample locations. The soil sampling locations from the current study are illustrated in Figure 3.8. For clarity, not all of the sample labels have been included. A summary of the drill hole information, including survey coordinates and depth, is included in Appendix A.

Figure 3.7: Dutch auger used for soil sample collection.

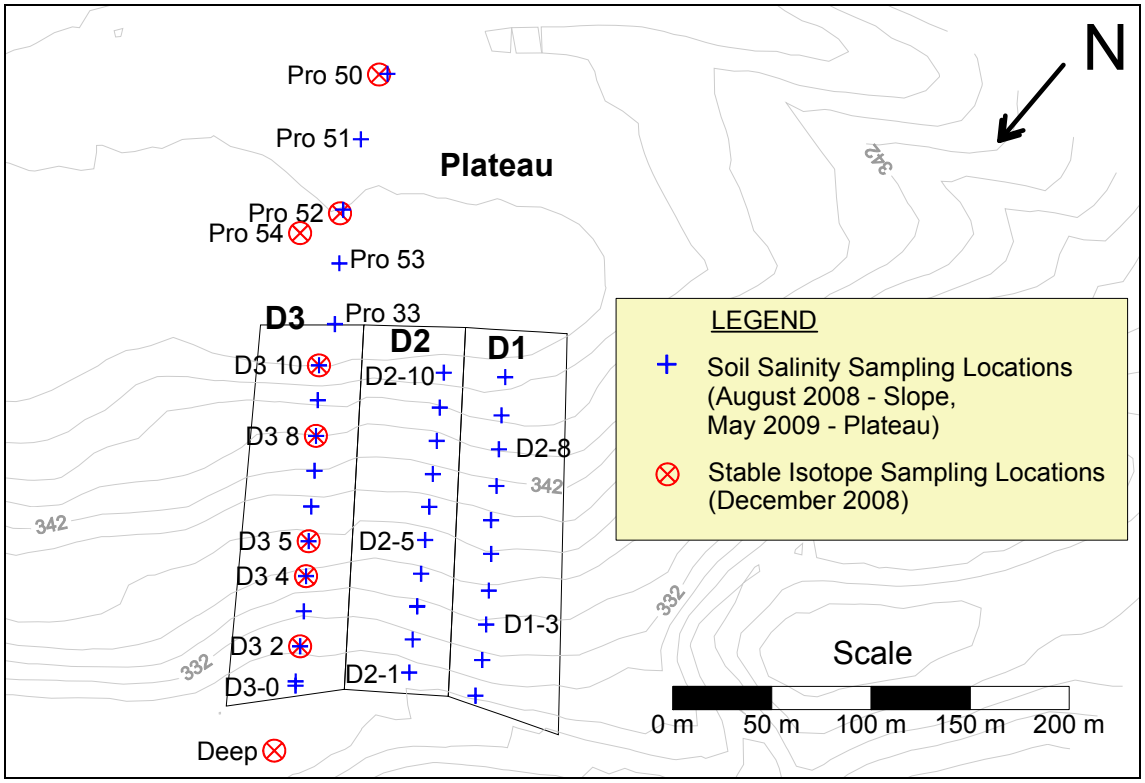

Figure 3.8: 2008 and 2009 soil sampling locations.

A separate drilling program was undertaken in December 2008 for the purpose of obtaining soil samples to analyze for stable pore water isotopes. A small tracked drill rig, approximately 3 m long by 2 m wide, was used for drilling on the cover as it provided good manoeuvrability with minimal ground pressure, limiting disturbance to trees and the peat layer on the ground surface. Three holes were drilled on the SBH plateau and five holes were drilled along a transect extending down the slope of the D3 cover. The locations of these drill holes are illustrated in Figure 3.8. The details of the isotope sampling drill holes are included in Appendix A.

The isotope sampling holes were cored by pushing a split-spoon sampler through the cover and into the shale to a depth of approximately 3 m below ground surface. The split-spoon sampler had a maximum 0.6 m sample length and, therefore, core runs ranged from 0.2 – 0.6 m in length. The split-spoon sampler had an outside diameter of 50 mm and an inside diameter of 35 mm.

An additional core hole was pushed below the access road at the base of the slope during the December 2008 drilling program. This hole was drilled using a larger truck-mounted auger rig because there was no cover in this location and, therefore, ground disturbance was not an issue. The method of drilling was the same (i.e. pushing a split-spoon sampler). The depth of this hole was 9.25 m below ground surface and was intended to provide background stable pore water isotope values for the shale at depth.

The cover soil and shale overburden were competent enough to keep the core holes from closing in between sampling runs. However, sample recovery was typically poor due to sample compression or lack of recovery. Lower recovery or sample compression seemed to be most severe in the till, especially in regions where the till was soft and wet or had peat mixed in. The heterogeneous nature of the cover, results in layers and pockets of varying soil stiffness and moisture content. It is believed that when the split-spoon was pushed through hard or dry cover soil or overburden, this material would become lodged in the shoe of the sampler. The softer soil below these hard zones would have had insufficient stiffness to push the hard soil further into the split-spoon barrel.

Consequently these softer zones were compressed or pushed aside by the plugged barrel until the next zone of sufficient resistance was encountered.

It was also observed that the poorest recovery seemed to be occurring in the uppermost portion of the cover. It is suspected that, as the split-spoon sampler was pushed through the cover surface, frozen peat would become lodged in the split-spoon. The soil just below the frost zone would therefore be compressed or pushed aside. After recognizing this problem, the sampling interval at the top of the cover was shortened from 0.6 m to 0.2 m. However, the recovery in the top 0.6 m still remained poor.

Sample recovery would have likely been better if thin-walled Shelby tubes were used to collect samples instead of the relatively thick-walled, and smaller inside diameter, split-spoon sampler. However, these tubes could not be obtained on short notice during this brief drilling contract.

For the softer soils within the cover, the recovered sample length was often less than 50% of the core run length. This necessitated the application of judgment in determining the sampling depth interval. Though best efforts were made during drilling, the assigned depths of samples could potentially be inaccurate by as much as ±0.3 m in the zones of poor recovery.

The recovery in the shale was generally better than the cover soil with an average recovery of approximately 70%. It is believed that the range of error in sample locations for the shale is approximately ±0.1 m.

3.1.7 Other Data Collection

Data from the automated soil and weather stations are collected semi-annually by OKC. Care and maintenance of these instruments is also provided by OKC to ensure that the equipment is in good working order. Some of the automated data that were especially relevant to this study include:

- climate data recovered from the mid-slope and plateau weather stations, especially temperature and daily and hourly precipitation amounts;
- daily snow pack height measurements from the plateau weather and soil station; and,
- soil temperature and soil moisture profiles collected from the three mid-slope soil stations on the cover plots and one soil station on the plateau.

In addition to the automated data collected at the soil and weather stations, OKC measured soil moisture profiles from Diviner 2000 access tubes distributed across the SBH site. In 2009, these profiles were measured monthly from May to September.

3.2 Laboratory Testing

3.2.1 Water Sample Testing

Water samples collected for the purposes of water chemistry analysis included interflow and groundwater samples. These samples were tested for pH, EC, and alkalinity in the University of Saskatchewan's Environmental Engineering laboratory. Major ion concentrations were measured using the Ion Chromatography (IC) apparatus in the University of Saskatchewan's Aqueous Geochemistry Laboratory. Water samples were analyzed for the following major ions: Ca^{2+}, Mg^{2+}, Na^{+}, K^{+}, NH_4^{+}, Cl^{-}, and SO_4^{2-}. Prior to chemistry analysis, all water samples were filtered in the laboratory using 0.45 μm cellulose nitrate filters.

Water samples to be tested for the stable isotopes, ^{2}H and ^{18}O, included melted snow, precipitation (rain), interflow, and groundwater. Isotopic compositions of the water samples were measured at the National Water Research Institute (NWRI) in Saskatoon. This laboratory utilizes an off-axis integrated cavity output spectroscopy laser (OA-ICOS) to directly measure absolute ratios of deuterium and oxygen-18 in the liquid water molecules (Lis et al. 2007). These absolute ratios are converted to delta notation (i.e., $\delta^{2}H$ and $\delta^{18}O$) using bracketing calibration standards that have known isotopic ratios relative to the VSMOW standard. The OA-ICOS laser is a recent technological innovation that some researchers are advocating over the established technology, isotope

ratio mass spectrometers (IRMS) (Lis et al. 2007, Wassenaar et al. 2008). The accuracy of the OA-ICOS laser for stable isotope testing of liquid water is reported to be 0.8‰ for δ^2H and 0.1‰ for $\delta^{18}O$ (Lis et al. 2007).

All water samples were stored in refrigerated conditions from the day that they were sampled until the day they were delivered to the laboratory. The exception is the period that samples were in transit from Fort McMurray to Saskatoon. During transit, samples were kept in insulated beverage coolers along with frozen ice packs. Transit time was approximately 48 hours. Once the samples were received in Saskatoon, they were immediately returned to refrigerators.

To assure the quality of water chemistry and stable isotope testing, approximately 10% of samples were resubmitted to the laboratory as duplicates. This was easily facilitated because test methods for both water chemistry and stable isotopes only required a fraction of the water sample collected. Test results for duplicate samples were then compared to original results to check repeatability of test methods.

3.2.2 Soil Sample Testing

Soil salinity testing was conducted at Exova Laboratory (formerly Bodycote) in Edmonton, Alberta using the saturated paste method, described in Rhoades (1982). While this method underestimates the total soluble salts in the soil compared to higher dilution extracts (Kessler 2007, Buckland and Hendry 1986) it is applicable when studying the effects of soil salinity on vegetation as the saturated paste extract is more representative of the pore water to which plants are exposed (USDA Salinity Laboratory 1954). However, the primary reason for using the saturated paste method in this study was to maintain consistency with the testing methods of Kessler (2007). Saturated paste extracts were tested for pH, EC, and the following major ions: Ca^{2+}, Mg^{2+}, Na^{+}, K^{+}, Cl^{-}, and SO_4^{2-}.

Isotopic testing of soil samples was conducted in the U of S Aqueous Geochemistry Laboratory. The stable isotope composition of the soil pore water was measured using

the $H_2O_{(liquid)}$-$H_2O_{(vapour)}$ equilibration laser spectroscopy method as described by Wassenaar et al. (2008). In the past researchers have often relied on water samples obtained from piezometers or lysimeters to represent the pore water isotopic composition (Remenda et al. 1996, Hendry and Wassenaar 1999). Standpipe piezometers generally provide quite coarse resolutions as the screen length of the well has to be sufficiently long to allow a reasonable flow of groundwater into the well. Even so, the time required to obtain a sufficiently large sample can be in the order of months for low permeability soils (Wassenaar and Hendry 1999). Alternatively, some researchers have proposed methods of physical extraction of pore water from soil samples (Allison and Hughes 1983, Edmunds and Bath 1976, Fontes et al. 1986, Manheim 1966, Patterson et al. 1977). Extraction of pore water from soil samples can provide much better resolution in stable isotope profiles than piezometer or lysimeter sample collection depending on the drilling and soil sampling methodology and the degree of care practiced by field technicians. However, physical extraction of pore water from soil samples can still be time consuming and expensive and may, in fact, cause direct or indirect fractionation of the sample which would be difficult to quantify (Koehler et al. 2000, Kelln et al. 2001, Wassenaar et al. 2008).

Hendry et al. (2004) showed that stable isotope profiles in a clay aquitard could be obtained much faster and at less expense than previously established pore water extraction methods by using the direct equilibration method (Koehler et al. 2000). Direct equilibration methods test gases that are in isotopic equilibrium with the pore water of the soil. Soil samples can be tested directly allowing good profile resolution, but the pore water does not need to be extracted from the sample. The isotopic signature of the gas is measured and, using well established fractionation factors between liquid water and the gas being tested, the isotopic composition of the liquid pore water can be calculated. Earlier direct equilibration methods tested H_2 and CO_2 gases in equilibrium with pore water samples (Koehler et al. 2000), but the latest generation of laboratory technology tests H_2O vapour that is isotopically equilibrated with the liquid pore water (Wassenaar et al. 2008). This eliminates interference effects from other gases and the need for gas purification (Wassenaar et al. 2008).

Soil samples were given approximately three days to equilibrate with the air in the sample container, a resealable air-tight plastic bag. The ^{2}H and ^{18}O content of the water vapour was then measured using the same OA-ICOS technology as described in Section 3.2.1. The $\delta^{2}H$ and $\delta^{18}O$ values were then calculated for the pore water using the known fractionation factors between liquid water and water vapour at the given sample temperature. As described in Section 2.6.3, the $\delta^{2}H$ and $\delta^{18}O$ values are referenced to the VSMOW international standard and are presented in ‰.

Duplicate testing of soil samples was not conducted for major ions because the entire soil sample was required for the saturated paste tests. Quality assurance testing might have been possible if "twin" holes had been drilled in the field with samples collected from the same sampling depth. However, even if twin holes had been drilled as closely as possible to each other, the heterogeneity of soils virtually guarantees some degree of variation in test results. An alternative solution would be to use a larger diameter Dutch auger for select drill holes, producing larger soil sample volumes which could then be split into duplicate samples. Neither of these options was considered at the time of soil sampling.

Likewise, duplicate testing of stable pore water isotopes in the soil samples was not conducted. After the stable isotope testing, a portion of each of the soil samples was used for gravimetric water content testing. In some cases, this portion amounted to most or all of the soil sample. It is also believed that this handling of the soil samples might have introduced an opportunity for evaporation to affect the isotopic content of the soil sample pore water. Therefore, duplicate testing was not conducted and was not considered to be possible.

3.3 Numerical Modelling

One-dimensional contaminant transport models were constructed for the SBH site using the Geoslope® finite element software package Seep/W (for water flow) coupled with CTran/W (for contaminant transport). The primary objective of the numerical modelling

in this study was to derive a more accurate estimate of net percolation through the cover and into the shale overburden. Previous research on the SBH site has helped to elucidate various parameters needed to characterize the water and salt dynamics in the cover and shale. These parameters include hydraulic conductivity (Meiers et al. 2003; 2006), effective diffusion coefficient (Kessler 2007), pyrite oxidation rate in the shale (Nichol et al. 2006, Wall 2005), matrix and fracture porosity (Kelln et al. 2009), and interflow mass transport rates (Kelln et al. 2009). However, to date, attempts to measure or calculate net percolation into the shale have been crude or unsuccessful (Kelln et al. 2008, unpublished tests by SCL).

3.3.1 Conceptual Model

Prior to undertaking the development of the numerical model a conceptual model was developed to summarize the processes involved in salt and moisture transport for the SBH cover system. The conceptual model as illustrated in Figure 3.9 was based on earlier modelling work by Kelln (2008) and Nichol et al. (2006).

The conceptual model was developed for the cover prescription of the D3 plot and the plateau area. As described in Section 1.2, the soil cover in these areas is nominally 1 m thick; 0.2 m of peat-mineral mix overlying 0.8 m of clayey till. In the conceptual model however, the cover was represented for simplicity as one material with the properties of the clayey till. The basis for this simplification is that the modelling for this study was primarily focused on salt and moisture transfer at the interface of the soil cover and the shale overburden. Previous research (Kessler 2007, Merrill et al. 1983) has shown that upward salt diffusion was limited to the bottom 15 - 20 cm of the cover. Previous and current salinity profiles also confirm that salt transport is not significant in the middle and upper portions of the cover. This simplification eliminates the difficult challenge of trying to accurately model the physical properties of the highly variable and heterogeneous peat-mineral mix layer.

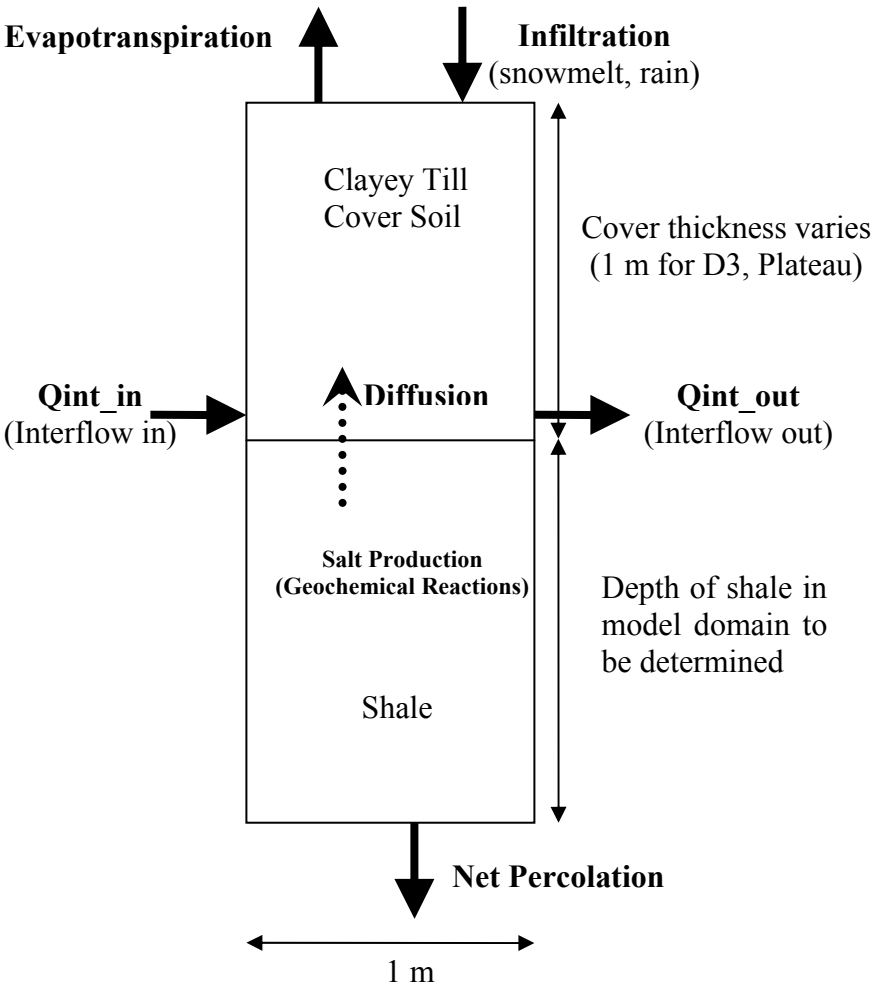

Figure 3.9: Quasi one-dimensional conceptual model.
(Adapted from Nichol et al. 2006)

As indicated in Figure 3.9, the depth of the shale in the conceptual model domain was not conclusively established prior to modelling. The depth of the 1D profile was limited to reduce calculation time and minimize file sizes during numerical modelling; however, a sufficient depth was used to ensure the lower boundary condition would not influence the model results. Simplifications to the interflow boundary conditions (described below) allowed the 2D conceptual model to be converted to a 1D numerical model. This meant that the width of the column is not important and was set at 1 m for simplicity.

Water ingress to the model was assumed to occur by two processes: interflow and infiltration. Differences between the rate of interflow entering and exiting the domain,

both in terms of water flow and contaminant mass, were accommodated by assigning the net difference (positive or negative) to the model nodes at the interface. Infiltration can be either rain water or melted snow that percolates down through the cover. Some of this infiltrating water may contribute to lateral interflow and some of it may be removed from the model domain as evapotranspiration. The remainder of the infiltrating water that passes through the cover/shale interface is termed "net percolation".

The primary objective of this modelling was to determine the net percolation through the cover and into the shale overburden. As a consequence, rather than trying to accurately simulate the dynamics of all of the advective processes (infiltration, evapotranspiration, percolation), it was determined that a "net percolation" variable could account for all of these processes. The origin for this net percolation flow was set at the till-shale interface since it is the net percolation into the shale that is of interest in this study.

The use of a net percolation variable would not be appropriate when seasonal variations cause reversals of flow direction and cycling of solutes. This would appear to be the case in the cover soil, which experiences downward percolation during the spring snow melt and summer rains, and upward advection due to transpiration and evaporation during the summer growing season. However, it is assumed that the shale, with a low hydraulic conductivity and at a depth of 1 m below the ground surface, would not experience significant upward water flux during the summer growing season. This assumption is supported by previous studies that have shown that the D3 cover soil provides much more available water than is required by the vegetation over the growing season (Shurniak 2003). As a consequence, the use of a net percolation variable would seem appropriate. This net percolation was assumed to be downward for the model (positive net percolation), but could easily be reversed (negative net percolation) to simulate groundwater discharge and evapotranspirative losses.

One-dimensional advective transport in the model was simulated by the following equation:

$$J_q = qC \qquad [3.1]$$

Where: J_q = mass flux due to advective contaminant transport ($g/m^2/s$)

q = specific discharge (m/s)

C = concentration of contaminant in pore water (g/m^3)

Upward or downward diffusive and dispersive transport of contaminants can also occur in the model depending on concentration gradients. The combination of diffusion and mechanical dispersion is referred to as hydrodynamic dispersion. This process is defined by Fick's First Law as follows (Shackelford 1991):

$$J_d = -\theta_e D_h \frac{\partial C}{\partial z} \qquad [3.2]$$

Where: J_d = mass flux transport by hydrodynamic dispersion ($g/m^2/s$)

θ_e = effective volumetric water content

$\frac{\partial C}{\partial z}$ = concentration gradient ($g/m^3/m$)

D_h = coefficient of hydrodynamic dispersion (m^2/s); comprising a molecular diffusion component and a mechanical dispersion component as follows:

$$D_h = D_o\tau + \alpha v \qquad [3.3]$$

Where: D_o = free solution molecular diffusion coefficient for a particular solute at a particular temperature (m^2/s)

τ = tortuosity factor (unitless)

α = dispersivity (m)

v = advective velocity (m/s) = $\frac{q}{\theta}$

The product of D_o and τ is referred to as the effective diffusion coefficient for the porous media, D_e.

The process of mechanical dispersion is considered by some to be inseparable from molecular diffusion and the two are collectively referred to as hydrodynamic dispersion (Fetter 1993). Molecular diffusion as a process is responsible for driving mass in the direction of a negative concentration gradient regardless of advective direction. Mechanical dispersion, on the other hand, is conceptualized as an 'apparent' mixing that occurs as a result of sampling across a range of different fluid pathways which are advecting the contaminant at different rates. The apparent mixing is described with a similar form of equation as that of molecular diffusion; however, it is not understood to be fundamentally a diffusion type process.

In this conceptual model, where molecular diffusion is responsible for transporting contaminants upward and net percolation is downward, it is not clear how mechanical dispersion could be responsible for transporting salt mass up into the cover. Consequently, in this conceptual model the transport of salts into the cover in response to concentration gradients was attributed solely to molecular diffusion. However, where the numerical model is simulating diffusion and advection in the same direction, mechanical dispersion could not be overlooked. This was the case for transport of stable isotopes where the pore water in the cover was enriched in ^{2}H and ^{18}O, and therefore both diffusion and advection would cause downward transport of the "contaminant". While this scenario is not shown in Figure 3.9, it is described in Sections 3.3.2 and 5.1

In addition to the transport processes described above, the model also had to account for production of salts in the shale through the oxidation of pyrite, as described in Section 2.3. Finally, depending on the solute assessed in the model, ion exchange between the pore water and clay minerals was considered as a potentially important factor in attenuating salt transport.

3.3.2 Stable Isotope Model

There were a number of unknown variables in the conceptual model of salt and water migration in the SBH cover system. Some of these unknowns were estimated based on previous research while other unknowns had to be varied in the model. The use of stable

isotopes as the tracer in the soil profile allows some simplifications to the model. The primary advantage to using stable isotopes of water is that they are conservative tracers. There is no production of ^{2}H and ^{18}O in the model domain and there is no exchange between the water and minerals in the soil profile. After some initial trial runs, it was determined that ^{2}H would be the tracer used in the model. Although water and soil samples were tested for both ^{2}H and ^{18}O, and thus either of these could have been used, the ^{2}H soil profiles showed less scatter.

The use of a net percolation variable (described in Section 3.2.1) and constant volumetric water content for the soils (described below) meant that the hydraulic conductivity and pressure gradients had no bearing on the model results. This simplification allowed the hydraulic conductivity to be nominally set at a very high value (e.g. 1 m/s).

A second simplifying assumption used in the model was to set the upper boundary condition for the model at the cover-shale interface. This simplification would be unacceptable if one was trying to accurately model all of the processes occurring in the cover soil, including any potential seasonal cycles of salt and water movement. However, as discussed above, the use of a net percolation variable eliminates the need to characterize cyclical water movement. The net percolation was assigned as a source of enriched ^{2}H applied directly to the surface of the underlying shale and, therefore, the transport of ^{2}H would be downward by both diffusion and advection, assuming net percolation is downward as described above.

The volumetric water content of the shale in the model was assumed to be constant year-round. A value of 0.4 was chosen which corresponds with the value used in previous 1D transport modelling performed by Kelln (2008). This value may be slightly higher than the average annual volumetric content for the shale, but is representative of conditions in the shale when the majority of transport occurs. Recent volumetric water content readings from the SBH site confirm that 0.4 is a reasonable value for the model. Diviner 2000 sensors were measured each year from approximately May to September across the

SBH site at various locations. Between 2008 and 2009, these Diviner 2000 readings provided average volumetric water contents of 0.37 for the shale from the plateau locations and 0.36 for the shale from the D3 test plot locations. Converted gravimetric water contents from the soil salinity samples collected in August 2008 and May 2009 indicated average volumetric water contents of 0.38 for the shale for both the plateau and D3 slope locations. The total porosity of the shale was estimated to be between 0.44 (Chapman 2008) and 0.46 (Boese 2003) based on in-situ density measurements and specific gravity testing.

The coefficient of molecular diffusion, D_e, was varied, along with the net percolation, to fit the field measured profiles. An initial estimate of D_e was selected based on the values from published studies where the soil type was similar to the overburden shale. Kessler (2007) conducted diffusion experiments pairing half-cells of shale with half-cells of till, using material from the site at field condition volumetric water contents (approximately 0.3). This work yielded a mean D_e for total salinity of $6x10^{-11}$ m²/s.

Hendry et al. (2009) used double reservoir diffusion tests in the laboratory to calculate D_e for δ^2H diffusing in clayey till. They also showed that D_e varies with porosity of the soil. For a saturated porosity of 0.4, which is approximately the porosity of the till and shale of the SBH site (Kelln 2008), Hendry et al. calculated a D_e value of $4x10^{-10}$ m²/s. This value was adopted as an upper limit for the current study at saturated conditions. Extrapolating from the porosity vs D_e relationship developed by Hendry et al. yields a D_e value of approximately $1.5x10^{-10}$ m²/s for a saturated porosity of 0.2. This value of 0.2 has been suggested as an approximate residual water content for the shale and cover soil based on water content sensor readings and measured water contents in soil samples (Kelln et al. 2008, Shurniak 2003, Boese 2003). It is not strictly accurate to assume that D_e for a soil with n=0.4, θ=0.2 is the same as D_e for a saturated soil with n=0.2; however, the D_e value from Hendry et al. (2009) is only used for comparison purposes.

Other measured diffusion coefficients from the literature include $1.7x10^{-10}$ m^2/s for δ^2H in shale with n=0.4 (Hendry and Wassenaar 1999) and $2.2x10^{-10}$ m^2/s for δ^2H in shale

with n=0.37 (Hendry et al. 2010). A diffusion coefficient of $1.7x10^{-10}$ m^2/s was also measured for δ^2H in clay till samples with an effective porosity of approximately 0.3 by Hendry and Wassenaar (1999) and van der Kamp et al. (1996). Shurbaji and Phillips (1995) suggested a higher diffusion coefficient of $7x10^{-10}$ m^2/s in a saturated soil with n=0.35. The diffusion coefficients in the model were generally kept within the range of diffusion coefficient values established by these previous studies. However, the coefficient values were modified slightly between model runs to improve the fit to field data.

As mentioned in Section 3.3.1, the stable isotope transport model required consideration of mechanical dispersion due to the fact that molecular diffusion and advection are acting in the same direction (downward). There has been no work to date for the SBH study site to quantify α in the cover soil or the shale. This variable is notoriously difficult to quantify as it is typically divided into longitudinal and transverse dispersivity components (Fetter 1993, van der Kamp et al. 1994) and has been shown to vary with the scale of measurement (Pickens and Grisak 1981, Gelhar et al. 1992). For the purposes of this modelling, dispersivity was assumed to be 0.01 m. This is roughly 1/100 of the scale of the model, which is reasonable based on the work of other researchers (Pickens and Grisak 1981, Gelhar et al. 1992).

The final important parameters in the δ^2H transport model were the background and source δ^2H values. The current study was the first time that a set of soil samples was collected and tested for stable isotopes of water at the SBH site. Therefore, there were no previous isotopic profiles, pre-construction or otherwise, to use in establishing baseline values. However, this fact was considered during the 2008 drilling program and it was decided that a single hole drilled deep into the shale might provide a reasonable estimate of baseline conditions. Based on the isotopic profile of the deep hole a baseline value was established for the shale.

Determining a source δ^2H value for the net percolation water that flows from the cover soil into the shale was not as simple. Stable isotope analysis of snow and rain samples

from the SBH site verified that the δ^2H values of waters contributing to net percolation vary over the year. This variation is especially evident in the isotopic profiles within the cover soil (upper 1 m). Similar variations in isotopic profiles have been observed in natural soil profiles across the oxidized zone of glacial till near ground surface (Hendry et al. 2010). Some effort was spent on numerical modelling to understand how isotopic content fluctuations in the percolating water might affect the isotopic profiles in the shale. However, in the end, the source value for net percolation was largely based on the δ^2H values measured in samples taken from the interface at specific sites.

It is important to note that the interflow process was not incorporated into the stable isotope model. This does not suggest that interflow is unimportant in defining the stable isotope profiles. On the contrary, the interflow water flowing down slope along the till-shale interface likely has the greatest impact on the source value of net percolation. However, by assigning the upper boundary at the interface, the stable isotope content of the interflow water is accounted for in the source value boundary condition in the model. The flow volume of interflow is not important in the stable isotope model because the model is quasi-one dimensional as described in Section 3.3.1 and, therefore, there is no net change between interflow in and interflow out. Any flow contribution or removal by interflow would be accounted for in the net percolation variable.

3.3.3 Geochemical Modelling to Determine Major Ion Field Concentrations

Saturated paste extract testing is a relatively fast and efficient way of assessing the concentrations of major ions in soil samples. For monitoring temporal changes in soil salinity, results from successive years can be compared directly. However, the saturated paste extracts do not provide the true insitu concentration of major ions in the soil pore water. Therefore, saturated paste concentrations cannot be used directly to determine the input concentrations for the numerical contaminant transport model, nor can the saturated paste concentration profiles be directly compared to simulated profiles from the contaminant transport model. Instead, it was necessary to convert the saturated paste concentrations to insitu pore water concentrations as was done by Nichol et al. (2006). The concentration conversion was accomplished using the geochemical modelling

software, PHREEQCI version 2.15 (Parkhurst and Appelo 1999), available from the USGS. This software allows the user to simulate various geochemical processes including dissolution and precipitation of minerals, equilibrium gas dissolution, and cation exchange on a soil or mineral surface.

In converting the saturated paste concentrations to field concentrations, the primary change was to reduce the water content of the samples in PHREEQCI. However, prior to doing this, the properties of the cation exchange surface were defined in the PHREEQCI model. The proportions of the cations, Ca^{2+}, Mg^{2+}, Na^{+}, and K^{+}, were established based on the proportions in solution of the saturated paste. The number of potential exchange sites on the soil surface was set at 0.15 equivalents per kg of soil. This was an average value from cation exchange capacity tests on shale and till samples performed by Kessler (2007) and used for previous geochemical modelling (Craig Nichol personal communication on June 10, 2010). The modelled solution was also forced to equilibrate with CO_2 gas at concentrations typical of the lower cover and upper shale based on measurements by Wall (2005). At the same time as the water content was reduced in the geochemical model, the temperature of the solution was reduced from 22°C (assumed temperature of the saturated paste in the lab) to 5°C (approximate groundwater temperature near the interface).

As the water content in the geochemical model was decreased from saturated paste levels to field water content, the concentrations of the dissolved constituents increased. The minerals calcite, dolomite and gypsum were allowed to precipitate as required to reach a saturation index of zero. The removal of certain cations, particularly Ca^{2+}, for mineral precipitation changed the proportion of the cations in solution, which thus changed the proportion of cations on the exchange surface. The resulting concentrations in the PHREEQCI model were exported to develop new field concentration profiles that could then be used for comparison to simulated profiles from the contaminant transport model.

3.3.4 Salt Transport Model

The second phase of transport modelling was to use the net percolation rates determined from the stable isotope model and apply them to a salt transport model. As described in Section 2.6.1, chloride is the most conservative of the salt ions and would therefore be the best option for a salt tracer. However, after reviewing the laboratory test results and looking at the salt profiles for the cover, it was decided that the concentrations of chloride were too low relative to the accuracy of testing, resulting in scatter and a general lack of confidence in the trends.

Sulphate was considered to be the next most conservative salt ion and is also the salt ion present in the highest concentrations in the shale and cover soil. The salt transport model was built from the stable isotope model with a few important variations.

One of the most important changes from the isotope model was the incorporation of the till cover in the model. Initial model runs showed that the upward transport of SO_4^{2-} would change the concentration at the interface and to accurately simulate this as a variable boundary condition would prove difficult. The 1 m thick till cover was therefore included to provide a buffer for upward salt diffusion. The net percolation was still applied to the till-shale interface, implying that all net percolation occurred as the result of 'ponded' water at the shale interface. It is assumed that most of the net percolation water that ponds at the base of the cover, arrives in the spring during frozen ground infiltration, as described by Kelln et al. (2009).

While the volumetric water content of the shale was left unchanged from the ^2H transport model at 0.4, the till was assigned a constant average volumetric water content of 0.30. This was again based on water content sensor readings from the site as well as converted gravimetric water contents from the collected soil samples. A constant volumetric water content in the cover is unrepresentative of field conditions, particularly in the summer when wetting and drying cycles can have a major impact on the upper 0.5 m of cover (Shurniak 2003). However, the water content of the lower till in the 1 m thick cover is more consistent and this is the portion of the cover that is of primary concern for

salt transport mechanisms (Kessler 2007). In addition, the use of an average volumetric water content is consistent with the rationale used to defend the use of a net percolation variable in the transport model.

Another important difference in the salt transport model is the inclusion of a pyrite oxidation zone in the upper shale. This oxidation zone adds additional sulphate to the model. The production rate and the depth of the oxidation zone were varied in the model to obtain a reasonable fit to the data. The production rate and oxidation zone depth were then compared to values obtained by other researchers (Wall 2005, Nichol et al. 2006) to ensure that the calculated values were reasonable.

The interflow process was neglected in the stable isotope model because of simplifications to the model and the higher values of δ^2H in the percolating water relative to the shale. However, these conditions do not apply to the salt transport model where interflow is a factor in salt transport (i.e., at slope locations) and must be incorporated into the model. The addition or removal of water in the model by interflow was deemed insignificant because of the quasi-one dimensional nature of the model and because of the use of a net percolation variable. On the other hand, the potential removal of salt by interflow had to be considered. This flushing of salts by interflow was accounted for through the use of contaminant mass removal nodes placed at the cover/shale interface. The rate of mass removal was calculated from salt concentrations measured in the interflow system from 2001 to 2009.

Baseline salt concentrations for the shale and cover soil pore water were obtained from previous research from the SBH site. The baseline salinity concentrations for shale were obtained from the work of Nichol et al. (2006) and to a lesser extent from Kessler (2007). The data from these reports came from samples collected from deep profiles drilled into the shale from the SBH plateau in 2001 (Wall 2005) and from samples collected in 1999 during an investigation at the SBH site six months after cover placement (Macyk 1999). The baseline concentrations of soil salinity for the secondary

cover soil were taken from samples collected in 2003 from a salvaged till stockpile (Kessler 2007).

Another difference between the stable isotope and salt transport models is the potential need to adjust the molecular diffusion coefficient. Using the Nernst equation, Li and Gregory (1974) calculated the free water molecular diffusion coefficient for a wide range of dissolved ions at infinite dilution and showed that the values can vary by up to an order of magnitude. While the work of Li and Gregory is qualitatively valuable to this study, the magnitude of diffusion in porous media is complicated by factors such as ion exclusion (Shackelford and Daniel 1991, Barone et al. 1989). In addition, infinitely dilute solutions do not apply to real world conditions because electrical neutrality must be maintained. Consequently, the measured diffusion coefficient for an individual ion will vary when in solution with multiple dissolved species at various concentrations (Barone et al. 1989).

Deuterium is considered to be part of the water molecule and is not a dissolved ion like sulphate. The ion exclusion effects and electrical neutrality effects that can reduce the diffusion coefficient of SO_4^{2-} in a porous media would not likely do so for ^2H. Therefore, it was expected that the diffusion coefficient for SO_4^{2-} in the cover soil and shale would be lower than that of ^2H but it was not known by how much. The calculated diffusion coefficient or range of coefficients from the stable isotope modelling were considered to be a starting estimate of the diffusion coefficient for sulphate in the salt transport model, with the knowledge that the diffusion coefficients would likely have to be decreased to accurately model transport of SO_4^{2-}. The coefficient of diffusion for total salinity between the till and shale measured by Kessler (2007) in the laboratory was also considered to be a guideline for selection of SO_4^{2-} diffusion coefficients. This value measured by Kessler was $6x10^{-11}$ m/s.

As described in Section 3.1.1, the process of mechanical dispersion was believed to be incapable of transporting salt into the cover, in opposition to the advective flow. Therefore mechanical dispersivity for the model was set to a negligible value.

4. PRESENTATION OF DATA

This chapter presents the results of the field program and laboratory analysis. The first part of the chapter includes an interpretation of the results of laboratory testing for stable isotope content of the water and soil samples. The focus of the second part of the chapter is on major ion chemistry of water and soil samples.

4.1 Interpretation of Stable Isotope Testing

4.1.1 Water Samples and Local Meteoric Water Line

Despite a decade of water sample collection and chemical analysis from the SBH site, very few of these samples have been analyzed for stable isotopes of water. A review of the literature and consultation with experts turned up only a few studies from the Athabasca oil sands region of Alberta where water samples had been analyzed for δ^2H and $\delta^{18}O$. Kelln et al. (2007) used stable isotopes to perform an isotope hydrograph separation to attempt to quantify the amount of recent precipitation in interflow at the SBH study site. Kelln et al. made no attempt to develop a local meteoric water line (LMWL) for the SBH study site. Researchers from the University of Alberta have collected and analyzed precipitation and surface water samples for δ^2H and $\delta^{18}O$ between 2005 and 2009 from two study sites near Utikuma Lake and Lac la Biche, Alberta. These sites are both approximately 250 km from the SBH study site to the southwest and south, respectively. It is expected that this research, led by Kevin Devito, will result in published LMWLs for these sites; however, this information was not available at the time of publishing. It appears that no local meteoric water line (LMWL) exists for any other site in the Athabasca oil sands mining area. Therefore, an objective was established for this study to develop a LMWL for the SBH site using the stable isotope data from water samples collected in 2009.

The water samples collected from the SBH site were analyzed for ^2H and ^{18}O. As mentioned in Section 3.2.1, the reported accuracy of the OA-ICOS laser for stable isotope testing is 0.8‰ for δ^2H and 0.1‰ for $\delta^{18}O$ (Lis et al. 2007). Duplicate testing of

samples revealed mean absolute duplicate-to-original discrepancies of 0.7‰ for δ^2H and 0.3‰ for $\delta^{18}O$, with standard deviations of 0.6‰ and 0.2‰, respectively.

The results of these analyses are plotted as δ^2H versus $\delta^{18}O$ as shown in Figure 4.1. The plot distinguishes the various types of water samples including rain, snow, interflow, shallow groundwater samples from standpipes and local surface water samples. Also included in Figure 4.1 is a linear best-fit interpolation for the 2009 snow and rain samples. This line is an estimate of the LMWL for the SBH site. Ideally, the LMWL should be based on data over a much longer period, for example, at least a decade. However, to the author's knowledge, such a database does not yet exist for any site in the Athabasca oil sands region.

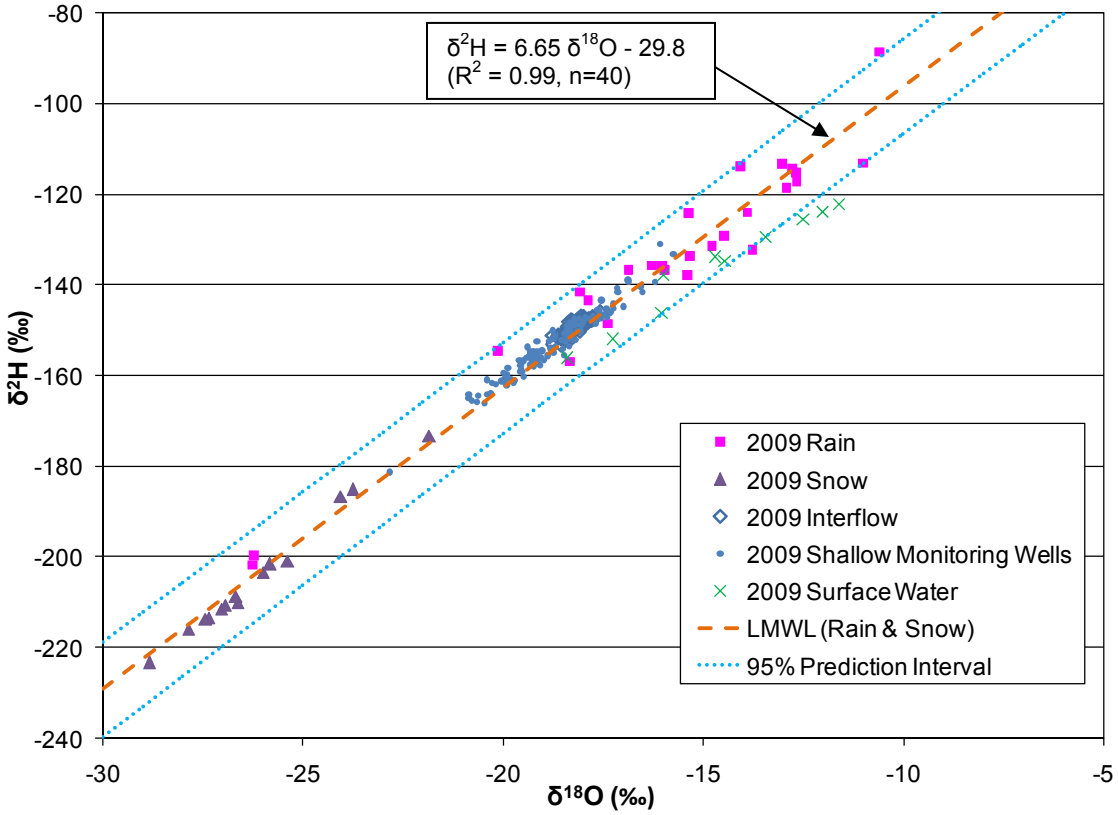

Figure 4.1: Stable isotope contents of 2009 water samples.

The equation of the LMWL based on the 2009 rain (n=26) and snow (n=14) samples is as follows:

$$\delta^2H = 6.65\ \delta^{18}O - 29.8 \quad (R^2 = 0.99, n=40) \qquad [4.1]$$

Figure 4.1 shows that the surface water samples (indicated by X symbols) show a clear divergence from the LMWL. These surface water samples are from multiple different sources including various ponds and streams, as described in Section 3.1.5. Therefore, the surface water samples will have different divergence points (i.e., the δ^2H vs $\delta^{18}O$ point along the LMWL prior to evaporation effects) and different evaporative lines.

Conversely, a remarkably tight relationship exists between the precipitation results and the results from interflow and shallow monitoring wells. This suggests that these samples have not been perceptibly altered by evaporation and plot on the LMWL. If the interflow and shallow monitoring well samples are considered to be unaffected by evaporation, then these samples could be included with the precipitation samples to increase the size of the dataset. The LMWL based on this new dataset is as follows:

$$\delta^2H = 6.63\ \delta^{18}O - 28.9 \quad (R^2 = 0.98, n=216) \qquad [4.2]$$

Equations 4.1 and 4.2 are very similar which is to be expected from the relationship illustrated in Figure 4.1.

The 2009 precipitation samples could also be bolstered using precipitation samples collected in 2005 (data not included). However, the inclusion of these data is done with caution as it is not known whether the sampling methodology varied from that followed in 2009. The equation of the LMWL generated from the 2005 and 2009 precipitation results, including snowpack samples, is as follows:

$$\delta^2H = 6.68\ \delta^{18}O - 26.5 \quad (R^2 = 0.97, n=54) \qquad [4.3]$$

If the 2003 to 2007 interflow and shallow monitoring well samples are included in the LMWL calculation, the following equation is developed:

$$\delta^2H = 6.25\ \delta^{18}O - 36.5 \quad (R^2 = 0.84, n=341) \qquad [4.4]$$

This equation shows some variation from the LMWL calculated using only the 2009 precipitation samples (Eq. 4.1), especially the value of the y-intercept. However, the larger dataset also shows considerably more scatter as evidenced by the lower R^2 value. Again, all data prior to 2009 must be considered with caution as the sampling procedures for these years are unknown.

The equation of the GMWL defined by Gat (1980) as presented in Chapter 2 is:

$$\delta^2H = 8.17\ \delta^{18}O + 10.56‰ \qquad [4.5]$$

The y-intercept of the GMWL is 36 to 46‰ higher than any of the y-intercepts developed in Equations 4.1 to 4.4. LMWLs with y-intercept values lower than that of the GMWL are common in North America (Kendall and Coplen 2001) and are caused by climatic variations including atmospheric temperature, weighted seasonality of precipitation and the source of water vapour (Clark and Fritz 1997). In addition, the GMWL has a considerably greater slope, indicating that the precipitation falling on the SBH site has likely experienced multiple evaporation-condensation cycles. This might suggest that much of the precipitation that falls on the SBH site was evaporated from inland water bodies or evapotranspirated from the surrounding boreal forest, or it might suggest that the rain that eventually falls on the SBH site has a marine origin but was cycled within the weather system prior to falling to the ground (i.e. the precipitation cycled from vapour to liquid and back to vapour within the cloud, possibly numerous times) (Gat et al. 2001).

A comparison with LMWLs developed for other nearby locations (within 700 km) shows that the divergence from the GMWL is mirrored in the LMWL for Fort Smith, Northwest Territories (Hage et al. 1975). This divergence is not, however, observed in

the LMWLs developed for Calgary (Peng et al. 2004), Edmonton (Hage et al. 1975) or Saskatoon (unpublished data from Len Wassenaar at NWRI). The LMWLs for these three locations are closer to the GMWL. The LMWLs are summarized in Table 4.1.

Table 4.1: Summary of LMWLs for locations in close proximity to SBH site.

Location	Distance from SBH	LMWL Equation	Data Years
SBH site	n/a	$\delta^2H = 6.68\ \delta^{18}O - 26.5‰$	2005, 2009
Fort Smith, NT[1]	330 km N	$\delta^2H = 6.8\ \delta^{18}O - 20.9‰$	1961 - 1965
Edmonton, AB[1]	400 km SSW	$\delta^2H = 7.7\ \delta^{18}O + 0.4‰$	1961 - 1966
Calgary, AB[2]	680 km SSW	$\delta^2H = 7.67\ \delta^{18}O - 0.4‰$	1992 - 2001
Saskatoon, SK[3]	630 km SE	$\delta^2H = 7.73\ \delta^{18}O - 1.5‰$	1990 - 2007

Data sources:
1: Hage et al. 1975; 2: Peng et al. 2004; 3: Unpublished data from Len Wassenaaar, NWRI, Saskatoon

Hage et al. (1975) suggested an alternate method of presenting δ^2H versus $\delta^{18}O$ data that would separate winter and summer precipitation into two separate LMWLs, each having similar slopes to the GMWL but with significantly different y-intercepts. However, while their data showed a strong and consistent correlation for winter precipitation, summer precipitation was much more scattered. The authors suggested that this was indicative of winter precipitation originating directly from ocean vapour and summer precipitation originating from inland sources. This trend identified by Hage et al. was also observed in the SBH data. Figure 4.2 clearly shows that winter precipitation, i.e. snowpack samples, plot on a LMWL that very closely approximates the GMWL. However, the LMWL for summer precipitation has a lower slope and lower y-intercept.

4.1.2 Soil Samples

The isotopic results for soil samples collected at the SBH site in December 2008 are plotted as δ^2H versus $\delta^{18}O$ and compared to the SBH LMWL developed from 2005 and 2009 precipitation samples (Eq. 4.3) in Figures 4.3 and 4.4. This version of the LMWL is used as it represents the largest dataset of pure precipitation samples. Soil samples are grouped in terms of drillhole location, as shown in Figure 4.3 and in terms of the soil type, as shown in Figure 4.4.

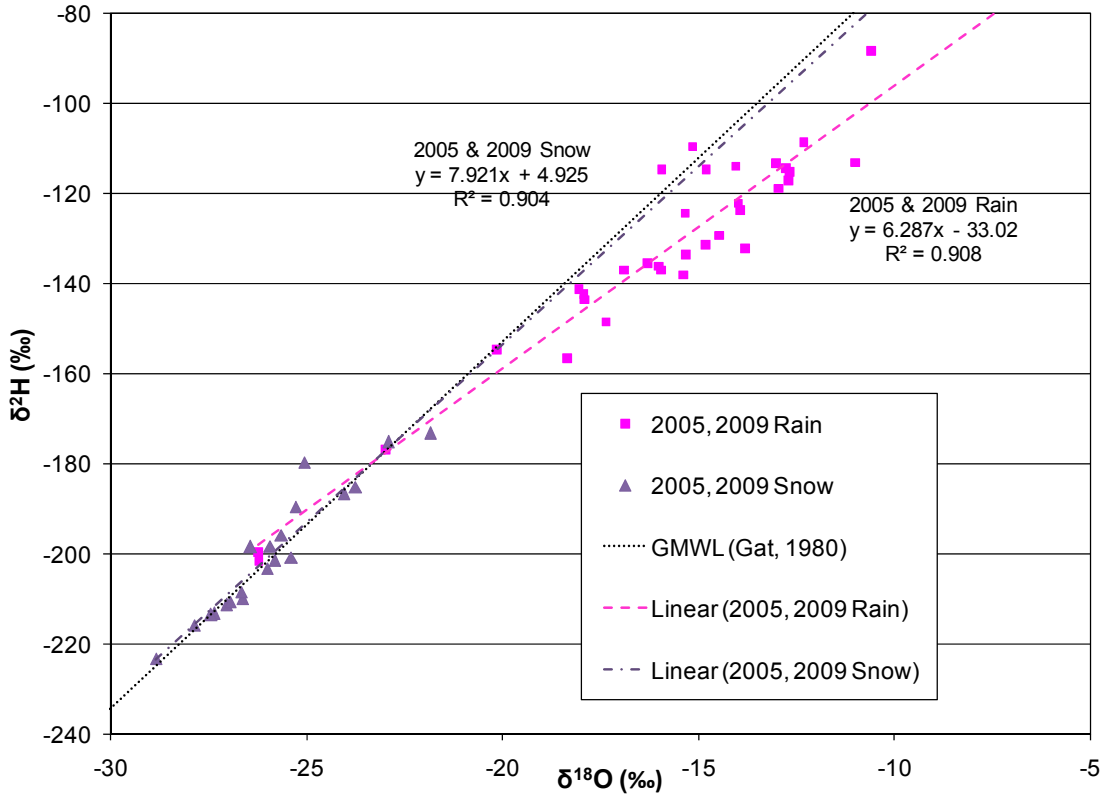

Figure 4.2: Separation of summer and winter precipitation LMWLs.

One interesting characteristic of Figures 4.3 and 4.4 is the location of nearly all of the soil samples just below the LMWL. This might suggest that evaporation has affected the isotopic content of the soil pore water. However, it might also suggest that the dataset used to construct the LMWL is too small. Figure 4.2 shows that summer precipitation at the SBH site plots over a wide range on the LMWL and presumably this variation also occurs from year to year. The LMWL in Figures 4.3 and 4.4 was developed using only two years of data, and the data from 2005 are incomplete. To demonstrate the significance of the separation between the soil samples and the LMWL, the 95% prediction intervals for the LMWL developed using only precipitation sample results (Eq. 4.3) are included in Figure 4.4. These prediction intervals envelop almost all of the soil samples, showing that the variation between the soil samples and the LMWL is not significant relative to the variation in the precipitation samples used to generate the LMWL.

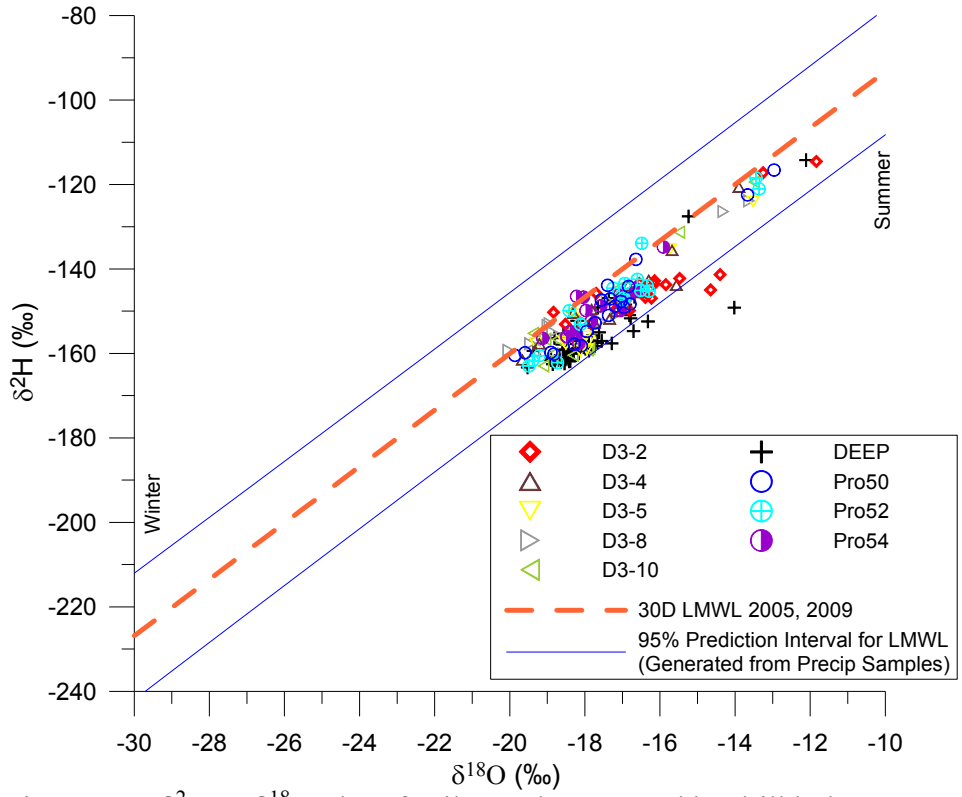

Figure 4.3: δ^2H vs $\delta^{18}O$ plot of soil samples grouped by drill hole.

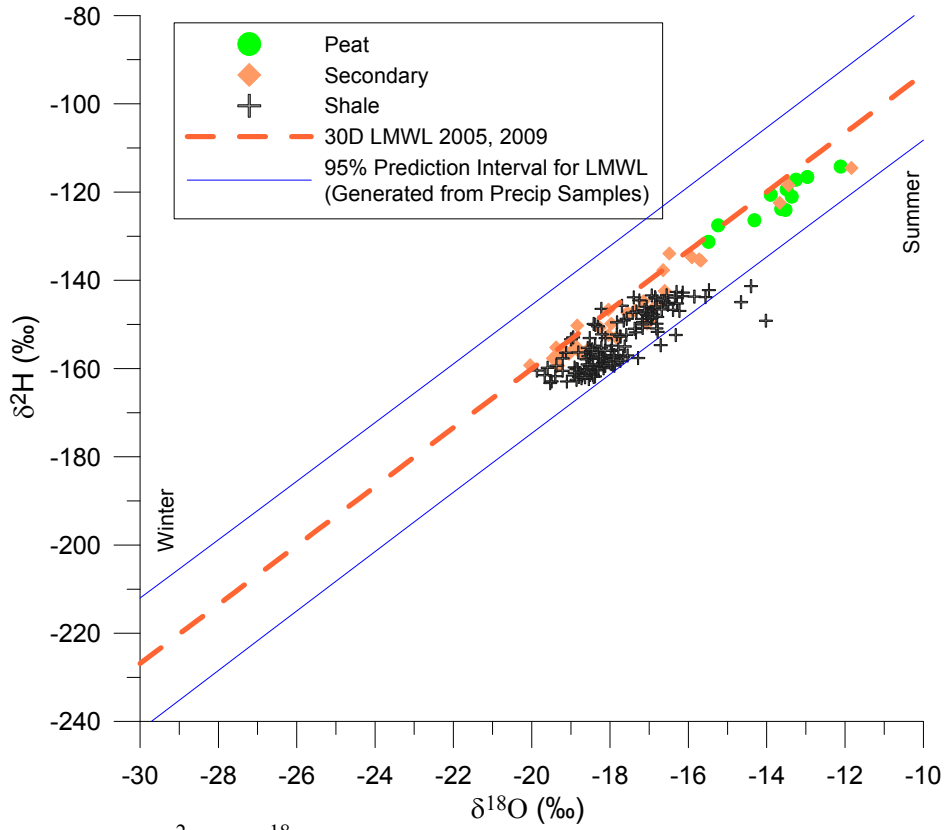

Figure 4.4: δ^2H vs $\delta^{18}O$ plot of soil samples grouped by soil type.

In addition, only a very slight change to the slope or y-intercept of the LMWL is necessary to fit the majority of the soil sample data. For example, if the slope of the LMWL was increased slightly from 6.68 to 7.00, or if the y-intercept was reduced from -26.5 to -32.0, then the revised LMWL would fit the soil data exceptionally well. The equation of the best-fit linear regression through the soil samples is:

$$\delta^2H = 6.27\ \delta^{18}O - 40.9 \quad (R^2 = 0.83,\ n=341) \qquad [4.6]$$

The similarity of this line to the LMWL developed from the complete dataset of precipitation, shallow groundwater and interflow samples from the SBH site (Eq. 4.4) is striking.

An observation of interest from Figure 4.3 is that the samples showing the greatest divergence from the LMWL are from D3-2 and the deep hole at the base of the slope. These two drill holes are only 55 m apart, but more importantly, they have nearly identical ground elevations. Because this portion of the SBH was constructed in 5 m horizontal lifts (Chapman 2008), it is quite likely that the uppermost shale overburden at these locations was placed at approximately the same time. Therefore the upper shale from these two drill holes may have experienced slightly more evaporation than shale from other sampling locations. Because the study site portion of the SBH was constructed upward in lifts over the course of two years (Chapman 2008), it is likely that the shale at the lower slope locations may have been exposed for two more years than shale in the upper slope locations, giving more opportunity for evaporation of original pore water to occur.

4.1.3 Fractionation Effects

Evaporation

The lack of divergence from the LMWL for the shallow groundwater and interflow water samples suggests that the water percolating through the cover were not subjected to much evaporation. In addition, the soil samples plot very close to the LMWL. This

suggests that even over a longer duration, the groundwater in upper few metres of the soil profile experiences little to no fractionation.

It is not unexpected that infiltrating rain water has experienced no evaporation. The porous, permeable peat layer at the surface of the cover is designed to allow rapid infiltration and storage of rain water (Qualizza et al. 2004). As the infiltrating water travels farther from the cover surface and the radiation of the sun, the evaporative potential decreases significantly. During the summer growing season, transpiration removes a large proportion of the pore water in the cover soil as roots draw moisture into the structure of the plant or tree. While transpiration is a fractionating process, the fractionation occurs in the plant leaves as liquid water evaporates, leaving the residual water enriched in heavier isotopes (Hillaire-Marcel 1980). However, the osmotic absorption of soil pore water by plant roots has not been shown to cause any fractionation (Gat 1996). Therefore, fractionation by transpiration is only important if one is studying the stable isotope composition of the plant water and not, as in this study, the soil pore water. There are, however, several other fractionation processes which could affect the soil water in the SBH cover but apparently do not.

Sublimation

The process of sublimation is a change of the physical state of water molecules from solid to vapour. Similar to the process of evaporation, this change of physical state removes isotopically lighter water molecules and leaves behind isotopically heavy molecules, specifically those water molecules containing either deuterium or oxygen-18 (Neumann et al. 2008, Taylor et al. 2002). In addition to enriching the heavy stable isotopes in the remaining snow, the sublimation process has the same effect as evaporation in that it causes a divergence from the meteoric water line (Sokratov and Golubev 2009). That is, water samples that have experienced sublimation or evaporation will plot along a shallower slope on a δ^2H vs $\delta^{18}O$ plot than precipitation samples unaffected by these processes.

Devito and Mendoza (2007) state that sublimation in the Boreal Plains region of Canada, the region in which the study site is located, can be 30 to 40 mm/yr or more of snow water equivalent. This would represent over 30% of the accumulated snow pack based on an average annual snow fall of approximately 90 mm/yr as reported by Kelln et al. (2008). These sublimation values reported by Devito and Mendoza are upper estimates for cold, dry winters and where snow has been intercepted by forest canopies. As the SBH study site has only immature trees and is situated on a north facing slope with less sun exposure it would have lower rates of sublimation. However, based on Devito and Mendoza's research it would appear that sublimation cannot be neglected.

Despite the likelihood that sublimation occurs at the 30D study site, the stable isotope results from snow pack samples and shallow groundwater samples suggest that no significant fractionation has occurred before or after the snow has melted and infiltrated the cover soil (see section 4.1.1). The expectation of sublimation paired with the lack of fractionation effects seems contradictory. However, the important difference between sublimation and other water fractionating processes is that the frozen water molecules in a snow pack are essentially locked in position and, therefore, the snow pack cannot easily equilibrate by self diffusion. This limitation of isotopic mixing between layers within a snowpack is the concept that allows paleoclimatic researchers to use glacier ice cores as an historical record of atmospheric changes over short time periods or hundreds of millennia (Gat 1996, Moser and Stichler 1980, Dansgaard et al. 1973).

To further clarify this concept, the following simplified model is used. Sublimation primarily removes snow mass from the upper few centimetres of the snow pack (Neumann et al. 2009, Sokratov and Golubev 2009). The sublimation process selectively removes the isotopically lighter water molecules first, leaving a higher concentration of isotopically heavier water molecules in the snow crust. The snow crust becomes enriched in these heavier isotopes but because the frozen conditions preclude diffusion, the snow pack cannot equilibrate. The "solid" physical structure of snow allows those frozen water molecules or ice grains that are not sublimated first, to stand out rather than settle back down to a smooth planar surface. The isotopically heavy molecules at the

outer edge of the snow pack are now more likely to be sublimated than lighter water molecules slightly deeper down, due to exposure to wind and solar energy. This "layer-by-layer" sublimation (Gat 1996) limits the transmission of the fractionation effect through the snow pack. This process is illustrated in Figure 4.5.

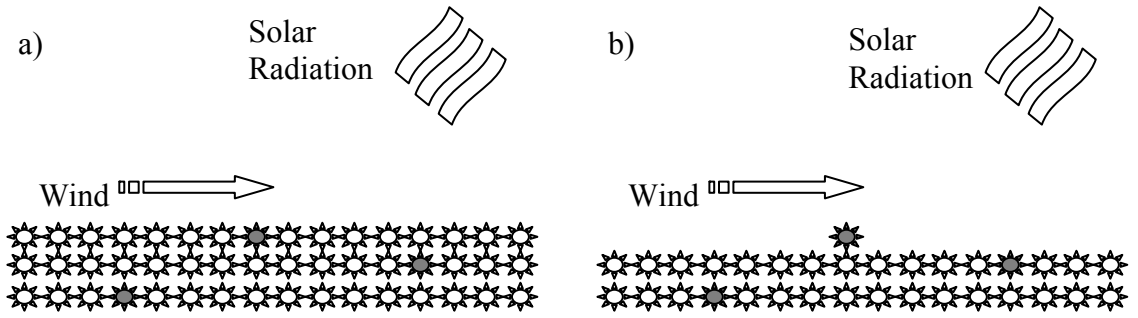

Figure 4.5: Fractionation in a snowpack.
Grey snowflakes indicate isotopically heavy molecules. White snowflakes indicate isotopically light molecules
a) Conditions at start of sublimation process.
b) Conditions after first stage of sublimation.

This model is, admittedly, overly simplistic. One complication is that the water molecules that are sublimated are part of mulitmolecular ice grains rather than individual molecules as shown. In addition, snow packs are constantly evolving as new snow falls covering previous snow pack crusts, warm spells cause melting, and the overall snow pack compresses under its own weight. Various processes can allow isotopic changes to penetrate the snow pack including diffusion of water vapour through voids in the snow, melting of surface snow followed by percolation and recrystallization, and disturbance of the bulk snow pack by drifting (Gat 1996, Moses and Stichler 1980, Dansgaard et al. 1973). However, the data available for the 30D site and results from other studies (Moser and Stichler 1974) suggest that fractionation effects by sublimation are only significant at the outer surface of the snow pack and, depending on the overall snow pack thickness and porosity, may be negligible when averaged over the entire mass of the snow pack.

Snowmelt

Taylor et al. (2002) have shown that the process of snow melt causes isotopic fractionation. However, due to the finite supply of snow in an annual snow pack, the fractionation is transient and the melt water isotopic signature transitions from depleted to enriched relative to the snow over the course of the melting process. In a closed system where sublimation and evaporation are negligible during the snowmelt process, the average δ^2H and $\delta^{18}O$ values of the melt water will be equal to the average δ^2H and $\delta^{18}O$ values of the snow pack. In other words, if the early snow melt and late snow melt reach the same destination and are remixed, there will be no perceptible difference between the meltwater isotopic signature and the snowpack isotopic signature. This concept might apply to the SBH site if equal proportions of early snowmelt and late snow end up infiltrating and mixing in the cover. However, the soil pore water will not have the same isotopic signature as the original snowpack because of the existing pore water in the soil prior to snowmelt infiltration.

As part of an isotope hydrograph separation exercise Kelln et al. (2007) made the assumption that melt water for the SBH site is isotopically enriched relative to snow. Sample measurements from 2009 also confirm that groundwater from the shallow monitoring wells in the cover and interflow water samples are isotopically enriched relative to snow from the site. However, comparison of these samples to the new LMWL gives evidence that the enrichment is most likely due to mixing with antecedent pore water in the soil cover, rather than fractionation caused by the snow melt.

Frost Front Advance

When water changes from a lower energy physical state to a higher energy physical state the molecules containing lighter isotopes have a greater tendency to make this transition. As discussed above, examples of this include evaporation, sublimation and melting. The opposite is true when water changes from a higher energy state to a lower energy state. A good example of this is water vapour condensing to form rain droplets in clouds. Another example is the freezing of liquid water. As discussed in Section 2.4, frost formation in the SBH cover system could be a factor in salt transport. However, it would

appear that frost formation in the cover could be creating or at least affecting existing isotopic gradients through the cover soil. To test this theory, a simple 1D contaminant transport model was created, similar to those discussed later in this chapter.

The numerical model simulated the formation of frost in shale. Frost advance was nominally simulated at 1 cm per day. This value was deemed reasonably for the shale based on daily readings of soil temperature data for the SBH site. As each progressive 1 cm element of the model was frozen it was made null in the model and a fractionation factor was used to calculate the δ^2H shift that must be applied to the next lower element. Numerous researchers have investigated fractionation of water by freezing and reported fractionation factors of 1.02 for δ^2H and between 1.002 and 1.003 for $\delta^{18}O$ (O'Neil 1968, Friedman et al. 1974). Applying this fractionation factor results in the newly formed pore ice being more enriched in ^2H than the original pore water, while the next lower element becomes more depleted in ^2H by an equal amount. For example, the pore water in the shale was assumed to have an original δ^2H value of -160‰. The first element of pore ice formed would have a δ^2H value of -143‰ while the pore water in the next lower element would have a δ^2H value of -177‰. This depleted element was then allowed to equilibrate by diffusion for 1 day until it too was frozen, continuing the advance of the frost. The model used a diffusion coefficient of $4x10^{-10}$ m^2/s, which is likely an upper limit for the diffusion coefficient in the cover.

The model results showed that even with this high diffusion coefficient and a reasonable frost advance rate the fractionation effects could not diffuse away from the frost front fast enough to be preserved. After only three days, the model predicted that the ice forming was more depleted than the original pore water. This indicates that the fractionated water is being frozen at a rate faster than equilibration by diffusion. Therefore, it is likely that fractionation by ice formation is very localized and does not affect the isotopic distribution for the entire cover profile.

4.1.4 δ^2H Soil Profiles

The measured δ^2H values for each soil sample were plotted against the sample depth to develop one-dimensional, vertical δ^2H profiles for each sampling location. These profiles are separated based on the region of the SBH overburden dump from where they were sampled. Figure 4.6 shows the δ^2H profiles for the three drill holes (Pro 50, Pro 52, and Pro 54) located on the plateau. Figure 4.7 shows the δ^2H profiles for the five drill holes (D3-2, D3-4, D3-5, D3-8, and D3-10) located along the north facing slope. Figure 4.8 presents the single deep profile drilled at the base of the SBH overburden dump. The solid grey lines in the plots were hand drawn to assist the reader in following the general trend of the data.

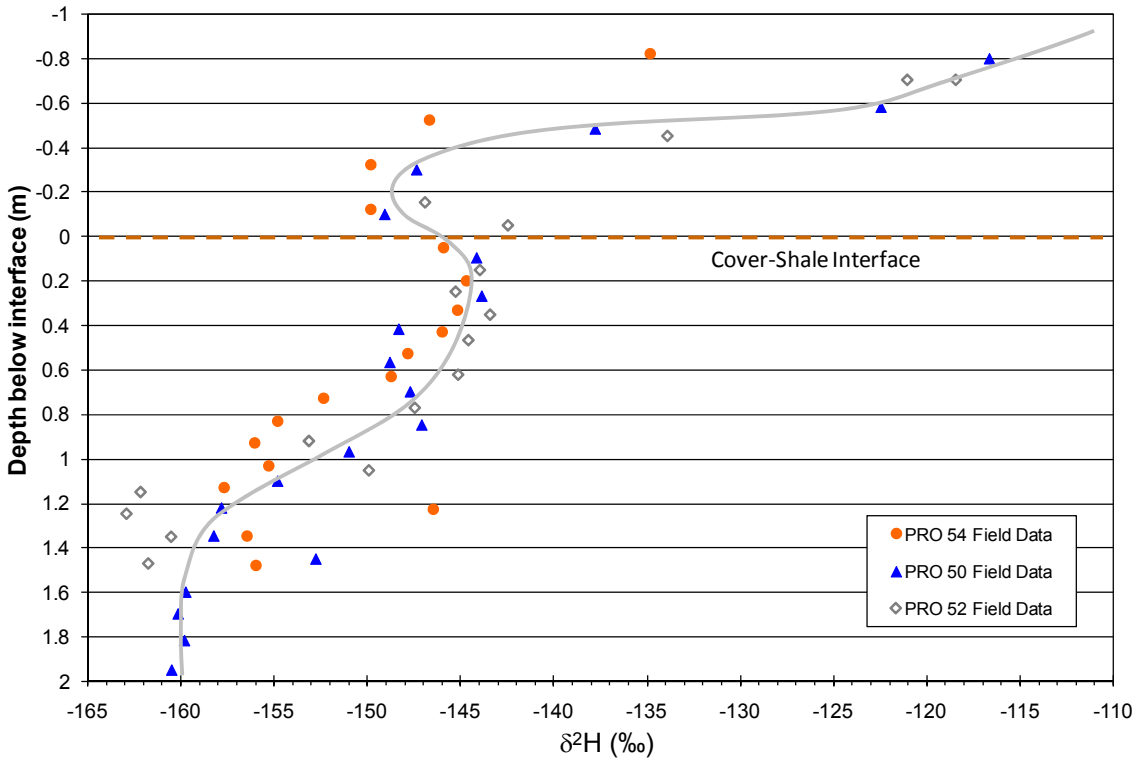

Figure 4.6: Field measured δ^2H vs depth profiles for the plateau sampling locations.

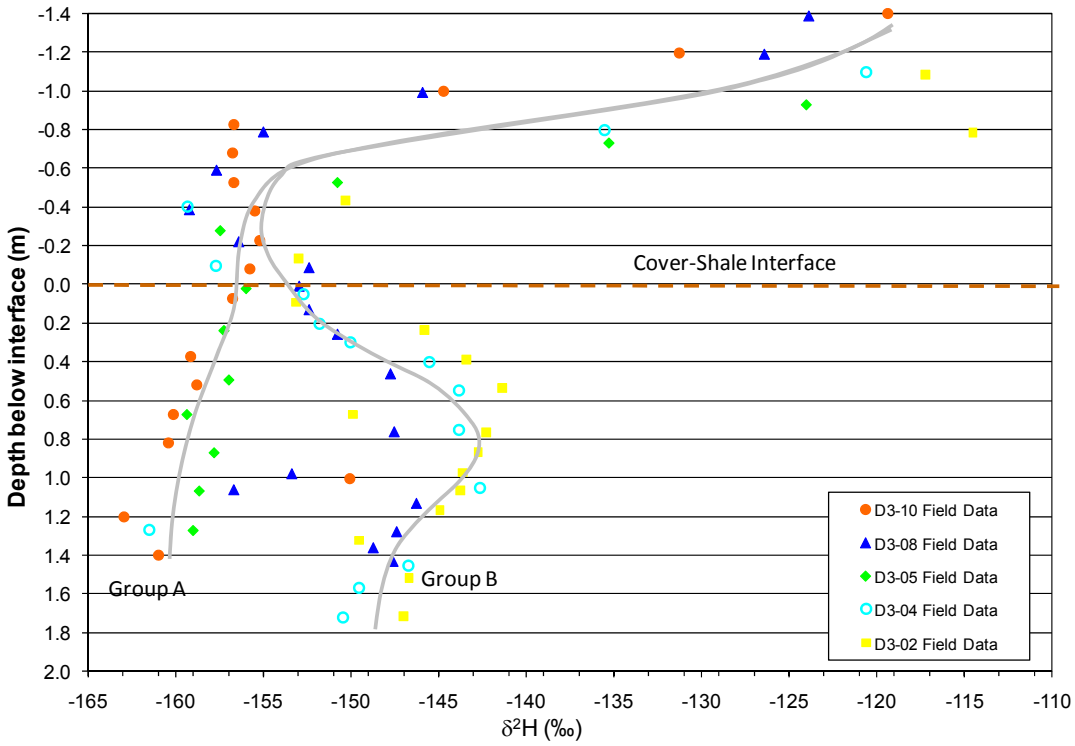

Figure 4.7: Field measured δ^2H vs depth profiles for the D3 sampling locations.

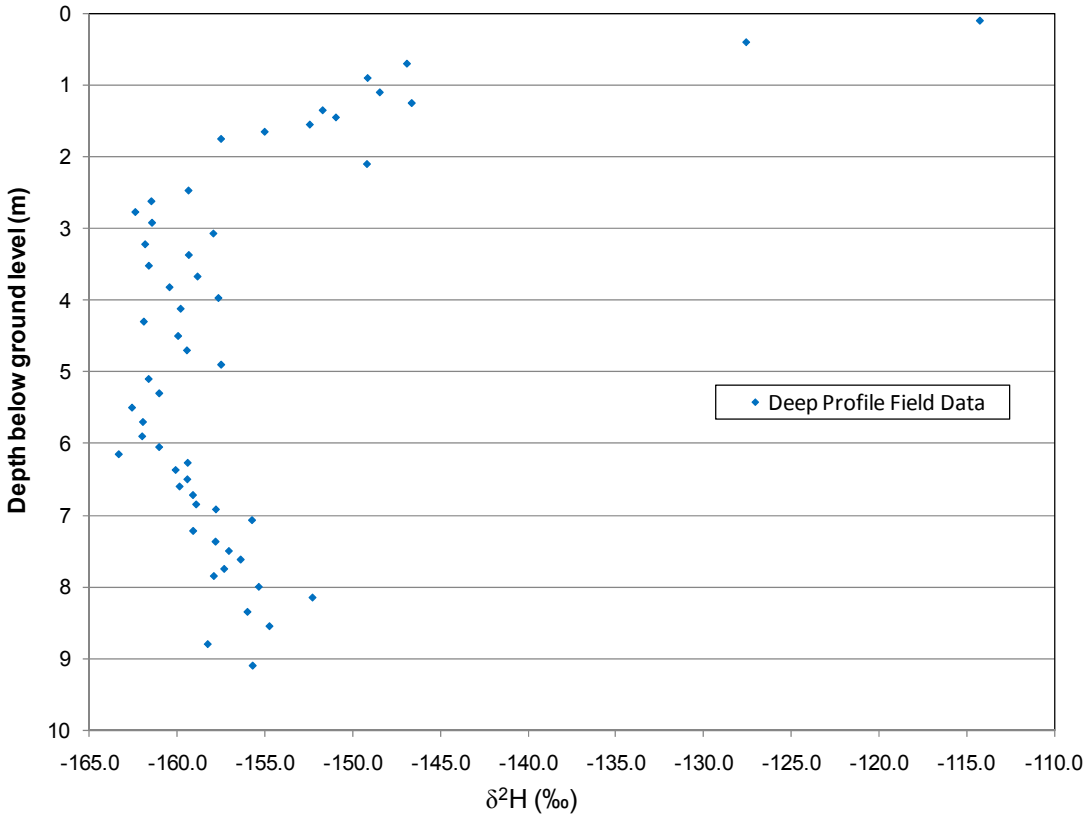

Figure 4.8: Field measured δ^2H vs depth profiles for the "deep" drill hole.

In general, the isotopic profiles for the majority of the drill holes can be described as being most depleted in the lower shale and most enriched in the peat and uppermost till material of the cover. Exceptions to this generalization exist, especially in the shale of the D3 profiles (Figure 4.7). The enrichment of heavy isotopes near ground surface might suggest that evaporation is occurring; however, based on the reasoning provided in Sections 4.1.3, this does not appear to be the case. Therefore, it is likely that the enrichment near ground surface is due to infiltration of summer rains. The till at the base of the cover, just above the interface, would receive less of this summer rain as a large proportion of it is stored within the cover and released by transpiration. Therefore, the lower cover soil tends to reflect the isotopic content of the infiltrating water that is able to penetrate the entire cover, this being the spring snow melt water. Maule et al. (1994) found similar results when studying infiltration at a prairie site in east-central Alberta. They showed that porewater collected from shallow soil samples (0-0.9 m below ground surface) had a lower composition of snowmelt than porewater from greater depths (3-4 m).

Upon plotting the isotopic profiles from the plateau sampling locations (Figure 4.6), it became apparent that the three profiles, from different sampling locations on the plateau, are quite similar in shape and in range of δ^2H values. The baseline values in the shale vary only slightly for the three profiles. Pro 50 has a baseline value of -160‰. The baseline value for Pro 52 is not well-established but appears to be between -160‰ and -162‰. Similarly, Pro 54 was not drilled deep enough to conclusively establish the baseline value for this location, but it appears to be between -156‰ and -157‰. For the purposes of numerical model input, it was assumed that the baseline shale value of -160‰ is the most representative value for the plateau.

The source values for the three plateau field profiles are very similar. The profiles from Pro 50 and Pro 52 suggest source values of -144‰ while the source value for Pro 54 is slightly lower at -145‰. A value of -144‰ was determined to be a representative average source value for the general plateau model.

An initial evaluation of the δ^2H profiles from the D3 test plot (Figure 4.7) revealed that the five profiles are dissimilar to the plateau profiles and dissimilar to each other. However, it did appear that the D3 profiles fell into two distinct groups: Group A, which comprises D3-05 and D3-10; and Group B, which comprises D3-02, D3-04, and D3-08.

The two soil profiles in Group A (D3-5 and D3-10) have baseline values of -159‰ and -161‰, respectively, which are very near the assumed shale baseline value of -161‰ for the plateau. The source value at the interface for these two profiles is between -156‰ and -157‰. This source value is less than the source values from the plateau profiles (-144‰). The exact reason for this is not known but most likely lies in the seasonal proportions of percolation water. On the plateau, it is believed that the till cover soil stays saturated for much of the year and acts like a mixing reservoir for snow melt and summer rain water that has infiltrated the cover before this water percolates into the shale. Therefore the source value at the interface likely represents a more evenly distributed mix of summer and winter precipitation than the profiles from the slope. The slope of the D3 cover tends to promote runoff and interflow. Therefore, waters from relatively brief precipitation events (i.e. summer rains) likely do not have the opportunity to percolate through the shale before the water flows down slope. During spring snow melt, however, the large amount of water present and the longer duration of this event relative to individual summer rains, give the snow melt water a greater opportunity to infiltrate the shale overburden. Therefore the mix of precipitation in the net percolation at the D3 slope locations is weighted more towards snow melt than summer rain. This would result in a more depleted source δ^2H value.

The δ^2H profiles from Group B of the D3 slope reflect an altogether different set of initial conditions or transport processes. One of the unexpected characteristics of these profiles is the large isotopic enrichment bulge over nearly the entire shale profile. Shurbaji and Phillips (1995) describe broad bulges in δ^2H profiles as being common in unsaturated soils and developed a numerical model that simulates these bulges. However, the bulges in that study were observed and simulated close to ground surface (maximum 40 cm depth) where extensive evaporation occurs. The bulges observed in

Group B of Figure 4.7 occur at least 1.2 m below ground surface in low permeability shale that is saturated or nearly saturated for most of the year. In addition, the plot of δ^2H versus $\delta^{18}O$ for these soil samples (Figure 4.4) suggested that any evaporation effects are negligible.

The other interesting characteristic of the Group B profiles is the fact that the profiles have more enriched δ^2H values in the shale at the bottom of the profile, compared to the Group A and plateau profiles. The δ^2H value at the bottom of these three profiles ranged from about -147‰ to -150‰. However it does appear that the Group B profiles are trending towards more depleted δ^2H values with depth. This suggests that the Group B drill holes did not penetrate deep enough to encounter baseline conditions.

The source values (at the interface) of the Group B profiles were quite consistent within the group at approximately -153‰, which was again more depleted than the source values for the plateau profiles. The explanation is believed to be the same as that described above for Group A. However, the source δ^2H values for Group B were slightly more enriched than for Group A. This is believed to be due to the enrichment bulges within the shale.

An explanation was required for both the enrichment bulges and potentially different baseline values in Group B. In examining the drilling logs from the isotopic soil sampling program it was discovered that the three Group B drill holes all contained considerable proportions of either glacial till or lean oil sand (LOS) mixed in with the shale overburden. Such mixtures are not completely unexpected as it has been noted that, while the SBH is primarily a shale overburden dump it can include glacial till and LOS (Chapman 2008). It is not known how the presence of other materials in the shale might have affected the initial isotopic content of the mixture primarily because the initial or baseline values of till and LOS are unknown. However, it is assumed that the presence of these materials is responsible for the unusual patterns in the Group B δ^2H profiles.

Because the "deep" drill hole from which samples were collected to develop the deep profile (Figure 4.8), was not located on the D3 cover plot, the source value is not comparable to the other profiles. In fact, the cover prescription at this location is not documented. However, the purpose of this drillhole was to obtain a baseline δ^2H value for the SBH shale. The profile in Figure 4.8 illustrates that there are some fluctuations in the δ^2H values in the deeper shale. However, most of the deeper shale sample results fall within a range of -156‰ to -162‰. The average δ^2H value for the deeper shale (>250 cm below ground surface) is -159‰.

It is also interesting to note that the deep isotopic profile seems to have a distinct shift at approximately 5 m below ground surface. As this portion of the SBH was built in 5 m lifts (Chapman 2008), it appears likely that this isotopic shift occurs at the interface of two consecutive lifts. The cause of the shift in isotopic profile may be due to equilibration with precipitation in the time interval between lift placements, or simply the placement of one material with a slightly different isotopic signature over top of another. Fortunately, these shifts in the isotopic signature within the shale between lift placements should be well below the shallow profiles measured on the plateau and D3 slope.

4.2 Interpretation of Major Ion Chemistry Testing

4.2.1 Water Samples

A moderate water sampling program for major ion analysis was first undertaken at the SBH site in the summer of 2000. In subsequent years the frequency of sampling was increased through the summer season with water samples being collected from shallow monitoring wells, the three interflow collection systems and the surface runoff collection system. In 2009, interflow water samples were collected regularly from each of the three interflow collection systems until interflow ceased completely on July 24. Four rounds of shallow groundwater sample collection were undertaken on May 1, 15, 29, and August 5. In addition, the EC of the groundwater in these shallow monitoring wells was measured frequently in the field concurrently with water level measurements.

The majority of monitoring wells demonstrated an increase in salinity from the start of the summer season (May 1) until the last sample was recovered or the last EC measurement was taken. This pattern corresponds with the conceptual model proposed by Kelln et al. (2009) that suggests subsurface flow is dominated by macropores in the cover. Kelln et al. suggested that snowmelt infiltrates the cover through macropores each spring and, as the ground begins to thaw, the water in the macropores equilibrates with matrix pore water. It is reasonable to assume that the more mobile water flowing through the monitoring well would be moving through these macropores and thus would demonstrate the same seasonal chemistry evolution. Therefore, the overall trend for salinity in monitoring wells at the SBH study site can be described as having highest salinity at the beginning of each year, followed by a reduction in salinity with the spring melt and finally, showing increasing salinity throughout the summer as water is lost to evapotranspiration.

It is to be expected that the interflow samples would reflect the same increasing salinity trend through the year as that displayed by the monitoring wells. This trend was observed in the D1 and D3 interflow collection systems, as displayed in Figure 4.9. This figure plots the EC of the interflow water samples as measured in the laboratory. The 2009 seasonal chemistry trend for the D2 interflow system was flatter with very little increase in salinity through the year. It is believed that this constancy is due to the fact that the D2 interflow system was not pumped out in 2007 or 2008. Therefore, the high salinity interflow water from late 2008 would still have been in the interflow barrel, collection pipe, trench and cover soil at the toe of the D2 slope, resulting in higher initial concentrations measured in the interflow at the start of 2009. However, by approximately May 27, the D2 and D1 interflow chemistry plots are nearly identical. This suggests that, after approximately one month of pumping from the D2 interflow system, all of the residual water from 2008 had been pumped out and the water passing through the interflow collection system was now 2009 water.

Figure 4.9 also shows that the concentration of salts in the D3 interflow system is lower than the D1 and D2 systems. This is due to the dilution effect of greater volumes of

water passing through the D3 system, as shown in Figure 4.10. The thicker cover of the D3 plot provides greater storage, especially macropore storage, for infiltrating snowmelt. This might have been confirmed if a lower volume of snowmelt runoff was observed to be coming from the D3 plot compared to the D1 and D2 plots; however, the runoff measurement weirs were decommissioned between 2005 and 2008 due to regular failures and data inconsistencies.

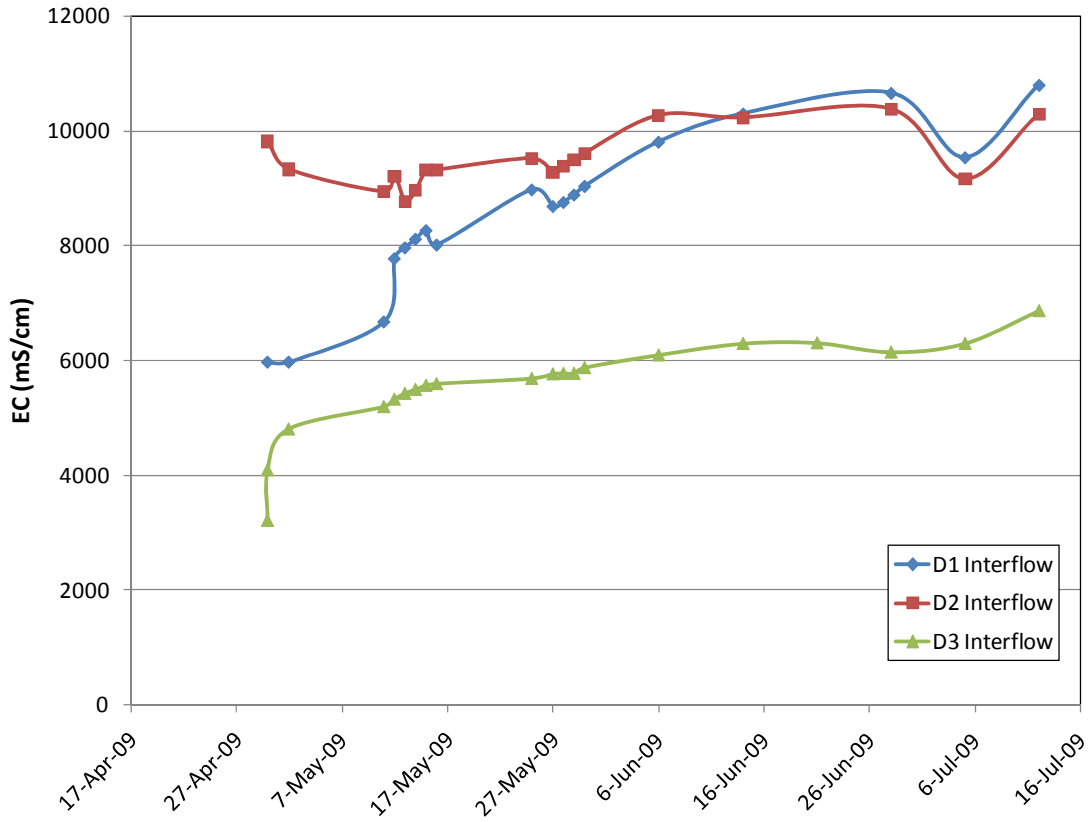

Figure 4.9: Interflow chemistry for 2009.

Despite the lower concentrations of salts in the D3 interflow waters, the total mass of salt flushed from the D3 system is considerably higher than from the D1 and D2 systems. Figures 4.11 displays the cumulative SO_4^{2-} mass output from each of the interflow systems. This figure shows that the total salt output from the D3 system is nearly four times greater than from the D1 system. Again, this higher mass loading is attributed to the greater interflow volumes passing through the D3 cover.

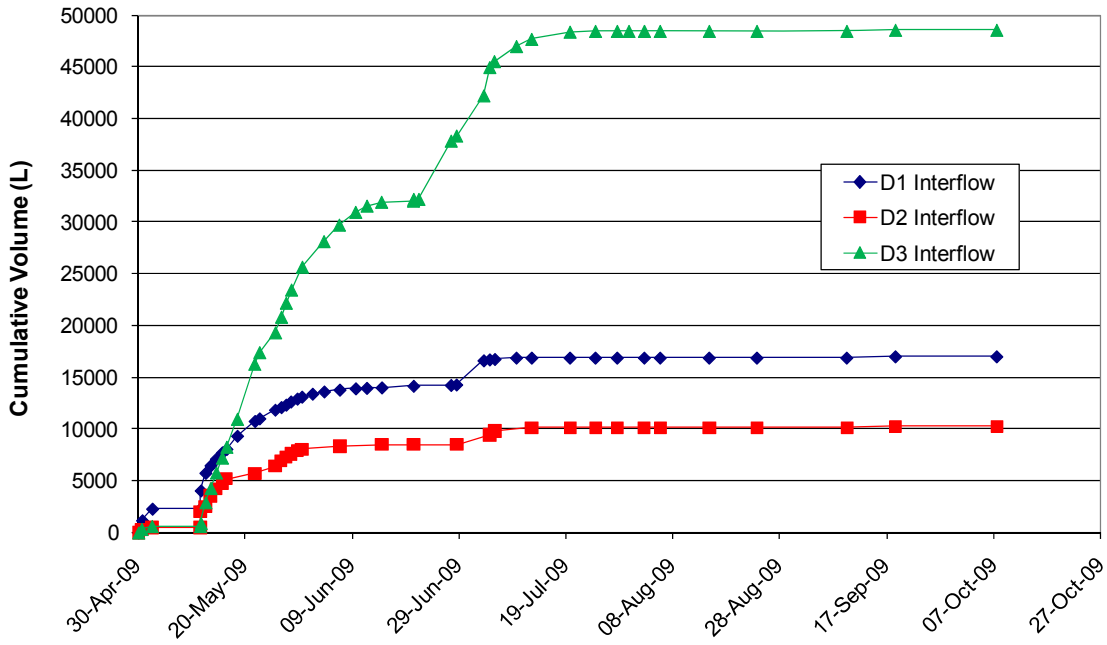

Figure 4.10: Cumulative interflow volumes for 2009.

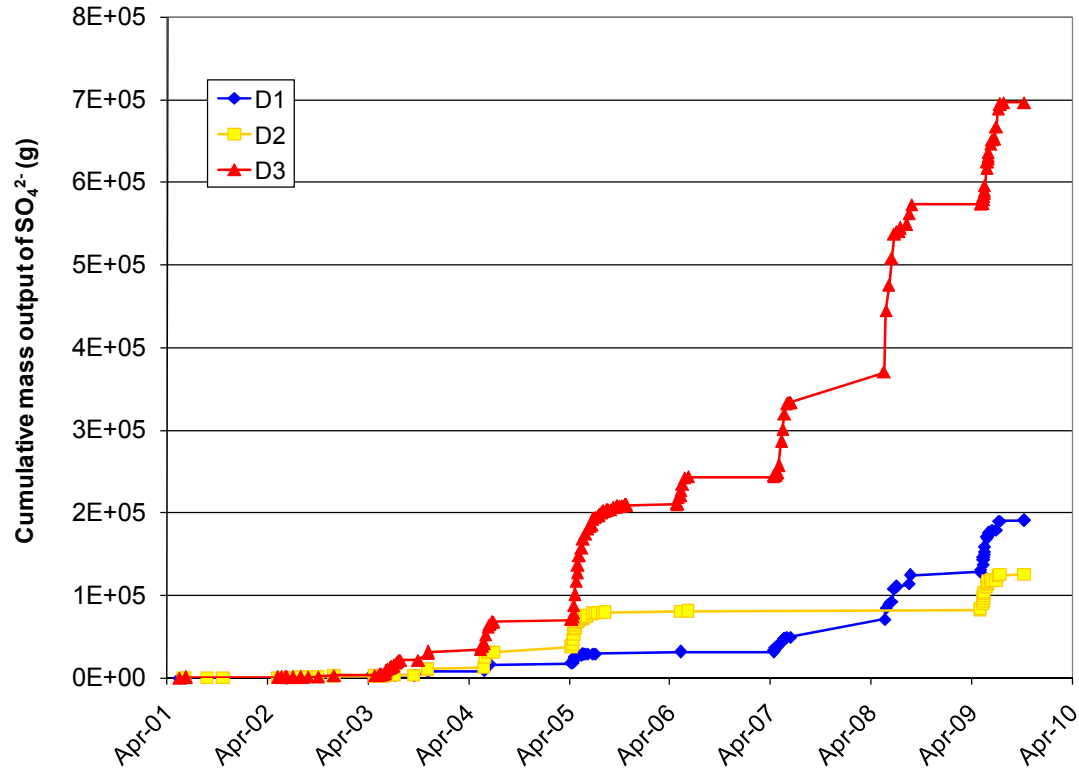

Figure 4.11: Cumulative SO_4^{2-} output from interflow systems for 2000 – 2009.

4.2.2 Soil Profiles

The salinity concentrations from the saturated paste extracts were used in the PHREEQCI geochemical modelling software to calculate true field concentrations. These calculated field concentrations from the D1, D2, and D3 test plots in August 2008 and the plateau area in May 2009 were plotted versus sample depth to generate salinity profiles for each of the sampling locations. The soil salinity profile for D3-05 is included in Figure 4.12 as an example. This figure includes concentration profiles for Na^{+}, SO_4^{2-}, and Ca^{2+}. The data used to generate these plots are tabulated in Appendix B.

The plots also include profiles generated from earlier soil sampling programs to illustrate how salt transport processes may be altering the salinity profiles. It should be noted that the SO_4^{2-} concentrations in these salinity profiles are presented as the mass concentration of sulphur as sulphate (indicated as $S\text{-}SO_4^{2-}$) per volume of solution. For example, if a sample contains 96 mg/l of SO_4^{2-}, this would equate to 32 mg/l of $S\text{-}SO_4^{2-}$. This unit of measurement is an industry standard used by many soil analysis laboratories and was, therefore, adopted for soil sample concentrations in this study, despite the fact that water sample concentrations are presented as mg/l of SO_4^{2-}.

The most recent 2008 and 2009 salinity profiles were visually compared to the salinity profiles from 2002 and 2004 to make note of any temporal changes. The 2008 salinity profiles from the D1 test plot were generally quite similar to the profiles from 2002. Six of the sampling locations (D1-3, 4, 7, 8, 9, and 10) indicated decreasing salt concentrations in the upper shale which suggests salt flushing by either net percolation or upward transport into the cover and removal by interflow. Three of the sampling locations at approximately mid-slope (D1-4, 5, and 6) showed slight to moderate degrees of salt accumulation in the cover. These salts might have diffused up into the cover from the shale below or might have been transported by interflow from upslope locations.

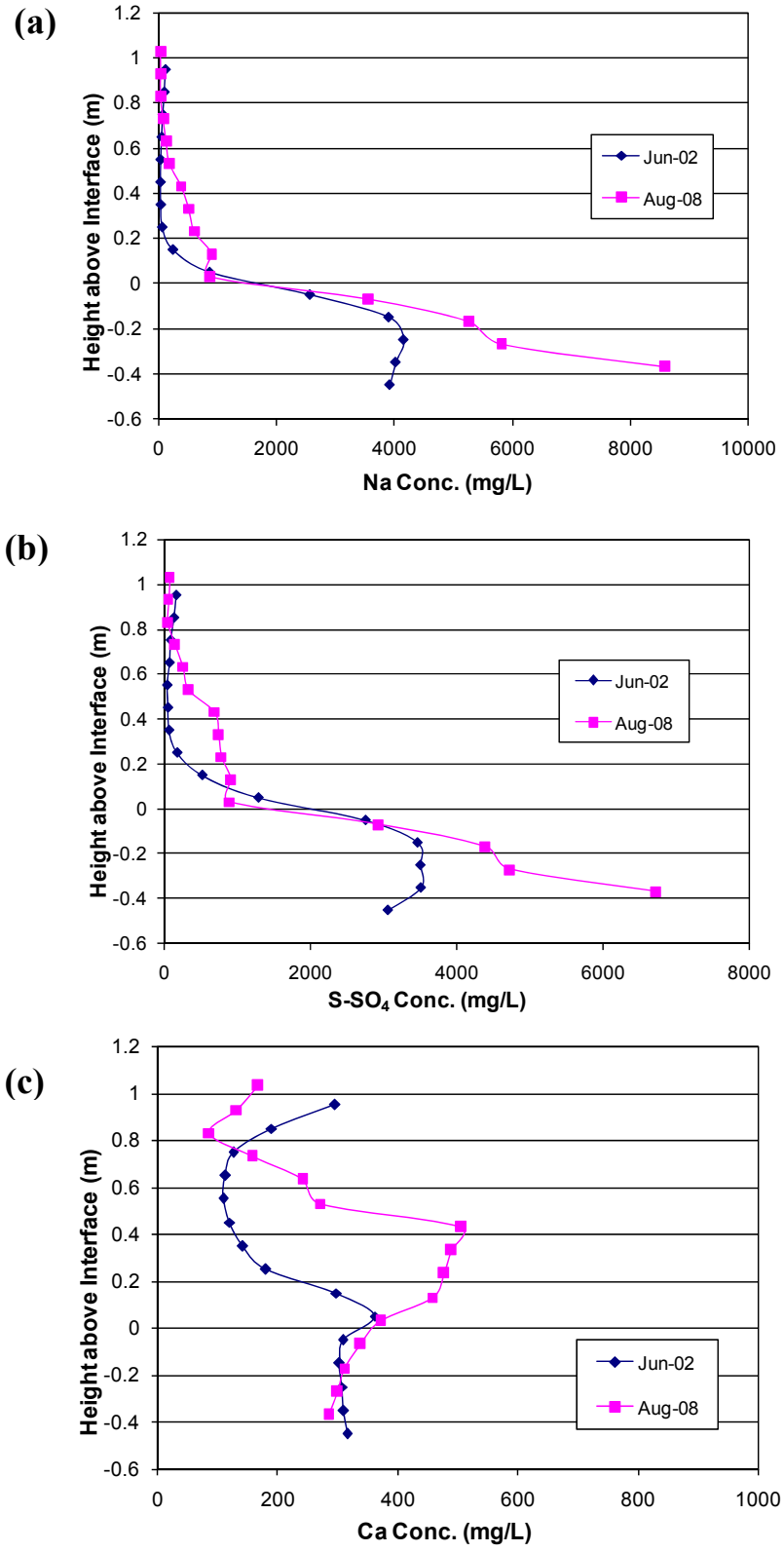

Figure 4.12: Example soil salinity profiles for D3-05 location. (a) Na^{+}, (b) $S\text{-}SO_4^{2-}$, and (c) Ca^{2+}.

The majority of the salinity profiles from D2 showed no sign of salt accumulation in the cover between 2002 and 2008. Seven of the sampling locations (D2-1, 3, 4, 6, 7, 9 and 10) showed decreased salt concentrations in the upper shale, particularly the upper 50 cm of shale. This suggests that salt has been removed by flushing or interflow removal. The two sampling locations at the toe of the slope (D2-1 and 2) showed slight to moderate accumulation of salts in the cover. This might suggest that some of the salts from the shale below have been transported up into the cover, but for D2-1, a mass balance indicates that there has been an overall loss of salts from the profile, either by percolation or interflow flushing. Five sampling locations spread across the slope (D2-3, 5, 6, 8 and 10) show increasing salt concentrations in the shale at depths greater than 50 cm below interface. This suggests that either the pyrite oxidation zone in the shale is progressing downward or that salts from the upper shale are being flushed downward.

Generally, the salinity profiles from D1 and D2 test plots indicate little change or decreasing salt concentrations in the cover and upper shale. Conversely, many of the sampling locations in the D3 test plot indicate accumulating salts in the cover. Nine of the ten sampling locations (D3-0 to 9) show higher salt concentration in the cover in 2008 compared to 2002. While the increase is slight in the upper slope locations, the two locations at the toe of the slope (D3-0 and D3-2) show more pronounced increases. Again, this might indicate that these lower slope locations are experiencing more upward salt transport or that the accumulating salts in the cover were transported down slope by interflow. There was generally little change between 2002 and 2008 in the salt concentrations within the shale of the D3 test plot. Most sampling locations showed no change, but one location (D3-3) showed a considerable decrease in salt concentrations in the upper shale. Another location (D3-5) showed a clear increase in salt concentrations in the shale between 2002 and 2008.

There are several potential explanations as to why the D3 test plot might be accumulating salts in the lower cover while the D1 and D2 plots seem to be flushing salts. The first explanation could be differences in the stage of pyrite oxidation. As described by Nichol et al. (2006), the zone of pyrite oxidation in the shale is initially just

below the interface but as the finite supply of pyrite is exhausted, the oxidation zone progresses deeper. The rate of the pyrite oxidation reaction is limited by the supply of oxygen (Wall 2005) and, therefore, the oxidation rate decreases as the oxidation zone extends deeper due to the increased distance that the oxygen must travel. Because the D1 and D2 covers are thinner, oxygen can pass through them more easily than the D3 cover, especially since the thinner covers are more susceptible to desaturation, as shown by Boese (2003) and Shurniak (2003). It is assumed that these thinner covers would have experienced higher initial oxidation rates in the upper shale. It is also assumed that the oxidation zone in the thinner covers would consequently progress downward at a faster rate than for the D3 cover. Therefore, the oxidation zone in the D3 cover is likely closer to the interface which might allow more of the produced salts to diffuse upward into the cover.

A second explanation for the salt accumulation in the D3 cover, could be due to higher volumetric water contents and, thus, higher diffusion coefficients in the cover soil of the D3 test plot relative to the D1 and D2 test plots. Boese (2003) and Shurniak (2003) demonstrated that the thicker D3 cover maintains higher moisture contents than the D1 or D2 covers. Other researchers have provided evidence that the diffusion coefficient increases with an increase in volumetric water content (Lim et al. 1998; Conca and Wright 1992; Rowe and Badv 1996a, 1996b). This suggests that the rate of salt diffusion into the D3 cover could be higher than in the D1 and D2 covers. This theory is supported by modelling work performed by Merrill et al. (1983) that showed increased diffusion rates for thicker covers.

Similar to the D1 and D2 cover sampling locations, the salinity profiles generated on the plateau indicate either no change or slight salinity decreases with time in the cover and upper shale. This was unexpected as the cover prescription for the plateau is the same as that of the D3 cover plot. The thick cover combined with the lack of interflow on the plateau lead to the highest degrees of saturation among the SBH site study areas and, thus, the average diffusion coefficient for the cover soil of the plateau should be equal to or greater than that of the D3 test plot. This suggests then that downward flushing of

salts by net percolation is occurring on the plateau to attenuate the upward diffusion of salts. The profiles also indicate that salt concentrations for two of the sampling locations (Pro 51 and Pro 53) are increasing at depths greater than 20 cm below the till-shale interface. This supports the theory that salt is being driven downward by percolation.

The trend of decreasing salinity in the cover soil on the plateau is in contrast to the conclusions of Nichol et al. (2006) who stated that salt transport into the cover is progressing faster on the plateau. Their work was based on 2004 salinity profiles and numerical modelling. Therefore, it may be possible that the observed salinity decreases in the cover are a recent reversal.

5. ANALYSIS AND DISCUSSION

This chapter presents the results of numerical modelling of δ^2H and SO_4^{2-} transport for the SBH study site and a discussion of the implications of these model results. In the first part of the chapter, the δ^2H transport numerical model results are presented and summarized. The second part of the chapter focuses on the SO_4^{2-} transport numerical model results. The chapter concludes with a discussion on the model results and implications for the characterization of the SBH cover system.

5.1 δ^2H Transport Model Results

The interpretation of stable isotope analysis for the SBH site was critical to the development of a transport model. The establishment of a LMWL for the SBH site was an important first step towards using stable isotopes of water as tracers in the cover soil. The lack of fractionation effects observed in groundwater samples and soil pore water confirms that δ^2H is a conservative tracer in the soil profile and can thus be incorporated into the numerical transport models.

5.1.1 Establishing Model Parameters

Shale Baseline δ^2H Value

To develop the numerical model, a baseline δ^2H value was required for the shale overburden. The δ^2H values for the deepest portions of the eight shallow sampling locations as well as the entire range of the single deep profile were visually interpreted to determine whether a consistent baseline value exists. These profiles are presented in Figures 4.6 to 4.8. Three of these soil profiles (D3-02, D3-04, D3-08) do not seem to penetrate deep enough to establish baseline values. The baseline δ^2H value in the remaining sample locations are consistently near to -160‰. Therefore, the baseline value for the shale overburden was established at -160‰.

No data from other studies were found that could provide δ^2H values for in-situ Clearwater formation shale of the Athabasca region. However, a study by Lemay (2002)

reported δ^2H values for three water samples collected from Clearwater Formation aquifers (i.e., not shale). These samples were collected from within the Athabasca Oil Sands Area approximately 150 km south of the SBH study site. The measured δ^2H values for these samples ranged from -147‰ to -148‰. These values are considerably more enriched than the selected baseline isotope signature for the shale at the SBH study site. The reason for this may be due to variations in the δ^2H values between shale and the more permeable strata sampled from in the Lemay (2002) study.

In another study, Hendry and Wassenaar (1999) measured a baseline δ^2H value of -144‰ in Bearpaw formation shale in south central Saskatchewan. This is similar to the results of the Lemay (2002) study and, again, more enriched than the selected SBH shale baseline value. However, deep isotopic profiles from the Saskatchewan site as well as an adjacent study site show that the δ^2H values in the shale vary from approximately -160‰ at the glacial till – shale boundary to baseline values between -139‰ and -144‰ (Hendry et al. 2010). The baseline value in the shale was typically reached at a depth of 20 to 40 m below the till-shale interface. Therefore, the shale that was placed at the SBH study site seems to resemble the upper shale from the Saskatchewan study sites.

Infiltrating Water δ^2H Value

The numerical model required an upper boundary condition to simulate the infiltration of water with a different δ^2H value than the original pore water. Two types of boundary conditions were considered. The first type of boundary condition considered is known as a "1st type" or "Dirichlet" boundary condition and requires that the nodes along the boundary be assigned a specific δ^2H value. In this approach the mass flux into the domain is due to both advection with the applied boundary water flux at the δ^2H value assigned to the boundary nodes and also by diffusion due to concentration gradients. The other type of boundary condition considered is known as a "Cauchy" boundary condition and requires that the mass flux be specified along the boundary.

Each of these two boundary conditions was incorporated into preliminary model runs. It was observed that the concentration boundary condition (Dirichlet) provided a more

representative simulation of the SBH cover system because the mass of infiltrating contaminant from the cover soil is small compared to the "pool" of potential contaminant mass being stored in the cover. In addition, the Dirichlet type boundary condition allowed simulation of an instantaneous concentration step function which would have occurred when the glacial till origin cover soil was placed on the saline-sodic overburden. This stepped concentration was necessary for accurate diffusion modelling.

Several options were considered in determining the source δ^2H value. One option was to use the measured δ^2H values from the shallow monitoring wells. However, the locations of monitoring wells do not coincide with the soil sampling locations, particularly on the D3 cover where monitoring wells were only installed in the lower half of the slope. In fact, only the Pro 50 and Pro 54 sampling locations on the plateau are located immediately adjacent to monitoring wells. In addition, these monitoring wells only provide water samples during the wettest part of the year.

Another option considered was to use the δ^2H values measured in water samples from the interflow collection system. Because the interflow moves through the soil overlying the interface it could provide a good representation of the δ^2H value of pore water just above the interface. However, it would only provide average conditions for the entire D3 cover plot and may not represent any one location particularly well. In addition, it may not represent the plateau sample locations at all as interflow is believed to be negligible in the plateau. The interflow water samples would also only provide an estimate of δ^2H values for a short period of the year after spring thaw or during especially heavy rains.

It was determined that the upper boundary δ^2H values would be selected based on the values obtained from the soil samples themselves (i.e. the field profiles in Figure 4.6 and 4.7) as average values to be applied over the entire model duration. The source values at the interface are as follows:

- -144‰ for the plateau profiles;
- -156‰ and -157‰ for Group A of the D3 profiles; and,

- -153‰ for Group B of the D3 profiles.

Explanations for the variations in the source conditions between the plateau and slope profiles are proposed in Section 4.1.4.

These source values, measured 8-10 years after cover placement (depending on location) would not likely provide a good representation of field conditions immediately after cover placement, but it is believed that the relatively high permeability of the till has allowed sufficient infiltration and water redistribution to establish a unique isotopic signature at the cover-shale interface within one to two years. This assumption is supported by the large fluctuations in volumetric water content observed in the till cover (from approximately 0.4 in the spring to approximately 0.15 in the summer) and the presence of perched water and interflow on the till/shale interface..

Although a constant δ^2H value boundary condition was used throughout the simulation, it is likely that the δ^2H value of the pore water at the interface varies seasonally and possibly varies from year to year. Several model simulations were performed to examine the effect of varying the boundary condition from one year to the next. The results, which are excluded for brevity, showed that, for the range of diffusion coefficients considered, the evidence of these δ^2H value fluctuations is lost after 1-3 years. These simulations demonstrated that if the simulated boundary condition δ^2H value is approximately equal to the average δ^2H value at the interface, and as long as no extreme annual δ^2H value fluctuations have occurred in the previous 1-3 years, the modelled profile should be a good representation of actual field conditions.

5.1.2 Modelling Frost Effects

Accurate numerical modelling of contaminant transport processes in a shallow soil profile can be difficult for temperate zones where seasonal climate changes cause extreme variations in precipitation and evapotranspiration. The average monthly air temperature for the SBH study site varies from approximately -20°C in January to nearly +20°C in July (Shurniak 2003). Frozen, saturated ground is an efficient barrier to water

flow and contaminant transport; however, the penetration of ground frost, in itself, can cause contaminant transport as liquid water is drawn to the frost front (Rehm et al. 1982).

In the past, researchers performing numerical modelling of contaminant transport at the SBH site have handled frost differently. Rather than attempting to quantify frost-induced transport, Kessler (2007) chose to ignore frost effects in a numerical model of salt diffusion in the cover. In her model, Kessler allowed diffusion to occur 365 days per year. Conversely, Kelln (2008) reasoned that diffusion and advection could not occur when the ground is frozen. Therefore, the numerical models created by Kelln allowed transport processes to occur for only 185 days per year; the period considered to be frost-free. With these contrasting viewpoints in mind, the numerical model for the current study was initially set up to examine the effects of limiting or restricting diffusion and advection over a defined period each year.

Soil temperature data from 2000 to 2009 were examined for the D3 cover soil station as well as the plateau soil station to estimate the depth of frost penetration and the number of days per year during which the soil is frozen. Temperature data are available for most years from two different sources; thermistor sensors and thermal conductivity sensors used to measure soil suction (see Boese 2003 for description of instrumentation). This provides an additional level of confidence to the values. The temperature data were obtained from SCL's SBH database but are not included in this report.

The soil temperature data from the plateau suggest that from 2001 to 2003 frost penetrated as deep as 1.8 m below ground surface and persisted in the shale for about 100 days per year. However a surprising shift occurred in the winter of 2003/04 and every year thereafter. The maximum depth of frost penetration over this time period was between 0.25 m and 0.4 m below ground, and at least 0.6 m above the cover-shale interface. In fact, for the winters of 2007/08 and 2008/09, the soil sensors indicate that frost did not penetrate to the 0.15 m sensor. A review of daily minimum and maximum air temperatures recorded from the SBH plateau and mid-slope weather stations between

2001 and 2009 revealed that, while the winter of 2005/06 did appear to be warmer, most other winters seemed to be consistent. The winters of 2007/08 and 2008/09 appeared to be as cold as the winters of 2001/02 and 2002/03.

Therefore, the very shallow frost penetration in later years is unexpected and may be caused by improper calibration of both sets of soil temperature sensors or by some unnatural heat source or insulation preventing the soil from freezing in the vicinity of the sensors. It is also possible that snow fall occurring early in the winter combined with the accumulation of vegetation at surface creates a natural insulation layer, preventing frost penetration. Vegetative insulation might better explain the evolution in frost behaviour with time, as it would have taken several years for this vegetation to establish itself.

The soil temperature data from the D3 cover soil station show deeper frost penetration. For the first five years after cover placement (winters of 1999/2000 to 2004/05), the frost penetration was to a depth of at least 1.6 m below ground surface and persisted for approximately 120 days at depth. Over the next five years (winters of 2005/06 to 2008/09) frost penetration did not exceed 1.25 m and persisted for approximately 60 days at depth. Again, this shows a reduction in frost severity with time, though the exact reason is unknown.

Based on these soil temperature readings, it was determined that soil frost is not likely to be restrictive to contaminant transport in the plateau cover. However, in the D3 cover, frost almost certainly interrupts contaminant transport processes for a portion of each year. Therefore, a simple numerical model was set up to determine the effects of this interruption by frost.

This simple numerical model was meant to represent general field conditions for the D3 cover but was not intended to represent any specific location exactly. The baseline value of the shale was set to -160‰, while the value at the cover-shale interface was set to -150‰. This is a reasonable approximation of boundary conditions in the D3 cover. The first set of simulations in the frost evaluation model incorporated diffusion as the only

transport process. The diffusion coefficient was set to $4x10^{-10}$ m²/s, which is considered an upper limit for the values used in all of these modelling exercises. Three cases were analyzed for comparison: Case I allowed diffusion year round with no frost; Case II had frost penetration to 0.60 m below the cover-shale interface (1.60 m below ground surface) for 120 days per year; and Case III had frost penetration to 0.25 m below the cover-shale interface for 60 days per year. A 10-year period was simulated for each of the three cases. For Cases II and III, the frost-affected region of the model were set to null elements during the portion of each year over which frost occurred.

The results of these diffusion-only model simulations show that transport interruption by frost has a slight but perceptible effect in the smoothing of the diffusion profile, as shown in Figure 5.1. Not surprisingly, the effects are greater for longer durations of frost and deeper frost penetration. The comparison between Case I and Case III suggests that shallow frost penetration (<0.25 m below interface) for short durations (<60 days per year) has a negligible effect on the diffusion process in the soil profile.

The next step in evaluating frost effects was to include net percolation in the numerical model. Net percolation was modeled as a downward total water volume of 10 mm entering the shale each year. The same three evaluation cases were used as described above. For Cases II and III, the frost in the soil profile prevents percolation during the frozen months and thus the 10 mm of net percolation is spread over a shorter time period. Thus, the water flux rate is highest for Case II followed by Case III, although the total volume of water passing through the soil profile in one year is the same for all three cases. The diffusion coefficient was left unchanged from the previous set of analyses. The results for the advection-diffusion frost evaluation model runs are also shown in Figure 5.1. The magnitude of the differences between the three profiles is almost identical to that observed for the diffusion-only profiles. This does not imply that frost penetration has no effect on advective transport. It does, however, demonstrate that when using a net annual percolation variable in a numerical model, it makes little to no difference whether this net percolation is occurring over part of the year or the whole year. Of course, one must still consider how the presence of frost serves to increase the

advective velocity for a given annual net percolation rate. This advective velocity should be evaluated based on the bulk hydraulic conductivity of the soil and reasonable hydraulic gradients to ensure that the velocity is possible.

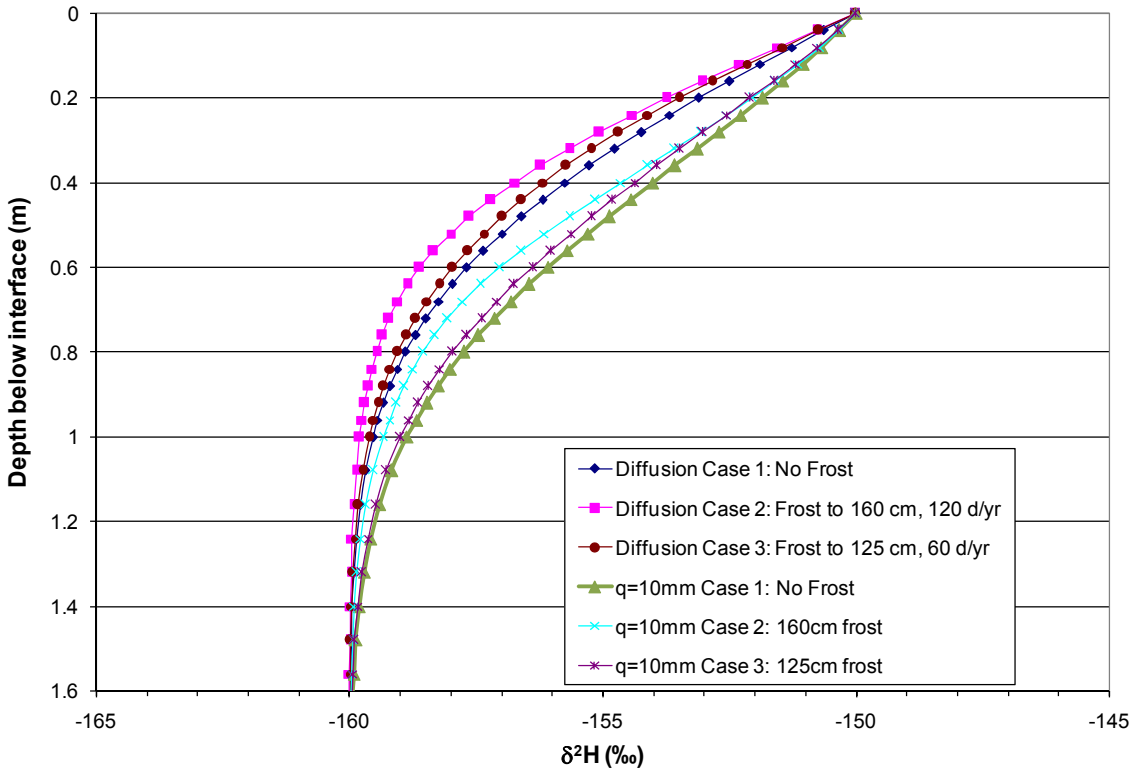

Figure 5.1: Simulated δ^2H profiles demonstrating frost interruption effects.

A final set of frost evaluation analyses were performed with a net percolation rate of 50 mm/yr (results not shown). It was found that the relative difference between profiles was even less perceptible than for 10 mm/yr. This is because diffusion, which is more affected by frost penetration in the model, becomes relatively less important as net percolation increases.

5.1.3 δ^2H Transport Model Results for Plateau

The three field measured isotopic profiles from the plateau sampling locations (Pro 50, Pro 52, and Pro 54) are plotted in Figure 4.6. While these plots include the portions of the measured profiles in the cover soil (upper 1 m), the numerical model did not include the cover soil for reasons described earlier. Based on the similarities in profile shape

between these three drill holes, it was decided that the three profiles would be considered collectively with simulated model results bracketing the measured field results. As described in Section 4.1.4, an average baseline value of -160‰ and a source value δ^2H value of -144‰ were used for the general plateau model. The net percolation rate and molecular diffusion coefficient were varied in the model to match the shape of the field profiles.

The volumetric water content for the shale in the numerical model was held constant at 0.4, as described in Chapter 3. It is noted that the volumetric water content of the soil has an impact on the results due to its effect on advective velocity. For example, with the diffusion coefficient fixed, the profile created by a net percolation rate of 10 mm/yr at a volumetric water content of 0.4 would be the same as for a net percolation rate of 7.5 mm/yr at a volumetric water content of 0.3. Therefore, if a net percolation rate is modeled at saturated conditions, the results must be qualified as such. If the volumetric water content varies widely for a soil profile over the course of a year but net percolation is assumed to only occur when the soil is saturated, then it follows that the model should use the higher volumetric water content year round to model the average annual net percolation.

The simulated δ^2H profiles for the plateau are shown with the field measured profiles in Figure 5.2 in terms of depth below the cover/shale interface. The simulations shown in Figure 5.2 are meant to bracket the field results without specifically providing an exact match to any particular set. Additional simulations were performed to provide more accurate fits to individual data sets, but these results are not included in Figure 5.2. The simulated profiles suggest that, for saturated conditions, the net percolation rate on the plateau is between 35 and 50 mm/yr for a volumetric water content of 0.4. With dispersivity held constant at 0.01 m, the coefficient of mechanical dispersion, αv, ranges from $2.8x10^{-11}$ to $4x10^{-11}$ m²/s. It was observed that, in order to simulate the shapes of these three field profiles, the range of molecular diffusion coefficients is quite narrow, falling between $5x10^{-11}$ and $8x10^{-11}$ m²/s, although Figure 5.2 only shows the simulations with $D_e = 8x10^{-11}$. The model uses a constant diffusion coefficient implying that

diffusion occurs year round at the same rate. Realistically, variations in water content would affect the diffusion coefficient and therefore, the estimated hydrodynamic dispersion coefficient is an average value for the year.

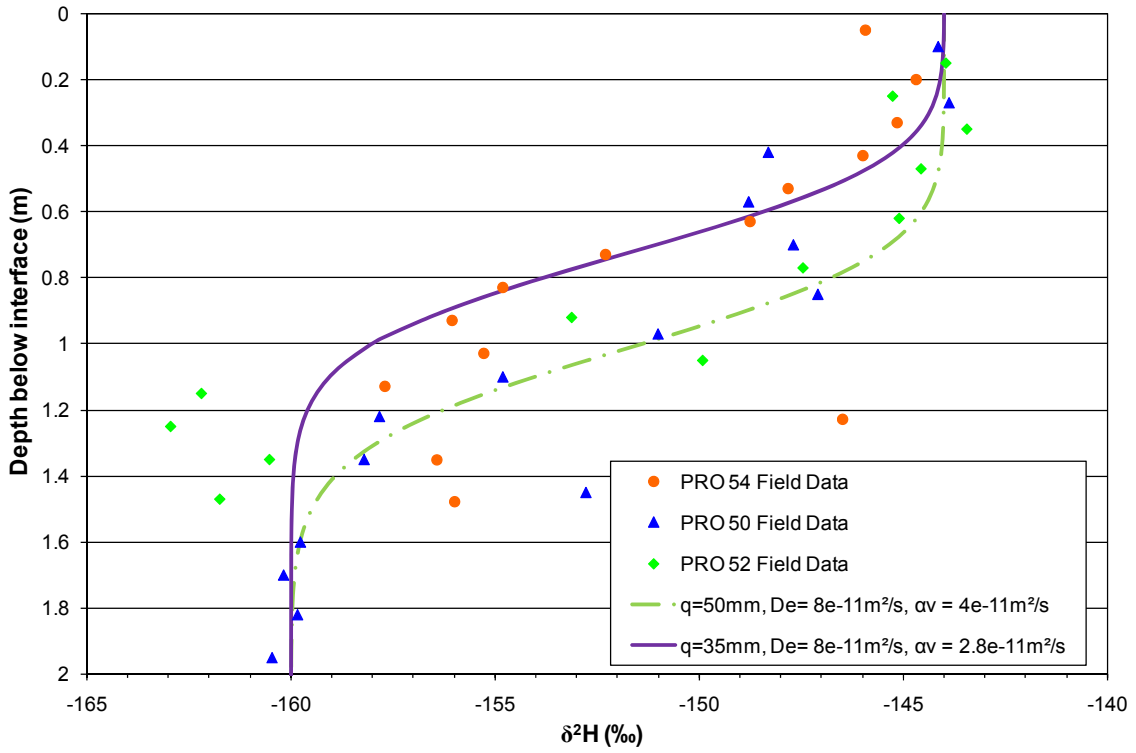

Figure 5.2: Simulated δ^2H profiles for the plateau.

Although the δ^2H profiles from the three plateau sampling locations are generally quite smooth and continuous, Figures 4.6 and 4.7 clearly show that several individual soil samples have δ^2H values that plot far from the smooth profile. In addition, the Pro 50 profile features an unexpected depletion bulge from 0.4 m to 0.6 m below the interface. Individual spurious data points might be explained by errors in testing or sampling. However, a bulge such as the one observed at Pro 50 likely requires an alternative explanation. This bulge could be caused by heterogeneity in the shale overburden. It is possible that a block of shale with comparatively lower porosity, lower hydraulic conductivity or lower diffusivity has caused transport to largely bypass this block preventing its δ^2H value from changing at the same rate as the zones above and below.

An alternative explanation might lie in the δ^2H value of the percolating water. In the model, the δ^2H value of the percolating water was controlled by setting fixed concentration boundary nodes at the interface (upper boundary). This boundary condition is based on the assumption that fluctuations in the δ^2H value of the percolating water either do not exist or do not significantly affect the resulting profile. If fluctuations do occur, diffusion would smooth these fluctuations over a reasonably short time. For a bulge such as that observed in Pro 50 to exist then, the δ^2H value fluctuation must have occurred for a sufficiently long period of time that it has not yet been smoothed out. Although an exact fit to these data was not obtained, additional modelling showed that by varying the source value for a year or several consecutive years, a δ^2H bulge could be produced in the upper shale. However, it was found that approximately 3 years after the δ^2H value fluctuation, evidence of these bulges disappeared from the soil profile.

5.1.4 δ^2H Transport Model Results for D3 Slope

The five isotopic profiles from the D3 sampling locations are plotted in Figure 4.7. As described above, the plots include the portions of the profiles in the cover soil (upper 1 m), while the numerical model did not include the cover soil. Because the D3 cover profiles are not collectively similar in shape, it was decided that they should be simulated individually rather than collectively, as was done for the plateau profiles. However, slight similarities within some D3 profiles allow them to be subdivided into two groups as described in Section 4.1.4. The measured δ^2H profiles for the D3 drill holes are replotted in Figure 5.3 without the upper cover soil.

As described in Section 5.1.3, the plot of δ^2H vs depth for the D3 profiles (Figure 5.3) shows that there are a number of spurious data points and smaller localized bulges that depart from the smooth δ^2H profiles. No attempt was made to exactly simulate these outliers in the soil profiles. Potential explanations for the outliers are the same as those provided for the plateau in Section 5.1.3. An attempt was made to simulate the larger enrichment bulges of the Group B profiles, however. The results are described below.

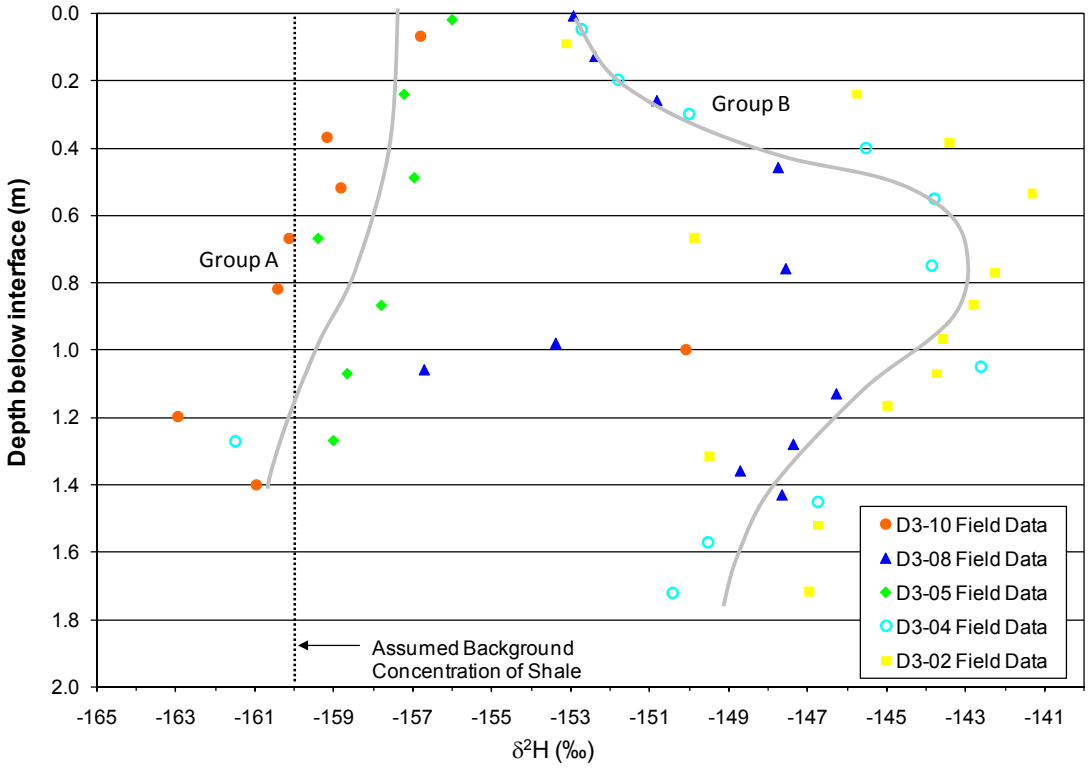

Figure 5.3: δ^2H profiles from soil samples collected on the D3 test plot.

Simulated profiles for Group A from the D3 slope are plotted in Figure 5.4. The numerical model simulations for the D3-05 location reveal that the molecular diffusion coefficient is not an especially sensitive parameter for this profile, due to the narrow range of δ^2H values for this profile. Reasonable simulations were achieved with molecular diffusion coefficients ranging between $2x10^{-11}$ and $4x10^{-10}$ m²/s. Conversely, the profile could only be simulated using a narrow range of net percolation values: 32 to 35 mm/yr. This range of net percolation rates results in mechanical dispersion coefficients, αv, of $2.6x10^{-11}$ to $2.8x10^{-11}$ m²/s.

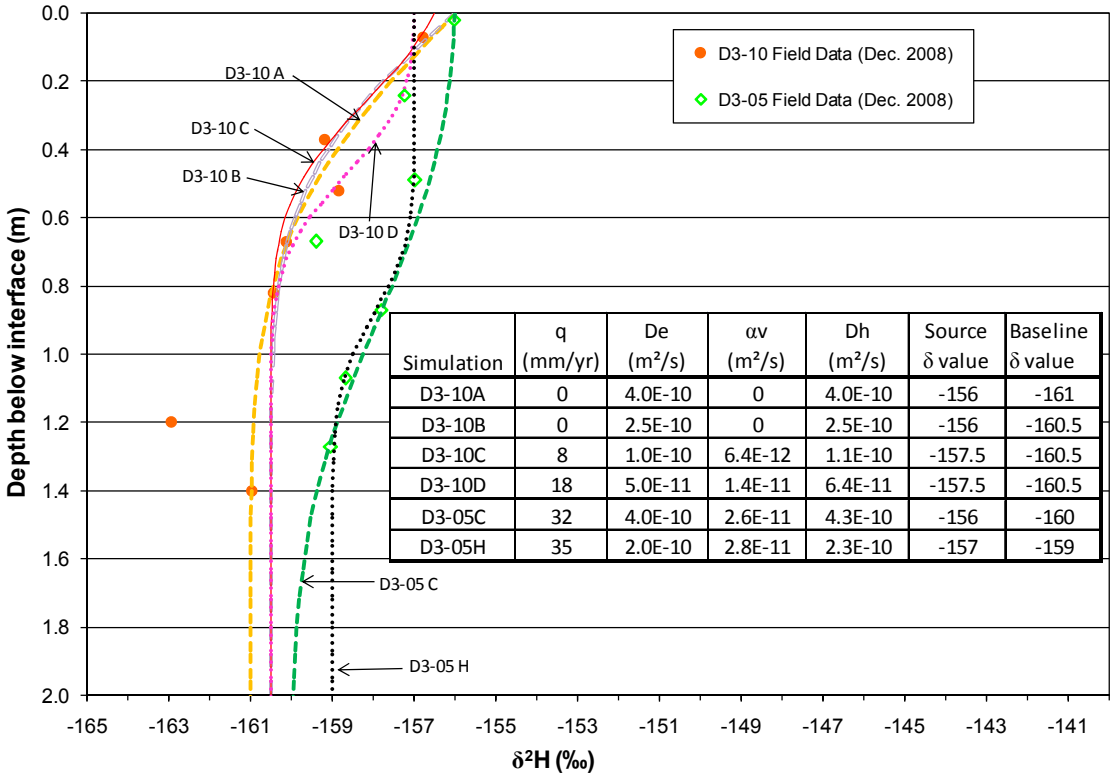

Simulation	q (mm/yr)	De (m²/s)	αv (m²/s)	Dh (m²/s)	Source δ value	Baseline δ value
D3-10A	0	4.0E-10	0	4.0E-10	-156	-161
D3-10B	0	2.5E-10	0	2.5E-10	-156	-160.5
D3-10C	8	1.0E-10	6.4E-12	1.1E-10	-157.5	-160.5
D3-10D	18	5.0E-11	1.4E-11	6.4E-11	-157.5	-160.5
D3-05C	32	4.0E-10	2.6E-11	4.3E-10	-156	-160
D3-05H	35	2.0E-10	2.8E-11	2.3E-10	-157	-159

Figure 5.4: Simulated δ^2H profiles for the D3 slope – Group A.

The stable isotope profile from D3-10 could be simulated using a range of molecular diffusion coefficients and net percolation values in various combinations. The visually interpreted best fit for D3-10 was obtained with a molecular diffusion coefficient of $1.0x10^{-10}$ m²/s, a net percolation rate of 8 mm/yr, and an αv value of $6x10^{-12}$ m²/s. However, the D3-10 profile could also be simulated reasonably well with no net percolation and a molecular diffusion coefficient of $4x10^{-10}$ m²/s if the baseline value of the shale is increased to -161‰.

The δ^2H profiles from Group B have much different shapes and δ^2H ranges than those of Group A, as described in Section 4.1.4. Primarily, these differences appear as enrichment bulges in the shale, which are thought to be caused by the presence of till and LOS mixed in with the shale. Chapman (2008) noted that heterogeneity is common within the overburden waste in this region of the SBH and may have been caused by the type of excavation equipment used for mining at that time. Additional mixing of

different material types, especially in the top metre of overburden, may have occurred during final grading of the slopes and plateau.

Simulations were performed for each of the three Group B profiles with modified initial δ^2H values in the shale over the range of depth where the drill hole logs indicated glacial till or LOS mixed in. For each of the three drill holes in Group B model simulations were performed using: (a) diffusion only, and (b) diffusion and net percolation. The simulated profiles are illustrated in Figures 5.5, 5.6, and 5.7.

As shown in Figure 5.5 (a), the D3-08 profile was simulated reasonably well using diffusion only. The diffusion coefficient is estimated to be between $1.5x10^{-10}$ m²/s and $4.0x10^{-10}$ m²/s. The field-logged description of the soil samples included a considerable amount of glacial till mixed with the shale from 0.6 m to at least 1.5 m below the interface. The model simulations utilized till-shale mixtures from 0.3 to 1.6 m, 0.5 to 1.4 m, and 0.4 to 1.6 m below the interface for simulations B, E, and F, respectively. The δ^2H values for the mixtures in each of these simulations were -145‰, -141‰, and -143‰. Given that the average δ^2H value for the till in the SBH profiles is approximately -142‰, the δ^2H value of the mixed soil represents 85 - 100% till. This proportion of till seem unlikely, suggesting either the simulated processes are inaccurate or the assumed δ^2H value for the till in the till-shale mixture is not correct.

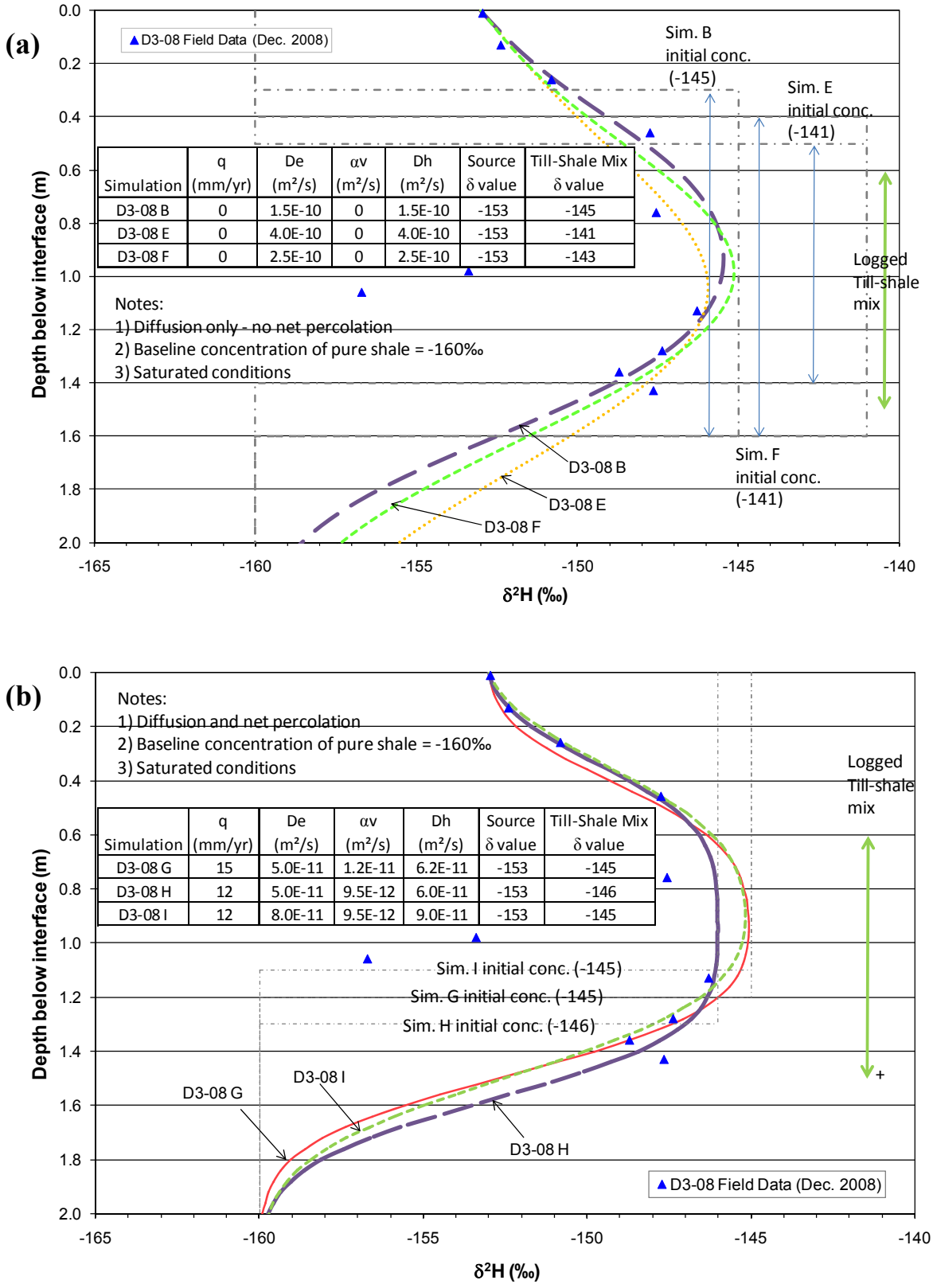

Simulation	q (mm/yr)	De (m²/s)	αv (m²/s)	Dh (m²/s)	Source δ value	Till-Shale Mix δ value
D3-08 B	0	1.5E-10	0	1.5E-10	-153	-145
D3-08 E	0	4.0E-10	0	4.0E-10	-153	-141
D3-08 F	0	2.5E-10	0	2.5E-10	-153	-143

Simulation	q (mm/yr)	De (m²/s)	αv (m²/s)	Dh (m²/s)	Source δ value	Till-Shale Mix δ value
D3-08 G	15	5.0E-11	1.2E-11	6.2E-11	-153	-145
D3-08 H	12	5.0E-11	9.5E-12	6.0E-11	-153	-146
D3-08 I	12	8.0E-11	9.5E-12	9.0E-11	-153	-145

Figure 5.5: Simulated δ^2H profiles for the D3-08.
(a) Diffusion only, and (b) diffusion and net percolation.

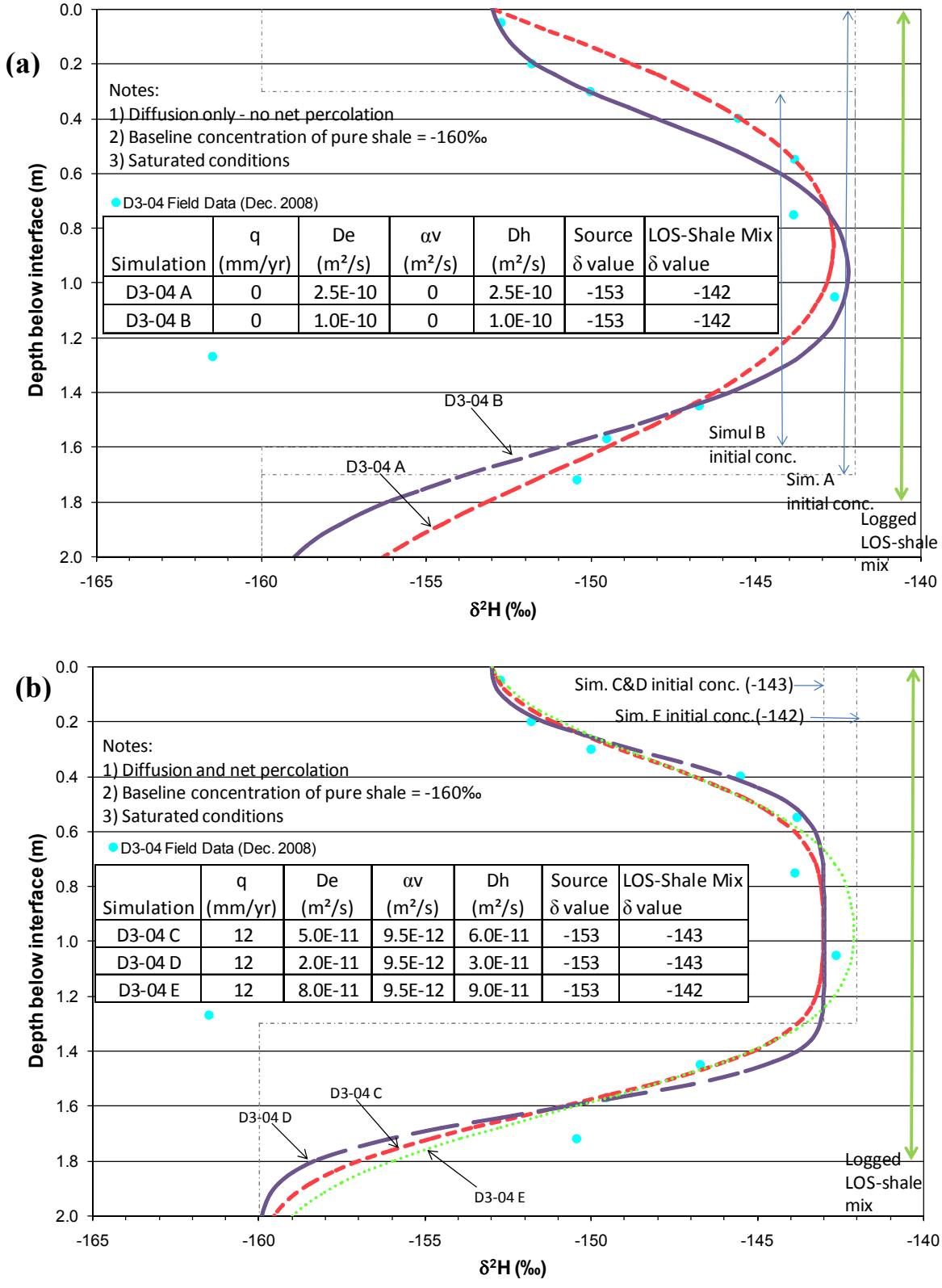

Figure 5.6: Simulated δ^2H profiles for the D3-04.
(a) Diffusion only, and (b) diffusion and net percolation.

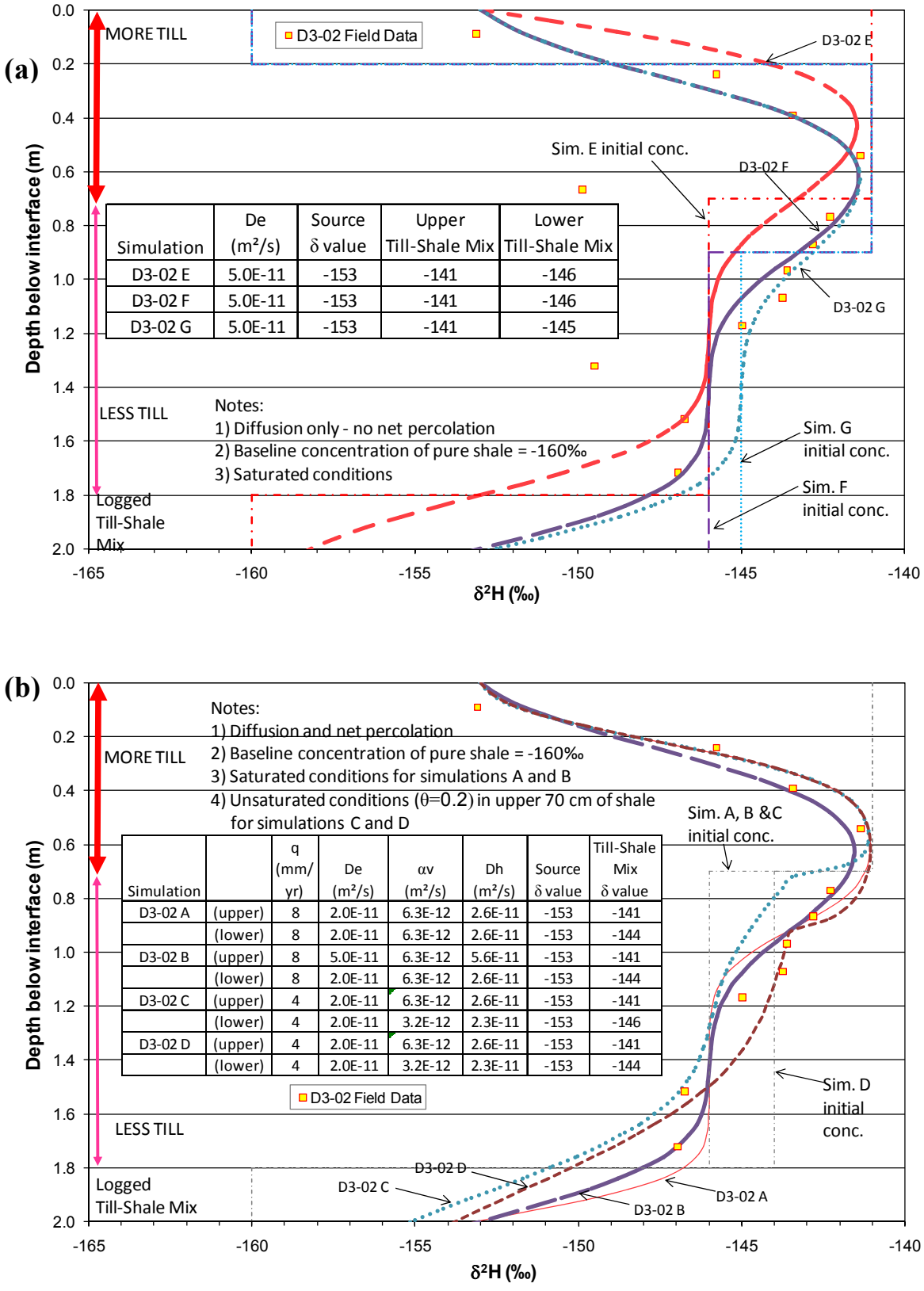

Figure 5.7: Simulated δ^2H profiles for the D3-02.
(a) Diffusion only, and (b) diffusion and net percolation.

The simulated profiles for D3-08 with both diffusion and percolation occurring are illustrated in Figure 5.5 (b). Reasonably good fitting simulated profiles were obtained using net percolation values ranging from 12 to 15 mm/yr but this required till mixture depths much different from the logged description. The estimated molecular diffusion coefficients range from $5x10^{-11}$ m²/s to $8x10^{-11}$ m²/s, with αv values ranging from $9.5x10^{-12}$ to 1.2 x 10^{-11}. While the till-shale mixture was logged from 0.6 to at least 1.5 m below the interface, the simulations required mixtures from 0 to 1.1 m, 0 to 1.3 m and 0 to 1.2 m for simulations G, H and I, respectively. The δ^2H values for the mixtures in each of these simulations were between -145‰ and -146‰. This implies mixtures with till proportions of between 79 and 85%. Again, this proportion seems suspiciously high given that the field logs identified the material as "shale with some till", or "shale and till". These descriptions suggest that the mixture might have up to 50% till. Therefore the δ^2H value for till in the mixture is either far more enriched than -142‰ or some other unknown combination of processes and initial conditions has affected the δ^2H profile.

The shape of the D3-04 profile is similar to that of D3-08 and, therefore, the same modelling approach was used. However, while D3-08 includes a mixture of till and shale below the cover, D3-04 includes a mixture of shale and lean oil sand (LOS). No data were found to provide baseline δ^2H values for LOS, in situ or otherwise. Therefore, while the LOS-shale mixture in the model can be assigned a δ^2H value, no assessment can be made on its validity or on the percentage composition of the mixture as was done for the till-shale mixture.

The diffusion-only simulated profiles for D3-04 are plotted in Figure 5.6 (a). The molecular diffusion coefficient is estimated to be between $1.0x10^{-10}$ m²/s and $2.5x10^{-10}$ m²/s. While the drill hole log describes LOS mixed with the shale from 0 to 1.8 m below the interface, the model simulations required mixes from 0 to 1.7 m below the interface (D3-04 Simulation A) or from 0.3 to 1.6 m below the interface (D3-04 Simulation B). The baseline δ^2H value for the LOS-shale mixture used for both of these simulations was -142‰.

The simulated profiles for D3-04 with both diffusion and percolation occurring are illustrated in Figure 5.6 (b). Three alternate best fit profiles are shown but each featured a net percolation rate of 12 mm/yr. The calculated molecular diffusion coefficients used in these simulations ranged from $2x10^{-11}$ m²/s to $8x10^{-11}$ m²/s. The αv values were the same for the each of the three simulations at $9.5x10^{-12}$ m²/s. The simulated LOS-shale mixture depth was 0 to 1.3 m below interface and the δ^2H value for the mixture was between -143 and -142‰.

Of all of the isotopic profiles collected from the SBH site, the profile for D3-02 is the most complex. As shown in Figure 5.7, the field data appears to plot along a double-hump or two stage enrichment bulge. Initially it might appear that this drillhole has a much more enriched δ^2H baseline value of approximately -147‰, which is attained at a depth of 1.5 m below interface. However, it is noted from the D3-02 drill hole log that the deepest sample collected still contained an appreciable amount of till mixed with the shale and, therefore, it is believed that the hole was not drilled deep enough to return to a baseline δ^2H value. The two stage enrichment bulge was explained in the model through the use of a two stage mixture of till and shale. The upper shale was deemed to have a higher proportion of till resulting in more enriched initial conditions. The lower shale contains less till resulting in initial δ^2H values that lie somewhere between the baseline value for pure shale and that of the upper till-shale mixture. This concept is qualitatively supported by the descriptions in the drill hole log where the upper shale from 0 to 0.7 m below interface is described as having more till while the lower shale from 0.7 to at least 1.8 m below interface is described as having less till.

The profiles depicted in Figure 5.7 (a) are the diffusion-only simulated profiles for D3-02. The visually-interpreted best fit profile (simulation "D3-02 F" in Figure 5.7 a) was obtained using a diffusion coefficient of $5x10^{-11}$ m²/s. The model configuration featured the higher till proportion mixture from 0.2 to 0.9 m below interface with a δ^2H value of -141‰. The lower till proportion mixture was simulated from 0.9 to 2.0 m below interface with a δ^2H value of -146‰.

Figure 5.7 (b) shows the simulated profiles for D3-02 with both diffusion and percolation occurring. Simulations A and B both used net percolation rates of 8 mm/yr and αv values of $6.3x10^{-12}$ m^2/s. The molecular diffusion coefficients for these simulations were $2x10^{-11}$ m^2/s and $5x10^{-11}$ m^2/s, respectively. These model simulations featured the higher till proportion mixture from 0 to 0.7 m below interface with a δ^2H value of -141‰. The lower till proportion mixture was simulated from 0.7 to 1.8 m below interface with a δ^2H value of -146‰. Neither of these two simulations provided a good fit to the field data and thus an attempt was made to model this location with variable volumetric water contents through the till. A corresponding decrease in diffusion coefficient was included in the model to accompany the decrease in water content. However, this concept could not be effectively utilized to match the field data profile, as evidenced by simulations C and D, and was abandoned.

5.1.5 Summary of δ^2H Transport Model Results

Simulated profiles were primarily evaluated for goodness of fit based on visual interpretation. An attempt was made to evaluate simulations based on the absolute mean difference (AMD) and root mean square difference (RMSD) between the field results and the simulated results. These methods of evaluation are unbiased and numerical, and therefore, ideal for many scientific analyses. However, for this study it was found that the δ^2H profiles generated from soil samples had frequent outlier points and deviations from a smooth profile. Without more detailed knowledge of the heterogeneity of the soil structure and the exact properties of the soil at the time of cover placement, such outliers cannot easily be simulated in the model. The scope of this modelling exercise was limited to the study of the cover and shale overburden as equivalent porous media and these materials were assumed to be homogeneous. Therefore, outliers and deviations from smooth profiles had to be ignored. It was deemed that human judgment was the best way to accomplish this and thus visual interpretation was accepted as the primary means of evaluating goodness of fit for simulated profiles.

The model parameters (diffusion coefficient and net percolation) used to generate the best fitting simulated profiles for each of the sampling locations are summarized in Table 5.1.

The analysis results from the 1D numerical transport model for deuterium demonstrate a notable difference in the estimated net percolation rates between the plateau region of the SBH study site and the locations from the D3 cover plot on the slope. With the exception of the D3-05 sampling location, the calculated net percolation rates for the slope are considerably lower than those from the plateau. The range of net percolation rates calculated for the plateau is 35–50 mm/yr. The range for D3-05 is only slightly lower at 32-35 mm/yr. The range of net percolation rates for the other slope locations is 0 to 12 mm/yr.

Table 5.1: Summary of estimated transport parameters from ^2H transport model.

Sample Location	Net Percolation (mm/yr)	Effective Molecular Diffusion Coefficient (m^2/s)	Mechanical Dispersion Coefficient, αv (m^2/s) [1]	Hydro-dynamic Dispersion Coefficient (m^2/s)
Plateau – Upper envelope	35	8×10^{-11}	3×10^{-11}	1.1×10^{-10}
Plateau – Lower envelope	50	8×10^{-11}	4×10^{-11}	1.2×10^{-10}
D3-02 – flat, toe of slope	8	5×10^{-11}	6×10^{-12}	6×10^{-11}
D3-04 – steep, mid-slope	12	5×10^{-11}	1×10^{-11}	6×10^{-11}
D3-05 – mid-slope bench [2]	32	4×10^{-10}	3×10^{-11}	4.3×10^{-10}
	35	2×10^{-11}	3×10^{-11}	5×10^{-11}
D3-08 – slight bench near upper slope [2]	12	8×10^{-11}	1×10^{-11}	9×10^{-11}
	0	1.5×10^{-10}	0	1.5×10^{-10}
D3-10 – steep, upper slope	8	1×10^{-10}	6×10^{-12}	1.1×10^{-10}

Notes: 1 – The mechanical dispersion coefficient (αv) varies only because the net percolation rate, and thus, velocity varied. The dispersivity (α) in the model simulations was fixed at 0.01 m

2 – Locations D3-05 and D3-08 each had two simulations that appeared to be equally good fits.

A simple Darcian flux calculation was applied to determine if these net percolation rates were reasonable. The estimated net percolation from the plateau is 35 to 50 mm/yr or $1.1x10^{-9}$ to $1.6x10^{-9}$ m/s. For an assumed hydraulic gradient of 1 over the entire year, the hydraulic conductivity of the shale would have to be approximately $1.1x10^{-9}$ to $1.6x10^{-9}$ m/s. However, it is more likely that the ponded water driving net percolation at a gradient of 1 would only be available for a portion, possibly segmented, of each year between spring and fall. Measurement of monitoring well water levels from the plateau indicate that ponded water was present for at least 3 months in the spring and early summer of 2009. Therefore, if we assume that the unity gradient is available for 3 months per year, then the required hydraulic conductivity to permit an equivalent 35 to 50 mm/yr of net percolation, would be approximately $4.5x10^{-9}$ to $6x10^{-9}$ m/s.

Net percolation rates lower than 35 mm/yr in Table 5.1 (i.e., at slope locations) might suggest lower hydraulic conductivities, shorter ponding periods, or possibly both. For example 12 mm/yr at a hydraulic conductivity of $4.5x10^{-9}$ m/s would require approximately 31 days of ponded water. The presence of ponded water on the SBH study site slopes, is typically 30 to 60 days as reported by Kelln et al. (2009) and supported by interflow measurement data.

The estimated range of hydraulic conductivity values above is reasonable based on the field measurements by Meiers (2002) who measured an average hydraulic conductivity of the upper shale (maximum depth of 1.7 m below ground surface) of $5x10^{-9}$ m/s in 2000.

The estimated hydraulic conductivities also compare well to estimates by Kelln et al. (2008), who used an alternate method to estimate net percolation rates and saturated hydraulic conductivity of the shale at the SBH site. Three monitoring wells were installed in large pockets of lean oil sand within the upper shale that became saturated in the spring and subsequently drained, presumably via percolation through the shale. By measuring the rate of drop of the perched water tables, Kelln et al. estimated that the saturated hydraulic conductivity for the shale was $3x10^{-9}$ m/s.

It is believed that the high net percolation at the D3-05 location, relative to other slope locations is due to the mesotopography of the site. This drill hole was located on a flat mid-slope bench that formed after the placement of the reclamation cover. It is likely that the flat bench is also mirrored by the cover-shale interface. The low gradient of the surface and interface at D3-05 could allow greater infiltration, less runoff and less interflow, resulting in a higher net percolation rate. It may even be possible that the interface at this location is back-sloped, which would create a ponded water table that would persist much longer than other slope locations in a manner similar to the plateau locations. However, it is not understood why the D3-02 location, which is located on the flat toe region of the slope would not have similarly high net percolation rates. Perhaps the interflow collection system provides sufficient drainage to prevent the perched water table from persisting as long as it would on the plateau or at D3-05. In addition, D3-08 is located on a slight bench, though not as wide and flat as the D3-05 bench. However, D3-08 shows no indications of greater net percolation.

The estimated molecular diffusion coefficients are similar between the plateau and slope locations. Most values fall between $5x10^{-11}$ and $1.5x10^{-10}$ m²/s. These values are comparable but somewhat lower than diffusion coefficients published by other authors for similar conditions. As described in Section 3.3.2, diffusion coefficients from the literature vary from $1.7x10^{-10}$ to $4.0x10^{-10}$ m²/s for diffusion of δ^2H in clayey soil with a saturated porosity of 0.4.

The lower diffusion coefficient values calculated in this study are reasonable given that they are average values applied over the entire year in the model. Desaturation of even the upper few centimetres of shale overburden in the profile would greatly reduce the effective diffusion coefficient over dry periods, thus reducing the average diffusion coefficient for the year. Soil moisture content data collected from access tubes across the study site suggest that in many locations, the upper shale may indeed be desaturating seasonally.

5.2 Salt Transport Model Results

The proposed salt transport mechanisms driving changes in the salinity profiles as described in Section 4.2.2 were assessed by means of a one-dimensional salt transport model for selected locations from the plateau and D3 cover plot. The locations chosen for salt transport modelling were those locations that had been sampled for both salinity and stable isotopes. The results from the numerical modelling of ^{2}H transport, as described in Section 5.1.4, were used to help define the model inputs for salt transport modelling.

5.2.1 Establishing Model Parameters

The primary focus of this modelling was to apply the net percolation rates calculated from the $\delta^{2}H$ transport modelling to evaluate the effect of other mechanisms on salt transport in the SBH cover. To accommodate upward salt migration into the cover from the shale, the cover was included in the salt transport model; however, matching the salinity profile in the cover soil was not emphasized due to the complex water dynamics within the cover itself (e.g. preferential flow, evaporation/transpiration releases, etc).

It is known from the work of previous investigators (Shurniak 2003, Boese 2003, Kessler 2007, Kelln 2008) that the cover soil tends to become drier than the underlying shale over the course of each summer. Therefore, while the shale was assigned a volumetric water content of 0.4, the till material of the cover was assigned a volumetric water content of 0.3. This value for the till was selected from water content sensor readings from the lower till (deeper than 0.5 m below ground surface) at various locations across the SBH site. The soil stations for the plateau and the D3 cover recorded an average volumetric water content of 0.3 based on data from 1999 to 2009. Diviner 2000 sensors readings taken between May and September of 2008 and 2009 from 17 locations across the plateau indicated an average volumetric water content of 0.31 in the lower till. The same sensor readings from the D3 test plot suggested a slightly higher volumetric water content of 0.36. Soil samples collected from the SBH site in August 2008 and May 2009 were tested for gravimetric water content and then converted to volumetric water content using a measured dry density for till of 1430 kg/m³ (Boese

2003, Shurniak 2003, OKC unpublished data). The average volumetric water content estimated from these soil samples is 0.34 in the lower till of the plateau and 0.31 in the lower till of the D3 test plot. Thus, a volumetric water content of 0.3 for the till would seem to be representative for the entire site.

The inclusion of the 1 m thick cover in the model produced additional challenges for modelling net percolation. The stable isotope transport model simulated the net percolation as a boundary condition at the shale surface. For the SO_4^{2-} transport model some experimental model runs were conducted to examine the difference between setting the net percolation boundary condition at the top of the cover or at the interface. It was found that modelling the net percolation as originating at the interface provided more representative simulated profiles. This boundary condition is supported by the conceptual model established by Kelln et al. (2009) that proposes snowmelt infiltration and percolation through the cover occurs primarily through macropores during frozen ground conditions. This rapid transport of fresh water through frozen ground to the interface largely bypasses the soil matrix limiting the occurrence of top-down salt flushing from the cover.

The baseline concentrations of SO_4^{2-} for the model were obtained from previous studies on the SBH site. The baseline SO_4^{2-} concentration in the till was estimated from the 2003 analysis of till samples obtained from a salvaged till stockpile (Kessler 2007). These samples indicated an average concentration of 0.14 g of SO_4^{2-} per kg of soil (or 0.05 g of S-SO_4^{2-}/kg soil). Based on the average bulk dry density for the till of 1430 kg/m^3 (Boese 2003, Shurniak 2003, OKC unpublished data) and a volumetric water content of 0.3 in the model, the baseline concentration in the till is approximately 230 mg/l of S-SO_4^{2-}. Nichol et al. (2006) estimated the baseline concentration of dissolved SO_4^{2-} in the shale to be 1.3 g of S-SO_4^{2-} per kg of soil. Using a bulk dry density for the shale of 1500 kg/m^3 (Boese 2003, Shurniak 2003, OKC unpublished data) and a volumetric water content of 0.4, the baseline concentration of S-SO_4^{2-} in the shale is approximately 4900 mg/l.

These baseline concentrations are averages for the materials from across the SBH study site. It is unlikely that the average baseline concentration actually applies to individual sampling locations. Salinity profiles from various locations across the study site from 2002/04 and 2008/09 suggest that baseline concentrations vary across the site and that, in general, the chosen average baseline concentration for the shale is too high. Therefore, the values above were used as a starting point for modelling but were adjusted as necessary to suit individual profiles.

Another difference in the SO_4^{2-} model compared to the δ^2H transport model was the exclusion of mechanical dispersion. As described in Section 3.3.1, mechanical dispersion and molecular diffusion are often considered collectively as hydrodynamic dispersion by researchers studying contaminant transport. However, in this conceptual model, molecular diffusion is driving salt from the higher concentration shale upward into the lower concentration till cover. Meanwhile, advection is driving salts downward by bulk transport. Mechanical dispersion is directly dependent on advective velocity and therefore, it is not believed that mechanical dispersion can cause contaminant transport in the opposite direction to advection. In other words, if molecular diffusion were temporarily removed from the equation, it should be impossible for mechanical dispersion to cause contaminant mass flux upward if advection is downward. While mechanical dispersion is still believed to occur, the currently accepted contaminant transport modelling equations will not provide accurate simulations of its effect. Therefore, in the SO_4^{2-} transport model, the dispersivity was set to zero and molecular diffusion was considered to be the sole contributing process to hydrodynamic dispersion.

5.2.2 Sulphate Transport Model Results for Plateau

A total of five locations (Pro 33, 50, 51, 52, and 53) were drilled on the plateau in May 2009 for soil salinity measurements. One of these locations, Pro 33, did not encounter a distinct till-shale interface over the entire 2.5 m depth of drill hole. The field salinity profiles for the remaining four profiles are shown in Figure 5.8. The field concentrations in Figure 5.8 were calculated from saturated paste concentrations using the geochemical modelling software, PHREEQCI, as described in Section 3.3.3. The salinity profiles

from the plateau, depicted in Figure 5.8, have a greater variation in shape than the stable isotope profiles for the plateau.

The initial model parameters for the plateau locations were based on the results of the stable isotope transport model. The molecular diffusion coefficient was set at $8x10^{-11}$ m^2/s for the shale at a volumetric water content of 0.4. The till cover soil, at a volumetric water content of 0.3, was initially assigned a molecular diffusion coefficient of $4x10^{-11}$ m^2/s. This ratio is reasonable based on the "D vs θ" relationship proposed by Conca and Wright (1992) and is further supported by the relationship proposed by Lim et al. (1998). It should also be noted that Kessler (2007) obtained an average diffusion coefficient of $6x10^{-11}$ m^2/s based on half cell diffusion tests that measured the diffusion of total salinity from shale to till. This value equals the average of the selected diffusion coefficients for shale and till.

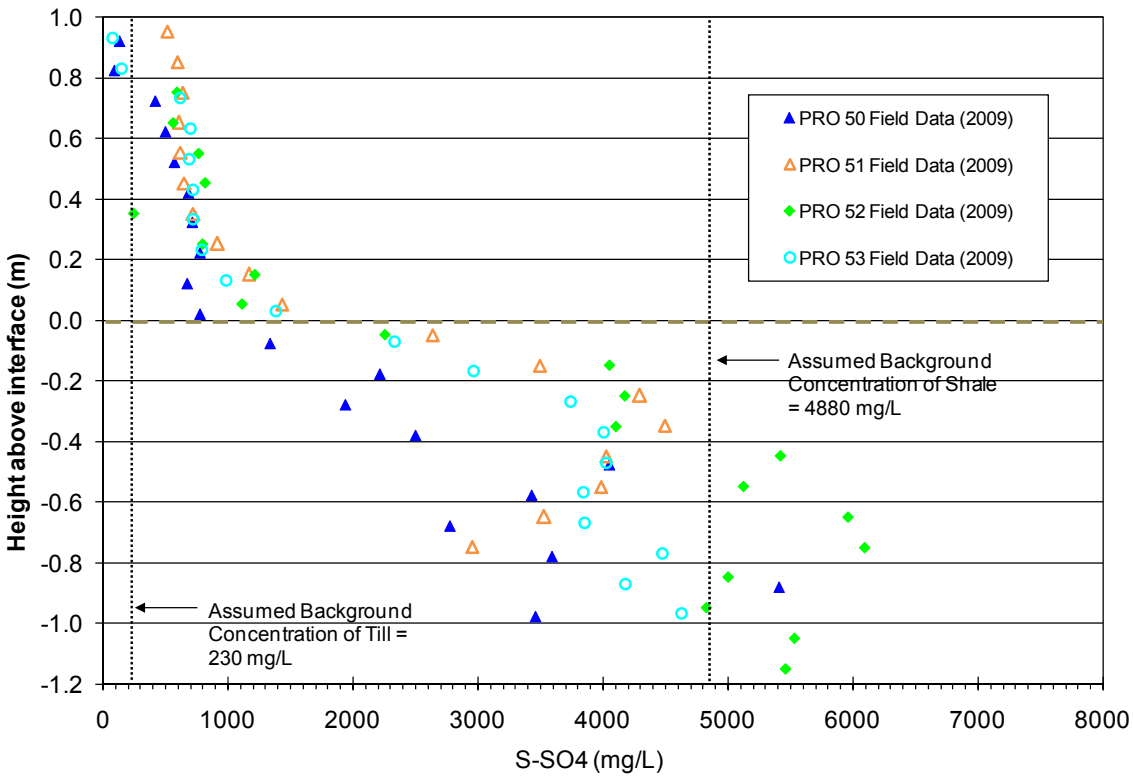

Figure 5.8: SO_4^{2-} profiles from plateau sampling locations from May 2009.

With these parameters fixed, an initial set of model runs was performed to see how the simulated profile compared with the field profiles. For this initial modelling, it was assumed that no pyrite oxidation was occurring in the shale and, thus, no SO_4^{2-} was added to the model. A range of net percolation values was used in the model from a low of 5 mm/yr to a high of 50 mm/yr. The δ^2H transport model results predicted a range of 35 – 50 mm/yr for the net percolation on the plateau. Therefore 50 mm/yr was expected to be the upper limit of net percolation. The simulated profiles with no pyrite oxidation are shown in Figure 5.9.

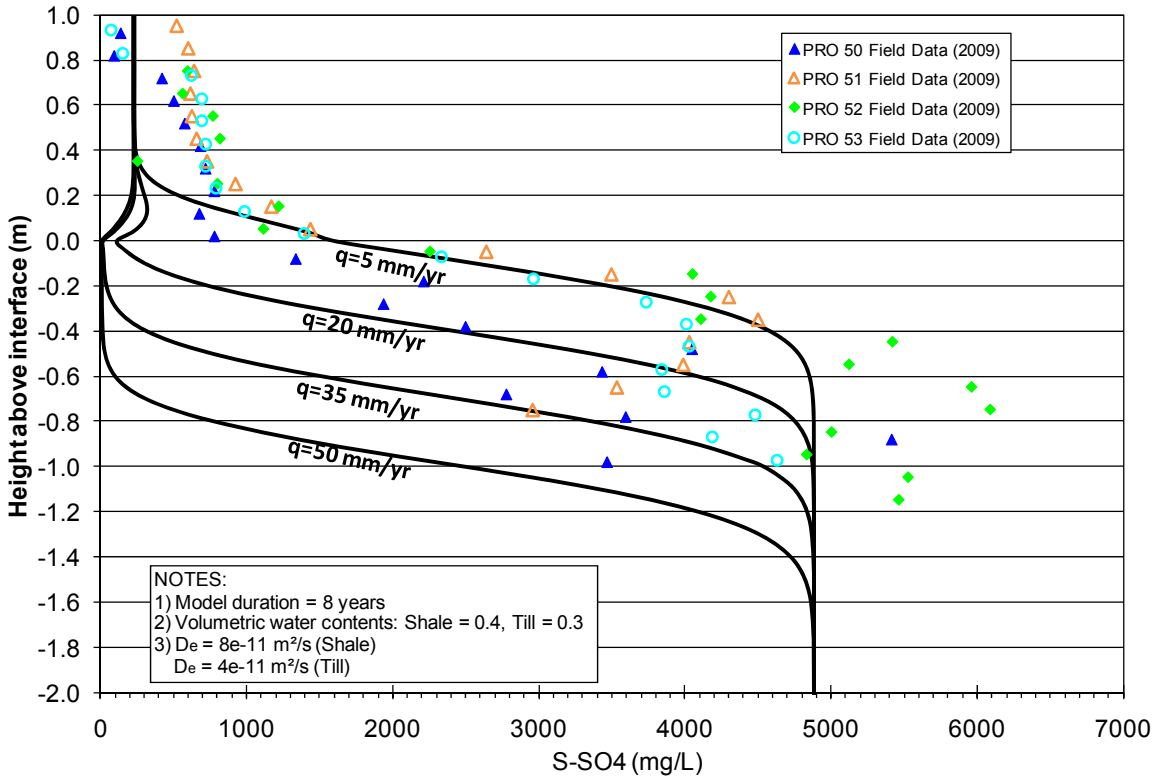

Figure 5.9: Simulated SO_4^{2-} profiles for plateau locations with no pyrite oxidation.

The simulated profiles with no pyrite oxidation are poor matches to the field data at the higher net percolation rates although the simulation with a net percolation rate of 5 mm/yr fits the data reasonably well in the upper shale for three of the profiles (Pro 51, 52, and 53). However, the δ^2H transport model results indicated that the net percolation should be within a range of 35-50 mm/yr. Therefore, SO_4^{2-} production was incorporated into the model and parameters were adjusted to individually fit the measured SO_4^{2-} profiles. The work of Nichol et al. (2006) was used to provide an initial estimate of the

oxidation rates in the shale. Nichol et al. estimated that oxidation of pyrite in the upper shale produced 0.35 – 0.48 g/m²/day of $S\text{-}SO_4^{2-}$ for the first 4 years after cover placement and 0.13 – 0.29 g (of S)/m²/day in the following 4 years.

Of the other four sampling locations shown in Figure 5.8, only two corresponded to stable isotope sampling locations. Therefore, only the Pro 50 and Pro 52 sample locations were modelled in detail to obtain fits to the field concentrations. Both of these sampling locations were modelled with net percolation rates of 35 mm/yr and 50 mm/yr, as suggested from the results of the δ^2H transport model.

The results of the SO_4^{2-} transport model for Pro 50 are shown in Figure 5.10. The baseline concentration in the till of 230 mg/l appeared to be too low for this profile and was increased to 700 mg/l to provide a better fit, especially in the lower till and upper shale. For both the 35 mm/yr and 50 mm/yr simulations, the pyrite oxidation zone was established as the upper 0.6 m of the shale. This was based on the field data profile. The required $S\text{-}SO_4^{2-}$ production rates in the model were 0.4 g/m³/day for the 35 mm/day net percolation rate and 0.6 g/m³/day for the 50 mm/day net percolation rate. However, the numerical model results for Pro 50 revealed that the fit of simulated profiles to field profiles was poor at the cover-shale interface, as indicated in Figure 5.10. To remedy this, additional $S\text{-}SO_4^{2-}$ production was generated at the till-shale interface. Although the model allows for this "point-source" addition of contaminant, it actually represents an increased $S\text{-}SO_4^{2-}$ production from the uppermost row of model elements in the shale and/or the lowermost row of elements in the till (i.e. assuming the production in the till is due to dissolution of recently precipitated gypsum). This additional oxidation rate was 0.05 g/m²/day for the 35 mm/yr net percolation and 0.10 g/m²/day for the 50 mm/day net percolation.

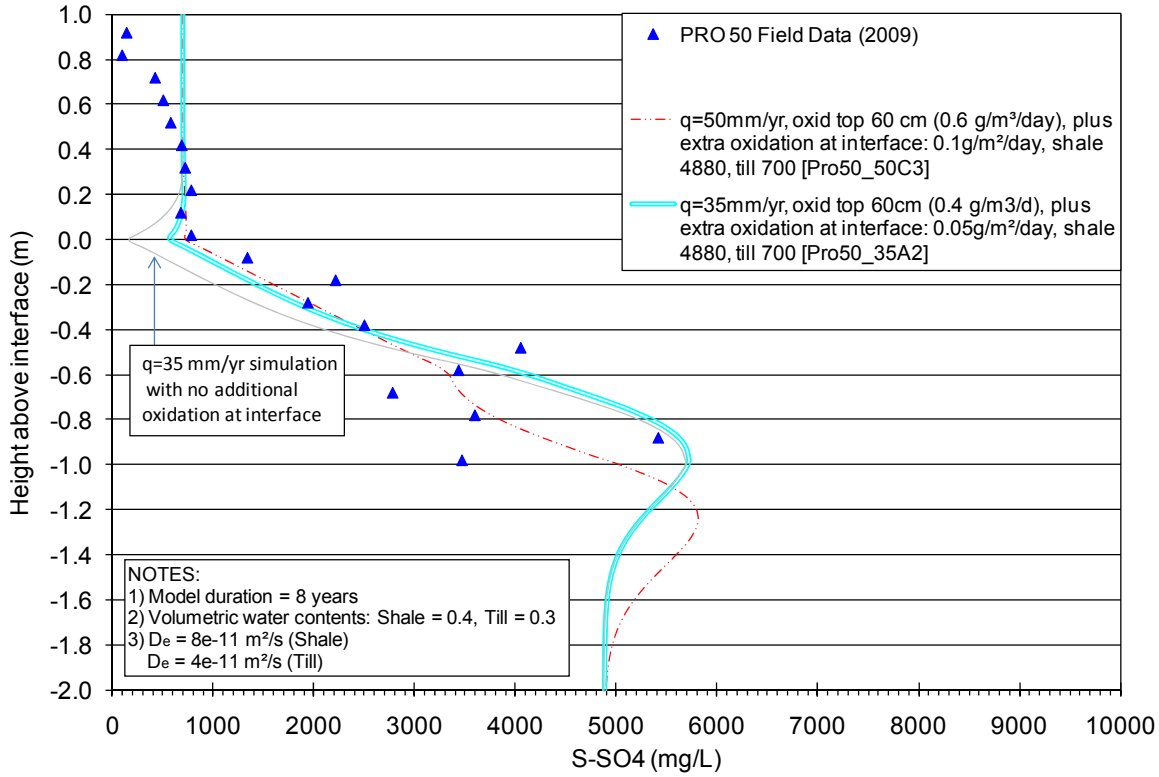

Figure 5.10: Simulated SO_4^{2-} profiles for Pro 50 plateau location.

In order to compare these oxidation rates to those of Nichol et al. (2006), the S-SO_4^{2-} production rates for the upper 0.6 m of the shale need to be converted into production rates per area. These production rates then need to be added to the additional shallow production added to the interface. Thus the oxidation rates are 0.29 g/m²/day and 0.46 g/m²/day for net percolation rates of 35 mm/yr and 50 mm/yr, respectively. Both of these values are in the upper range of the pyrite oxidation rates estimated by Nichol et al. (2006).

The results of the SO_4^{2-} transport modelling for the Pro 50 location are shown in Figure 5.11. The baseline S-SO_4^{2-} concentrations used for Pro 50 were also found to be suitable for Pro 52. These baseline concentrations were 700 mg/l for the till and 4900 mg/l for the shale.

The numerical model for Pro 52 utilized a two-stage oxidation zone, similar to the simulations for Pro 50. However, whereas Pro 50 required a concentrated addition of

SO_4^{2-} near the interface of the cover and shale, the upper oxidation zone for Pro 52 extended over the top 0.12 m of the shale. The required oxidation rate in this upper zone was 3.0 g/m³/day for q=35 mm/yr and 4.0 g/m³/day for q=50 mm/yr. The lower oxidation zone extended to a depth of 0.6 m below interface and had an oxidation rate of 0.3 g/m³/day for q=35 mm/yr and 0.6 g/m³/day for q=50 mm/yr. These oxidation rates are summarized in Table 5.2, including a conversion to the oxidation rate per area for the entire profile.

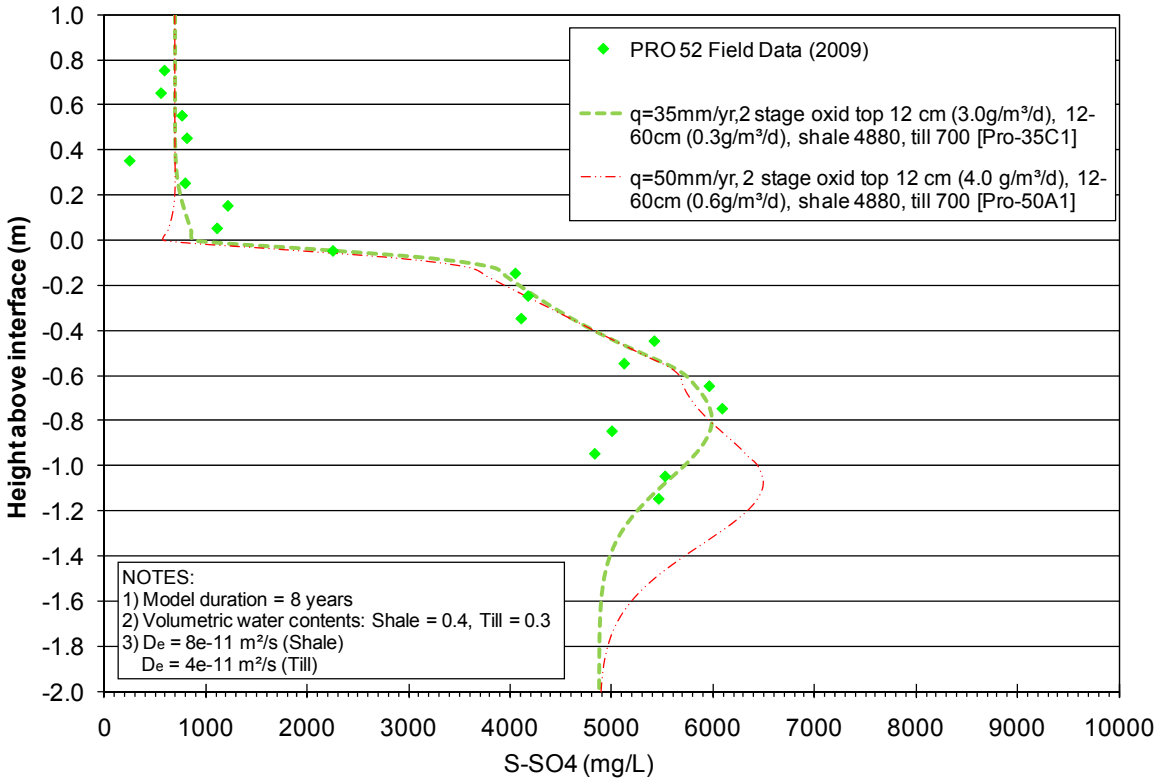

Figure 5.11: Simulated SO_4^{2-} profiles for Pro 52 plateau location.

Table 5.2: Estimated two-stage oxidation rates for Pro 52.

Net Percolation Rate	Upper Zone (top 0.12 m of shale) Oxidation Rate (g of S-SO_4^{2-}/m³/day)	Lower Zone (0.12 -0.6 m below interface) Oxidation Rate (g of S-SO_4^{2-}/m³/day)	Total Oxidation Rate per Landscape Surface Area (g of S-SO_4^{2-}/m²/day)
35 mm/yr	3.0	0.3	0.50
50 mm/yr	4.0	0.6	0.768

The simulated fit for q=35 mm/yr in Figure 5.11, appears to be better than that of q=50 mm/yr. In addition, the oxidation rate for q=35 mm/yr is more in line with the predictions of Nichol et al. (2006).

5.2.3 Sulphate Transport Model Results for D3 Slope

A total of 10 locations were drilled and sampled along the D3 slope in August 2008 as shown in Figure 3.8. Although each of the 10 profiles developed for these D3 sampling locations could have been used for model calibration, it was decided that only the five drillholes that correspond to stable isotope sampling locations would be used. These five locations (D3-2, 4, 5, 8 and 10) are distributed across the length of the D3 cover providing a good representation of the different topographic aspects from the toe of the slope to the crest. The $S\text{-}SO_4^{2-}$ concentration profiles for these five locations are shown in Figure 5.12.

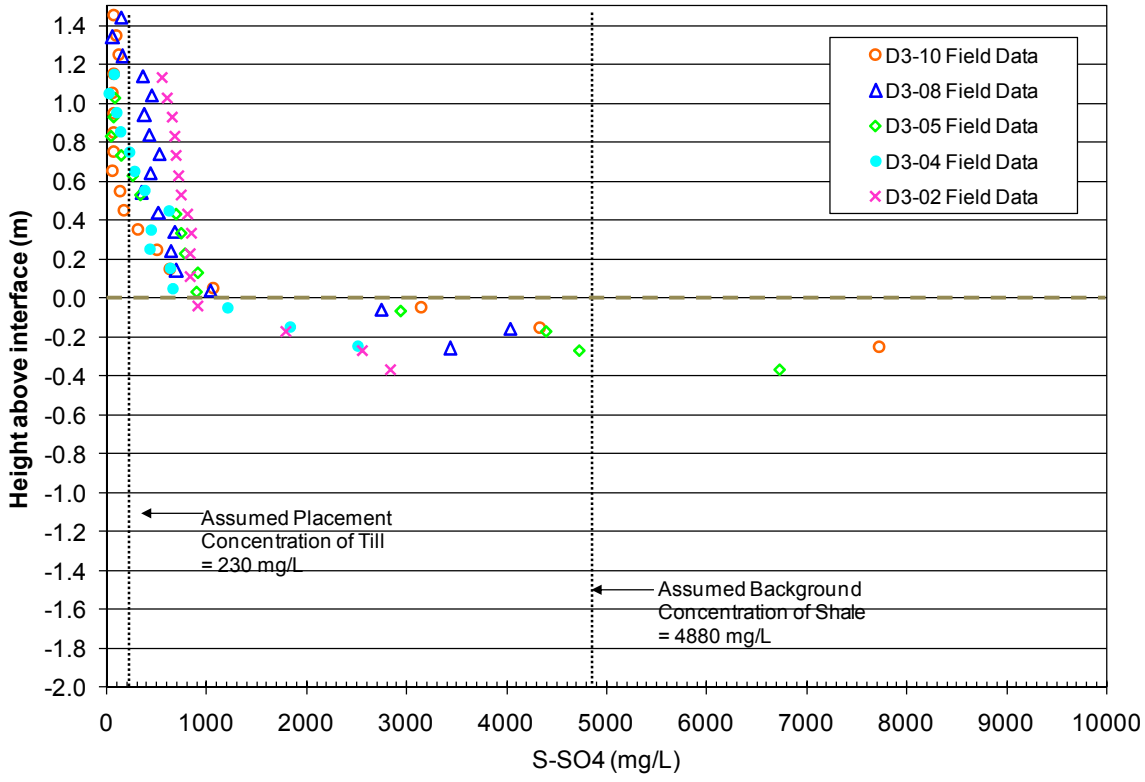

Figure 5.12: SO_4^{2-} profiles from D3 slope sampling locations from August 2008.

While the SO_4^{2-} profiles for the plateau locations extend to a maximum depth of 1.2 m below the cover-shale interface, the sampling drill holes from the D3 slope extended to a maximum of 0.4 m below the interface. The hole depths and sampling locations were selected to correspond with an earlier drilling and sampling program (Kessler 2007). This earlier drilling program was focussed on the till soil within the cover which justified the minimal drill hole penetration into the shale. During the 2008 drilling and sampling program, it was believed that the portion of the profiles in the cover would be the most important for modelling. The importance of extending these drill holes was not understood at that time. Unfortunately, this lack of profile depth makes it difficult to estimate local baseline concentrations in the shale and leads to inconclusive model results. Nonetheless, an attempt was made to produce reasonable simulations using the net percolation rates calculated from the stable isotope numerical modelling.

The molecular diffusion coefficient for the shale in the D3 slope model was left unchanged from the plateau model, at $D = 8x10^{-11}$ m²/s. Based on the stable isotope transport model results, this value seems to be representative for most D3 sample locations. Although it was expected that the till cover soil of the sloped D3 test plot would be drier on average than the plateau, a review of the water content sensor data for the site revealed no perceptible difference for the lower cover soil. Therefore, the molecular diffusion coefficient for the till was left at $4x10^{-11}$ m²/s. For each of the D3 sampling locations, the estimated net percolation rate or range of rates from the ^2H transport modelling was used in the SO_4^{2-} transport model. These net percolation rates are summarized in Table 5.1. As with the plateau simulations, the dispersivity was set to zero for the D3 slope simulations.

An additional element of the D3 slope model was the inclusion of interflow as a means of mass removal from the profile. This was accomplished using mass flux boundary nodes placed at the cover-shale interface. The interflow boundary condition removed SO_4^{2-} from the model at a fixed rate. To establish the rate of mass outflow from the profile by interflow, the D3 interflow collection system data were assessed. Historical measurements of SO_4^{2-} concentrations in the interflow water and recordings of

cumulative interflow volumes allowed the calculation of cumulative mass outflow from the system, as illustrated in Figure 4.11. Beginning in the spring of 2001 until the fall of 2009, the cumulative mass outflow from the D3 collection system was approximately $7x10^5$ g of SO_4^{2-} or $2.34x10^5$ g of $S\text{-}SO_4^{2-}$. Dividing this value by the number of years over which the data were recorded (9 years), and the area of the D3 test plot (10, 000 m²) returns an average annual interflow mass output of 2.6 g (of S)/m²/yr or $7.1x10^{-3}$ g (of S)/m²/day. Although Figure 4.11 and the work of Meiers et al. (2006) suggest that interflow volumes and, thus, mass removal are escalating with time, for the purposes of this study it has been assumed that the mass removal by interflow was constant over the model duration. Given the small mass removal rate by interflow relative to the mass production rate by pyrite oxidation and the uncertainty in this oxidation rate, the error in this assumption is considered negligible.

The oxidation rate and oxidation zone in the model were adjusted as required to match the field profiles and were then compared to the range of oxidation rates estimated by Nichol et al. (2006).

The simulated profiles for the five sampling locations on the D3 test plot are shown in Figures 5.13 to 5.17. The simulated profiles are for a model duration of 10 years (1999 – 2008) instead of the eight year model duration of the plateau, as the cover over the D3 slope was installed two years earlier than the cover on the plateau.

The net percolation rate for the D3-02 SO_4^{2-} transport model simulation was fixed at 8 mm/yr based on the results of the δ^2H transport model results. The baseline $S\text{-}SO_4^{2-}$ concentration in the till was set at 600 mg/l. The baseline $S\text{-}SO_4^{2-}$ concentration in the shale was varied for the two simulations shown in Figure 5.13 from 2500 to 4900 mg/l. The oxidation rate was also varied for the two simulations. With a baseline concentration of 4900 mg/l in the shale, the oxidation rate had to be set to zero in order to provide a reasonably good fit to the data. With the reduced baseline concentration of 2500 mg/l in the shale, the oxidation rate was set to 0.15 g/m³/day in the top 0.4 m of the shale. This equates to a $S\text{-}SO_4^{2-}$ production rate of 0.06 g/m²/day when considering the

oxidation rate per landscape surface area. This value is somewhat lower than the range of oxidation rates estimated by Nichol et al. (2006) but still appears to be reasonable.

The measured S-SO_4^{2-} profiles for D3-04 is quite similar in shape and magnitude to the D3-02 profile. The net percolation rate for the D3-02 simulation was set at 12 mm/yr. The baseline S-SO_4^{2-} concentration in the till was set at 300 mg/l. The baseline S-SO_4^{2-} concentration in the shale was varied for the two simulations shown in Figure 5.14 from 2500 to 4900 mg/l. The oxidation rate was set at 0.2 g/m³/day for the lower baseline concentration and 0.1 g/m³/day for the higher baseline concentration. The oxidation zone was the upper 0.4 m of shale for both of these simulations. These oxidation rates equate to 0.08 g/m²/day and 0.04 g/m²/day, respectively, when considering the S-SO_4^{2-} production per landscape area. Again these oxidation rates are lower than those predicted by Nichol et al. (2006).

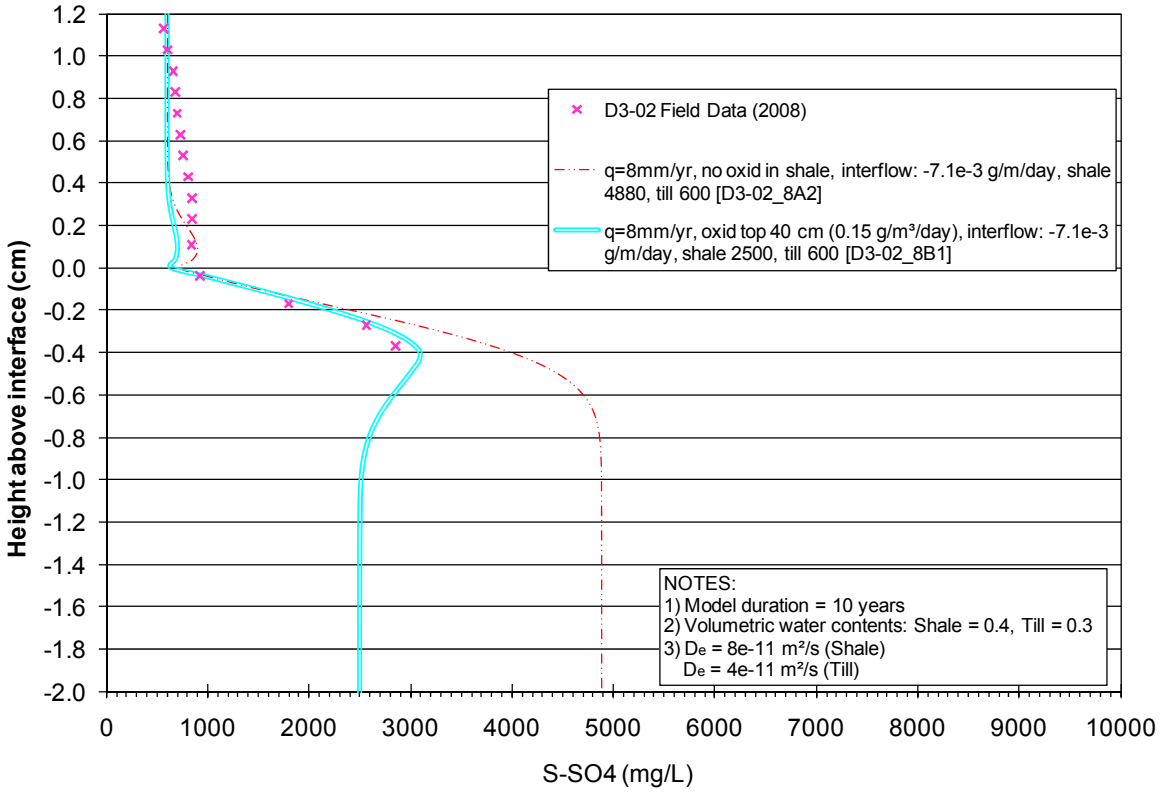

Figure 5.13: Simulated SO_4^{2-} profiles for D3-02 sampling location.

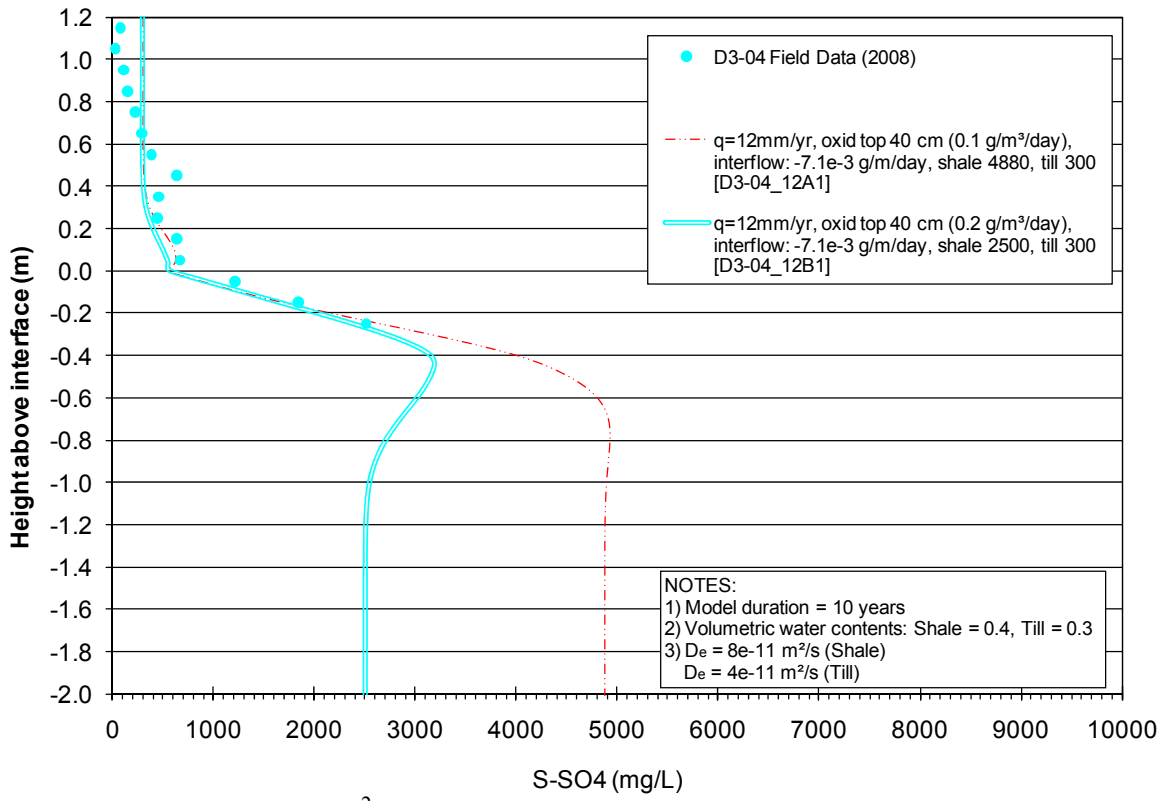

Figure 5.14: Simulated SO_4^{2-} profiles for D3-04 sampling location.

The calculated best-fit range of net percolation rates from the stable isotope transport model for D3-05 was 32 to 35 mm/yr. Therefore the simulations shown in Figure 5.15 feature a net percolation rate of 33 mm/yr, which is approximately in the middle of the calculated range. Similar to the plateau simulations with high net percolation rates, this resulted in a sharp decrease in concentration at the interface that led to a divergence from the measured profile. This is believed to be caused by inaccuracies in the simulated transport mechanisms within the lower till. A second simulation is shown without interflow mass removal at the interface which seems to better simulate the measured profile. The reduction or lack of interflow mass removal at D3-05 could be due to the bench that has formed in the surface topography and, presumably, the underlying shale surface. As discussed in Section 5.1.5, this flat topography likely allows a perched water table to persist longer which could be responsible for the higher than average net percolation rates. The benched topography may also affect the interflow mechanics. For example, if the shale surface is slightly back-sloped at this location, the interflow spill-over point could be above the interface.

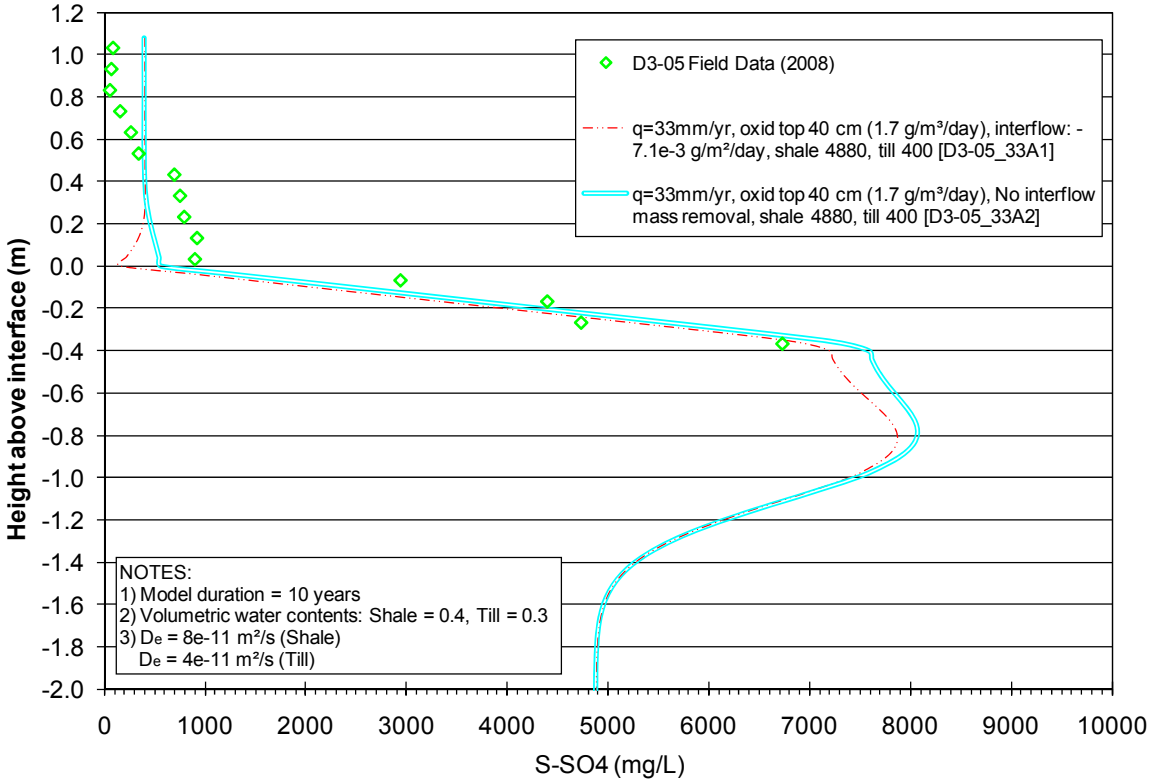

Figure 5.15: Simulated SO_4^{2-} profiles for D3-05 sampling location.

The oxidation rate for the D3-05 simulations was set at1.7 g/m³/day over the top 0.4 m of shale. This oxidation rate equates to 0.68 g/m²/day when considering the S-SO_4^{2-} production per landscape area. This oxidation rate is higher that the range of rates estimated by Nichol et al. (2006). It is not known why the oxidation rate in this location would be higher than average.

The results from the stable isotope transport model suggest that the net percolation rate for the D3-08 sampling location is between zero (diffusion only) and 12 mm/yr. These two bracketing values were simulated in the S-SO_4^{2-} transport model. The simulations for D3-08 are shown in Figure 5.16.

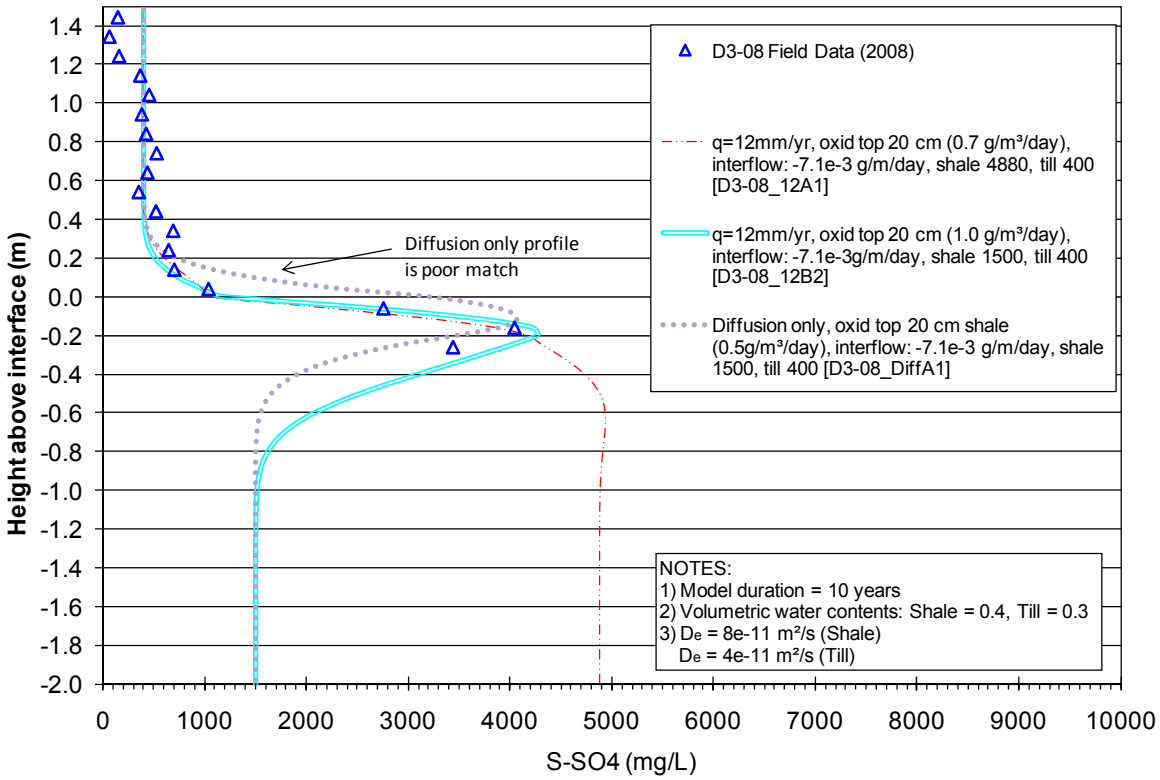

Figure 5.16: Simulated SO_4^{2-} profiles for D3-08 sampling location.

Due to the shallow penetration of the D3-08 sampling hole, it is not known if the deepest sampling point indicates a true concentration reduction or simply a spurious data point. Therefore the baseline concentration in the shale was modelled at both 1500 mg/l and 4900 mg/l. The simulated profile for a net percolation rate of zero (diffusion only) does not provide a good fit to the measured data points. Using a net percolation rate of 12 mm/yr the calculated range of oxidation rates is 0.7 to 1.0 g/m³/day over the top 0.2 m of shale. Converting these values to oxidation rates per landscape surface area results in 0.14 to 0.2 g/m²/day, which is considered reasonable based on the work of Nichol et al. (2006). However, the oxidation zone in the model comprises only the upper 20 cm of shale which is shallower than expected.

The stable isotope transport model results indicate that the net percolation rate at the D3-10 location is 8 mm/yr. Using this rate of 8 mm/yr in the SO_4^{2-} transport model, a reasonable fit was obtained as shown in Figure 5.17. The baseline concentration of the shale was set at 4900 mg/l. The pyrite oxidation zone was established as the top 0.36 m

of the shale and the oxidation rate was set at 0.8 g/m³/day. This equates to 0.29 g/m²/day, which is reasonable when compared to the estimates of Nichol et al (2006)

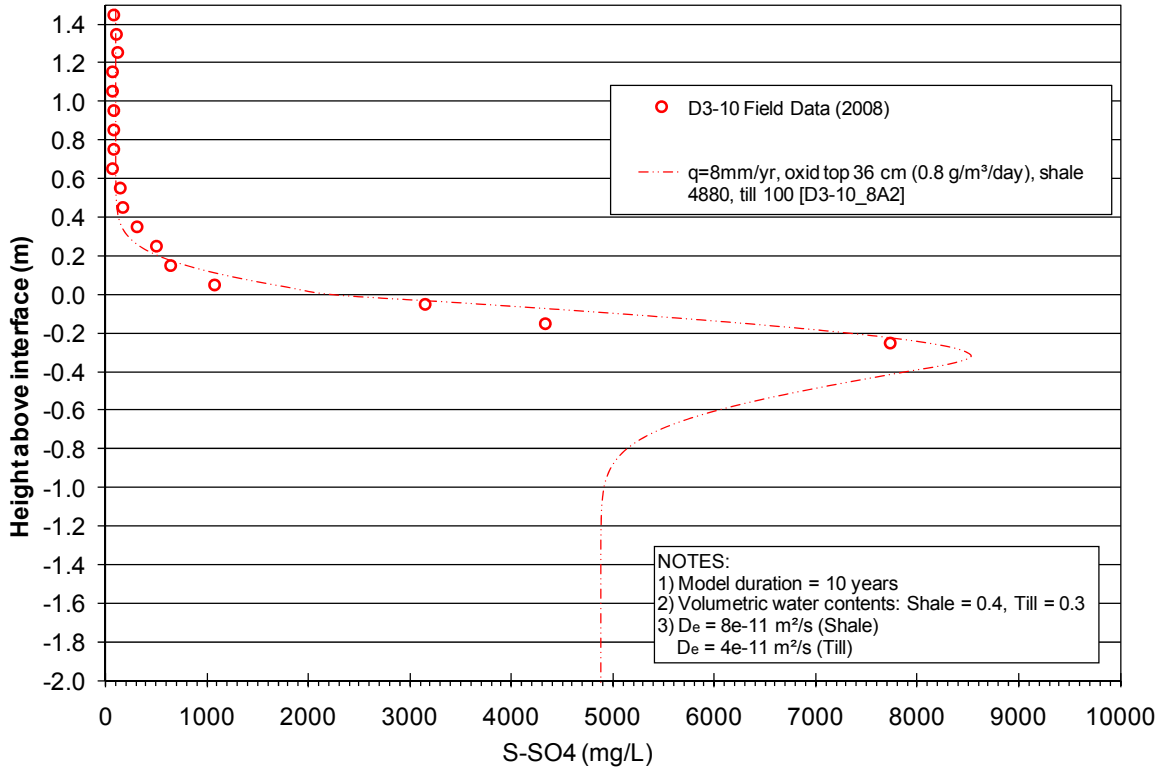

Figure 5.17: Simulated SO_4^{2-} profiles for D3-10 sampling location.

5.2.4 Accounting for Exposure Prior to Cover Placement

In addition to oxidation rates decreasing with depth, it is to be expected that the oxidation rate in the shale will decrease with time (Nichol et al. 2006). This is especially true if the oxidation rate is significant relative to the reservoir of available pyrite. This relationship between oxidation rate and time was not specifically investigated in this study. Instead, it should be assumed that the oxidation rates reported in this study are average values over the duration of the model simulation. In addition, the model simulations up to this point have considered only the time period after cover placement until the time of sampling (i.e. 8 years for the plateau, 10 years for the D3 test plot). Nichol et al. (2006) state that the shale overburden from the plateau area was likely exposed to air for 3 to 5 years prior to cover placement, while the D3 test plot was likely exposed for 6 months to 3 years. This potentially significant and sudden change in the

oxidation rate was investigated using the D3-10 sampling location as an example. A model simulation was conducted using an increased initial concentration just below the interface to simulate the higher concentrations that would arise due to oxidation of exposed shale and the results are shown in Figure 5.18.

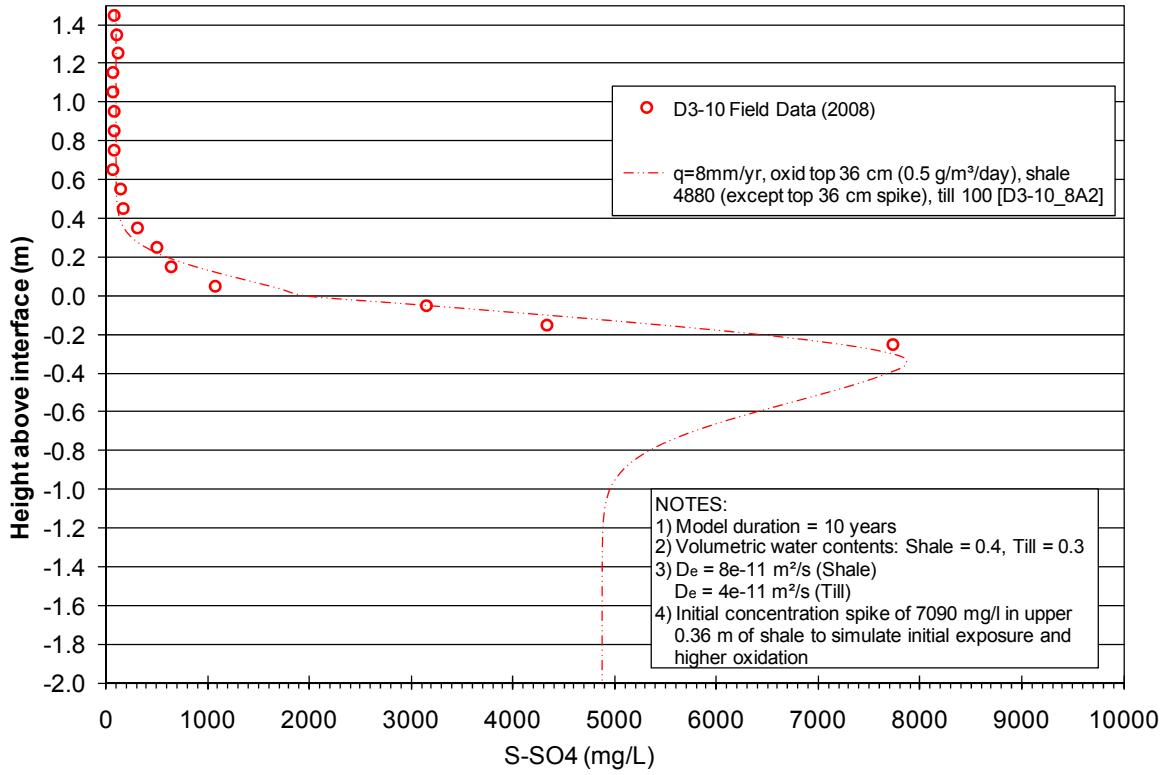

Figure 5.18: Simulated SO_4^{2-} profiles for D3-10 with initial concentration spike in upper shale.

It was assumed that the shale D3-10 was exposed for two years prior to cover placement. The baseline concentrations of the till and shale were set at 100 mg/l and 4900 mg/l, respectively. A concentration spike was simulated in the top 36 cm of shale. Based on the work of Nichol et al. (2006) it was assumed that the oxidation rate for this exposure period was 0.48 g/m²/day of $S\text{-}SO_4^{2-}$ which equates to 1.33 g/m³/day in the top 36 cm of shale. To simplify the model, it was assumed that the sulphate produced by oxidation accumulated in the upper 36 cm of shale with negligible transport by advection or diffusion. This equates to an additional 2190 mg/l of $S\text{-}SO_4^{2-}$ in the top 40 cm of shale. Therefore the spiked concentration in the upper 40 cm in the model was set at 7090

mg/l. With a net percolation rate of 8 mm/yr, and a post-cover oxidation rate of 0.5 g/m³/day of $S\text{-}SO_4^{2-}$, this simulation provided a reasonable fit to the measured concentration profile. As expected, this oxidation rate of 0.5 g/m³/day is lower than the originally calculated value of 0.8 g/m³/day.

This suggests that, while the simulations shown in Figures 5.10 to 5.17 did not account for the potential oxidation prior to cover placement, this early oxidation might have been important and would certainly affect the calculated post-cover-placement oxidation rate. Therefore, the oxidation rates calculated from Figures 5.10 to 5.17 are likely inaccurate as they are inadvertently accounting for this early oxidation. Thus, the oxidation rates calculated in this study cannot be extrapolated indefinitely into the future for prediction purposes.

5.2.5 Summary of Sulphate Transport Model Results

The simulated sulphate profiles from this study were assessed for goodness of fit based on visual interpretation only. It was apparent that the simple transport model used for this study was less effective at modelling salt transport processes in the cover soil than in the shale. Therefore, the goodness of fit of the simulated profiles to the measured data points was evaluated primarily for the shale. While visual interpretation introduces human judgement as a potential source of error, that same human judgement is necessary to omit measured spurious data points, which may be caused by heterogeneity in the soil, sampling error or testing errors.

Some of the model parameters used to generate the best fitting simulated profiles for each of the sampling locations are summarized in Table 5.3. It should be noted that the molecular diffusion coefficient used for all model simulations was 8×10^{-11} m²/s for the shale and 4×10^{-11} m²/s for the till. The volumetric water contents used were 0.4 for the shale and 0.3 for the till. The net percolation rates used in the simulations were the same as those estimated from the stable isotope modelling.

Table 5.3: Summary of estimated model parameters from sulphate transport model.

Sample Location	Net percolation, "q" (mm/yr)	Oxidation zone depth (cm below interface)	Oxidation rate per landscape surface area (g/m²/day of $S\text{-}SO_4^{2-}$)	Baseline $S\text{-}SO_4^{2-}$ concentration in shale (mg/l)
Pro 50	35	60	0.29	4900
	50	60	0.46	4900
Pro 52	35	60	0.50	4900
	50	60	0.77	4900
D3-02	8	0	0	4900
	8	40	0.06	2500
D3-04	12	40	0.04	4900
	12	40	0.08	2500
D3-05	33	40	0.68	4900
D3-08	12	20	0.14	4900
	12	20	0.20	1500
D3-10	8	36	0.29	4900

The results from the salt transport modelling are generally in agreement with those of the stable isotope transport modelling. For the plateau locations, simulations were conducted with high net percolation rates (35 – 50 mm/yr) that fit the measured data reasonably well. The net percolation rates for the D3 sampling locations were unchanged from the rates estimated from the stable isotope transport model.

The oxidation rates used in these simulations are generally within the range of values estimated by Nichol et al. (2006). It is interesting to note that the highest oxidation rates in the model are required for the simulations with the highest net percolation rates. This seems counter-intuitive as one might expect that the higher net percolation rates occur in the locations where the cover stays saturated longer. These locations should have a reduced exposure to atmospheric oxygen with consequently lower pyrite oxidation rates.

One possible explanation is that the higher net percolation rates may be due to increased hydraulic conductivity within the shale in these locations. This increase in hydraulic conductivity could be caused by a localized increase in macroporosity or by heterogeneity in the shale matrix. This higher hydraulic conductivity might allow the shale to drain faster, promoting desaturation and thus allowing more exposure to gaseous oxygen. However, a more likely explanation is that the increased $S\text{-}SO_4^{2-}$ production in locations of higher net percolation is due to increased gypsum dissolution. The model is unable to differentiate between the $S\text{-}SO_4^{2-}$ derived from gypsum dissolution and $S\text{-}SO_4^{2-}$ derived from pyrite oxidation.

The oxidation rates summarized in Table 5.3 are presented as the oxidation per landscape surface area, which is useful when considering the amount of oxygen that must transfer through a 1 m² horizontal plane in order to cause the predicted amount of pyrite oxidation. The pyrite oxidation process, described by Wall (2005), utilizes 1.875 moles of O_2 for every mole of SO_4^{2-} produced. Therefore, the oxidation rates presented in Table 5.3 must be converted to molar rates and multiplied by 1.875 to determine the required rate of oxygen transfer through the soil column. For example, the highest estimated oxidation rate in Table 5.3 was an oxidation rate of 0.77 g/m²/day of $S\text{-}SO_4^{2-}$ which equates to 0.024 mol/m²/day of $S\text{-}SO_4^{2-}$. This would require an O_2 flux of 0.045 mol/m²/day or 1.44 g/m²/day. Using measured concentration gradients of O_2 gas in the soil profile and Fick's First Law, Wall (2005), estimated O_2 gas fluxes ranging from 0.03 to 0.16 moles/m²/day. Therefore, the estimated oxidation rates in Table 5.3 are generally lower than the range of oxidation rates reported by Wall. This could be due to the fact that Wall's measurements were obtained in 2002, approximately 6 years earlier than the measurements from this study. The oxidation rates estimated from this study are averages over the 8-10 years of the model duration.

Another consideration for pyrite oxidation rates is the mass of pyrite in the shale available for oxidation and how quickly this reservoir is depleted at the estimated oxidation rates. For this calculation, one must consider the bulk oxidation rate, not the oxidation rate per landscape surface area as summarized in Table 5.3. Bulk oxidation

rates are detailed in the legends of Figures 5.10 to 5.17. These rates vary from less than 0.1 g/m³/day to as high as 3.0 g/m³/day. Nichol et al. (2006) estimated that the shale contains an average of 3.7 g/kg of unoxidized sulphur (e.g. pyrite and organosulphur) and 1.8 g/kg of sulphur as gypsum. Because the model is unable to differentiate between dissolution of gypsum and oxidation of pyrite as sources of dissolved S-SO_4^{2-}, both sources must be considered. Using a dry density of 1500 kg/m³, there would be approximately 8250 g/m³ of sulphur as gypsum and pyrite that could contribute to sulphate production. For each of the estimated oxidation rates, the time required for complete depletion of gypsum and pyrite within the assumed oxidation zone (see Table 5.3) was calculated and is summarized in Table 5.4.

Table 5.4: Time required for depletion of pyrite and gypsum.

Sample Location	Net percolation, "q" (mm/yr)	Volumetric oxidation rate (g/m³/day of S-SO_4^{2-})	Time required for depletion of pyrite and gypsum (years)
Pro 50	35	0.6	38
	50	0.4	57
Pro 52	35	Top 0-12 cm: 3.0 Btm 12-60 cm: 0.3	Top: 7.5 Btm: 75
	50	Top 0-12 cm: 4.0 Btm 12-72 cm: 0.6	Top: 5.7 Btm: 38
D3-02 (shale baseline= 2500 mg/l)	8	0.15	151
D3-04 (shale baseline= 4900 mg/l)	12	0.1	226
D3-04 (shale baseline= 2500 mg/l)	12	0.2	113
D3-05	33	1.7	13
D3-08 (shale baseline= 4900 mg/l)	12	0.7	32
D3-08 (shale baseline= 1500 mg/l)	12	1.0	23
D3-10	8	0.8	28

Of special note in Table 5.4 are the estimated depletion times for Pro 52 which are less than 10 years for the upper oxidation zone. Because the model duration is 10 years, it would appear that these simulations are not applicable; however, it is also possible that

the pyrite or gypsum concentrations at these locations are higher than average. The estimated time to depletion for D3-05 is also quite short at 13 years.

It should be noted that the time for depletion of pyrite and gypsum summarized in Table 5.4 only applies to the oxidation zone in the model. This does not suggest that the shale will cease to produce SO_4^{2-} after this time. However, the rate of oxidation will decrease as the oxidation zone extends deeper.

5.3 Discussion of Numerical Model Results

From the analysis and modelling of stable isotopes, the molecular diffusion coefficient and net percolation rates were estimated for individual sampling locations. The estimated molecular diffusion coefficients are generally between $5x10^{-11}$ and $1.5x10^{-10}$ m²/s. An approximate average value of $8x10^{-11}$ m²/s has been adopted for both the plateau and D3 sample locations. The estimated net percolation rates vary considerably between the plateau and the sloping D3 test plot. Estimated net percolation rates for the plateau are in the range of 35-50 mm/yr, while those of the D3 slope are generally closer to 10 mm/yr. One D3 sampling location on a flat bench at mid-slope (D3-05) has a higher estimated net percolation rate at between 32-35 mm/yr.

The higher net percolation rates for the plateau and, to a lesser extent, the D3-05 mid-slope bench are believed to be caused by a perched water table that persists longer in these locations. It is noted that, with the exception of D3-05, the calculated net percolation rate for the D3 slope are consistent at approximately 8-10 mm/yr. It had been expected that lower slope locations might have higher net percolation rates due to more persistent water tables and greater cover soil moisture. In particular, the sampling location D3-02, which is located on the flat portion of the toe of the slope was expected to have a higher calculated net percolation rate than upper slope locations. In fact, the net percolation rate at D3-02 appears to be one of the lowest of the locations sampled.

It is noted that the stable isotope profile for the D3-02 sample location is the most complex of the measured profiles due to an unusual 2-stage enrichment bulge. This

bulge is attributed to the presence of considerable amounts of glacial till mixed in with the shale. Simulation of this profile was accomplished by making assumptions on the initial δ^2H signature of the profile below the cover-shale interface. If these assumptions were erroneous, the calculated net percolation rate would also be inaccurate. Similar, albeit less complicated, δ^2H enrichment bulges were also noted for D3-04 and D3-08. Again, the accuracy of the calculated net percolation rates at these locations is dependent on the assumptions made to explain the enrichment bulges.

The molecular diffusion coefficients and net percolation rates from the stable isotope model results were incorporated into the SO_4^{2-} transport model. The pyrite oxidation rate (production of $S\text{-}SO_4^{2-}$) and oxidation zone were manipulated to achieve reasonable fits to the measured data. In general, the estimated oxidation rates were within a range of expected values reported by Nichol et al. (2006). In some cases it was also necessary to adjust the baseline $S\text{-}SO_4^{2-}$ concentration in the till and/or shale. However, the range of potential $S\text{-}SO_4^{2-}$ concentrations in the till and shale, reported by Nichol et al. (2006) and Kessler (2007) do not suggest an absolute baseline concentration. Therefore, adjustments of the initial concentrations in the model are considered acceptable and should be expected given the heterogeneity within the overburden waste of the SBH waste dump (Chapman 2008).

The calculated pyrite oxidation rates for the plateau region of the SBH are within a range of 0.29 – 0.77 g of $S\text{-}SO_4^{2-}$ produced per day per m² of ground surface area. The calculated oxidation rates for the D3 slope locations, excluding D3-05, are between 0-0.29 g/day/m². The calculated oxidation rate for D3-05 is 0.68 g/day/m².

It is noted that the estimated $S\text{-}SO_4^{2-}$ production rates for the D3 slope tend to be greater for the upper slope locations and reduced for the lower slope locations. It is, therefore, not surprising to note from the soil salinity profiles measured in this study and from the work of Kessler (2007) that the upper slope locations tend to have higher overall salinity.

5.4 Sources of Error in Study

5.4.1 "Pincushion Effect" of Frequent Sampling

In most locations on the plateau and D3 slope, only two sets of soil samples have been collected. However, in some locations along the D3 slope, sampling was performed in 2002, 2005, 2007, and 2008. In addition, if drilling refusal was encountered prior to reaching the target depth, the hole was abandoned and redrilled in close proximity. Thus, in some locations, it is estimated that there could be as many as 6 drill holes. Each of these drillholes was approximately 80 mm in diameter. The majority of the auger cuttings from these drill holes were retained for soil samples. This left little material for backfilling the holes. Bentonite chips are often used in geological drill programs to backfill holes, but for this site, it was believed that the high sodium concentration of the bentonite could affect the soil chemistry for future sampling and testing. Therefore, holes were only backfilled with available cuttings which was often insufficient for complete backfilling.

Each of these open or partially open drill holes acts as a conduit that allows infiltration into the cover and percolation into the shale. It might be argued, with good reason, that the radial extent of this effect would be limited by the low hydraulic conductivity of the till and shale. However, if a sample collection hole is inadvertently drilled in very near proximity to a previous hole, it may well fall within the affected radius. Therefore the simulated net percolation rates calculated in this study might be slightly higher than the true net percolation rates in undisturbed ground.

Or alternatively, if the majority of water is infiltrating through previously drilled holes, this might have reduced the volume of water infiltrating through the porous media where the most recent sampling was conducted. This would result in predicted net percolation rates that are lower than the true average for the local region around the sample location.

5.4.2 Post-collection Oxidation of Soil Samples

The soil sampling methodology undertaken for this study as well as the sample collection work by Kessler in 2002 and 2004 did not ensure anoxic conditions for soil samples after collection. Therefore, the sampling procedure would have increased the exposure to oxygen and allowed additional oxidation of pyrite to occur prior to testing of the samples.

During the drilling programs, samples were recovered from the hand auger and placed into plastic soil sampling bags that were twisted shut and wrapped with electrical tape. This first bag was then placed in a second bag, which was sealed in the same manner. This bagging arrangement would have minimized air transfer but it is acknowledged that the bags were not completely air tight. The airspace in these bags was intentionally kept low to permit easier packing, but the bags were not evacuated of air. The samples collected in 2008 and 2009 were tested within 7-10 days of collection.

Previous attempts have been made to obtain anoxic soil samples from the SBH study site. Wall (2005) collected one set of anoxic samples and one set of samples using standard collection procedures. However, difficulties in the collection procedure led to issues with quality assurance. The data from this sample set were considered unreliable by other researchers (Nichol et al. 2006) and were not included in subsequent analyses. Therefore, it was determined that standard sample collection procedures should be followed to avoid similar problems.

5.4.3 Gypsum Precipitation and Dissolution

Gypsum precipitation and dissolution is believed to be occurring in the shale, but primarily in the zone of oxidation where sulphate production is occurring. The effect with respect to sulphate concentrations in the salt transport model would be a simulated oxidation rate that is lower or higher than the true oxidation rate. In other words, the model would misinterpret the dissolution or precipitation as a difference in the sulphate production by pyrite oxidation, but this should not significantly affect other transport parameters.

6. CONCLUSIONS AND RECOMMENDATIONS

6.1 Conclusions

The global objective of this study was to improve the understanding of the salt and moisture dynamics for the SBH instrumented watershed. Principally, this meant developing better estimates for net percolation rates through the cover soil and into the underlying shale for various topographic locations on the study site. This objective was achieved in this study by means of a rigorous sampling, testing and numerical modelling program that used both stable isotopes of water and major ion chemistry as tracers in the system.

This study showed that net percolation of precipitation is occurring through the cover soil and into the underlying saline-sodic overburden waste. While net percolation was calculated to be occurring throughout the study site, the highest rates are estimated to be occurring on the plateau and a mid-slope bench. This is not unexpected as these locations have the flattest topography and most persistent perched water tables. The net percolation is opposing the upward diffusion of salts from the shale into the cover. Comparison of salinity profiles collected several years apart indicates that, in some locations, the downward advection of salts by net percolation is likely causing a decrease in salinity in the cover and upper shale.

The numerical modelling results suggested that SO_4^{2-} production is occurring at various rates in the upper shale, throughout the SBH study site. This SO_4^{2-} production is primarily attributed to pyrite oxidation. The highest oxidation rates were calculated for the plateau and mid-slope bench. This was unexpected as these locations are believed to remain saturated longer than other areas and thus should have lower oxidation rates. The higher calculated oxidation rates in these areas may be due to gypsum dissolution which is not distinguished from pyrite oxidation in the model. The model results also showed that the mass removal from the cover-shale interface by interflow is much less than the calculated SO_4^{2-} production rates at these locations. Therefore, the SO_4^{2-} transport model

results suggest that net percolation is the dominant salt flushing mechanism across the site (both plateau and sloped areas) for estimated average net percolation rates of 8 mm/yr and greater. Although salt flushing by interflow is less than flushing by net percolation, mass transport by interflow remains an important component of the salt mass budget for the site, particularly because interflow is typically discharged to surface water courses and water bodies and may accumulate in wetland areas.

This study has shown that stable isotopes of water are an effective means of estimating contaminant transport parameters in geochemically complex systems. These conservative tracers allow researchers to overcome numerical model challenges such as estimating adsorption and geochemical reaction rates. However, greater confidence in this method of analysis would have been achieved had there been a better understanding of initial conditions in the shale and cover soil at the time of construction. Ideally, a set of soil samples would have been collected immediately after construction which would provide the baseline concentrations. This would have eliminated the need for estimating baseline concentrations and for guessing the cause of unexpected concentration variations.

6.2 Specific achievements

Through the completion of this study, several important achievements have been made. This section of the report summarizes these achievements.

6.2.1 Calculated Range of Net Percolation Rates

The results of the δ^2H transport numerical model have provided a range of net percolation rates for various topographic locations within the study site. These net percolation rates in relation to their topographic position are summarized in Table 6.1.

Table 6.1: Summary of calculated net percolation rate vs topographic location.

Topographic Location	Sample Locations	Range of net percolation rates (mm/yr)
Plateau	Pro 50, Pro 52, Pro 54	35 - 50
Upper Slope	D3-08, D3-10	0 - 12
Mid-slope Bench	D3-05	32 - 35
Lower Slope	D3-02, D3-04	8 - 12

6.2.2 Calculated Pyrite Oxidation Rates

By incorporating the calculated net percolation rates from the δ^2H transport model into the SO_4^{2-} transport model, the oxidation zone and rate was adjusted in the model to obtain reasonable fits to the measured profiles. The oxidation rates and zone depths are summarized in Table 6.2. Oxidation rates are presented as g of $S\text{-}SO_4^{2-}$ per m^2 of cover per day.

Table 6.2: Summary of calculated oxidation rates and zones vs topographic location.

Topographic Location	Sample Locations	Calculated oxidation rates (g of $S\text{-}SO_4^{2-}/m^2/day$)	Calculated Oxidation Zone Depth (m)
Plateau	Pro 50, Pro 52, Pro 54	0.29 – 0.77	0.60
Upper Slope	D3-08, D3-10	0.14 – 0.29	0.20 – 0.36
Mid-slope Bench	D3-05	0.68	0.40
Lower Slope	D3-02, D3-04	0 – 0.08	0 – 0.40

6.2.3 Procedure for Obtaining Shallow Isotopic Profiles through Reclamation Covers

The procedure developed for obtaining isotopic profiles in the SBH reclamation cover was developed with assistance from, and based on the past experience of researchers at the University of Saskatchewan, led by Dr. M.J. Hendry. Although the sampling and test

procedures were not flawless and in some areas can be improved upon, the procedures did provide a defendable collection of isotopic data.

The technologies and techniques employed for sample collection are simple and readily available through drilling contractors. One of the primary challenges for sample collection was how to mobilize drilling equipment on to the site without damaging the sensitive vegetation or compacting the cover soil. To this end, it was determined that a smaller tracked drill rig would be used in the winter after the soil cover had completely frozen. The second challenge was how to obtain soil samples without affecting the pore water in the samples or cross contaminating samples. This led to a decision to use a dry core or pushed core technique. This could have been accomplished with thin-walled Shelby tubes but was achieved reasonably well in this study using a split-spoon sampler.

Another challenge was to ensure that samples were not exposed to external sources which might affect the isotopic content of the pore water. Examples of this include evaporation of water from the sample or equilibration with atmospheric water vapour. This challenge was achieved by double sealing samples in readily available Ziplock bags and storing the samples in insulated coolers.

The direct equilibration stable isotope testing is the one aspect of the overall procedure that requires specialized equipment and expertise. However, the soil samples collected can be easily transported to equipped laboratories by normal transport routes without affecting the isotope content

6.2.4 LMWL developed for SBH site

A basic requirement for any study involving stable isotopes of water is to obtain a LMWL for the study site. For this study, the LMWL was needed for comparisons to the isotopic signatures of the soil, groundwater, and interflow samples. A review of relevant literature did not turn up any results for LMWLs developed for the Athabasca region of Alberta. The closest LMWLs to the study site were from Edmonton, Alberta and Fort Smith, Northwest Territories.

The LMWL for the SBH study site was developed by obtaining precipitation samples from the site during the spring, summer and fall of 2008, and submitting them to the NWRI laboratory in Saskatoon for analysis of δ^2H and $\delta^{18}O$. Snow samples collected from sited during the annual snowpack measurement of the 2007/08 winter were also submitted for testing. In addition, these data were supplemented with isotopic test results of rain and snow samples collected during 2005.

The LMWL developed from the 2005 and 2009 data from the SBH site is:

$$\delta^2H = 6.68\ \delta^{18}O - 26.5$$

6.3 Opportunities for Future Research

6.3.1 Application of Results to 2D or 3D Numerical Transport Model

The results from the 1D contaminant transport model in this study have provided some improved estimates of net percolation through the SBH cover for various topographic locations from the plateau down to the toe of the slope. In addition, the model results have provided new estimates of molecular diffusion coefficients for δ^2H and SO42-. However, these net percolation rates have not yet been incorporated into a 2D or 3D numerical transport model. It is suggested that a revised 2D transport model could be created by building upon the model of Kelln (2008).

6.3.2 Extension of Procedures to Other Sites

The procedures to develop and utilize isotopic profiles for this study could be applied to other reclaimed landscapes to obtain a better understanding of the water and contaminant transport mechanisms including evaporation, net percolation and molecular diffusion. Examples of reclaimed landscapes that might benefit from the use of isotopic profiling include reclaimed coarse and fine tailings piles in the Athabasca region.

6.3.3 Long-term LMWL for Athabasca Oil Sands Region

The development of a LMWL for the SBH study site was a necessary objective for this research and was done using the all of the data available at the time. However, it is recommended that precipitation samples should continue to be collected and measured for δ^2H and $^{\delta 18}O$ over a much longer period of time (e.g. 10 to 20 years) to provide a better representation of the LMWL at the SBH study site. The data collected for this study provide an important base for future measurements.

6.4 Specific Improvements for Similar Studies

6.4.1 Improvements in Soil Sample Collection Methodology

The challenges experienced during the stable isotope soil sampling program were described in Section 3.1.5. The sampling method used in December 2008 resulted in sample compression and core loss. This led to a decreased confidence in the depths from which samples were recovered and, therefore, less confidence in the depth of samples. It is suggested that for future stable isotope soil sampling programs, sampling should be done using thin-walled Shelby tubes, as a minimum. It may even be necessary to use a sonic or vibratory casing advancement rig to in order to obtain complete samples.

6.4.2 Development of Additional Stable Isotope Profiles

In order to further develop stable isotope profiling as a means of characterizing salt and moisture dynamics in reclaimed landscapes, industry and academia would benefit from an improved understanding of the seasonal variability of stable isotope contents in soils. For the SBH site, this could be achieved by collecting soil samples at previously sampled locations during spring and summer.

During the spring and summer, it would be impossible to access the drilling locations with a wheeled or tracked drill rig without causing damage to the vegetation and compaction of the cover soil. On the other hand, hand-augering is believed to cause too much smearing and mixing of soil samples allowing cross contamination and making it difficult to obtain discrete samples. Therefore, collection of samples would have to be

achieved using man-powered coring devices. It is not known whether these devices would be able to achieve the required penetration depth of at least 3 m for the plateau and D3 areas that is necessary to obtain complete isotopic profiles.

6.4.3 Establishing Baseline Stable Isotope Profiles for Other Study Sites

As mentioned earlier, the current study would have benefited with an improved understanding of the baseline stable isotope contents of the till and shale. This could have been achieved by conducting a soil sampling program in the first year after construction of the cover, and prior to vegetation of the site. While it is no longer possible to obtain these baseline concentrations for the SBH site, it is recommended that researchers studying other similar constructed reclamation landscapes should develop isotopic profiles immediately after construction.

6.4.4 Isotopic Profiling Using Water Vapour

The same principles that allow direct equilibration testing for the stable water isotopes in soil samples in the laboratory could be relied upon for direct testing of pore gas through a soil profile. Provided that the soil is not fully saturated, a sample of pore gas could be withdrawn from discrete depths through the cover and shale overburden using pore gas sampling tubes. The pore gas samples could be tested in a laboratory where the δ^2H and $\delta^{18}O$ could be measured for the water vapour and then, using known fractionation factors, the isotopic content of the pore water could be calculated.

A total of 87 gas probes were installed in 13 drill holes across the SBH site between 2000 and 2004. Most of these instrumented bore holes are between 2 m and 4 m deep but one instrumentation location on the plateau extends to 25 m depth. Installation details are described by Wall (2005). It is currently not known how many of the existing gas probes remain serviceable. Sampling was last performed in 2006 with indications that up to 20% of the probes may be leaking (unpublished data). Despite this, the gas probes provide the potential for additional stable isotope profiles that can be obtained quicker and at less expense than collection of soil samples.

Pore gas samples should be collected each day for at least 3 days to ascertain whether the pore gas is in equilibrium. A diffusive or advective gas flux could cause an imbalance between the pore water and pore vapour isotopic signatures which might be identified by fluctuating δ^2H and $\delta^{18}O$ values. OKC are currently studying the sampling and testing procedure to identify potential challenges in this methodology (Tyler Birkham, personal communication, 08 April 2010).

6.4.5 Laboratory Modelling of Mechanical Dispersion

In the field of contaminant hydrogeology, there is an apparent lack of understanding about the process of mechanical dispersion when advection and molecular diffusion act in opposite directions. As a result, in this study the coefficient of molecular diffusion could not be regarded independently of mechanical dispersion for the salt transport model and, therefore, the coefficient of hydrodynamic dispersion was presented. It is recommended that a column experiment be performed in a laboratory setting to address this issue.

As an initial experiment, the porous media used for this study need not be the same soil material from the SBH site. For example, a fine grained sand may be easier to work with for this column study. For all tests, the soil should be kept at the same density or level of compaction. For simplicity, it is recommended that the soil be maintained under saturated conditions; however, future variations of this lab experiment may be used to investigate unsaturated soil conditions.

A molecular diffusion coefficient should first be established for the saturated soil for the tracer that is to be used. It is suggested that Cl- could be used as a tracer as it is conservative but more easily measured than stable isotopes. The molecular diffusion coefficient can be measured using a variety of methods described by Shackelford (1991) including double reservoir methods, column testing, or the half-cell method. Another alternative is to use the radial diffusion method described by van der Kamp et. al. (1996).

The next step would be to evaluate the longitudinal mechanical dispersivity for the soil in the column. The pore water of the soil column would have an initial zero concentration and the injected fluid would have a known concentration. The breakthrough curve would be plotted for the column. As the molecular diffusion coefficient is known, the mechanical dispersion effect could be distinguished and the longitudinal dispersivity could be calculated. This phase of testing might be accomplished using a double reservoir setup as described by Shackelford (1991) and illustrated in Figure 6.1a.

The final stage of testing would be to set up the column with a concentration gradient that opposes the flow direction. For example, if the double reservoir method is used as described by Shackelford (1991), then the receiving or effluent reservoir would contain the initial spike of Cl- while the influent water and reservoir would have no Cl-, as illustrated in Figure 6.1b. Breakthrough would be measured at the influent side of the column unlike a standard double reservoir test. Another variation to the test would be the addition of Cl- to the effluent reservoir with some means of mixing. The reservoir could then be maintained at a constant concentration, providing a constant gradient across the soil column. This would simplify the analysis of the test. The concentration of the effluent reservoir should be made very high to maximize the concentration gradient. The flow rate through the column could be varied for different tests but should be initially kept as low as possible to increase the speed of diffusive breakthrough.

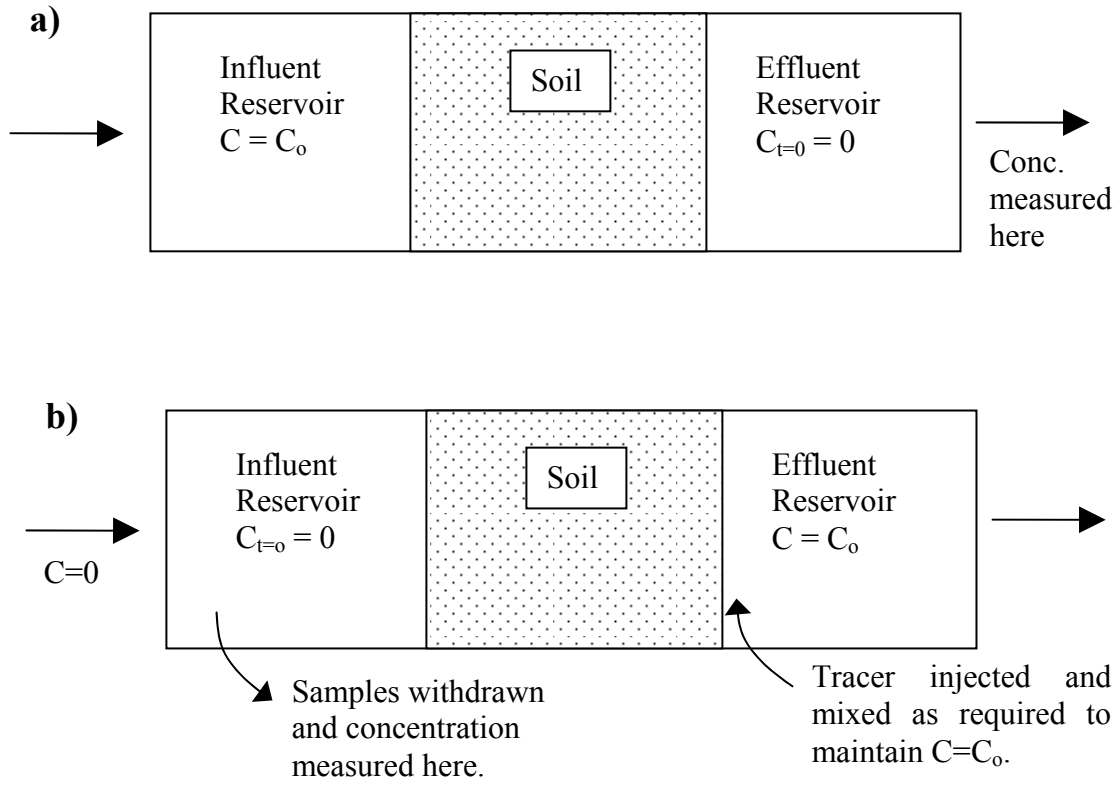

Figure 6.1: Double reservoir test for testing diffusion, dispersion, and advection
a) Standard double reservoir test set-up.
b) Opposing diffusion and advection double reservoir test set-up.
(adapted from Shackelford)

REFERENCES

Agriculture and Agri-Food Canada 2002. Gross evaporation for the 30-year period 1971-2000 in the Canadian prairies. Hydrology report #143. Prairie Farm Rehabilitation Administration Technical Service. Regina, Saskatchewan.

Alberta Agriculture. 1987. Soil quality relative to disturbance and reclamation, revised edition. Alberta Soils Advisory Committee, Soil Reclamation Subcommittee, Soil Quality Working Group, Edmonton, AB.

Alberta Environment. 2008. Environmental Protection and Enhancement Act, Conservation and Reclamation Regulation. Alberta Regulation 115/93. Alberta Queen's Printer. Available from: http://www.qp.alberta.ca/574.cfm?page=1993_115.cfm&leg_type=Regs&isbncln=9780779731343 [cited 21 July 2009]

Alberta Environment. 2007. Environmental Protection and Enhancement Act, Approval No. 26-02-00. Approval to Syncrude Canada Limited for construction, operation, and reclamation.

Alberta Energy. 2009. Alberta's Leased Oil Sands Areas (map). Available from: http://www.energy.alberta.ca/OilSands/pdfs/OSAagreesStats_June2009vkb.pdf [cited 09 April 2010]

Alberta Energy and Utilities Board. 2000. An atlas of lithofacies of McMurray formation, Athabasca oil sands deposit, northeastern Alberta: surface and subsurface." Earth Sciences Report 2000-07. Calgary, AB, June 2000

Alberta Energy Resources Conservation Board. 2009. Alberta's Energy Reserves 2008 and Supply/Demand Outlook 2009-2018, ST98-2009. Calgary, AB, June 2009. Available from: http://www.ercb.ca/docs/products/STs/st98_current.pdf [cited 21 July 2009]

Allison, G.B., and Hughes, M.W. 1983. The use of natural tracers as indicators of soil-water movement in a temperate semiarid region. Journal of Hydrology 60: 157–173.

Aubertin, M., Bussiere, B., Chapuis, R.P., and Barbera, J. 1996. Construction of experimental cells with covers on acid producing tailings. *In* Proceedings of the 49th Annual Canadian Geotechnical Conference, St. John's, Newfoundland, pp. 655-662.

Aubertin, M., Cifuentes, E., Martin, V., Apithy, S., Bussiere, B., Molson, J., Chapuis, R.P., and Maqsoud, A. 2006. An investigation of factors that influence the water diversion capacity of inclined covers with capillary barrier effects. *In* 4th International Conference on Unsaturated Soils, 2-5 April 2006, pp. 613-624.

Bailey, D.L.H. 2001. Properties of soil profiles over sodic mine spoil 16 years after construction. M.Sc. thesis, Univ. of Alberta, Edmonton, AB. [from Kessler 2007]

Barbour, L., Hendry, J., Nichol, C., Chanasyk, D., Mendoza, C., Purdy, B., Leskiw, L., Macyk, T., O'Kane, M., Qualizza, C. 2006. Soil capping technology transfer, Phase 2: Salt. Report issued to Syncrude Canada Ltd. Spring 2006.

Barone, F. S., Yanful, E.K., Quigley, R.M. and Rowe, R.K. 1989. Effect of multiple contaminant migration on diffusion and adsorption of some domestic waste contaminants in a natural clayey soil. Canadian Geotechnical Journal 26: 189-198.

Boese, C. D. 2003. The design and installation of a field instrumentation program for the evaluation of soil-atmosphere water fluxes in a vegetated cover over saline/sodic Shale overburden. M.Sc. Thesis, University of Saskatchewan, Saskatoon, SK.

Buckland, G.D., and M.J. Hendry. 1986. Dilution effects on mineral dissolution in a sulfate-dominated soil. p. 240–245. In G. Van der Kamp, and M. Maunicky (ed.) Proceedings Of the Third Canadian Hydrogeological Conference, 3rd, Saskatoon, SK. 20-23 April 1986. International. Association of. Hydrogeologists, Canadian National Chapter, Saskatoon, SK.

Bussiere, B., Aubertin, M., and Chapuis, R.P. 2003. The behavior of inclined covers used as oxygen barriers. Canadian Geotechnical Journal, **40**(3): 512-535.

Bussiere, B., Nicholson, R.V., Aubertin, M., and Benzaazoua, M. 1997. Evaluation of the effectiveness of covers built with desulfurized tailings for preventing acid mine drainage. *In* Proceedings of the 50th Annual Canadian Geotechnical Conference, Ottawa, Ontario, pp. 17-25.

Chapman, D.E. 2008. Hydrogeologic characterization of a newly constructed saline-sodic clay overburden hill. M.Sc. Thesis, University of Saskatchewan, Saskatoon.

Clark, I.D. and Fritz, P., 1997. Environmental Isotopes in Hydrogeology, Lewis Publishers, New York. 328pp.

Conca, J.L., and Wright, J. 1992. Diffusion and flow in gravel, soil, and whole rock. Applied Hydrogeology, **1**(1): 5-24.

Craig, H. 1961. Isotopic variations in meteoric waters, Science, 133:1702-1733.

Crank, J. 1956. The Mathematics of Diffusion. 347 pp. Oxford University Press.

Dansgaard, W., Johnsen, S.J., Clausen, H.B., and Gundestrup, N. 1973. Stable isotope glaciology, Meddelelser om Gronland, 197: 1-53.

Desaulniers, D.E., Kaufmann, R.S., Cherry, J.A., and Bentley, H.W. 1986. The 37Cl-35Cl variations in a diffusion-controlled groundwater system, Geochimica et Cosmochimica Acta, **50**(8): 1757-1764.

Devito, K., and Mendoza, C. 2007. Maintenance and dynamics of natural wetlands in western boreal forests: Synthesis of current understanding from the Utikuma research study area. pp.C2-C46. In: Harris, M.L. (ed.) 2007. Guideline for wetland establishment on reclaimed oil sands leases, Revised (2007) edition. Prepared by Lorax Environmental for CEMA Wetlands and Aquatics Subgroup of the Reclamation Working Group, Fort McMurray, AB. Dec.2007.

Domenico, P. A. and W. Schwartz. 1998. Physical and Chemical Hydrogeology. New York, John Wiley and Sons, Inc.

Dowuona, G.N., Mermut, A.R., and Krouse, H.R. 1993. Stable isotope geochemistry of sulfate in relation to hydrogeology in southern Saskatchewan, Canada, Applied Geochemistry **8**(3): 255-263.

Drever, J.I. 1988. The Geochemistry of Natural Waters. 437 pp. Prentice Hall, Englewood Cliffs, NJ, USA.

Edmunds, W.M., and Bath, A.H. 1976. Centrifuge extraction and chemical analysis of interstitial waters. Environmental Science and Technology 10: 467–472.

Elshorbagy, A., Jutla, A., Barbour, S.L., and Kells, J. 2005. System dynamics approach to assess the sustainability of reclamation of disturbed watersheds. Canadian Journal of Civil Engineering, 35(1): 144-158.

Environment Canada 2011. National climate data and information archive - Canadian climate normals or averages 1971-2000. Available from: http://www.climate.weatheroffice.gc.ca/climate_normals/index_e.html [cited July 15 2011].

Feth, J.H. 1981. Chloride in natural continental water: A review. U.S. Geological Survey Water Supply Paper 2176, 30 pp.

Fetter, C.W. 1993. Contaminant Hydrogeology. New York, Macmillan Publishing Company.

Fontes, J.C., Yousfi, M., and Allison, G.B. 1986. Estimation of long-term, diffuse groundwater discharge in the northern Sahara using stable isotope profiles in soil water. Journal of Hydrology 86: 315–327.

Fritz, P. and Fontes, J.C. 1980. Introduction. In: Fritz, P. and Fontes, J.C. (Editors), Handbook of Environmental Isotope Geochemistry, 1, The Terrestrial Environment, A. Elsevier, Amsterdam, pp. 1-19.

Friedman, I., Redfields, A.C., Schoen, B. and Harris, J. 1964. The variation of deuterium content of natural waters in the hydrologic cycle. Rev. Geophys. 2: 177-224.

Gat, J.R., 1996. Oxygen and hydrogen isotopes in the hydrologic cycle. Annual Rev. Earth Planet. Sci. 24: 225-262.

Gat, J.R., Mook, W.G, and Meijer, A.J. 2001. Environmental isotopes in the hydrological cycle – Principles and applications, Vol. 2 – Atmospheric water. W.G. Mook (ed.), IHP-V, Technical document No. 39, UNESCO, Paris. 139p.

Gelhar, L.W., Welty, C., and Rehfeldt, K.R. 1992. A critical review of data on field-scale dispersion in aquifers. Water Resources Research **28**(7): 1955-1974.

Geo-Slope International Ltd. 2010. Seepage modelling with SEEP/W 2007: An engineering methodology, 4th edition. February 2010. Calgary, Alberta.

Google. 2010. Google Maps Canada. Available from: http://maps.google.ca/ [cited on 09 January 09].

Hendry, M.J., Barbour, S.L., Boldt-Leppin, B.E.J., Reiffersheid, L.J. and Wassenaar, L.I. 2009. A comparison of laboratory and field based determinations of molecular diffusion coefficients in a low permeability geologic medium. Environmental Science and Technology, **43**(17): 6730-6736.

Hendry, M.J., Barbour, S.L., Zettyl, J., Chostner, V., and Wassenaar, L.I. 2010 (in prep). Controls on the long-term downward transport of δD of water in a regionally extensive, two-layered aquitard system. In preparation.

Hendry, M.J., Cherry, J.A., and Wallick, E.I. 1986. Origin and distribution of sulfate in a fractured till in southern Alberta, Canada, Water Resources Research, 22(1):45-61.

Hendry, M.J. and Wassenaar, L.I. 1999. Implications of the distribution of D in pore waters for groundwater flow and the timing of geologic events in a thick aquitard system, Water Resources Research, **35**(6): 1751-1760.

Hendry, M.J. and Wassenaar, L.I. 2004. Transport and geochemical controls on the distribution of solutes and stable isotopes in a thick clay-rich till aquitard, Canada. Isotopes in Environmental and Health Studies, **40**(1): 3-19.

Hillaire-Marcel, G. 1980. Isotopes and food. In: Fritz, P. and Fontes, J.C. (Editors), Handbook of Environmental Isotope Geochemistry, 2, The Terrestrial Environment, B. Elsevier, Amsterdam, pp. 507-548.

Isaac, B.A., Dusseault, M.B., Loebb, G.D., and Root, J.D. 1982. Characterization of the lower cretaceous overburden for oil sands surface mining within Syncrude Canada Ltd. leases in northeast Alberta, Canada. p. 371–384. In Proc. Congr. Int. Assoc. Engineering Geology, 4th, New Dehli, India. Dec. 1982. A.A. Balkema, Rotterdam, Netherlands.

Jordaan, S.M., Keith, D.W., and Stelfox, B. 2009. Quantifying land use of oil sands production: a life cycle perspective. Environmental Research Letters, 4(2) 024004: 1-15

Kelln, C.J., Wassenaar, L.I., and Hendry, M.J. 2001. Stable isotopes of pore water in clay-rich aquitards: A comparison and evaluation of measurement techniques, Ground Water Monitoring & Remediation **21**(2): 108-116.

Kelln, C., Barbour, L., and Qualizza, C. 2007. Preferential flow in a reclamation cover: Hydrological and geochemical response. Journal of Geotechnical and Geoenvironmental Engineering, **133**(10): 1277-1289.

Kelln, C., Barbour, S.L., and Qualizza, C. 2008. Controls on the spatial distribution of soil moisture and solute transport in a sloping reclamation cover. Canadian Geotechnical Journal, **45**(3): 351-366.

Kelln, C.J. 2008. The effects of meso-scale topography on the performance of engineered soil covers. Ph.D. Thesis, University of Saskatchewan, Saskatoon.

Kelln, C.J., Barbour, S.L., and Qualizza, C. 2009. Fracture-dominated subsurface flow and transport in a sloping reclamation cover. Vadose Zone Journal, **8**(1): 96-107.

Kendall, C. and Coplen, T.B. 2001. Distribution of oxygen-18 and deuterium in river waters across the United States. Hydrological Processes 15: 1363–1393.

Kessler, S. 2007. Salinity Profiles in Reconstructed Soils Over Saline-Sodic Waste from the Oil Sands Industry. M.Sc. Thesis, University of Saskatchewan, Saskatoon, SK.

Khire, M.V., Benson, C.H., and Bosscher, P.J. 2000. Capillary barriers: Design variables and water balance. Journal of Geotechnical and Geoenvironmental Engineering, **126**(8): 695-708.

Khire, M.V., Meerdink, J.S., Benson, C.H., and Bosscher, P.J. 1995. Unsaturated hydraulic conductivity and water balance predictions for earthen landfill final covers. *In* Proceedings of the Conference of the Geotechnical Engineering Division of the ASCE in Conjunction with the ASCE Convention, 22-26 October 1995, pp. 38-57.

Koehler, G., Wassenaar, L.I., and Hendry, M.J. 2000. An automated technique for measuring δD and δ18O values of pore water by direct CO2 and H2 equilibration. Analytical Chemistry, **72**(22): 5659-5664.

Lawrence, J. R. and Taylor, H. P. 1972. "Hydrogen and oxygen isotope systematics in weathering profiles." Geochimica Cosmochimica Acta 36, 1377–1393.

Lazorko, H.M. 2005. Root distribution, activity, and development for boreal species on reclaimed oil sand mine soils in Alberta, Canada. M.Sc. Thesis, University of Saskatchewan, Saskatoon, SK.

Lemay, T.G. 2002. Geochemical and isotope data for formation water from selected wells, Cretaceous to Quaternary succession, Athabasca Oil Sands (in situ) Area, Alberta. EUB/AGS Geo-Note 2002-02. Alberta Energy and Utilities Board, Alberta Geological Survey, Edmonton, AB. December 2002.

Leskiw, L.A. 1998. Land capability classification system for forest ecosystems in the oil sands region. Alberta Environmental Protection, Environmental Sciences Division, Edmonton, Alberta. Report ESD/LM/98-1.

Lim, P.C., Barbour, S.L., and Fredlund, D.G. 1998. The influence of the degree of saturation on the coefficient of aqueous diffusion. Canadian Geotechnical Journal, 35: 811-827.

Lis, G.P., Wassenaar, L.I., and Hendry, M.J. 2007. High precision laser spectroscopy D/H and $^{18}O/^{16}O$ measurements of microliter natural water samples. Analytical Chemistry 80: 287-293.

Macyk, T.M. and Drozdowski, B.L. 2008. Comprehensive report on operational reclamation techniques in the mineable oil sands region. Report prepared for Cumulative Environmental Management Association (CEMA). Alberta Research Council, Edmonton, AB.

Macyk, T.M. 1999. Soil monitoring at the 30 dump overburden area. Report prepared for Syncrude Canada Ltd. Alberta Research Council, Edmonton, AB.

Manheim, F.T. 1966. A hydraulic squeezer for obtaining interstitial waters from consolidated and unconsolidated sediments. U.S. Geol. Surv. Prof. Paper 550–C: 256–261.

Maule, C.P., Chanasyk, D.S., and Muehlenbachs, K. 1994. Isotopic determination of snow-water contribution to soil water and groundwater. Journal of Hydrology, 155: 73-91.

McKenna, G.T. 2002. Sustainable mine reclamation and landscape engineering. Ph.D. Thesis, University of Alberta, Edmonton.

McKnight, T.L., and Hess, D. 2005. Physical Geography: A Landscape Appreciation. Pearson Prentice Hall, Upper Saddle River, NJ.

Meiers, G. 2002. The use of field measurements of hydraulic conductivity to characterize the performance of reclamation covers with time. M. Eng. thesis, University of Saskatchewan, Saskatoon, SK.

Meiers, G.P., Barbour, S.L., and Meiers, M.K. 2003. The use of field measurements of hydraulic conductivity to characterize the performance of reclamation soil covers with time. *In* 6th International Conference on Acid Rock Drainage, Cairns, Australia.

Meiers, G.P., Barbour, S.L., and Qualizza, C.V. 2006. The use of *in situ* measurements of hydraulic conductivity to provide an understanding of cover system performance over time. *In* 7th International Conference on Acid Rock Drainage, St. Louis, MO.

Mermut, A.R. and Arshad, M.A. 1987. Significance of sulfide oxidation in soil salinization in southeastern Saskatchewan, Canada. Soil Sci. Soc. Am. J. **51**: 247–251.

Merrill, S.D., Doering, E.J, Power, J.F, and Sandoval, F.M. 1983. Sodium movement in soil-minespoil profiles: Diffusion and convection. Soil Science 136:308–316.

Moran, S.R., Trudell, M.R., Macyk, T.M., and Cheel, D.B. 1990. Plains hydrology and reclamation project: summary report. Report prepared for the Plains Coal Reclamation Research Program. Alberta Land Conservation Reclamation Council, Edmonton, AB.

Morris, C.E. and Stormont, J.C. 1997. Capillary barriers and subtitle D covers: Estimating equivalency. Journal of Environmental Engineering - ASCE, **123**(1): 3-10.

Moser, H. and Stichler, W. 1974. Deuterium and oxygen-18 contents as an index of the properties of snow covers. In: Snow Mechanics, Proceedings of Grindewald Symposium, April 1974. IASH Publication 114: 122-135.

Moser, H. and Stichler, W. 1980. Environmental isotopes in ice and snow. In: Fritz, P. and Fontes, J.C. (Editors), Handbook of Environmental Isotope Geochemistry, 1, The Terrestrial Environment, A. Elsevier, Amsterdam, 141-178.

National Energy Board. 1996. Canada's oil sands opportunities and challenges to 2015: an update. National Energy Board of Canada, Calgary, Alberta. Available from: http://www.neb-one.gc.ca/clf-nsi/rnrgynfmtn/nrgyrprt/lsnd/pprtntsndchllngs20152006_/pprtntsndchllngs20152006-eng.pdf. [cited 17 May 2010].

Natural Regions Committee 2006. Natural regions and subregions of Alberta. Compiled by D.J. Downing and W.W. Pettapiece. Government of Alberta. Pub. No. T/852.

Neumann, T.A., Albert, M.R., Lomonaco, R., Engel, C., Courville, Z., and Perron, F. 2008. Experimental determination of snow sublimation rate and stable-isotopic exchange. Annals of Glaciology, 49: 1-6

Nichol, C., Kessler, S., Wall, S.N., Barbour, S.L., and Hendry, J. 2006. 30 Dump instrumented watersheds geochemical analysis: A report prepared for Syncrude Canada Ltd., University of Saskatchewan, Saskatoon.

Nicholson, R.V., Gillham, R.W., Cherry, J.A., and Reardon, E.J. 1989. Reduction of acid generation in mine tailings through the use of moisture-retaining cover layers as oxygen barriers. Canadian geotechnical journal, **26**(1): 1-8.

O'Kane Consultants Inc. 2001. As-built report for the Southwest Sands Storage and 30-Dump automated water balance monitoring systems at Syncrude Canada Ltd. Report No. 653-2

O'Neil, J.R. 1968. Hydrogen and oxygen isotope fractionation between ice and water. Journal of Physical Chemistry, 72(10): 3683-3684.

Ogg, J.G., Ogg, G., and Gradstein, F.M. 2000. The Concise Geologic Time Scale. Cambridge University Press. New York, NY.

Parkhurst, D.L., and Appelo, C.A.J. 1999. User's guide to PHREEQC (Version 2)--a computer program for speciation, batch-reaction, one-dimensional transport, and inverse geochemical calculations: U.S. Geological Survey Water- Resources Investigations Report 99-4259, 312 p.

Patterson, R.J., Krape, S.K., Dykes, L.S., and Mcleod, R.A.. 1977. A coring and squeezing technique for the detailed study of subsurface water chemistry. Canadian Journal of Earth Science 15: 162–169.

Pauls, D.R. 1988. Plains Hydrology and Reclamation Project: Investigation of the settlement behavior of surface mine backfill. Alberta Land Conservation and Reclamation Council Report #88-4. [from Moran et al. 1990]

Peng, H., Mayer, B., Harris, S., and Krouse, H.R. 2004. A 10-yr record of stable isotope ratios of hydrogen and oxygen in precipitation at Calgary, Alberta, Canada. Tellus, Series B: Chemical and Physical Meteorology 56: 147-159.

Pickens, J. F. and Grisak, G.E. 1981. Scale-dependent dispersion in a stratified granular aquifer. Water Resources Research **17**(4): 1191-1211.

Qualizza, C., Chapman, D., Barbour, S.L., and Purdy, B. 2004. Reclamation research at Syncrude Canada's Mining Operation in Alberta's Athabasca Oil Sands Region. *In* 16th International Conference, Society for Ecological Restoration, Victoria, Canada.

Remenda, V.H., Van, D.K., and Cherry, J.A. 1996. Use of vertical profiles of 18O to constrain estimates of hydraulic conductivity in a thick, unfractured aquitard, Water Resources Research, **32**(10): 2979-2987.

Rhoades. J.D. 1982. Soluble salts. p. 167–179. *In* A.L. Page, R.H. Miller and D.R. Keeney (ed.) Methods of soil analysis, Part 2. Chemical and microbiological properties. Agronomy Monograph No. 9. American Society of Agronomy and Soil Science Society of America, Madison, WI.

Rose, S. E. 1995. Introduction to isotope hydrology, Principles and applications. Course notes, 23-24 March 1995. Atlanta, Georgia. Environmental Education Enterprises, Columbus, Ohio. 119 pp.

Ross, B. 1990. The diversion capacity of capillary barriers, Water Resources Research, **26**(10): 2625-9.

Rowe, R.K. and Badv, K. 1996a. Chloride migration through clayey silt underlain by fine sand or silt. ASCE, Journal of Geotechnical Engineering **122** 1 (1996), pp. 60–68

Rowe, R.K. and Badv, K. 1996b. Advective-diffusive contaminant migration in unsaturated sand and gravel. ASCE Journal of Geotechnical Engineering, 122(12): 965-975

Sandoval, F.M., and Gould, W.L. 1978. Improvement of saline- and sodium-affected disturbed lands. p. 485–504. In F.W. Schaller, and P. Sutton (ed.) Reclamation of drastically disturbed lands. ASA, Madison, WI.

Savin, S.M. 1980. Oxygen and hydrogen isotope effects in low-temperature mineral-water interactions. In: Fritz, P. and Fontes, J.C. (Editors), Handbook of Environmental Isotope Geochemistry, 1, The Terrestrial Environment, A. Elsevier, Amsterdam, pp. 283-327.

Shackelford, C.D. 1991. Laboratory diffusion testing for waste disposal – A review. Contaminant Hydrology **7**:177-217

Shackelford, C.D. and Daniel, D.E. 1991. Diffusion in saturated soil I: Background. Journal of Geotechnical Engineering **117**(3): 467-484.

Shurniak, R. 2003. Predictive Modeling of Moisture Movement within Soil Cover Systems for Saline/Sodic Overburden Piles. M.Sc. Thesis, University of Saskatchewan, Saskatoon, SK.

Shurbaji, A.-R.M.; and Phillips, F.M. (1995) A numerical model for the movement of H_2O, $H_2{}^{18}O$, and ^2HHO in the unsaturated zone: Journal of Hydrology, 171: 125-142.

Simpkins, W.W. and Bradbury, K.R. 1992. Groundwater flow, velocity, and age in a thick, fine-grained till unit in southeastern Wisconsin. Journal of Hydrology, **132**(1-4): 283-319.

Sokratov, S.A. and Golubev, V.N. 2009. Snow isotopic content change by sublimation. Journal of Glaciology, **55**(193): 823-828.

Spokas, K., Bogner, J., Chanton, J.P., Morcet, M., Aran, C., Graff, C., Golvan, Y.M., and Hebe, I. 2006. Methane mass balance at three landfill sites: What is the efficiency of capture by gas collection systems? Waste Management, **26**(5): 516-525.

Stormont, J.C. and Anderson, C.E. 1999. Capillary barrier effect from underlying coarser soil layer. Journal of Geotechnical and Geoenvironmental Engineering, **125**(8): 641-648.

Taylor, S., Feng, X., Williams, M., and McNamara, J. 2002. How isotopic fractionation of snowmelt affects hydrograph separation. In 59th Eastern Snow Conference, Stowe, Vermont, USA, pp. 285-293.

USDA Salinity Laboratory. 1954. Diagnosis and improvement of saline and alkali soils. USDA Handbook No. 60. U.S. Government Printing Office, Washington, DC.

van der Kamp, G., Luba, L.D., Cherry, J.A., and Maathuis, H. 1994. Field study of a long and very narrow contaminant plume. Ground Water **32**(6): 1008-1016.

van der Kamp, G., Van Stempvoort, D.R., and Wassenaar, L.I. 1996. The radial diffusion method 1: using intact cores to determine isotopic composition, chemistry, and effective porosities for groundwater in aquitards, Water Resources Research, **32**(6), 1815–1822.

Wall, S.N. 2005. Characterizing the geochemical reactions in an overburden waste pile: Syncrude mine site, Fort McMurray, Alberta, Canada. M.Sc. Thesis, University of Saskatchewan, Saskatoon.

Wassenaar, L.I. and Hendry, M.J. 1999. Improved piezometer construction and sampling techniques to determine pore water chemistry in aquitards. Ground Water. **37**(4): 564–571.

Wassenaar, L.I., Hendry, M.J., Chostner, V.L., and Lis, G.P. 2008. High resolution pore water δ^2H and $\delta^{18}O$ measurements by $H_2O_{(liquid)} - H_2O_{(vapour)}$ equilibration laser spectroscopy. Environmental Science and Technology **42** (24), 9262-9267.

Yanful, E.K., Bell, A.V., and Woyshner, M.R. 1993. Design of a composite soil cover for an experimental waste rock pile near Newcastle, New Brunswick, Canada. Canadian Geotechnical Journal, **30**(4): 578-587.

Yeh, H., and Epstein, S. 1978. Hydrogen isotope exchange between clay minerals and sea water. Geochimica et Cosmochimica Acta, 42: 140-143.

Appendix A:
Drill Hole Details and Logs

Table A1: Drill hole details from soil chemistry sampling.

Drill hole ID	Easting (m)	Northing (m)	Elevation (masl)	Drill Date	Total Depth (m)	Depth to Secondary (m)	Depth to Shale (m)
D1 1	462247	6317110	328.7	20-Aug-08	1.5	0.09	0.33
D1 2	462256	6317094	331.5	20-Aug-08	1.1	0.10	0.36
D1 3	462266	6317079	*333.8*	20-Aug-08	1.1	0.37	0.66
D1 4	462276	6317065	*335.6*	20-Aug-08	1.1	0.14	0.49
D1 5	462287	6317050	*337.7*	20-Aug-08	1.1	0.30	0.50
D1 6	462298	6317037	*339.3*	20-Aug-08	1.1	0.20	0.45
D1 7	462307	6317022	*341.3*	20-Aug-08	1.1	0.20	0.53
D1 8	462318	6317007	*343.7*	20-Aug-08	1.1	0.30	0.69
D1 9	462328	6316993	*346.0*	20-Aug-08	1.1	0.15	0.48
D1 10	462339	6316977	*347.9*	20-Aug-08	1.1	0.33	0.70
D2 1	462280	6317123	328.6	19-Aug-08	1.0	0.20	0.30
D2 2	462289	6317109	331.1	19-Aug-08	1.0	0.13	0.37
D2 3	462298	6317094	333.2	19-Aug-08	1.0	0.22	0.32
D2 4	462308	6317081	335.3	19-Aug-08	1.0	0.37	0.53
D2 5	462317	6317066	337.1	19-Aug-08	1.0	0.18	0.49
D2 6	462326	6317052	338.8	19-Aug-08	1.0	0.19	0.38
D2 7	462335	6317038	341.1	19-Aug-08	1.0	0.18	0.44
D2 8	462345	6317024	343.2	19-Aug-08	1.0	0.07	0.20
D2 9	462354	6317010	345.1	19-Aug-08	1.0	0.20	0.28
D2 10	462364	6316996	348.4	19-Aug-08	1.0	0.19	0.31
D3 0	462320	6317165	328.4	19-Aug-08	1.5	0.17	0.80
D3 2	462331	6317148	330.0	19-Aug-08	1.5	0.20	1.18
D3 3	462341	6317133	331.8	19-Aug-08	1.5	0.20	0.79
D3 4	462351	6317119	334.9	19-Aug-08	1.5	0.10	1.20
D3 5	462362	6317105	337.2	19-Aug-08	1.5	0.12	1.08
D3 6	462372	6317090	338.8	19-Aug-08	1.5	0.27	1.10
D3 7	462382	6317075	341.4	19-Aug-08	1.5	0.25	1.18
D3 8	462393	6317061	343.6	19-Aug-08	1.8	0.43	1.49
D3 9	462404	6317047	345.9	19-Aug-08	2.1	0.25	1.80
D3 10	462415	6317033	349.6	19-Aug-08	1.5	0.29	1.50
Pro 33	462422	6317012	*351.0*	26-May-09	2.5	0.06	>2.50
Pro 50A	462483	6316898	*349.0*	26-May-09	2.0	0.20	0.98
Pro 51	462472	6316932	*350.0*	26-May-09	2.0	0.10	0.80
Pro 52	462456	6316965	*350.0*	26-May-09	2.0	0.10	1.20
Pro 53	462440	6316987	*351.0*	26-May-09	2.0	0.10	0.97

Table A2: Drill hole details from soil stable isotope sampling.

Drill hole ID	Easting (m)	Northing (m)	Elevation (masl)	Drill Date	Total Depth (m)	Depth to Secondary (m)	Depth to Shale (m)
D3-2	462331	6317148	330.0	12-Dec-08	1.5	3.00	1.18
D3-4	462351	6317119	334.9	12-Dec-08	1.1	3.00	1.15
D3-5	462362	6317105	337.2	12-Dec-08	1.1	2.40	0.90
D3-8	462393	6317061	343.6	12-Dec-08	1.1	3.00	1.45
D3-10	462415	6317033	349.6	9-Dec-08	1.1	3.00	1.50
Pro 50	462486	6316901	*349.0*	9-Dec-08	1.1	3.00	1.00
Pro 52	462456	6316967	*350.0*	9-Dec-08	1.1	2.35	0.90
Pro 54	462465	6316988	*350.0*	9-Dec-08	1.1	2.75	1.25
Deep	462307	6317197	*330.0*	13-Dec-08	1.1	9.25	0.80

Notes from Tables A1 and A2:

- All coordinates are in UTM NAD 83.
- Coordinates listed are staked locations (prior to drilling) and were recorded with handheld GPS units. Accuracy is reported to be within approximately 5 m.
- Elevations in italics were not surveyed but were estimated from 2004 Lidar survey. Accuracy is approximately 0.5 m.
- Peat-till and till-shale interface depths from isotope sampling are accurate within approx. 0.3 m. Depths from major ion chemistry sampling are accurate within <0.1 m.

Table A3: Drill hole logs from soil salinity sampling on D3 cover in 2008.

Hole ID	Depth (cm)	Material	Comments
D3-0	**0 - 17**	Peat	
	17 - 80	Till	20 - 38cm wood debris and shale mix
	80 - 150	Shale	125 - 150cm softer crumbly shale
Note: D3 -1 was not sampled because weeping tile now exists there			
D3-2	**0 - 20**	Peat	mostly till with some peat
	20 - 118	Till	between 30-40cm large pocket of sphagnum moss. 95 -110cm fine-medium grained sand with some silt, wet, brown. 110 - 118 cm till again.
	118 - 150	Shale	
D3-3	**0 - 20**	Peat	
	20 - 79	Till	
	79 - 150	Shale	
D3-4	**0 - 10**	Peat	
	10 - 120	Till	
	120 - 150	Shale	
D3-5	**0 - 12**	Peat	
	12 - 108	Till	
	108 - 150	Shale	
D3-6	**0 - 27**	Peat	Heavy on the mineral mix percentage
	27 - 110	Till	
	110 - 150	Shale	
D3-7	**0 - 25**	Peat	17 - 25cm till mixed in with peat
	25 - 118	Till	At 73 cm small 1cm thick sand lens
	118 - 150	Shale	
D3-8	**0 - 43**	Peat	
	43 - 149	Till	
	149 - 180	Shale	
D3-9	**0 - 25**	Peat	
	25 - 180	Till	25 -85cm mixed peat and till. At 85cm solid till.
	180 - 210	Shale	
D3-10	**0 - 29**	Peat	
	29 - 150	Till	
	150 - 180	Shale	

Sampling Notes:
Date: August 19,2008
Weather: partially cloudy, 15 - 20 C

Table A4: Drill hole logs from soil salinity sampling on plateau cover in 2009.

Hole ID	Depth (cm)	Material	Comments
Pro33	**0 - 6**	Peat	some till
	6 - 250	Till	6-20 cm some peat 80-92 cm Soft till with some shale mixed in. 92-100 cm: Shale 107-120 cm: Trace to some peat mixed in. 250 cm: max. depth, shale not reached
Pro53	**0 - 20**	Peat	
	20 - 98	Till	20 - 30cm trace peat
	98 - 200	Shale	Trace glauconitic sand.
Pro52	**0 - 10**	Peat + Till	Peat mixed with Till
	10 - 36	Till	trace peat mixed in
	36 - 80	Peat +Till	36 - 70 cm: Mainly peat with till mixed in. 70 - 80 cm: Till with peat
	80 - 200	Shale	110 - 200cm: Trace glauconitic sand Trace lean oil sand
Pro51	**0 - 10**	Peat	
	10 - 120	Till	10-30cm trace peat 50 cm: becomes soft wet 60-70cm: Some peat
	120 - 200	Shale	
Pro50	**0 - 10**	Peat	Some till mixed in
	10 - 97	Till	40-50cm: trace peat 86-92cm: Peat only
	97 - 200	Shale	110 cm - Hit large obstruction (siltstone block?) in original hole and several subsequent holes. Had to move approx. 7m S and 9 m W to avoid obstruction. 110-120cm: some glauconitic sand, trace lean oil sand 180-200cm: some lean oil sand

Sampling Notes:
Date: May 26, 2009
Weather: am - Light rain, cloudy, 5 - 10 C. p.m. - clearing, 10 - 15 C

Table A5: Drill hole logs and sample details for soil isotope sampling.

Hole ID	Core Start Depth (mbgl)	Core End Depth (mbgl)	Recovery (m)	Recovery (%)	Sample ID	Sample Top (mbgl)	Sample Bottom (mbgl)	Material Description	Notes
PRO 50	0	0.58	0.38	66%	PRO 50-01	0	0.38	Peat	Assume sample compression occurred here
					PRO 50-02	0.38	0.48	Peat-Till mixture	
					PRO 50-03	0.48	0.58	Till	
	0.58	1.2	0.3	48%	PRO 50-04	0.58	0.8	Till	
					PRO 50-05	0.8	1	Till	
					PRO 50-06	1	1.2	Shale	
	1.2	1.8	0.43	72%	PRO 50-07	1.2	1.35	Shale	Samples not frozen below this depth
					PRO 50-08	1.35	1.5	Shale	
					PRO 50-09	1.5	1.65	Shale	
					PRO 50-10	1.65	1.76	Shale	4 cm lost from bottom of sampler
	1.8	2.4	0.53	88%	PRO 50-11	1.8	1.92	Shale	
					PRO 50-12	1.92	2.04	Shale	
					PRO 50-13	2.04	2.16	Shale	
					PRO 50-14	2.16	2.28	Shale	
					PRO 50-15	2.28	2.4	Shale	
	2.4	3	0.46	77%	PRO 50-16	2.4	2.52	Shale	
					PRO 50-17	2.52	2.64	Shale	
					PRO 50-18	2.64	2.76	Shale	
					PRO 50-19	2.76	2.88	Shale	
					PRO 50-20	2.88	3	Shale	

Hole ID	Core Start Depth (mbgl)	Core End Depth (mbgl)	Recovery (m)	Recovery (%)	Sample ID	Sample Top (mbgl)	Sample Bottom (mbgl)	Material Description	Notes
PRO 52	0	0.6	0.14	23%	PRO 52-01	0	0.14	Peat	Frozen
						0.14	0.6	Till?	No Recovery
	0.6	1.2	0.4	67%	PRO 52-02	0.6	0.9	Till	Assume compression occurred here
					PRO 52-03	0.9	1	Shale	
					PRO 52-04	1	1.1	Shale	
					PRO 52-05	1.1	1.2	Shale	
	1.2	1.8	0.45	75%	PRO 52-06	1.2	1.35	Shale	
					PRO 52-07	1.35	1.5	Shale	
					PRO 52-08	1.5	1.65	Shale	
					PRO 52-09	1.65	1.8	Shale	
	1.8	2.35	0.53	96%	PRO 52-10	1.8	1.9	Shale	Water in hole (sampler wet)
					PRO 52-11	1.9	2	Shale	
					PRO 52-12	2	2.1	Shale	
					PRO 52-13	2.1	2.2	Shale	
					PRO 52-14	2.2	2.35	Shale	
PRO 52A	0	0.2	0.18	90%	PRO 52A-01	0	0.2	Till w some peat	
	0.2	0.8	0.23	38%	PRO 52A-02	0.2	0.5	Till	
					PRO 52A-03	0.5	0.8	Till	

Hole ID	Core Start Depth (mbgl)	Core End Depth (mbgl)	Recovery (m)	Recovery (%)	Sample ID	Sample Top (mbgl)	Sample Bottom (mbgl)	Material Description	Notes
PRO 54	0	0.2	0.02	10%	No sample	0	0.2	Peat	Frozen, insufficient recovery for sample
	0.2	0.6	0.13	33%	PRO 54-01	0.2	0.6	Peat-Till mixture	Poor recovery
	0.6	1.2	0.31	52%	PRO 54-02	0.6	0.8	Till	
					PRO 54-03	0.8	1	Till	
					PRO 54-04	1	1.2	Till	
	1.2	1.8	0.53	88%	PRO 54-05	1.2	1.35	Shale	Top 5 cm was till, Shale starts at 1.25 m bgl
					PRO 54-06	1.35	1.5	Shale	
					PRO 54-07	1.5	1.6	Shale	
					PRO 54-08	1.6	1.7	Shale	
					PRO 54-09	1.7	1.8	Shale, minor LOS	Some lean oil sand
	1.8	2.4	0.58	97%	PRO 54-10	1.8	1.9	Shale	Initial refusal at 1.8 m. Hole relocated 0.5 m away. Sampling resumed at 1.8 m.
					PRO 54-11	1.9	2	Shale	Trace oil sand, bitumen odour
					PRO 54-12	2	2.1	Shale	Trace oil sand, bitumen odour
					PRO 54-13	2.1	2.2	Shale	mm scale seam of clean fine grained sand
					PRO 54-14	2.2	2.3	Shale	
					PRO 54-15	2.3	2.4	Shale	
	2.4	2.75	0.34	97%	PRO 54-16	2.4	2.52	Shale	
					PRO 54-17	2.52	2.64	Shale	
					PRO 54-18	2.64	2.75	Shale	

Hole ID	Core Start Depth (mbgl)	Core End Depth (mbgl)	Recovery (m)	Recovery (%)	Sample ID	Sample Top (mbgl)	Sample Bottom (mbgl)	Material Description	Notes
D3-10	0	0.2	0.06	30%	D3-10-01	0	0.2	Peat	
	0.2	0.6	0.2	50%	D3-10-02	0.2	0.4	Peat-Till mixture	
					D3-10-03	0.4	0.6	Till	
	0.6	1.2	0.37	62%	D3-10-04	0.6	0.75	Till	
					D3-10-05	0.75	0.9	Till	
					D3-10-06	0.9	1.05	Till	
					D3-10-07	1.05	1.2	Till	
	1.2	1.65	0.35	78%	D3-10-08	1.2	1.35	Till	
					D3-10-09	1.35	1.5	Till	
					D3-10-10	1.5	1.65	Shale	Good recovery across the till-shale interface.
					No sample	1.65	1.8	Shale	Hard rock encountered at 1.65 m (likely siltstone). Bypassed rock with auger.
	1.8	2.4	0.4	67%	D3-10-11	1.8	1.95	Shale	
					D3-10-12	1.95	2.1	Shale	
					D3-10-13	2.1	2.25	Shale	Some glauconitic sand
					D3-10-14	2.25	2.4	Shale	Some glauconitic sand
	2.4	3	0.4	67%	D3-10-15	2.4	2.6	Peat-Till mixture	Likely sloughed material
					D3-10-16	2.6	2.8	Shale	
					D3-10-17	2.8	3	Shale	

Hole ID	Core Start Depth (mbgl)	Core End Depth (mbgl)	Recovery (m)	Recovery (%)	Sample ID	Sample Top (mbgl)	Sample Bottom (mbgl)	Material Description	Notes
D3-08	0	0.2	0.06	30%	D3-08-01	0	0.2	Peat-Till mixture	Mainly till with some peat
	0.2	0.6	0.16	40%	D3-08-02	0.2	0.4	Peat-Till mixture	Mainly peat with some till
					D3-08-03	0.4	0.6	Till	
	0.6	1.2	0.3	50%	D3-08-04	0.6	0.8	Till	
					D3-08-05	0.8	1	Till	
					D3-08-06	1	1.2	Till	
	1.2	1.7	0.35	70%	D3-08-07	1.2	1.35	Till	
					D3-08-08	1.35	1.45	Till w. some shale	Interface not well defined, assumed at 1.4 m
					D3-08-09	1.45	1.55	Shale	
					D3-08-10	1.55	1.7	Shale	Siltstone inclusions
	1.7	1.8	0.07	70%	D3-08-11	1.7	1.8	Shale	Grey, crumbling
						1.8	1.95	Shale	1.8 m - Rock encountered, bypassed with augers
	1.95	2.4	0.09	20%		1.95	2.4	Shale	Grey, crumbling, very poor recovery, no sample
	2.4	3	0.22	37%	D3-08-12	2.4	2.7	Shale	Clay shale with lenses of grey, crumbling clay
					D3-08-13	2.7	3	Shale	

Hole ID	Core Start Depth (mbgl)	Core End Depth (mbgl)	Recovery (m)	Recovery (%)	Sample ID	Sample Top (mbgl)	Sample Bottom (mbgl)	Material Description	Notes
D3-08A	1.8	2.4	0.26	43%	D3-08A-14	1.8	2.1	Shale	D3-08A offset 1 m from D3-08, sampled from 1.8 m
					D3-08A-15	2.1	2.4	Shale with Till	Mostly shale with some clay till mixed in
	2.4	3	0.41	68%	D3-08A-16	2.4	2.55	Shale with Till	
					D3-08A-17	2.55	2.7	Shale with Till	
					D3-08A-18	2.7	2.85	Shale with Till	
					D3-08A-19	2.85	3	Shale with Till	
D3-05	0	0.2	0.1	50%	D3-05-01	0	0.2	Peat-Till mixture	
	0.2	0.6	0.24	60%	D3-05-02	0.2	0.4	Till	
					D3-05-03	0.4	0.6	Till	
	0.6	1.2	0.16	27%	D3-05-04	0.6	0.9	Till	
					D3-05-05	0.9	1.2	Shale	
	1.2	1.35	0.14	93%	D3-05-06	1.2	1.35	Shale	
					no sample	1.35	1.45		1.35 m - rock encountered, bypassed with auger
	1.45	1.8	0.26	74%	D3-05-07	1.45	1.6	Shale	
					D3-05-08	1.6	1.8	Shale	some glauconitic sand
	1.8	2.4	0.32	53%	D3-05-09	1.8	2	Shale	trace pebbles and rocks (siltstone fragments?)
					D3-05-10	2	2.2	Shale	
					D3-05-11	2.2	2.4	Shale	Sand lens at 2.3 m, Refusal at 2.4 m

Hole ID	Core Start Depth (mbgl)	Core End Depth (mbgl)	Recovery (m)	Recovery (%)	Sample ID	Sample Top (mbgl)	Sample Bottom (mbgl)	Material Description	Notes
D3-04	0	0.2	0.1	50%	D3-04-01	0	0.1	Peat	
					D3-04-02	0.1	0.2	Till	Trace Peat
	0.2	0.6	0.1	25%	D3-04-03	0.2	0.6	Till	Sandy clay till, Poor recovery
	0.6	1.2	0.22	37%	D3-04-04	0.6	1	Till	
					D3-04-05	1	1.2	Shale	
	1.2	1.8	0.49	82%	D3-04-06	1.2	1.32	Shale w LOS	some lean oil sand
					D3-04-07	1.32	1.44	Shale	
					D3-04-08	1.44	1.56	Shale	some glauconitic sand
					D3-04-09	1.56	1.68	Shale	
					D3-04-10	1.68	1.8	Shale w LOS	some lean oil sand
	1.8	2.4	0.24	40%	D3-04-11	1.8	2.1	Shale w LOS	some lean oil sand
					D3-04-12	2.1	2.4	Shale w Till	some till inclusions
	2.4	3	0.47	78%	D3-04-13	2.4	2.55	Shale	Water in hole, Sampler came out very wet
					D3-04-14	2.55	2.7	Shale w LOS	some lean oil sand
					D3-04-15	2.7	2.85	Shale w LOS	some lean oil sand
					D3-04-16	2.85	3	Shale w LOS	some lean oil sand

Hole ID	Core Start Depth (mbgl)	Core End Depth (mbgl)	Recovery (m)	Recovery (%)	Sample ID	Sample Top (mbgl)	Sample Bottom (mbgl)	Material Description	Notes
D3-02	0	0.2	0.08	40%	D3-02-01	0	0.2	Peat, Till	Assumed peat from 0-0.1 m, till beginning at 0.1 m
	0.2	0.6	0.07	18%	D3-02-02	0.2	0.6	Till	
	0.6	1.2	0.24	40%	D3-02-03	0.6	0.9	Till	
					D3-02-04	0.9	1.2	Till	very oxidized, trace shale at bottom of sample
	1.2	1.8	0.42	70%	D3-02-05	1.2	1.35	Till-Shale mixture	wet, medium to high plasticity
					D3-02-06	1.35	1.5	Shale	medium to high plasticity
					D3-02-07	1.5	1.65	Shale w LOS	some lean oil sand
					D3-02-08	1.65	1.8	Shale w Till	some till inclusions
	1.8	2.4	0.54	90%	D3-02-09	1.8	1.9	Shale	
					D3-02-10	1.9	2	Shale-Till mixture	
					D3-02-11	2	2.1	Shale w Till	
					D3-02-12	2.1	2.2	Shale w Till	
					D3-02-13	2.2	2.3	Shale	some glauconitic sand, and rocks (siltstone?)
					D3-02-14	2.3	2.4	Shale	some glauconitic sand
	2.4	3	0.25	42%	D3-02-15	2.4	2.6	Shale w Till	some till inclusions
					D3-02-16	2.6	2.8	Shale w Till	some till inclusions, some glauconitic sand
					D3-02-17	2.8	3	Shale w sand	clean sand lenses

Hole ID	Core Start Depth (mbgl)	Core End Depth (mbgl)	Recovery (m)	Recovery (%)	Sample ID	Sample Top (mbgl)	Sample Bottom (mbgl)	Material Description	Notes
Deep	0	0.2	0.06	30%	DEEP-01	0	0.2	Till	with trace organics
	0.2	0.6	0.15	38%	DEEP-02	0.2	0.6	Till w trace Peat	with peat inclusions
	0.6	1.2	0.3	50%	DEEP-03	0.6	0.8	Till	with some sand lenses
					DEEP-04	0.8	1	Shale	
					DEEP-05	1	1.2	Shale	with some glauconitic sand
	1.2	1.8	0.58	97%	DEEP-06	1.2	1.3	Shale	
					DEEP-07	1.3	1.4	Shale	
					DEEP-08	1.4	1.5	Shale	
					DEEP-09	1.5	1.6	Shale	
					DEEP-10	1.6	1.7	Shale	
					DEEP-11	1.7	1.8	Shale	Hard, dry, crumbling shale at bottom
	1.8	2.4	0.05	8%	DEEP-12	1.8	2.4	Shale	Hard, dry, crumbling shale. Very poor recovery
	2.4	3	0.44	73%	DEEP-13	2.4	2.55	Shale	Some glauconitic sand; some hard, crumbling shale
					DEEP-14	2.55	2.7	Shale	Some hard, dry, crumbling shale
					DEEP-15	2.7	2.85	Shale	Some hard, dry, crumbling shale
					DEEP-16	2.85	3	Shale	Some hard, dry, crumbling shale
	3	3.6	0.44	73%	DEEP-17	3	3.15	Shale	
					DEEP-18	3.15	3.3	Shale	with some glauconitic sand
					DEEP-19	3.3	3.45	Shale	

Hole ID	Core Start Depth (mbgl)	Core End Depth (mbgl)	Recovery (m)	Recovery (%)	Sample ID	Sample Top (mbgl)	Sample Bottom (mbgl)	Material Description	Notes
Deep					DEEP-20	3.45	3.6	Shale	with some sand lenses
	3.6	4.2	0.44	73%	DEEP-21	3.6	3.75	Shale	with some glauconitic sand
					DEEP-22	3.75	3.9	Shale	with some sand lenses
					DEEP-23	3.9	4.05	Shale	with some sand lenses
					DEEP-24	4.05	4.2	Shale	with some sand lenses
	4.2	4.8	0.38	63%	DEEP-25	4.2	4.4	Shale	
					DEEP-26	4.4	4.6	Shale	
					DEEP-27	4.6	4.8	Shale	
	4.8	5.4	0.33	55%	DEEP-28	4.8	5	Shale	with some glauconitic sand
					DEEP-29	5	5.2	Shale	with some glauconitic sand
					DEEP-30	5.2	5.4	Shale	with some glauconitic sand and oxidized sand
	5.4	6	0.37	62%	DEEP-31	5.4	5.6	Shale	Hard, dry, crumbling with some glauconitic sand
					DEEP-32	5.6	5.8	Shale	
					DEEP-33	5.8	6	Shale	with some sand lenses
	6	6.77	0.71	92%	DEEP-34	6	6.11	Shale	with some sand lenses
					DEEP-35	6.11	6.22	Shale	with some sand lenses
					DEEP-36	6.22	6.33	Shale	
					DEEP-37	6.33	6.44	Shale	
					DEEP-38	6.44	6.55	Shale	
					DEEP-39	6.55	6.66	Shale	
					DEEP-40	6.66	6.77	Shale	Some very hard shale at bottom

Hole ID	Core Start Depth (mbgl)	Core End Depth (mbgl)	Recovery (m)	Recovery (%)	Sample ID	Sample Top (mbgl)	Sample Bottom (mbgl)	Material Description	Notes
Deep					No Sample	6.77	6.85	Shale	Refusal at 6.77 m. Bypassed with auger.
	6.85	7.45	0.48	80%	DEEP-41	6.85	7	Shale	some crushed rock fragments
					DEEP-42	7	7.15	Shale	
					DEEP-43	7.15	7.3	Shale	
					DEEP-44	7.3	7.45	Shale	Hard, dry, crumbling
	7.45	8.05	0.5	83%	DEEP-45	7.45	7.57	Shale	
					DEEP-46	7.57	7.69	Shale	
					DEEP-47	7.69	7.81	Shale	with some oxidized sand
					DEEP-48	7.81	7.93	Shale	with some glauconitic sand
					DEEP-49	7.93	8.05	Shale	with some glauconitic sand
	8.05	8.65	0.3	50%	DEEP-50	8.05	8.25	Shale	with some glauconitic sand
					DEEP-51	8.25	8.45	Shale	with some glauconitic sand
					DEEP-52	8.45	8.65	Shale	Hard, dry, crumbling shale, sandy (glauconitic sand)
	8.65	9.25	0.19	32%	DEEP-53	8.65	8.95	Shale	with some oxidized sand
					DEEP-54	8.95	9.25	Shale	Sandy (oxidized sand)

Appendix B:

Laboratory Test Results and PHREEQC Calculated Field Concentrations for Soil Salinity

Table B1: Laboratory and Phreeq-C soil salinity data for D1 locations.

Sample Location	Sample Date	Sample Depth (cm)	Point Depth (cm)	Above Shale (cm)	M.C. %	pH	EC dS/m	SAR	% Sat	Lab Measured Sat Paste Conc. Ca^{2+} mg/L	Mg^{2+} mg/L	Na^{+} mg/L	Cl^{-} mg/L	SO_4^{2-} mg/L	Phrq-C Calc. Field Conc. Na^{+} mg/L	Ca^{2+} mg/L	SO_4^{2-} mg/L
D1 - 1	1-Jun-02	0-10	5	23	14.8	7.3	3.0	6.4	42.9	265	58	440	91	557	698	448	844
D1 - 1	1-Jun-02	10-20	15	13	14.9	7.4	4.9	9.5	41.6	426	106	846	54	841	1227	483	973
D1 - 1	1-Jun-02	20-30	25	3	21.4	7.5	7.3	13.9	47.9	462	184	1400	32	1390	1908	400	1533
D1 - 1	1-Jun-02	30-40	35	-7	22.8	7.4	11.1	19.7	73.7	436	380	2328	26	2204	4943	319	4223
D1 - 1	1-Jun-02	40-50	45	-17	22.1	7.3	12.8	22.8	66.1	422	467	2861	41	2538	6071	307	5183
D1 - 1	1-Jun-02	50-60	55	-27	22.1	7.5	12.4	22.2	69.0	452	424	2731	46	2538	5854	306	5016
D1 - 1	1-Jun-02	60-70	65	-37	28.3	7.6	12.4	24.6	69.1	446	328	2803	51	2421	4983	321	3922
D1 - 1	1-Jun-02	70-80	75	-47	20.5	7.6	9.2	18.7	50.4	474	219	1964	51	1725	2896	375	2133
D1 - 1	1-Jun-02	80-90	85	-57	18.7	7.6	7.5	14.1	46.3	487	175	1429	48	1390	1978	407	1512
D1 - 1	1-Jun-02	90-100	95	-67	21.6	7.6	6.5	11.3	49.8	484	184	1151	41	1181	1584	427	1303
D1 - 1	1-Jun-02	100-110	105	-77	21.5	7.4	5.8	9.2	47.0	497	171	930	32	1044	1238	451	1098
D1 - 1	1-Jun-02	110-120	115	-87	22.7	7.6	5.3	8.8	45.7	472	146	856	28	988	1110	450	1034
D1 - 1	1-Jun-02	120-130	125	-97	17.9	7.6	5.2	10.0	51.4	405	132	902	32	932	1376	447	1143
D1 - 1	1-Jun-02	130-140	135	-107	22.4	7.4	5.2	8.3	45.8	476	164	820	32	951	1078	461	1017
D1 - 1	1-Jun-02	140-150	145	-117	19.8	7.5	5.9	9.8	48.5	499	166	989	51	1083	1368	448	1143
D1 - 1	1-Jun-02	150-160	155	-127	18.1	7.6	5.0	9.1	48.9	429	120	828	51	895	1216	463	1028
D1-1	20-Aug-08	0-10	5	28	31.8	7.4	1.1	1.3	95.0	135	40	68	22	73			
D1-1	20-Aug-08	10-20	15	18	24.0	7.8	1.2	4.0	53.0	83	24	162	13	152	278	233	333
D1-1	20-Aug-08	20-30	25	8	16.2	7.6	3.6	5.3	51.0	441	126	494	14	782	749	485	849
D1-1	20-Aug-08	30-40	35	-2	30.0	7.6	6.2	10.4	62.0	468	206	1073	13	1316	1459	387	1441
D1-1	20-Aug-08	40-50	45	-12	26.4	7.6	8.0	14.2	100.0	432	302	1580	14	1770	3589	327	3315
D1-1	20-Aug-08	50-60	55	-22	28.8	7.5	10.4	18.4	90.0	433	456	2311	27	2467	5258	297	5104

Sample Location	Sample Date	Sample Depth (cm)	Point Depth (cm)	Above Shale (cm)	M.C. %	pH	EC dS/m	SAR	% Sat	Lab Measured Sat Paste Conc. Ca^{2+} mg/L	Mg^{2+} mg/L	Na^{+} mg/L	Cl^{-} mg/L	SO_4^{2-} mg/L	Phrq-C Calc. Field Conc. Na^{+} mg/L	Ca^{2+} mg/L	SO_4^{2-} mg/L
D1-1	20-Aug-08	60-70	65	-32	30.4	7.6	9.9	17.5	99.0	431	419	2141	27	2283	4969	303	4752
D1-1	20-Aug-08	70-80	75	-42	24.6	7.8	9.0	17.0	76.0	428	325	1921	45	2026	3725	323	3344
D1-1	20-Aug-08	80-90	85	-52	17.9	7.8	8.1	15.8	70.0	436	271	1700	39	1786	3404	343	2841
D1-1	20-Aug-08	90-100	95	-62	19.8	7.7	6.9	12.8	70.0	457	230	1349	43	1514	2366	367	2020
D1-1	20-Aug-08	100-110	105	-72	22.9	7.5	5.9	9.6	67.0	479	222	1019	42	1278	1610	403	1468
D1-1	20-Aug-08	110-120	115	-82	22.4	7.5	5.5	8.9	72.0	469	200	911	53	1194	1496	397	1419
D1-1	20-Aug-08	120-130	125	-92	19.3	7.6	4.3	8.4	64.0	309	123	695	45	831	1188	415	1192
D1-1	20-Aug-08	130-140	135	-102	22.5	7.6	3.4	9.8	66.0	209	86	664	48	641	1230	432	1143
D1-1	20-Aug-08	140-150	145	-112	22.6	7.6	4.1	10.3	67.0	225	89	725	54	718	1305	414	1219
D1 - 2	1-Jun-02	0-10	5	25	48.6	6.6	1.3	1.4	175.4	160	50	81	41	147	211	592	532
D1 - 2	1-Jun-02	10-20	15	15	28.9	7.4	2.2	3.6	44.8	298	56	257	65	264	332	429	410
D1 - 2	1-Jun-02	20-30	25	5	19.3	7.7	4.0	8.1	40.7	355	79	648	98	610	924	506	823
D1 - 2	1-Jun-02	30-40	35	-5	17.8	7.6	7.1	12.1	47.1	509	184	1252	98	1283	1776	430	1353
D1 - 2	1-Jun-02	40-50	45	-15	19.3	7.4	7.1	13.1	63.3	464	166	1288	81	1304	2139	408	1593
D1 - 2	1-Jun-02	50-60	55	-25	18.3	7.4	7.9	14.6	64.8	476	192	1491	72	1434	2623	396	1893
D1 - 2	1-Jun-02	60-70	65	-35	16.5	7.4	7.8	14.7	70.5	481	183	1495	60	1390	2897	399	1996
D1 - 2	1-Jun-02	70-80	75	-45	33.6	7.4	7.7	14.1	67.4	501	167	1425	60	1412	1956	394	1565
D1 - 2	1-Jun-02	80-90	85	-55	15.9	7.4	7.6	14.2	67.3	462	166	1395	43	1346	2605	400	1847
D1 - 2	1-Jun-02	90-100	95	-65	18.4	7.3	8.0	14.4	77.5	460	210	1482	34	1434	2998	385	2182
D1-2	20-Aug-08	0-10	5	31	108.0	6.4	1.1	2.4	178.0	89	32	107	25	96	158	160	158
D1-2	20-Aug-08	10-20	15	21	21.6	7.6	2.1	5.4	64.0	159	48	302	19	348	591	473	807
D1-2	20-Aug-08	20-30	25	11	20.6	7.6	2.5	6.0	62.0	205	63	387	21	453	714	467	860
D1-2	20-Aug-08	30-40	35	1	21.6	7.5	4.9	7.1	64.0	483	156	706	38	1014	1070	428	1096

Sample Location	Sample Date	Sample Depth (cm)	Point Depth (cm)	Above Shale (cm)	M.C. %	pH	EC dS/m	SAR	% Sat	Lab Measured Sat Paste Conc. Ca^{2+} mg/L	Mg^{2+} mg/L	Na^{+} mg/L	Cl^{-} mg/L	SO_4^{2-} mg/L	Phrq-C Calc. Field Conc. Na^{+} mg/L	Ca^{2+} mg/L	SO_4^{2-} mg/L
D1-2	20-Aug-08	40-50	45	-9	19.8	7.4	6.0	10.7	68.0	466	182	1082	46	1291	1796	390	1565
D1-2	20-Aug-08	50-60	55	-19	22.1	7.4	6.9	12.8	78.0	455	209	1308	51	1487	2387	360	2064
D1-2	20-Aug-08	60-70	65	-29	21.4	7.6	6.4	11.8	74.0	457	181	1182	35	1365	2023	371	1771
D1-2	20-Aug-08	70-80	75	-39	21.7	7.6	7.5	14.2	68.0	437	193	1415	54	1559	2348	342	2132
D1-2	20-Aug-08	80-90	85	-49	19.6	7.5	7.4	14.2	77.0	439	187	1416	55	1558	2633	337	2333
D1-2	20-Aug-08	90-100	95	-59	23.8	7.6	7.7	14.9	76.0	432	187	1474	61	1618	2543	331	2346
D1-2	20-Aug-08	100-110	105	-69	24.2	7.5	7.7	15.2	76.0	438	183	1513	64	1632	2573	334	2298
D1-2	21-Oct-05	0-10	5	27		6.2	0.3	1.0	255.0	37	13	27	19	25			
D1-2	21-Oct-05	10-20	15	17		7.0	1.0	2.3	85.0	125	36	112	22	104			
D1-2	21-Oct-05	20-32	25	7		7.7	2.7	7.6	48.0	184	54	458	46	479			
D1-2	21-Oct-05	32-40	35	-3		7.5	5.7	9.6	57.0	504	188	993	49	1302			
D1-2	21-Oct-05	40-50	45	-13		7.4	5.9	10.7	50.0	484	202	1110	54	1368			
D1-2	21-Oct-05	50-60	55	-23		7.4	7.0	13.4	60.0	483	222	1432	65	1637			
D1-2	21-Oct-05	60-70	65	-33		7.5	7.2	15.2	64.0	478	211	1594	61	1734			
D1-2	21-Oct-05	70-80	75	-43		7.6	7.6	16.1	64.0	448	208	1641	70	1766			
D1-2	21-Oct-05	80-90	85	-53		7.5	7.6	15.6	70.0	463	239	1671	61	1829			
D1-2	21-Oct-05	90-100	95	-63		7.5	7.7	14.7	78.0	446	267	1590	58	1795			
D1-2	14-Aug-07	0-10	5	28	26.2	6.3	0.7	2.0	197.0	61	20	72	23	70			
D1-2	14-Aug-07	10-20	15	18	13.7	7.2	2.5	6.1	73.0	175	56	362	49	390			
D1-2	14-Aug-07	20-30	25	8	13.0	7.2	3.9	6.4	70.0	386	118	567	53	800			
D1-2	14-Aug-07	30-40	35	-2	16.4	7.3	5.3	8.4	64.0	488	166	847	56	1170			
D1-2	14-Aug-07	40-50	45	-12	13.6	7.4	6.4	11.0	68.0	479	197	1143	59	1397			
D1-2	14-Aug-07	50-60	55	-22	15.0	7.3	6.8	12.5	57.0	465	198	1286	63	1488			

Sample Location	Sample Date	Sample Depth (cm)	Point Depth (cm)	Above Shale (cm)	M.C. %	pH	EC dS/m	SAR	% Sat	Lab Measured Sat Paste Conc. Ca^{2+} mg/L	Mg^{2+} mg/L	Na^{+} mg/L	Cl^{-} mg/L	SO_4^{2-} mg/L	Phrq-C Calc. Field Conc. Na^{+} mg/L	Ca^{2+} mg/L	SO_4^{2-} mg/L
D1-2	14-Aug-07	60-70	65	-32	21.1	7.4	7.8	14.4	76.0	496	226	1539	53	1750			
D1-2	14-Aug-07	70-80	75	-42	22.1	7.4	8.1	15.2	68.0	460	235	1618	49	1779			
D1-2	14-Aug-07	100-110	105	-72	25.4	7.4	8.8	16.4	75.0	473	303	1867	56	2067			
D1-2	14-Aug-07	140-150	145	-112	27.7	7.2	9.2	16.6	78.0	477	324	1923	60	2128			
D1 - 3	1-Jun-02	0-10	5	55	71.7	5.9	0.7	0.9	146.5	91	30	38	14	81	64	197	166
D1 - 3	1-Jun-02	10-20	15	45	77.9	6.4	1.2	1.0	113.7	155	46	57	16	97	76	233	142
D1 - 3	1-Jun-02	20-30	25	35	80.8	6.2	1.2	1.0	122.3	159	52	59	12	130	80	249	197
D1 - 3	1-Jun-02	30-40	35	25	18.0	6.9	1.5	2.2	62.3	215	38	131	12	163	268	649	535
D1 - 3	1-Jun-02	40-50	45	15	16.1	7.4	2.2	6.0	53.8	222	28	355	12	315	668	547	675
D1 - 3	1-Jun-02	50-60	55	5	18.4	7.3	4.6	8.7	53.7	421	89	757	14	823	1147	467	971
D1 - 3	1-Jun-02	60-70	65	-5	14.3	7.3	6.4	10.4	66.4	501	184	1067	13	1181	1954	433	1471
D1 - 3	1-Jun-02	70-80	75	-15	18.3	7.1	7.3	11.3	75.5	540	282	1304	14	1390	2525	411	1910
D1 - 3	1-Jun-02	80-90	85	-25	20.0	7.2	7.5	11.0	83.1	579	313	1325	17	1434	2674	404	2050
D1 - 3	1-Jun-02	90-100	95	-35	19.0	7.2	7.9	12.9	83.5	511	267	1450	16	1503	3074	380	2354
D1 - 3	1-Jun-02	100-110	105	-45	16.3	7.2	8.3	14.1	78.3	487	269	1558	19	1574	3441	370	2634
D1-3	20-Aug-08	0-10	5	61	57.6	6.2	0.4	0.3	221.0	55	18	11	24	32	29	225	122
D1-3	20-Aug-08	10-20	15	51	138.0	6.0	0.5	0.7	321.0	55	16	23	17	45	45	137	104
D1-3	20-Aug-08	20-30	25	41	154.0	5.9	0.8	1.3	469.0	86	26	55	13	106	142	285	324
D1-3	20-Aug-08	30-40	35	31	73.2	6.8	1.7	2.0	218.0	210	54	128	17	233	299	563	623
D1-3	20-Aug-08	40-50	45	21	12.5	7.7	1.8	4.2	47.0	151	35	219	15	283	444	496	706
D1-3	20-Aug-08	50-60	55	11	11.0	7.7	2.3	5.4	46.0	193	53	333	17	422	625	466	819
D1-3	20-Aug-08	60-70	65	1	23.2	7.6	4.6	5.7	68.0	460	159	553	13	956	838	406	1086
D1-3	20-Aug-08	70-80	75	-9	23.6	7.5	5.3	6.8	78.0	456	224	708	12	1150	1175	378	1430

Sample Location	Sample Date	Sample Depth (cm)	Point Depth (cm)	Above Shale (cm)	M.C. %	pH	EC dS/m	SAR	% Sat	Lab Measured Sat Paste Conc. Ca^{2+} mg/L	Mg^{2+} mg/L	Na^{+} mg/L	Cl^{-} mg/L	SO_4^{2-} mg/L	Phrq-C Calc. Field Conc. Na^{+} mg/L	Ca^{2+} mg/L	SO_4^{2-} mg/L
D1-3	20-Aug-08	80-90	85	-19	22.1	7.4	5.7	7.6	84.0	442	255	807	11	1262	1482	358	1760
D1-3	20-Aug-08	90-100	95	-29	25.7	7.4	6.1	8.1	90.0	448	289	899	11	1400	1660	341	2059
D1-3	20-Aug-08	100-110	105	-39	22.8	7.6	6.3	9.0	76.0	441	276	982	14	1434	1678	343	1985
D1 - 4	1-Jun-02	0-10	5	35	97.7	5.7	0.8	0.9	165.3	95	33	40	14	97	60	168	165
D1 - 4	1-Jun-02	10-20	15	25	158.1	5.6	0.9	0.9	241.3	112	41	42	14	114	60	176	174
D1 - 4	1-Jun-02	20-30	25	15	128.2	5.7	1.2	1.6	161.1	129	49	82	22	147	99	167	185
D1 - 4	1-Jun-02	30-40	35	5	24.7	6.7	2.3	4.6	70.4	252	57	311	38	298	580	583	660
D1 - 4	1-Jun-02	40-50	45	-5	12.2	7.1	5.2	7.9	52.9	522	153	798	41	969	1310	499	1006
D1 - 4	1-Jun-02	50-60	55	-15	18.5	7.4	6.5	11.3	56.9	483	179	1141	46	1201	1775	426	1387
D1 - 4	1-Jun-02	60-70	65	-25	21.7	7.4	7.1	12.3	60.1	472	199	1262	46	1325	1945	405	1566
D1 - 4	1-Jun-02	70-80	75	-35	21.2	7.5	6.3	11.0	57.7	487	167	1101	54	1181	1637	426	1317
D1 - 4	1-Jun-02	80-90	85	-45	21.3	7.4	6.1	10.6	62.0	452	167	1042	41	1141	1634	421	1350
D1 - 4	1-Jun-02	90-100	95	-55	21.4	7.3	6.0	9.5	58.9	483	194	977	28	1141	1474	431	1282
D1 - 4	1-Jun-02	100-110	105	-65	23.4	7.3	5.7	8.8	65.3	473	182	885	22	1121	1364	424	1258
D1 - 4	20-Aug-08	0-10	5	44	104.0	5.9	0.3	0.5	183.0	36	13	13	13	26	19	66	46
D1 - 4	20-Aug-08	10-20	15	34	29.5	5.7	0.5	1.2	115.0	43	16	35	13	54	86	200	213
D1 - 4	20-Aug-08	20-30	25	24	59.4	5.6	0.8	2.1	146.0	66	23	78	29	101	150	190	249
D1 - 4	20-Aug-08	30-40	35	14	61.4	6.3	1.7	3.8	148.0	137	46	201	42	249	398	394	604
D1 - 4	20-Aug-08	40-50	45	4	27.4	7.2	2.2	4.7	74.0	180	59	288	43	354	545	486	784
D1 - 4	20-Aug-08	50-60	55	-6	19.8	7.4	4.1	4.5	66.0	474	149	442	33	839	704	454	908
D1 - 4	20-Aug-08	60-70	65	-16	21.8	7.4	4.9	6.2	72.0	494	183	642	38	1046	1019	413	1155
D1 - 4	20-Aug-08	70-80	75	-26	21.2	7.4	5.1	7.0	68.0	491	185	722	47	1101	1117	402	1224
D1 - 4	20-Aug-08	80-90	85	-36	24.4	7.5	5.2	7.8	71.0	485	177	794	44	1130	1215	398	1269

Sample Location	Sample Date	Sample Depth (cm)	Point Depth (cm)	Above Shale (cm)	M.C. %	pH	EC dS/m	SAR	% Sat	Lab Measured Sat Paste Conc. Ca^{2+} mg/L	Mg^{2+} mg/L	Na^{+} mg/L	Cl^{-} mg/L	SO_4^{2-} mg/L	Phrq-C Calc. Field Conc. Na^{+} mg/L	Ca^{2+} mg/L	SO_4^{2-} mg/L
D1 - 4	20-Aug-08	90-100	95	-46	25.8	7.5	5.3	8.0	78.0	482	176	803	38	1149	1278	385	1352
D1 - 4	20-Aug-08	100-110	105	-56	22.6	7.5	5.2	7.8	76.0	472	171	780	39	1109	1275	392	1320
D1 - 5	1-Jun-02	0-10	5	55	89.9	6.2	0.5	0.8	142.3	57	21	28	14	33	39	94	52
D1 - 5	1-Jun-02	10-20	15	45	94.2	5.8	0.6	0.8	162.1	70	23	29	13	65	44	126	112
D1 - 5	1-Jun-02	20-30	25	35	66.2	5.7	0.7	0.9	160.1	80	27	35	17	81	67	207	196
D1 - 5	1-Jun-02	30-40	35	25	61.4	6.5	1.1	1.3	154.5	141	41	70	14	81	138	354	205
D1 - 5	1-Jun-02	40-50	45	15	20.1	7.4	1.7	4.6	49.9	171	32	248	30	197	437	458	488
D1 - 5	1-Jun-02	50-60	55	5	13.3	7.5	3.7	9.2	52.9	269	68	651	57	575	1212	501	933
D1 - 5	1-Jun-02	60-70	65	-5	19.3	7.5	7.5	12.4	72.2	477	228	1316	60	1412	2433	391	1910
D1 - 5	1-Jun-02	70-80	75	-15	18.2	7.6	8.7	15.8	72.7	432	258	1682	81	1648	3479	358	2709
D1 - 5	1-Jun-02	80-90	85	-25	18.9	7.7	9.4	16.6	70.6	480	263	1822	143	1725	3615	365	2649
D1 - 5	1-Jun-02	90-100	95	-35	20.6	7.7	8.8	16.5	71.9	447	221	1708	190	1574	3269	378	2300
D1 - 5	1-Jun-02	100-110	105	-45	22.2	7.4	9.5	16.9	80.1	525	241	1860	239	1725	3740	373	2545
D1-5	20-Aug-08	0-10	5	40	100.0	6.3	2.9	4.5	168.0	304	113	360	29	595	536	444	870
D1-5	20-Aug-08	10-20	15	30	47.9	6.5	4.1	5.6	179.0	398	142	513	31	816	1162	402	1276
D1-5	20-Aug-08	20-30	25	20	129.0	6.8	5.0	7.7	164.0	440	157	738	44	1000	876	412	1062
D1-5	20-Aug-08	30-40	35	10	18.2	7.7	5.7	9.1	56.0	477	173	911	43	1186	1340	396	1308
D1-5	20-Aug-08	40-50	45	0	16.0	7.8	5.7	9.3	56.0	480	188	954	38	1259	1422	381	1426
D1-5	20-Aug-08	50-60	55	-10	23.6	7.8	7.4	11.2	69.0	464	322	1293	42	1652	2144	348	2194
D1-5	20-Aug-08	60-70	65	-20	22.6	7.6	8.3	12.0	90.0	443	414	1467	39	1889	3424	316	3710
D1-5	20-Aug-08	70-80	75	-30	24.4	7.5	9.1	13.2	87.0	451	479	1690	55	2138	3842	306	4253
D1-5	20-Aug-08	80-90	85	-40	24.8	7.5	8.3	12.0	92.0	440	421	1457	50	1891	3327	315	3659
D1-5	20-Aug-08	90-100	95	-50	30.2	7.5	9.2	13.4	92.0	430	480	1696	67	2130	3624	307	4022

Sample Location	Sample Date	Sample Depth (cm)	Point Depth (cm)	Above Shale (cm)	M.C. %	pH	EC dS/m	SAR	% Sat	Lab Measured Sat Paste Conc. Ca^{2+} mg/L	Mg^{2+} mg/L	Na^{+} mg/L	Cl^{-} mg/L	SO_4^{2-} mg/L	Phrq-C Calc. Field Conc. Na^{+} mg/L	Ca^{2+} mg/L	SO_4^{2-} mg/L
D1-5	20-Aug-08	100-110	105	-60	29.3	7.4	9.7	14.0	93.0	446	512	1828	75	2269	4093	302	4504
D1-5	21-Oct-05	0-10	5	55		5.7	0.8	0.6	200.0	144	46	31	28	116			
D1-5	21-Oct-05	10-20	15	45		5.8	0.5	0.5	295.0	114	34	22	17	71			
D1-5	21-Oct-05	20-32	25	35		5.7	1.0	0.7	233.0	169	60	40	12	182			
D1-5	21-Oct-05	32-40	35	25		5.5	1.1	0.8	279.0	189	63	50	15	218			
D1-5	21-Oct-05	40-50	45	15		6.8	1.9	2.0	71.0	266	69	145	23	269			
D1-5	21-Oct-05	50-60	55	5		7.2	2.3	4.1	51.0	237	67	275	33	392			
D1-5	21-Oct-05	60-70	65	-5		7.4	3.4	7.1	70.0	270	96	529	43	671			
D1-5	21-Oct-05	70-80	75	-15		7.4	5.9	9.4	74.0	488	228	1014	69	1378			
D1-5	21-Oct-05	80-90	85	-25		7.5	7.0	13.4	76.0	457	243	1434	99	1632			
D1-5	21-Oct-05	90-100	95	-35		7.5	7.6	15.8	81.0	464	244	1691	128	1790			
D1-5	21-Oct-05	100-110	105	-45		7.4	8.2	17.4	109.0	454	249	1853	150	1927			
D1-5	14-Aug-07	0-10	5	55	32.9	6.4	0.5	1.1	180.0	58	21	38	16	49			
D1-5	14-Aug-07	10-20	15	45	20.5	6.4	0.6	1.5	200.0	55	19	51	19	64			
D1-5	14-Aug-07	20-30	25	35	20.3	7.0	1.3	3.0	108.0	126	38	149	23	158			
D1-5	14-Aug-07	30-40	35	25	12.5	7.3	2.6	5.4	59.0	202	60	342	32	439			
D1-5	14-Aug-07	40-50	45	15	12.2	7.5	3.1	7.7	49.0	214	66	506	41	576			
D1-5	14-Aug-07	50-60	55	5	12.0	7.5	4.3	10.6	58.0	259	97	788	52	850			
D1-5	14-Aug-07	60-70	65	-5	20.0	7.5	7.3	12.6	81.0	507	247	1395	67	1667			
D1-5	14-Aug-07	70-80	75	-15	20.8	7.5	8.2	14.0	85.0	468	299	1576	87	1835			
D1-5	14-Aug-07	80-90	85	-25	24.4	7.4	8.1	13.5	95.0	459	311	1526	80	1800			
D1-5	14-Aug-07	120-130	125	-65	25.9	7.3	8.8	14.8	85.0	452	355	1729	111	1953			
D1-5	14-Aug-07	150-160	155	-95	24.7	7.3	8.9	14.4	86.0	474	359	1721	119	2000			

Sample Location	Sample Date	Sample Depth (cm)	Point Depth (cm)	Above Shale (cm)	M.C. %	pH	EC dS/m	SAR	% Sat	Lab Measured Sat Paste Conc. Ca^{2+} mg/L	Mg^{2+} mg/L	Na^{+} mg/L	Cl^{-} mg/L	SO_4^{2-} mg/L	Phrq-C Calc. Field Conc. Na^{+} mg/L	Ca^{2+} mg/L	SO_4^{2-} mg/L
D1 - 6	1-Jun-02	0-10	5	35	50.4	7.1	1.0	1.6	99.5	118	38	77	22	81	124	241	160
D1 - 6	1-Jun-02	10-20	15	25	28.9	7.4	1.2	1.6	64.3	147	40	83	15	130	139	351	291
D1 - 6	1-Jun-02	20-30	25	15	19.1	7.7	1.4	2.1	53.5	155	38	113	12	180	218	505	505
D1 - 6	1-Jun-02	30-40	35	5	18.0	7.8	2.2	6.1	54.1	219	50	386	12	315	708	530	745
D1 - 6	1-Jun-02	40-50	45	-5	19.2	7.5	6.2	8.8	87.5	499	251	970	15	1181	1992	418	1653
D1 - 6	1-Jun-02	50-60	55	-15	19.2	7.5	9.1	11.8	73.0	644	432	1573	14	1862	3054	366	2658
D1 - 6	1-Jun-02	60-70	65	-25	17.2	7.3	10.2	13.2	71.1	536	552	1829	21	2072	4226	332	4137
D1 - 6	1-Jun-02	70-80	75	-35	17.1	7.3	9.9	14.1	75.5	430	456	1760	21	2010	4416	317	4462
D1 - 6	1-Jun-02	80-90	85	-45	17.5	7.4	10.2	14.6	71.5	431	482	1850	22	2105	4444	316	4520
D1 - 6	1-Jun-02	90-100	95	-55	17.0	7.3	9.8	13.5	77.4	496	449	1729	21	1979	4249	327	4091
D1 - 6	1-Jun-02	100-110	105	-65	17.2	7.4	9.7	13.4	75.4	466	456	1698	18	1949	4085	327	4018
D1-6	20-Aug-08	0-10	5	40	57.9	7.0	2.0	2.9	81.0	180	72	180	27	332	233	273	467
D1-6	20-Aug-08	10-20	15	30	44.9	7.3	3.1	6.0	72.0	290	81	447	21	590	617	447	845
D1-6	20-Aug-08	20-30	25	20	20.4	7.8	3.5	6.6	55.0	345	89	531	13	735	789	421	960
D1-6	20-Aug-08	30-40	35	10	21.1	7.8	4.2	7.3	54.0	356	111	619	15	820	899	417	1037
D1-6	20-Aug-08	40-50	45	0	23.1	7.7	6.1	8.2	72.0	465	278	913	24	1343	1508	372	1675
D1-6	20-Aug-08	50-60	55	-10	24.8	7.5	8.2	11.2	82.0	441	449	1402	23	1902	2840	322	3251
D1-6	20-Aug-08	60-70	65	-20	24.2	7.6	9.4	13.3	85.0	438	532	1753	31	2224	4078	304	4633
D1-6	20-Aug-08	70-80	75	-30	25.2	7.7	10.4	14.5	81.0	451	590	2000	37	2469	4460	301	4979
D1-6	20-Aug-08	80-90	85	-40	28.3	7.7	10.0	14.2	88.0	435	549	1886	35	2375	4168	298	4740
D1-6	20-Aug-08	90-100	95	-50	32.1	7.7	10.3	14.9	88.0	430	564	2000	40	2455	4086	298	4610
D1-6	20-Aug-08	100-110	105	-60	34.1	7.7	11.2	15.7	86.0	433	652	2209	55	2686	4391	298	4931

Sample Location	Sample Date	Sample Depth (cm)	Point Depth (cm)	Above Shale (cm)	M.C. %	pH	EC dS/m	SAR	% Sat	Lab Measured Sat Paste Conc. Ca^{2+} mg/L	Mg^{2+} mg/L	Na^{+} mg/L	Cl^{-} mg/L	SO_4^{2-} mg/L	Phrq-C Calc. Field Conc. Na^{+} mg/L	Ca^{2+} mg/L	SO_4^{2-} mg/L
D1 - 7	1-Jun-02	0-10	5	45	74.0	6.4	0.5	0.8	105.3	62	20	28	18	49	35	91	69
D1 - 7	1-Jun-02	10-20	15	35	57.7	6.6	0.7	0.9	112.6	78	27	37	18	65	59	161	127
D1 - 7	1-Jun-02	20-30	25	25	23.6	7.2	1.1	1.2	58.1	129	39	61	12	97	107	338	240
D1 - 7	1-Jun-02	30-40	35	15	20.9	7.5	1.3	2.6	62.3	130	36	129	15	163	265	466	487
D1 - 7	1-Jun-02	40-50	45	5	17.6	7.5	3.8	8.3	43.6	301	96	644	12	662	989	470	950
D1 - 7	1-Jun-02	50-60	55	-5	21.2	7.3	8.3	10.2	64.3	479	469	1311	12	1725	2324	366	2440
D1 - 7	1-Jun-02	60-70	65	-15	19.0	7.3	9.9	10.6	61.8	511	691	1565	13	2137	3083	338	3637
D1 - 7	1-Jun-02	70-80	75	-25	17.7	7.4	10.9	11.1	58.4	465	858	1749	16	2538	3738	311	5073
D1 - 7	1-Jun-02	80-90	85	-35	18.9	7.4	10.8	14.3	62.4	465	608	1986	26	2239	4119	324	4253
D1 - 7	1-Jun-02	90-100	95	-45	19.4	7.2	12.1	19.4	66.7	453	523	2560	34	2459	5854	308	5344
D1 - 7	1-Jun-02	100-110	105	-55	19.8	7.1	12.9	21.0	70.5	409	532	2740	65	2137	6549	310	5561
D1-7	20-Aug-08	0-10	5	48	39.8	6.4	0.5	0.4	157.0	77	26	15	18	32	38	320	127
D1-7	20-Aug-08	10-20	15	38	35.8	6.3	0.4	0.6	117.0	55	17	19	12	26	41	193	87
D1-7	20-Aug-08	20-30	25	28	21.1	7.6	0.5	1.2	56.0	57	15	39	7	31	72	173	84
D1-7	20-Aug-08	30-40	35	18	21.5	7.7	0.5	2.0	50.0	40	11	56	8	38	96	114	87
D1-7	20-Aug-08	40-50	45	8	18.3	7.9	0.7	3.2	48.0	41	13	92	6	66	174	148	175
D1-7	20-Aug-08	50-60	55	-2	18.4	7.5	3.5	2.6	69.0	513	213	277	6	875	453	443	916
D1-7	20-Aug-08	60-70	65	-12	20.6	7.4	4.5	3.0	77.0	488	306	345	16	1004	615	435	1139
D1-7	20-Aug-08	70-80	75	-22	24.1	7.4	4.9	3.6	79.0	478	339	420	8	1101	730	409	1305
D1-7	20-Aug-08	80-90	85	-32	24.4	7.1	5.5	4.3	82.0	477	422	530	7	1280	976	388	1656
D1-7	20-Aug-08	90-100	95	-42	25.7	7.4	5.9	5.2	86.0	462	459	653	8	1407	1257	368	2002
D1-7	20-Aug-08	100-110	105	-52	25.6	7.4	5.8	5.0	87.0	462	440	626	8	1379	1192	367	1934
D1 - 8	1-Jun-02	0-10	5	55	68.1	6.9	0.8	0.7	91.6	100	36	30	46	65	37	137	87

Sample Location	Sample Date	Sample Depth (cm)	Point Depth (cm)	Above Shale (cm)	M.C. %	pH	EC dS/m	SAR	% Sat	Lab Measured Sat Paste Conc. Ca^{2+} mg/L	Mg^{2+} mg/L	Na^{+} mg/L	Cl^{-} mg/L	SO_4^{2-} mg/L	Phrq-C Calc. Field Conc. Na^{+} mg/L	Ca^{2+} mg/L	SO_4^{2-} mg/L
D1 - 8	1-Jun-02	10-20	15	45	27.7	7.4	0.9	0.8	54.1	112	34	38	30	49	58	230	95
D1 - 8	1-Jun-02	20-30	25	35	23.4	7.7	0.6	0.9	47.4	75	21	33	12	33	50	163	66
D1 - 8	1-Jun-02	30-40	35	25	21.5	7.7	0.8	1.3	48.9	102	27	58	12	81	96	256	185
D1 - 8	1-Jun-02	40-50	45	15	21.1	7.8	1.5	3.8	46.5	115	29	178	14	163	305	313	360
D1 - 8	1-Jun-02	50-60	55	5	19.2	8.0	4.5	12.3	48.6	268	74	881	30	716	1411	442	1134
D1 - 8	1-Jun-02	60-70	65	-5	22.9	7.7	8.8	13.4	66.5	563	319	1607	26	1752	2655	372	2209
D1 - 8	1-Jun-02	70-80	75	-15	20.5	7.6	10.9	15.9	70.9	443	455	1990	28	2239	4345	313	4299
D1 - 8	1-Jun-02	80-90	85	-25	19.4	7.6	11.6	15.5	64.7	462	571	2106	28	2421	4553	310	4740
D1 - 8	1-Jun-02	90-100	95	-35	18.3	7.4	10.8	15.7	67.4	474	478	2030	34	2239	4512	318	4354
D1 - 8	1-Jun-02	100-110	105	-45	18.6	7.4	11.3	16.7	68.7	451	481	2144	62	2310	5016	310	4872
D1 - 8	20-Aug-08	0-10	5	64	28.5	7.0	0.9	0.6	81.0	127	41	30	25	46	55	308	130
D1 - 8	20-Aug-08	10-20	15	54	32.6	6.5	0.5	0.4	149.0	64	22	15	28	27	43	314	125
D1 - 8	20-Aug-08	20-30	25	44	116.0	6.7	0.7	0.7	170.0	84	27	31	28	38	41	125	56
D1 - 8	20-Aug-08	30-40	35	34	20.5	7.7	0.7	1.8	58.0	63	17	64	12	62	123	217	177
D1 - 8	20-Aug-08	40-50	45	24	24.0	7.7	1.0	4.6	54.0	62	15	156	11	109	277	188	247
D1 - 8	20-Aug-08	50-60	55	14	24.7	8.1	1.7	8.8	54.0	60	17	300	13	220	552	201	484
D1 - 8	20-Aug-08	60-70	65	4	17.7	8.1	2.4	11.7	61.0	73	32	482	15	377	1192	415	1180
D1 - 8	20-Aug-08	70-80	75	-6	22.6	7.4	6.1	8.9	91.0	457	253	954	18	1341	1881	360	1948
D1 - 8	20-Aug-08	80-90	85	-16	15.7	7.5	6.7	9.6	94.0	439	310	1074	23	1489	2706	333	2868
D1 - 8	20-Aug-08	90-100	95	-26	18.8	7.4	7.9	11.4	90.0	432	424	1389	29	1833	3656	315	4061
D1 - 8	20-Aug-08	100-110	105	-36	23.6	7.3	8.5	12.1	94.0	432	486	1553	30	2021	3870	307	4454
D1-9	1-Jun-02	0-10	5	45	91.5	5.5	0.7	0.8	142.8	78	29	34	87	77	48	127	120
D1-9	1-Jun-02	10-20	15	35	30.2	6.7	1.5	1.8	68.2	171	55	105	53	142	181	416	321

Sample Location	Sample Date	Sample Depth (cm)	Point Depth (cm)	Above Shale (cm)	M.C. %	pH	EC dS/m	SAR	% Sat	Lab Measured Sat Paste Conc. Ca^{2+} mg/L	Mg^{2+} mg/L	Na^{+} mg/L	Cl^{-} mg/L	SO_4^{2-} mg/L	Phrq-C Calc. Field Conc. Na^{+} mg/L	Ca^{2+} mg/L	SO_4^{2-} mg/L
D1-9	1-Jun-02	20-30	25	25	14.2	7.6	1.2	2.7	48.0	109	29	125	58	170	270	478	576
D1-9	1-Jun-02	30-40	35	15	16.1	7.7	2.6	9.1	55.2	132	39	464	90	442	950	420	1008
D1-9	1-Jun-02	40-50	45	5	16.9	7.6	7.9	15.7	63.9	434	174	1526	112	1477	2759	384	1978
D1-9	1-Jun-02	50-60	55	-5	22.8	7.5	11.3	22.8	85.5	400	274	2422	117	2045	5900	317	4503
D1-9	1-Jun-02	60-70	65	-15	20.3	7.0	14.0	25.3	90.1	370	398	2942	144	2382	9299	286	7607
D1-9	1-Jun-02	70-80	75	-25	19.1	7.2	13.9	25.4	101.9	394	360	2893	164	2513	10974	268	9286
D1-9	1-Jun-02	80-90	85	-35	19.9	7.1	13.9	27.2	98.5	388	399	3190	174	2251	11265	275	8749
D1-9	1-Jun-02	90-100	95	-45	21.8	7.0	13.3	30.5	107.8	416	365	3529	203	2513	13174	265	9899
D1-9	1-Jun-02	100-110	105	-55	21.6	7.3	12.4	28.7	121.4	337	226	2773	146	1992	11031	282	7960
D1-9	20-Aug-08	0-10	5	43	24.8	5.8	0.5	0.8	162.0	53	20	27	23	34	97	407	220
D1-9	20-Aug-08	10-20	15	33	22.2	6.9	0.8	1.0	59.0	95	27	46	19	30	82	263	80
D1-9	20-Aug-08	20-30	25	23	17.7	7.9	0.6	2.0	48.0	45	12	56	17	25	108	154	70
D1-9	20-Aug-08	30-40	35	13	19.1	8.1	0.9	5.9	48.0	30	8	142	31	62	284	123	159
D1-9	20-Aug-08	40-50	45	3	28.6	8.0	1.7	11.3	64.0	37	13	313	44	191	600	140	424
D1-9	20-Aug-08	50-60	55	-7	34.3	5.7	6.4	10.6	92.0	466	210	1098	57	1359	1828	368	1742
D1-9	20-Aug-08	60-70	65	-17	31.4	6.5	9.4	18.2	118.0	422	288	1983	67	2034	5086	301	4546
D1-9	20-Aug-08	70-80	75	-27	27.0	7.3	11.2	23.2	123.0	409	303	2545	88	2431	8458	271	7451
D1-9	20-Aug-08	80-90	85	-37	29.2	7.5	12.3	25.8	134.0	403	334	2903	104	2701	10369	257	9170
D1-9	20-Aug-08	90-100	95	-47	31.8	7.0	13.1	27.2	137.0	402	394	3212	126	3015	11230	249	10173
D1-9	20-Aug-08	100-110	105	-57	28.8	7.2	14.7	29.7	127.0	409	452	3677	157	3441	13509	235	12354
D1-9	21-Oct-05	0-10	5	45		5.8	0.6	0.7	134.0	83	30	28	60	48			
D1-9	21-Oct-05	10-20	15	35		7.5	0.5	1.2	57.0	63	18	42	18	23			
D1-9	21-Oct-05	20-32	25	25		7.8	0.6	2.6	48.0	57	15	85	25	50			

Sample Location	Sample Date	Sample Depth (cm)	Point Depth (cm)	Above Shale (cm)	M.C. %	pH	EC dS/m	SAR	% Sat	Lab Measured Sat Paste Conc. Ca^{2+} mg/L	Mg^{2+} mg/L	Na^{+} mg/L	Cl^{-} mg/L	SO_4^{2-} mg/L	Phrq-C Calc. Field Conc. Na^{+} mg/L	Ca^{2+} mg/L	SO_4^{2-} mg/L
D1-9	21-Oct-05	32-40	35	15		7.8	2.1	8.8	49.0	102	29	388	71	306			
D1-9	21-Oct-05	40-50	45	5		7.6	3.8	12.0	63.0	187	65	778	79	698			
D1-9	21-Oct-05	50-60	55	-5		7.7	9.0	17.8	70.0	459	331	2057	107	2186			
D1-9	21-Oct-05	60-70	65	-15		7.5	11.6	20.8	78.0	438	571	2821	123	3026			
D1-9	21-Oct-05	70-80	75	-25		6.5	13.0	22.8	88.0	445	705	3341	148	3534			
D1-9	21-Oct-05	80-90	85	-35		6.8	14.3	27.8	97.0	447	751	4155	196	4062			
D1-9	21-Oct-05	90-100	95	-45		6.8	13.9	30.0	109.0	417	562	4000	208	3771			
D1-9	14-Aug-07	0-10	5	45	19.2	6.2	0.7	1.1	139.0	73	27	45	27	43			
D1-9	14-Aug-07	10-20	15	35	14.6	6.7	1.4	1.9	77.0	156	52	110	60	136			
D1-9	14-Aug-07	20-30	25	25	14.1	7.1	1.8	3.0	75.0	177	53	177	85	209			
D1-9	14-Aug-07	30-40	35	15	15.0	7.4	2.2	6.0	64.0	143	43	320	122	316			
D1-9	14-Aug-07	40-50	45	5	13.5	7.5	7.0	13.1	72.0	476	185	1331	111	1500			
D1-9	14-Aug-07	50-60	55	-5	15.7	7.5	8.3	15.7	87.0	451	261	1690	105	1839			
D1-9	14-Aug-07	60-70	65	-15	24.7	7.5	10.3	19.0	98.0	456	363	2245	114	2296			
D1-9	14-Aug-07	70-80	75	-25	23.7	7.5	11.7	21.5	104.0	443	452	2692	121	2750			
D1-9	14-Aug-07	80-90	85	-35	22.1	7.0	12.6	22.6	111.0	423	479	2865	138	2919			
D1-9	14-Aug-07	120-130	125	-75	30.7	7.3	13.2	27.0	146.0	432	408	3274	134	3110			
D1-9	14-Aug-07	140-150	145	-95	22.4	7.3	10.9	25.4	185.0	349	247	2541	110	2389			
D1 - 10	1-Jun-02	0-10	5	55	99.2	5.3	0.5	0.7	261.0	52	19	25	35	72	52	151	190
D1 - 10	1-Jun-02	10-20	15	45	82.4	5.0	0.7	0.8	206.2	84	27	34	28	105	68	226	264
D1 - 10	1-Jun-02	20-30	25	35	83.8	5.1	0.7	0.9	213.2	90	31	37	28	118	75	244	300
D1 - 10	1-Jun-02	30-40	35	25	17.5	7.2	1.5	3.3	49.5	164	41	180	32	251	345	525	653
D1 - 10	1-Jun-02	40-50	45	15	16.2	7.3	2.5	7.5	50.1	158	39	407	40	386	791	474	840

Sample Location	Sample Date	Sample Depth (cm)	Point Depth (cm)	Above Shale (cm)	M.C. %	pH	EC dS/m	SAR	% Sat	Lab Measured Sat Paste Conc. Ca^{2+} mg/L	Mg^{2+} mg/L	Na^{+} mg/L	Cl^{-} mg/L	SO_4^{2-} mg/L	Phrq-C Calc. Field Conc. Na^{+} mg/L	Ca^{2+} mg/L	SO_4^{2-} mg/L
D1 - 10	1-Jun-02	50-60	55	5	20.3	7.4	6.6	14.8	69.2	368	115	1268	39	1212	2224	388	1681
D1 - 10	1-Jun-02	60-70	65	-5	20.3	7.3	10.1	19.7	81.6	371	219	1938	46	1934	4437	302	3928
D1 - 10	1-Jun-02	70-80	75	-15	19.7	7.4	11.5	21.9	83.3	386	337	2442	55	2251	6753	296	5806
D1 - 10	1-Jun-02	80-90	85	-25	19.6	7.4	11.6	22.6	84.1	391	319	2483	51	2090	6824	306	5465
D1 - 10	1-Jun-02	90-100	95	-35	17.9	7.5	11.6	23.2	78.8	406	291	2503	67	2113	6740	309	5249
D1 - 10	1-Jun-02	100-110	105	-45	18.9	7.4	10.9	22.6	83.8	383	256	2327	90	2000	6278	312	4862
D1 - 10	20-Aug-08	0-10	5	65	69.5	5.8	0.4	0.3	194.0	49	19	11	26	19	22	145	52
D1 - 10	20-Aug-08	10-20	15	55	181.0	6.0	1.0	1.4	240.0	107	39	67	28	107	84	146	142
D1 - 10	20-Aug-08	20-30	25	45	92.7	5.1	1.4	2.3	276.0	143	50	125	34	209	307	476	626
D1 - 10	20-Aug-08	30-40	35	35	16.8	7.1	2.4	5.9	64.0	194	54	359	28	363	742	524	777
D1 - 10	20-Aug-08	40-50	45	25	16.0	7.5	1.8	5.9	49.0	117	31	280	16	249	601	511	742
D1 - 10	20-Aug-08	50-60	55	15	15.9	7.8	2.5	7.5	55.0	180	47	440	15	449	844	460	891
D1 - 10	20-Aug-08	60-70	65	5	15.7	7.9	3.1	10.9	65.0	150	53	611	23	542	1322	427	1167
D1 - 10	20-Aug-08	70-80	75	-5	27.3	7.6	6.8	11.8	98.0	448	227	1224	33	1439	2459	358	2191
D1 - 10	20-Aug-08	80-90	85	-15	30.8	7.6	8.4	15.4	102.0	434	286	1686	50	1833	3597	324	3263
D1 - 10	20-Aug-08	90-100	95	-25	27.3	7.5	9.4	17.7	102.0	423	322	1990	63	2069	4922	303	4494
D1 - 10	20-Aug-08	100-110	105	-35	25.6	7.5	10.4	20.6	103.0	430	341	2369	83	2311	6581	291	5810

Table B2: Laboratory and Phreeq-C soil salinity data for D2 locations.

Sample Location	Sample Date	Sample Depth (cm)	Point Depth (cm)	Above Shale (cm)	M.C. %	pH	EC dS/m	SAR	% Sat	Lab Measured Sat Paste Conc. Ca^{2+} mg/L	Mg^{2+} mg/L	Na^{+} mg/L	Cl^{-} mg/L	SO_4^{2-} mg/L	Phrq-C Calc. Field Conc. Na^{+} mg/L	Ca^{2+} mg/L	SO_4^{2-} mg/L
D2-1	1-Jun-02	0-10	5	15	37.5	7.0	1.9	5.9	82.7	133	39	301	67	225	538	362	497
D2-1	1-Jun-02	10-20	15	5	27.8	7.1	4.5	9.2	62.3	327	89	726	130	707	1122	472	956
D2-1	1-Jun-02	20-30	25	-5	20.1	7.5	8.4	16.2	62.7	397	216	1619	90	1517	2837	376	2151
D2-1	1-Jun-02	30-40	35	-15	24.5	7.1	11.9	20.9	83.4	377	407	2457	101	2251	5933	307	5153
D2-1	1-Jun-02	40-50	45	-25	27.5	7.0	14.0	24.4	100.0	373	503	3072	114	2777	8807	278	7912
D2-1	1-Jun-02	50-60	55	-35	26.0	7.1	15.3	26.0	95.8	372	545	3370	152	2777	9824	278	8425
D2-1	1-Jun-02	60-70	65	-45	25.2	7.2	16.3	28.6	91.2	375	568	3755	176	3043	10943	270	9271
D2-1	1-Jun-02	70-80	75	-55	26.3	7.1	16.0	28.7	94.4	370	536	3692	176	3043	10757	270	9112
D2-1	1-Jun-02	80-90	85	-65	28.0	7.1	15.5	30.1	100.5	389	479	3750	194	2777	10839	277	8477
D2-1	1-Jun-02	90-100	95	-75	28.8	7.1	14.7	29.1	108.2	394	398	3431	160	2513	10120	284	7681
D2-1	19-Aug-08	0-10	5	25	36.8	7.5	3.7	9.1	120.0	260	68	640	107	613	1326	448	1077
D2-1	19-Aug-08	10-20	15	15	127.0	7.4	4.7	11.2	192.0	299	84	854	116	786	1201	420	1104
D2-1	19-Aug-08	20-30	25	5	20.0	7.8	4.6	10.7	82.0	284	82	798	89	807	1569	413	1276
D2-1	19-Aug-08	30-40	35	-5	21.7	7.6	5.4	10.7	64.0	372	101	903	103	991	1419	397	1266
D2-1	19-Aug-08	40-50	45	-15	26.8	7.6	6.0	9.5	68.0	469	172	946	79	1215	1378	382	1381
D2-1	19-Aug-08	50-60	55	-25	29.8	7.2	8.4	13.6	101.0	430	318	1525	40	1832	3240	312	3314
D2-1	19-Aug-08	60-70	65	-35	34.1	7.1	8.7	14.8	103.0	417	298	1621	37	1874	3280	312	3279
D2-1	19-Aug-08	70-80	75	-45	29.2	7.3	9.4	16.6	113.0	416	314	1850	36	2053	4734	292	4667
D2-1	19-Aug-08	80-90	85	-55	30.8	7.3	10.2	19.3	116.0	412	297	2112	50	2216	5541	283	5288
D2-1	19-Aug-08	90-100	95	-65	30.3	7.1	11.4	21.2	114.0	411	351	2430	78	2509	6744	273	6488
D2-2	1-Jun-02	0-10	5	35	103.4	6.0	0.7	0.9	159.3	77	29	35	35	83	48	124	129
D2-2	1-Jun-02	10-20	15	25	147.0	5.8	0.6	1.0	307.3	71	25	40	30	82	72	158	171

Sample Location	Sample Date	Sample Depth	Point Depth	Above Shale	M.C.	pH	EC	SAR	% Sat	Lab Measured Sat Paste Conc. Ca^{2+}	Mg^{2+}	Na^{+}	Cl^{-}	SO_4^{2-}	Phrq-C Calc. Field Conc. Na^{+}	Ca^{2+}	SO_4^{2-}
D2-2	1-Jun-02	20-30	25	15	54.7	6.7	1.8	2.7	94.7	228	64	179	57	278	271	428	481
D2-2	1-Jun-02	30-40	35	5	23.2	7.4	2.3	5.9	55.3	181	47	346	86	358	619	491	764
D2-2	1-Jun-02	40-50	45	-5	21.3	7.3	6.0	10.0	31.8	459	147	961	107	1035	1108	449	1023
D2-2	1-Jun-02	50-60	55	-15	21.4	7.4	7.7	14.3	55.8	418	185	1397	145	1305	2164	409	1610
D2-2	1-Jun-02	60-70	65	-25	18.0	7.4	9.0	18.0	64.3	417	198	1784	178	1557	3365	382	2278
D2-2	1-Jun-02	70-80	75	-35	16.3	7.3	10.0	20.1	49.8	421	235	2075	242	1679	3535	389	2305
D2-2	1-Jun-02	80-90	85	-45	16.6	7.3	10.5	20.9	50.4	406	245	2162	278	1805	3769	374	2542
D2-2	1-Jun-02	90-100	95	-55	18.7	7.3	10.7	21.4	56.3	424	231	2207	298	1805	3917	373	2583
D2-2	19-Aug-08	0-10	5	32	80.1	7.2	1.6	4.3	146.0	116	33	205	27	140	319	216	256
D2-2	19-Aug-08	10-20	15	22	32.7	7.6	1.9	5.8	87.0	114	31	274	25	247	559	414	658
D2-2	19-Aug-08	20-30	25	12	19.6	7.9	2.5	7.3	54.0	160	43	406	39	411	753	449	879
D2-2	19-Aug-08	30-40	35	2	17.8	8.0	2.5	8.2	62.0	132	40	421	37	410	884	431	975
D2-2	19-Aug-08	40-50	45	-8	24.4	7.6	5.1	7.7	75.0	460	128	728	52	1007	1141	403	1171
D2-2	19-Aug-08	50-60	55	-18	20.8	7.6	6.7	11.8	66.0	448	173	1168	103	1344	1862	370	1660
D2-2	19-Aug-08	60-70	65	-28	20.1	7.6	8.5	16.5	66.0	433	208	1682	176	1697	2896	341	2396
D2-2	19-Aug-08	70-80	75	-38	23.5	7.5	9.0	17.8	72.0	422	219	1806	188	1792	3265	336	2660
D2-2	19-Aug-08	80-90	85	-48	17.2	7.6	9.3	19.1	64.0	422	211	1938	206	1859	3689	332	2891
D2-2	19-Aug-08	90-100	95	-58	18.2	7.7	9.5	20.2	60.0	433	188	2000	227	1900	3480	330	2734
D2-2	21-Oct-05	0-10	5	45		6.5	0.6	0.9	162.0	75	26	36	41	47			
D2-2	21-Oct-05	10-20	15	35		6.5	0.2	0.7	454.0	24	8	16	14	9			
D2-2	21-Oct-05	20-32	25	25		6.2	0.2	1.1	544.0	23	7	22	16	15			
D2-2	21-Oct-05	32-40	35	15		7.0	1.7	3.4	76.0	176	50	197	58	221			
D2-2	21-Oct-05	40-50	45	5		7.7	2.9	8.7	59.0	173	59	525	78	508			
D2-2	21-Oct-05	50-60	55	-5		7.5	5.4	9.5	73.0	473	167	945	74	1238			

Sample Location	Sample Date	Sample Depth	Point Depth	Above Shale	M.C.	pH	EC	SAR	% Sat	Lab Measured Sat Paste Conc. Ca^{2+}	Mg^{2+}	Na^{+}	Cl^{-}	SO_4^{2-}	Phrq-C Calc. Field Conc. Na^{+}	Ca^{2+}	SO_4^{2-}
D2-2	21-Oct-05	60-70	65	-15		7.6	6.6	13.3	73.0	462	188	1352	95	1521			
D2-2	21-Oct-05	70-80	75	-25		7.6	7.4	16.0	65.0	460	202	1631	132	1662			
D2-2	21-Oct-05	80-90	85	-35		7.5	8.5	18.5	63.0	462	252	2000	165	1984			
D2-2	21-Oct-05	90-100	95	-45		7.6	8.8	19.8	71.0	444	245	2099	176	2056			
D2-2	14-Aug-07	0-10	5	25	16.7	7.2	1.5	3.7	87.0	133	41	192	48	157			
D2-2	14-Aug-07	10-20	15	15	17.1	7.7	2.0	6.5	62.0	127	37	326	65	284			
D2-2	14-Aug-07	20-30	25	5	18.2	7.3	5.1	8.0	67.0	491	149	785	78	1058			
D2-2	14-Aug-07	30-40	35	-5	20.0	7.5	5.9	10.4	71.0	472	183	1056	92	1251			
D2-2	14-Aug-07	40-50	45	-15	17.7	7.6	7.1	13.5	63.0	475	213	1410	106	1521			
D2-2	14-Aug-07	50-60	55	-25	19.6	7.3	8.2	16.2	69.0	475	206	1681	142	1710			
D2-2	14-Aug-07	100-110	105	-75	19.8	7.5	8.3	17.7	67.0	460	201	1806	155	1731			
D2-3	1-Jun-02	0-10	5	35	98.6	5.8	0.7	1.4	163.3	74	24	55	30	90	80	131	149
D2-3	1-Jun-02	10-20	15	25	49.5	5.9	1.9	5.0	90.4	135	46	264	75	278	417	292	508
D2-3	1-Jun-02	20-30	25	15	31.9	6.9	5.9	9.6	66.2	451	143	912	131	949	1304	462	1067
D2-3	1-Jun-02	30-40	35	5	23.7	7.4	9.7	19.0	67.1	388	239	1934	135	1638	3464	366	2534
D2-3	1-Jun-02	40-50	45	-5	23.8	7.5	10.0	19.3	61.6	426	249	2031	171	1720	3361	370	2409
D2-3	1-Jun-02	50-60	55	-15	21.8	7.4	10.4	19.7	63.0	425	243	2053	196	1762	3634	365	2582
D2-3	1-Jun-02	60-70	65	-25	20.0	7.4	10.6	20.6	60.2	396	250	2130	205	1847	3912	354	2848
D2-3	1-Jun-02	70-80	75	-35	18.1	7.3	10.9	20.9	56.6	422	276	2244	218	1891	4133	359	2916
D2-3	1-Jun-02	80-90	85	-45	18.6	7.3	11.0	21.4	60.1	426	272	2301	208	1891	4399	357	3062
D2-3	1-Jun-02	90-100	95	-55	18.1	7.4	10.5	20.2	51.0	415	248	2110	220	1956	3520	350	2681
D2-3	19-Aug-08	0-10	5	27	120.0	5.7	1.9	3.2	191.0	172	54	190	69	269	279	295	429
D2-3	19-Aug-08	10-20	15	17	82.4	5.9	2.2	5.7	203.0	139	43	301	59	330	630	422	815

Sample Location	Sample Date	Sample Depth	Point Depth	Above Shale	M.C.	pH	EC	SAR	% Sat	Lab Measured Sat Paste Conc. Ca^{2+}	Mg^{2+}	Na^{+}	Cl^{-}	SO_4^{2-}	Phrq-C Calc. Field Conc. Na^{+}	Ca^{2+}	SO_4^{2-}
D2-3	19-Aug-08	20-30	25	7	32.9	7.0	3.8	7.3	95.0	286	89	548	73	619	1015	462	969
D2-3	19-Aug-08	30-40	35	-3	23.6	7.2	4.1	9.3	70.0	247	86	669	59	709	1175	418	1145
D2-3	19-Aug-08	40-50	45	-13	22.2	7.4	5.4	10.4	68.0	350	133	900	56	1028	1486	389	1401
D2-3	19-Aug-08	50-60	55	-23	27.0	7.3	6.5	10.9	75.0	444	181	1083	59	1292	1717	374	1608
D2-3	19-Aug-08	60-70	65	-33	26.9	7.4	7.4	13.0	73.0	440	211	1323	70	1507	2121	354	1954
D2-3	19-Aug-08	70-80	75	-43	17.6	7.5	7.9	14.5	71.0	430	214	1479	75	1606	2821	344	2410
D2-3	19-Aug-08	80-90	85	-53	18.7	7.4	9.2	17.0	71.0	427	282	1845	82	1930	3766	322	3303
D2-3	19-Aug-08	90-100	95	-63	25.0	7.2	8.7	15.5	89.0	411	283	1674	67	1831	3560	318	3302
D2-4	1-Jun-02	0-10	5	45	52.5	6.4	1.1	0.7	101.6	152	51	41	38	125	66	308	242
D2-4	1-Jun-02	10-20	15	35	52.4	6.0	1.1	0.9	105.0	129	42	44	43	134	72	274	269
D2-4	1-Jun-02	20-30	25	25	56.7	6.0	1.4	1.4	171.0	154	52	78	101	166	180	507	501
D2-4	1-Jun-02	30-40	35	15	19.2	7.0	2.8	4.8	49.3	262	72	340	215	345	602	617	643
D2-4	1-Jun-02	40-50	45	5	15.3	7.2	5.6	8.6	41.5	497	131	838	278	899	1226	544	855
D2-4	1-Jun-02	50-60	55	-5	17.0	7.3	9.4	18.3	52.2	431	220	1869	281	1597	3163	398	2073
D2-4	1-Jun-02	60-70	65	-15	18.9	7.3	11.4	21.2	53.7	415	288	2298	326	1934	4053	362	2835
D2-4	1-Jun-02	70-80	75	-25	16.3	7.4	12.3	22.4	49.3	444	305	2506	454	2644	4335	293	4274
D2-4	1-Jun-02	80-90	85	-35	20.2	7.3	12.7	23.2	51.8	427	297	2553	531	2644	4199	297	4052
D2-4	1-Jun-02	90-100	95	-45	19.2	7.2	13.1	24.0	47.5	425	319	2692	600	2777	4332	296	4190
D2-4	19-Aug-08	0-10	5	48	38.4	6.8	0.5	0.8	109.0	53	19	28	14	33	54	165	94
D2-4	19-Aug-08	10-20	15	38	33.5	6.8	0.5	1.1	102.0	46	16	33	11	38	70	160	115
D2-4	19-Aug-08	20-30	25	28	60.3	6.3	0.5	1.7	167.0	45	13	50	13	49	104	147	136
D2-4	19-Aug-08	30-40	35	18	41.7	7.5	1.7	5.4	55.0	106	28	244	20	225	299	155	296
D2-4	19-Aug-08	40-50	45	8	17.6	7.7	2.1	6.1	55.0	129	36	304	27	313	628	468	813
D2-4	19-Aug-08	50-60	55	-2	17.3	7.7	4.0	6.8	56.0	321	110	555	36	736	908	436	1009

Sample Location	Sample Date	Sample Depth	Point Depth	Above Shale	M.C.	pH	EC	SAR	% Sat	Lab Measured Sat Paste Conc. Ca^{2+}	Mg^{2+}	Na^{+}	Cl^{-}	SO_4^{2-}	Phrq-C Calc. Field Conc. Na^{+}	Ca^{2+}	SO_4^{2-}
D2-4	19-Aug-08	60-70	65	-12	18.7	7.5	6.0	9.1	60.0	457	205	937	50	1227	1457	394	1427
D2-4	19-Aug-08	70-80	75	-22	19.3	7.4	6.2	9.8	54.0	433	200	987	67	1233	1466	391	1433
D2-4	19-Aug-08	80-90	85	-32	19.2	7.4	4.9	10.0	58.0	262	138	807	64	916	1375	384	1426
D2-4	19-Aug-08	90-100	95	-42	16.5	7.3	6.9	11.1	59.0	458	246	1181	100	1468	1940	362	1847
D2-5	1-Jun-02	0-10	5	35	32.0	6.7	1.2	1.4	74.9	145	49	75	31	107	132	361	250
D2-5	1-Jun-02	10-20	15	25	16.6	7.3	1.1	2.0	45.3	113	33	95	26	140	177	367	382
D2-5	1-Jun-02	20-30	25	15	15.0	7.4	1.7	3.8	50.1	160	46	213	42	278	428	518	697
D2-5	1-Jun-02	30-40	35	5	15.5	7.5	3.1	8.3	40.5	195	57	510	78	527	859	437	945
D2-5	1-Jun-02	40-50	45	-5	22.6	7.4	8.3	14.9	63.4	427	221	1525	116	1557	2509	373	2017
D2-5	1-Jun-02	50-60	55	-15	31.6	7.4	10.2	19.9	76.3	403	275	2112	145	1934	3657	342	2915
D2-5	1-Jun-02	60-70	65	-25	22.1	7.3	10.7	20.7	71.3	421	281	2236	153	1934	4520	342	3366
D2-5	1-Jun-02	70-80	75	-35	16.3	7.1	10.3	19.7	47.6	425	285	2140	186	1783	3582	380	2484
D2-5	1-Jun-02	80-90	85	-45	6.2	7.2	8.9	18.4	46.6	369	190	1749	239	1361	3923	458	1984
D2-5	1-Jun-02	90-100	95	-55	12.1	7.6	7.8	35.0	71.4	106	56	1795	319	966	5985	381	3142
D2-5	19-Aug-08	0-10	5	44	54.8	6.8	0.8	0.8	143.0	90	35	34	24	39	68	234	101
D2-5	19-Aug-08	10-20	15	34	50.1	7.3	1.0	2.4	109.0	84	28	101	18	72	175	202	158
D2-5	19-Aug-08	20-30	25	24	17.1	7.7	1.5	4.8	47.0	90	28	200	17	188	403	349	521
D2-5	19-Aug-08	30-40	35	14	16.6	7.8	2.3	7.0	50.0	142	48	376	20	384	739	451	900
D2-5	19-Aug-08	40-50	45	4	24.3	7.8	4.8	11.5	52.0	250	115	881	40	892	1341	393	1330
D2-5	19-Aug-08	50-60	55	-6	23.1	7.7	8.2	14.6	78.0	462	271	1603	68	1731	3054	346	2609
D2-5	19-Aug-08	60-70	65	-16	19.0	7.6	9.9	17.5	74.0	447	369	2068	105	2189	4746	309	4318
D2-5	19-Aug-08	70-80	75	-26	32.7	7.3	10.1	17.0	53.0	430	434	2094	125	2245	2729	339	2593
D2-5	19-Aug-08	80-90	85	-36	12.8	7.5	8.9	18.5	53.0	432	242	1943	130	1881	3660	351	2752
D2-5	19-Aug-08	90-100	95	-46	20.0	8.2	5.8	37.2	109.0	47	33	1367	131	927	5298	316	3787

Sample Location	Sample Date	Sample Depth	Point Depth	Above Shale	M.C.	pH	EC	SAR	% Sat	Lab Measured Sat Paste Conc. Ca^{2+}	Mg^{2+}	Na^{+}	Cl^{-}	SO_4^{2-}	Phrq-C Calc. Field Conc. Na^{+}	Ca^{2+}	SO_4^{2-}
D2-5	21-Oct-05	0-10	5	41		7.4	0.6	0.8	66.0	86	28	32	100	36			
D2-5	21-Oct-05	10-20	15	31		7.6	0.8	1.3	47.0	103	29	57	134	94			
D2-5	21-Oct-05	20-32	26	20		7.8	1.8	3.8	45.0	183	48	224	189	298			
D2-5	21-Oct-05	32-40	36	10		7.7	3.2	6.4	45.0	282	87	489	98	622			
D2-5	21-Oct-05	40-50	45	1		7.8	3.8	11.0	56.0	200	82	732	82	696			
D2-5	21-Oct-05	50-60	55	-9		7.5	6.5	11.1	71.0	485	232	1186	76	1521			
D2-5	21-Oct-05	60-70	65	-19		7.6	8.2	16.1	90.0	473	294	1822	77	1989			
D2-5	21-Oct-05	70-80	75	-29		7.5	8.0	16.5	52.0	448	267	1798	165	1921			
D2-5	21-Oct-05	80-90	85	-39		7.5	8.1	19.3	53.0	396	194	1877	196	1828			
D2-5	21-Oct-05	90-100	95	-49		8.0	6.6	32.0	111.0	110	61	1676	113	1297			
D2-5	14-Aug-07	0-10	5	45	14.2	7.4	1.4	2.1	69.0	158	43	113	71	172			
D2-5	14-Aug-07	10-20	15	35	12.2	7.5	2.7	4.6	58.0	274	77	334	112	459			
D2-5	14-Aug-07	20-30	25	25	12.1	7.6	3.7	6.8	50.0	328	96	544	114	678			
D2-5	14-Aug-07	30-40	35	15	14.4	7.4	5.0	9.2	60.0	402	137	847	110	1007			
D2-5	14-Aug-07	40-50	45	5	15.1	7.7	7.8	14.6	67.0	481	252	1597	146	1687			
D2-5	14-Aug-07	50-60	55	-5	14.9	7.6	8.2	15.9	78.0	444	262	1718	126	1744			
D2-5	14-Aug-07	60-70	65	-15	26.3	7.5	9.3	18.6	119.0	445	300	2067	122	2042			
D2-5	14-Aug-07	70-80	75	-25	15.7	7.3	9.3	17.2	60.0	460	367	2050	133	2100			
D2-5	14-Aug-07	110-120	115	-65	9.9	7.2	7.0	13.2	50.0	396	264	1390	136	1476			
D2-6	1-Jun-02	0-10	5	35	81.1	6.1	0.7	0.9	168.7	77	26	37	41	53	64	170	110
D2-6	1-Jun-02	10-20	15	25	31.1	6.8	1.5	1.7	60.8	190	58	102	66	136	158	381	266
D2-6	1-Jun-02	20-30	25	15	14.8	7.0	2.1	3.2	40.4	226	58	207	22	225	367	606	608
D2-6	1-Jun-02	30-40	35	5	11.4	7.1	4.4	7.6	37.9	391	105	656	26	661	1014	530	848

Sample Location	Sample Date	Sample Depth	Point Depth	Above Shale	M.C.	pH	EC	SAR	% Sat	Lab Measured Sat Paste Conc. Ca^{2+}	Mg^{2+}	Na^{+}	Cl^{-}	SO_4^{2-}	Phrq-C Calc. Field Conc. Na^{+}	Ca^{2+}	SO_4^{2-}
D2-6	1-Jun-02	40-50	45	-5	17.8	7.3	7.6	13.6	56.6	416	199	1344	27	1267	2231	406	1709
D2-6	1-Jun-02	50-60	55	-15	16.4	7.3	9.0	15.9	64.4	430	270	1703	30	1638	3349	365	2606
D2-6	1-Jun-02	60-70	65	-25	15.6	7.3	9.2	15.8	62.6	413	288	1708	32	1638	3422	363	2708
D2-6	1-Jun-02	70-80	75	-35	14.4	7.3	9.9	16.7	55.7	417	336	1892	40	1741	3721	361	2936
D2-6	1-Jun-02	80-90	85	-45	17.3	7.2	10.2	17.1	58.6	427	354	1973	38	1805	3765	356	3012
D2-6	1-Jun-02	90-100	95	-55	19.7	7.2	10.6	18.5	68.4	406	367	2138	35	1847	4522	341	3630
D2-6	19-Aug-08	0-10	5	33	71.8	6.6	1.0	1.1	134.0	107	39	54	19	102	85	213	192
D2-6	19-Aug-08	10-20	15	23	34.8	7.0	1.7	1.5	103.0	217	71	97	12	255	200	569	623
D2-6	19-Aug-08	20-30	25	13	16.0	7.4	2.8	3.1	52.0	408	114	273	19	583	440	547	685
D2-6	19-Aug-08	30-40	35	3	22.0	7.6	3.2	4.2	47.0	438	119	383	21	711	515	476	776
D2-6	19-Aug-08	40-50	45	-7	22.7	7.6	5.5	8.2	67.0	491	191	843	22	1175	1291	402	1306
D2-6	19-Aug-08	50-60	55	-17	22.5	7.6	6.6	10.2	66.0	489	261	1124	27	1455	1778	374	1738
D2-6	19-Aug-08	60-70	65	-27	23.9	7.6	7.5	11.8	66.0	482	317	1358	27	1697	2173	355	2131
D2-6	19-Aug-08	70-80	75	-37	25.1	7.6	8.3	13.4	69.0	458	372	1594	32	1884	2746	341	2668
D2-6	19-Aug-08	80-90	85	-47	23.5	7.5	9.8	15.4	66.0	459	473	1985	42	2333	3633	309	3779
D2-6	19-Aug-08	90-100	95	-57	25.9	7.5	10.8	16.7	78.0	441	540	2218	46	2577	4760	294	5074
D2-7	1-Jun-02	0-10	5	45	30.4	6.8	0.9	0.9	77.8	116	40	47	25	41	83	277	106
D2-7	1-Jun-02	10-20	15	35	19.9	7.3	1.0	1.8	46.5	98	28	78	24	85	132	262	199
D2-7	1-Jun-02	20-30	25	25	22.3	7.1	3.3	2.1	54.1	538	135	208	25	601	301	585	615
D2-7	1-Jun-02	30-40	35	15	21.4	7.4	2.2	5.1	53.4	182	50	301	24	174	499	386	435
D2-7	1-Jun-02	40-50	45	5	19.2	7.4	6.0	10.1	58.3	422	153	953	22	1035	1504	432	1259
D2-7	1-Jun-02	50-60	55	-5	20.0	7.3	9.7	15.3	70.3	415	373	1784	24	1720	3663	351	3129
D2-7	1-Jun-02	60-70	65	-15	18.4	7.1	11.1	16.4	68.5	399	532	2128	27	2135	5035	318	4881
D2-7	1-Jun-02	70-80	75	-25	20.9	7.1	10.1	16.0	72.3	400	392	1880	33	1826	4000	341	3498

Sample Location	Sample Date	Sample Depth	Point Depth	Above Shale	M.C.	pH	EC	SAR	% Sat	Lab Measured Sat Paste Conc. Ca^{2+}	Mg^{2+}	Na^{+}	Cl^{-}	SO_4^{2-}	Phrq-C Calc. Field Conc. Na^{+}	Ca^{2+}	SO_4^{2-}
D2-7	1-Jun-02	80-90	85	-35	18.0	7.1	9.5	15.0	73.2	394	360	1711	41	1679	3874	349	3327
D2-7	1-Jun-02	90-100	95	-45	17.6	7.0	9.9	15.5	67.7	403	377	1801	46	1762	3903	349	3338
D2-7	19-Aug-08	0-10	5	39	22.7	7.3	0.7	0.5	68.0	87	27	22	19	31	42	260	91
D2-7	19-Aug-08	10-20	15	29	17.5	7.7	0.5	0.7	47.0	53	14	23	19	16	41	157	44
D2-7	19-Aug-08	20-30	25	19	15.2	7.8	0.5	1.4	48.0	38	10	38	23	17	78	149	54
D2-7	19-Aug-08	30-40	35	9	15.8	8.0	0.6	3.2	46.0	34	10	83	11	53	169	144	154
D2-7	19-Aug-08	40-50	45	-1	20.6	7.8	1.2	4.0	60.0	73	28	160	10	165	333	297	482
D2-7	19-Aug-08	50-60	55	-11	20.9	7.5	2.9	3.2	68.0	357	138	287	12	634	485	469	843
D2-7	19-Aug-08	60-70	65	-21	23.1	7.4	3.5	3.2	84.0	477	185	324	15	835	564	441	944
D2-7	19-Aug-08	70-80	75	-31	20.9	7.4	4.3	4.0	81.0	486	233	428	22	948	773	448	1070
D2-7	19-Aug-08	80-90	85	-41	22.2	7.4	4.6	4.7	88.0	469	245	505	15	1027	937	411	1265
D2-7	19-Aug-08	90-100	95	-51	24.0	7.4	5.3	6.1	82.0	467	294	683	12	1189	1232	397	1502
D2-8	1-Jun-02	0-10	5	25	67.3	6.5	1.4	4.2	118.3	109	36	197	43	160	305	219	281
D2-8	1-Jun-02	10-20	15	15	28.8	7.3	4.8	11.8	50.9	254	83	850	36	707	1239	438	1094
D2-8	1-Jun-02	20-30	25	5	26.8	7.3	8.1	14.8	72.9	421	215	1497	30	1438	2534	379	2021
D2-8	1-Jun-02	30-40	35	-5	22.0	7.3	8.7	14.7	62.1	412	273	1564	30	1557	2636	373	2185
D2-8	1-Jun-02	40-50	45	-15	15.5	7.3	7.4	11.4	45.1	453	252	1221	30	1361	1827	412	1557
D2-8	1-Jun-02	50-60	55	-25	18.9	7.4	5.6	8.1	47.5	438	200	811	17	1000	1167	450	1136
D2-8	1-Jun-02	60-70	65	-35	16.8	7.5	4.3	7.2	48.3	363	123	622	13	738	966	475	952
D2-8	1-Jun-02	70-80	75	-45	19.0	7.3	4.4	6.7	51.6	375	139	598	14	754	921	475	958
D2-8	1-Jun-02	80-90	85	-55	17.6	7.3	4.8	7.7	48.1	398	134	699	13	802	1050	472	987
D2-8	1-Jun-02	90-100	95	-65	18.0	7.4	5.0	9.3	50.7	335	123	781	14	850	1229	442	1125
D2-8	19-Aug-08	0-10	5	15	29.3	7.0	0.9	1.3	121.0	77	27	54	25	63	138	349	263

Sample Location	Sample Date	Sample Depth	Point Depth	Above Shale	M.C.	pH	EC	SAR	% Sat	Lab Measured Sat Paste Conc. Ca^{2+}	Mg^{2+}	Na^{+}	Cl^{-}	SO_4^{2-}	Phrq-C Calc. Field Conc. Na^{+}	Ca^{2+}	SO_4^{2-}
D2-8	19-Aug-08	10-20	15	5	13.8	7.7	0.9	2.5	54.0	67	23	94	17	87	221	350	337
D2-8	19-Aug-08	20-30	25	-5	23.1	7.4	3.5	3.0	73.0	495	190	312	10	878	488	423	944
D2-8	19-Aug-08	30-40	35	-15	21.3	7.4	5.7	5.8	74.0	461	368	696	9	1365	1220	357	1816
D2-8	19-Aug-08	40-50	45	-25	14.0	7.4	6.7	7.5	54.0	452	457	952	11	1644	1628	343	2242
D2-8	19-Aug-08	50-60	55	-35	12.0	7.7	4.2	3.7	46.0	485	215	389	11	946	558	421	983
D2-8	19-Aug-08	60-70	65	-45	13.6	7.6	4.5	4.5	48.0	465	208	469	10	975	676	409	1057
D2-8	19-Aug-08	70-80	75	-55	15.2	7.6	5.0	5.3	58.0	466	257	576	10	1110	903	393	1274
D2-8	19-Aug-08	80-90	85	-65	19.4	7.4	5.7	5.7	77.0	457	356	669	29	1325	1237	356	1854
D2-8	19-Aug-08	90-100	95	-75	15.5	7.4	6.2	7.8	74.0	443	314	884	19	1405	1706	344	2105
D2-9	1-Jun-02	0-10	5	25	71.7	6.0	0.6	1.3	128.3	62	22	46	27	56	69	120	100
D2-9	1-Jun-02	10-20	15	15	37.8	6.7	1.6	4.1	81.4	131	42	212	77	174	370	339	375
D2-9	1-Jun-02	20-30	25	5	21.0	7.3	7.2	13.4	68.9	450	164	1304	95	1140	2264	428	1548
D2-9	1-Jun-02	30-40	35	-5	26.3	7.3	11.4	23.5	104.0	396	249	2427	95	1891	6468	320	4677
D2-9	1-Jun-02	40-50	45	-15	23.5	7.4	12.9	28.0	109.0	381	294	2989	118	1608	9343	303	6177
D2-9	1-Jun-02	50-60	55	-25	19.2	7.4	14.9	30.4	98.0	393	350	3436	155	1992	12210	276	8599
D2-9	1-Jun-02	60-70	65	-35	17.5	7.4	14.1	28.2	98.2	395	327	3127	159	1992	11698	277	8500
D2-9	1-Jun-02	70-80	75	-45	16.8	7.3	14.3	28.8	95.6	402	338	3237	173	1992	12239	274	8808
D2-9	1-Jun-02	80-90	85	-55	16.6	7.3	13.8	30.0	101.0	384	293	3202	159	1992	13108	269	9335
D2-9	1-Jun-02	90-100	95	-65	17.0	7.3	13.6	30.6	105.4	390	246	3138	157	1992	13063	272	9047
D2-9	19-Aug-08	0-10	5	23	47.8	6.8	0.7	2.2	146.0	54	17	74	24	59	165	207	179
D2-9	19-Aug-08	10-20	15	13	47.2	7.4	1.0	5.0	128.0	58	15	166	11	71	338	187	194
D2-9	19-Aug-08	20-30	25	3	25.5	7.8	1.8	10.1	65.0	55	17	332	8	225	691	236	573
D2-9	19-Aug-08	30-40	35	-7	25.9	7.5	5.1	12.7	79.0	266	112	984	16	989	1789	376	1614
D2-9	19-Aug-08	40-50	45	-17	32.0	7.2	7.7	14.4	86.0	443	251	1535	23	1698	2653	341	2420

Sample Location	Sample Date	Sample Depth	Point Depth	Above Shale	M.C.	pH	EC	SAR	% Sat	Lab Measured Sat Paste Conc. Ca^{2+}	Mg^{2+}	Na^{+}	Cl^{-}	SO_4^{2-}	Phrq-C Calc. Field Conc. Na^{+}	Ca^{2+}	SO_4^{2-}
D2-9	19-Aug-08	50-60	55	-27	32.3	7.4	11.0	21.0	96.0	439	402	2542	41	2552	5647	296	5127
D2-9	19-Aug-08	60-70	65	-37	27.8	7.4	12.0	23.7	99.0	420	433	2909	57	2818	7886	275	7247
D2-9	19-Aug-08	70-80	75	-47	29.8	7.3	14.1	27.4	98.0	439	507	3571	84	3541	9582	253	9160
D2-9	19-Aug-08	80-90	85	-57	33.8	7.4	13.4	26.5	102.0	421	460	3294	90	3176	8186	269	7496
D2-9	19-Aug-08	90-100	95	-67	30.0	7.4	14.3	29.0	110.0	415	474	3655	129	3509	11114	245	10443
D2-9	21-Oct-05	0-10	5	25		6.3	0.4	1.8	170.0	46	14	54	24	39			
D2-9	21-Oct-05	10-20	15	15		6.1	0.4	3.0	270.0	33	9	74	18	44			
D2-9	21-Oct-05	20-30	25	5		7.3	2.1	12.0	81.0	63	21	432	17	272			
D2-9	21-Oct-05	30-40	35	-5		7.1	7.8	17.2	103.0	448	204	1757	38	1806			
D2-9	21-Oct-05	40-50	45	-15		7.2	11.0	25.2	108.0	440	313	2833	76	2731			
D2-9	21-Oct-05	50-60	55	-25		7.1	11.0	27.6	131.0	400	305	3023	76	2725			
D2-9	21-Oct-05	60-70	65	-35		7.2	12.3	30.6	128.0	407	354	3500	103	3172			
D2-9	21-Oct-05	70-80	75	-45		7.2	13.7	32.2	103.0	428	441	3990	156	3670			
D2-9	21-Oct-05	80-90	85	-55		7.3	14.3	34.6	95.0	421	461	4326	200	3821			
D2-9	21-Oct-05	90-100	95	-65		7.3	15.4	34.6	110.0	455	528	4582	244	4218			
D2-9	14-Aug-07	0-10	5	35	19.0	6.9	1.1	2.3	146.0	118	36	113	25	83			
D2-9	14-Aug-07	10-20	15	25	16.5	7.5	0.9	3.8	95.0	75	20	141	17	95			
D2-9	14-Aug-07	20-30	25	15	15.3	7.7	1.1	5.0	77.0	79	21	192	19	139			
D2-9	14-Aug-07	30-40	35	5	11.7	7.4	3.9	6.9	70.0	391	108	596	30	801			
D2-9	14-Aug-07	40-50	45	-5	19.5	7.4	6.1	11.0	89.0	482	192	1135	30	1348			
D2-9	14-Aug-07	50-60	55	-15	26.3	7.3	9.6	18.2	109.0	453	325	2092	52	2156			
D2-9	14-Aug-07	60-70	65	-25	32.5	7.4	9.3	17.8	122.0	457	292	1975	51	2123			
D2-9	14-Aug-07	70-80	75	-35	25.6	7.3	9.5	18.2	116.0	460	299	2052	53	2121			

Sample Location	Sample Date	Sample Depth	Point Depth	Above Shale	M.C.	pH	EC	SAR	% Sat	Lab Measured Sat Paste Conc. Ca^{2+}	Mg^{2+}	Na^{+}	Cl^{-}	SO_4^{2-}	Phrq-C Calc. Field Conc. Na^{+}	Ca^{2+}	SO_4^{2-}
D2-10	1-Jun-02	0-10	5	25	27.5	6.9	1.2	1.0	79.1	142	45	55	47	154	110	449	443
D2-10	1-Jun-02	10-20	15	15	34.7	6.6	1.9	4.1	85.9	152	48	226	79	357	426	434	841
D2-10	1-Jun-02	20-30	25	5	19.7	7.3	7.7	12.9	73.8	386	170	1213	79	1418	2145	333	2184
D2-10	1-Jun-02	30-40	35	-5	22.9	6.9	13.2	20.3	91.9	367	400	2361	91	2680	6639	261	7490
D2-10	1-Jun-02	40-50	45	-15	26.4	6.9	16.7	26.6	104.0	371	469	3266	113	3124	10317	255	9698
D2-10	1-Jun-02	50-60	55	-25	23.0	7.1	16.2	27.2	105.7	371	410	3201	128	3124	11470	241	11116
D2-10	1-Jun-02	60-70	65	-35	24.4	7.1	14.8	28.4	125.5	356	271	2920	120	3124	11598	226	12547
D2-10	1-Jun-02	70-80	75	-45	24.7	7.0	14.2	30.1	139.9	324	235	2920	113	2827	13005	229	12509
D2-10	1-Jun-02	80-90	85	-55	25.8	6.9	13.4	30.3	134.0	291	195	2721	112	2827	10888	229	11517
D2-10	1-Jun-02	90-100	95	-65	21.7	7.2	12.2	30.0	132.4	216	135	2460	118	2097	11198	251	9555
D2-10	19-Aug-08	0-10	5	26	47.9	6.8	0.7	2.8	87.0	50	18	91	21	59	140	107	107
D2-10	19-Aug-08	10-20	15	16	48.6	7.2	0.6	4.3	124.0	32	10	110	16	30	223	115	78
D2-10	19-Aug-08	20-30	25	6	30.9	7.6	1.8	9.3	62.0	61	22	331	16	231	572	178	464
D2-10	19-Aug-08	30-40	35	-4	36.6	6.4	4.4	13.4	97.0	167	82	845	18	770	1651	378	1544
D2-10	19-Aug-08	40-50	45	-14	42.6	4.9	9.9	20.5	107.0	441	320	2318	43	2262	4509	316	3856
D2-10	19-Aug-08	50-60	55	-24	47.7	4.3	13.3	26.4	126.0	418	452	3278	70	3143	7403	275	6728
D2-10	19-Aug-08	60-70	65	-34	42.6	5.2	12.6	26.5	156.0	399	364	3045	61	2865	9395	263	8323
D2-10	19-Aug-08	70-80	75	-44	40.4	6.6	14.6	30.7	142.0	421	451	3817	87	3662	11678	241	10848
D2-10	19-Aug-08	80-90	85	-54	34.4	6.9	14.8	32.0	154.0	413	427	3896	106	3617	15086	227	13647
D2-10	19-Aug-08	90-100	95	-64	36.9	7.2	15.3	31.8	138.0	417	467	3986	135	3775	12954	235	11972

Table B3: Laboratory and Phreeq-C soil salinity data for D3 locations.

Sample Location	Sample Date	Sample Depth (cm)	Point Depth (cm)	Above Shale (cm)	M.C. %	pH	EC dS/m	SAR	% Sat	Lab Measured Sat Paste Conc. Ca^{2+} mg/L	Mg^{2+} mg/L	Na^{+} mg/L	Cl^{-} mg/L	SO_4^{2-} mg/L	Phrq-C Calc. Field Conc. Na^{+} mg/L	Ca^{2+} mg/L	SO_4^{2-} mg/L
D3-0	1-Jun-02	0-10	5	75	29.3	6.2	3.5	4.1	86.8	390	130	369	27	594	672	562	764
D3-0	1-Jun-02	10-20	15	65	46.7	6.4	4.1	3.7	66.2	502	171	372	21	715	576	557	750
D3-0	1-Jun-02	20-30	25	55	30.3	6.4	3.3	2.7	64.3	414	145	251	19	545	393	578	682
D3-0	1-Jun-02	30-40	35	45	22.2	6.8	1.8	2.0	47.8	220	52	127	24	158	203	465	350
D3-0	1-Jun-02	40-50	45	35	21.6	7.2	1.2	1.1	45.1	170	32	59	39	148	103	460	367
D3-0	1-Jun-02	50-60	55	25	20.1	7.3	1.4	1.4	51.7	181	37	78	49	183	146	547	498
D3-0	1-Jun-02	60-70	65	15	18.5	7.2	2.5	4.4	50.4	228	41	275	68	269	481	580	615
D3-0	1-Jun-02	70-80	75	5	22.3	7.2	5.5	7.9	62.0	442	110	712	74	786	1094	487	927
D3-0	1-Jun-02	80-90	85	-5	21.9	7.3	9.7	13.7	60.8	456	310	1547	87	1676	2518	372	2146
D3-0	1-Jun-02	90-100	95	-15	23.0	7.0	12.0	16.1	80.4	420	476	2027	74	1443	3900	366	3072
D3-0	1-Jun-02	100-110	105	-25	19.8	6.8	12.6	17.9	84.7	399	442	2189	85	1443	4512	354	3427
D3-0	1-Jun-02	110-120	115	-35	19.2	6.8	12.6	20.4	91.5	395	339	2292	96	1443	5307	347	3720
D3-0	1-Jun-02	120-130	125	-45	22.4	7.0	11.7	21.7	95.6	385	226	2170	96	2005	4877	316	3924
D3-0	1-Jun-02	130-140	135	-55	22.6	6.9	11.3	22.7	88.8	366	199	2176	100	1917	4576	328	3496
D3-0	1-Jun-02	140-150	145	-65	20.1	7.1	9.9	23.4	98.3	280	136	1907	103	1460	4250	350	2954
D3-0	19-Aug-08	0-10	5	75	28.5	7.2	2.2	1.6	86.0	294	83	124	85	251	245	645	576
D3-0	19-Aug-08	10-20	15	65	26.8	7.3	1.7	1.9	76.0	199	53	118	79	205	237	612	575
D3-0	19-Aug-08	20-30	25	55	26.0	7.2	3.4	2.5	77.0	549	144	256	122	717	416	550	675
D3-0	19-Aug-08	30-40	35	45	37.4	7.4	4.6	5.0	85.0	518	166	512	160	878	762	470	893
D3-0	19-Aug-08	40-50	45	35	21.9	7.6	4.6	6.0	61.0	493	123	577	120	884	841	453	903
D3-0	19-Aug-08	50-60	55	25	21.3	7.7	5.6	9.4	58.0	467	124	888	102	1098	1248	398	1200
D3-0	19-Aug-08	60-70	65	15	19.7	7.8	6.6	11.6	59.0	449	165	1134	98	1308	1704	373	1548
D3-0	19-Aug-08	70-80	75	5	22.6	7.8	7.8	13.4	57.0	467	240	1432	102	1633	2060	351	1931

Sample Location	Sample Date	Sample Depth (cm)	Point Depth (cm)	Above Shale (cm)	M.C. %	pH	EC dS/m	SAR	% Sat	Lab Measured Sat Paste Conc. Ca^{2+} mg/L	Mg^{2+} mg/L	Na^{+} mg/L	Cl^{-} mg/L	SO_4^{2-} mg/L	Phrq-C Calc. Field Conc. Na^{+} mg/L	Ca^{2+} mg/L	SO_4^{2-} mg/L
D3-0	19-Aug-08	80-90	85	-5	18.3	7.7	8.3	13.6	70.0	440	307	1514	76	1786	2932	324	2855
D3-0	19-Aug-08	90-100	95	-15	27.1	7.7	9.5	16.1	71.0	448	338	1859	75	2085	3156	317	3057
D3-0	19-Aug-08	100-110	105	-25	28.0	7.6	10.0	18.4	108.0	431	300	2037	63	2157	5203	289	4898
D3-0	19-Aug-08	110-120	115	-35	26.4	7.8	8.0	23.8	133.0	190	120	1707	59	1504	5649	287	4870
D3-0	19-Aug-08	120-130	125	-45	27.2	7.8	9.3	23.5	106.0	321	138	2000	74	1840	4914	294	4190
D3-0	19-Aug-08	130-140	135	-55	31.6	8.0	6.5	29.5	167.0	92	48	1401	61	1120	5232	292	4292
D3-0	19-Aug-08	140-150	145	-65	27.0	7.9	7.2	27.6	137.0	139	62	1562	72	1270	5125	296	4110
D3-2	1-Jun-02	0-10	5	105	49.1	6.6	1.0	0.4	88.0	122	36	21	15	59	31	225	106
D3-2	1-Jun-02	10-20	15	95	48.1	6.7	0.9	0.5	74.8	103	31	22	19	46	29	165	72
D3-2	1-Jun-02	20-30	25	85	22.7	6.9	0.8	0.8	62.3	95	26	33	14	46	62	280	128
D3-2	1-Jun-02	30-40	35	75	21.7	7.4	0.5	1.3	62.1	46	8	37	8	42	72	157	120
D3-2	1-Jun-02	40-50	45	65	22.6	7.5	0.5	1.6	61.2	41	6	41	9	34	77	137	93
D3-2	1-Jun-02	50-60	55	55	20.6	7.6	0.5	1.3	54.4	45	8	36	11	34	66	139	90
D3-2	1-Jun-02	60-70	65	45	22.3	7.5	0.5	1.2	52.0	47	12	36	17	42	61	127	98
D3-2	1-Jun-02	70-80	75	35	20.9	7.5	0.8	1.4	45.0	76	26	57	32	83	91	185	178
D3-2	1-Jun-02	80-90	85	25	17.3	7.5	1.2	2.3	45.5	111	21	100	52	152	184	355	400
D3-2	1-Jun-02	90-100	95	15	19.8	7.6	2.0	5.4	43.6	164	29	284	81	296	491	464	655
D3-2	1-Jun-02	100-110	105	5	17.7	7.6	3.1	7.5	42.3	211	42	454	102	465	747	463	819
D3-2	1-Jun-02	110-120	115	-5	19.3	7.1	6.7	10.0	50.1	417	188	978	109	1187	1414	399	1360
D3-2	1-Jun-02	120-130	125	-15	20.8	6.9	8.9	13.8	55.6	400	277	1466	117	1522	2381	386	1979
D3-2	1-Jun-02	130-140	135	-25	20.8	7.0	9.4	15.0	66.4	391	292	1612	102	1712	2989	347	2629
D3-2	1-Jun-02	140-150	145	-35	23.6	7.3	10.2	17.3	65.3	401	279	1848	105	1777	3229	354	2611
D3-2	19-Aug-08	0-10	5	113	23.1	7.3	1.7	1.6	65.0	214	59	100	52	200	193	616	565

Sample Location	Sample Date	Sample Depth (cm)	Point Depth (cm)	Above Shale (cm)	M.C. %	pH	EC dS/m	SAR	% Sat	Lab Measured Sat Paste Conc. Ca^{2+} mg/L	Mg^{2+} mg/L	Na^{+} mg/L	Cl^{-} mg/L	SO_4^{2-} mg/L	Phrq-C Calc. Field Conc. Na^{+} mg/L	Ca^{2+} mg/L	SO_4^{2-} mg/L
D3-2	19-Aug-08	10-20	15	103	28.4	7.2	1.9	2.1	69.0	241	59	142	58	294	250	555	605
D3-2	19-Aug-08	20-30	25	93	19.7	6.9	2.4	2.8	75.0	299	74	212	75	423	412	538	662
D3-2	19-Aug-08	30-40	35	83	44.9	7.4	2.8	4.0	74.0	345	68	315	100	499	432	498	683
D3-2	19-Aug-08	40-50	45	73	23.0	7.7	2.7	4.3	53.0	321	59	321	83	496	482	491	701
D3-2	19-Aug-08	50-60	55	63	26.3	7.7	2.8	4.5	64.0	317	58	334	80	509	521	477	729
D3-2	19-Aug-08	60-70	65	53	22.3	7.5	2.7	5.2	61.0	275	56	364	75	482	604	481	756
D3-2	19-Aug-08	70-80	75	43	18.2	7.3	2.8	5.8	59.0	261	56	397	73	503	694	466	810
D3-2	19-Aug-08	80-90	85	33	24.9	7.3	3.0	6.8	65.0	257	56	466	77	529	781	460	850
D3-2	19-Aug-08	90-100	95	23	20.2	7.6	4.1	6.8	39.0	387	79	559	103	731	727	449	844
D3-2	19-Aug-08	100-110	105	13	17.4	7.7	3.1	7.4	29.0	257	54	500	90	566	686	443	841
D3-2	19-Aug-08	110-120	115	3	20.8	7.8	3.2	8.1	47.0	217	54	515	91	545	823	434	921
D3-2	19-Aug-08	120-130	125	-7	20.7	7.6	6.8	10.6	62.0	423	250	1108	97	1402	1778	362	1798
D3-2	19-Aug-08	130-140	135	-17	22.1	7.4	7.9	12.8	75.0	424	300	1413	103	1680	2642	335	2567
D3-2	19-Aug-08	140-150	145	-27	23.3	7.5	8.4	14.0	76.0	407	313	1539	95	1763	2978	330	2850
D3-2	21-Oct-05	0-10	5	109		7.3	0.6	0.4	76.0	97	27	17	29	29			
D3-2	21-Oct-05	10-20	15	99		7.4	0.5	0.4	58.0	84	21	17	14	19			
D3-2	21-Oct-05	20-30	25	89		7.6	0.4	0.5	52.0	65	15	15	8	13			
D3-2	21-Oct-05	30-40	35	79		7.6	0.4	0.6	53.0	68	15	21	6	16			
D3-2	21-Oct-05	40-50	45	69		7.7	0.4	0.8	54.0	54	12	26	11	24			
D3-2	21-Oct-05	50-60	55	59		7.7	0.8	1.4	50.0	96	20	58	38	84			
D3-2	21-Oct-05	60-70	65	49		7.5	1.5	2.7	56.0	178	35	152	70	227			
D3-2	21-Oct-05	70-80	75	39		7.5	2.5	4.6	54.0	278	63	315	109	444			
D3-2	21-Oct-05	80-90	85	29		7.5	2.6	5.5	57.0	237	54	368	116	439			
D3-2	21-Oct-05	90-100	95	19		7.4	3.4	6.3	54.0	344	81	500	146	611			

Sample Location	Sample Date	Sample Depth (cm)	Point Depth (cm)	Above Shale (cm)	M.C. %	pH	EC dS/m	SAR	% Sat	Lab Measured Sat Paste Conc. Ca^{2+} mg/L	Mg^{2+} mg/L	Na^{+} mg/L	Cl^{-} mg/L	SO_4^{2-} mg/L	Phrq-C Calc. Field Conc. Na^{+} mg/L	Ca^{2+} mg/L	SO_4^{2-} mg/L
D3-2	21-Oct-05	100-114	107	7		7.4	3.2	7.6	54.0	257	69	519	130	556			
D3-2	21-Oct-05	114-130	122	-8		7.3	6.6	11.1	49.0	488	257	1224	157	1473			
D3-2	21-Oct-05	130-140	135	-21		7.3	7.7	14.0	56.0	438	327	1604	130	1839			
D3-2	21-Oct-05	140-150	145	-31		7.1	8.8	17.5	69.0	436	319	1971	125	2145			
D3-2	21-Oct-05	150-160	155	-41		7.2	9.1	17.9	69.0	454	362	2116	116	2261			
D3-3	1-Jun-02	0-10	5	75	69.9	5.8	0.7	0.8	93.0	78	31	32	26	71	39	107	94
D3-3	1-Jun-02	10-20	15	65	49.1	6.2	0.7	1.0	104.5	79	24	38	26	58	63	180	124
D3-3	1-Jun-02	20-30	25	55	25.1	7.4	0.6	1.7	62.6	59	10	53	20	64	95	176	160
D3-3	1-Jun-02	30-40	35	45	17.6	7.5	0.7	2.2	44.2	54	10	69	39	58	124	172	146
D3-3	1-Jun-02	40-50	45	35	27.7	7.5	0.7	2.3	57.3	48	9	65	59	44	106	122	90
D3-3	1-Jun-02	50-60	55	25	21.7	7.4	1.0	2.5	60.3	72	13	89	95	69	175	253	192
D3-3	1-Jun-02	60-70	65	15	24.6	7.3	2.2	6.2	58.2	156	21	309	162	242	575	490	573
D3-3	1-Jun-02	70-80	75	5	24.7	7.3	5.9	9.2	63.6	422	95	804	216	867	1231	464	980
D3-3	1-Jun-02	80-90	85	-5	20.6	7.0	10.7	15.1	49.7	441	322	1708	287	1755	2587	375	2112
D3-3	1-Jun-02	90-100	95	-15	17.9	7.1	12.8	17.8	46.1	424	421	2166	419	2282	3529	326	3196
D3-3	1-Jun-02	100-110	105	-25	19.2	7.1	13.0	19.1	46.5	396	380	2220	463	2418	3498	310	3503
D3-3	1-Jun-02	110-120	115	-35	18.8	7.1	13.8	22.4	47.2	385	335	2494	500	2282	4166	327	3325
D3-3	1-Jun-02	120-130	125	-45	18.9	7.2	12.7	24.0	52.1	345	227	2340	479	2147	4071	316	3384
D3-3	1-Jun-02	130-140	135	-55	18.5	7.2	12.8	24.8	50.3	315	244	2408	511	2147	4294	316	3507
D3-3	1-Jun-02	140-150	145	-65	19.2	7.2	11.3	28.5	48.8	201	138	2146	473	1564	3945	350	2713
D3-3	19-Aug-08	0-10	5	74	34.0	6.0	0.7	1.0	93.0	65	21	38	34	68	74	201	186
D3-3	19-Aug-08	10-20	15	64	59.7	5.8	1.4	1.3	108.0	165	49	77	40	207	118	319	377
D3-3	19-Aug-08	20-30	25	54	30.4	7.1	2.2	2.3	87.0	301	58	166	60	366	304	554	602

Sample Location	Sample Date	Sample Depth (cm)	Point Depth (cm)	Above Shale (cm)	M.C. %	pH	EC dS/m	SAR	% Sat	Lab Measured Sat Paste Conc. Ca^{2+} mg/L	Mg^{2+} mg/L	Na^{+} mg/L	Cl^{-} mg/L	SO_4^{2-} mg/L	Phrq-C Calc. Field Conc. Na^{+} mg/L	Ca^{2+} mg/L	SO_4^{2-} mg/L
D3-3	19-Aug-08	30-40	35	44	28.6	7.6	1.9	3.4	67.0	206	33	203	52	304	353	505	637
D3-3	19-Aug-08	40-50	45	34	21.1	7.8	1.9	4.9	64.0	154	25	252	41	289	505	486	705
D3-3	19-Aug-08	50-60	55	24	28.4	7.8	2.0	5.5	69.0	138	28	271	39	296	515	446	725
D3-3	19-Aug-08	60-70	65	14	27.5	7.7	2.5	5.8	73.0	208	47	356	47	432	639	453	818
D3-3	19-Aug-08	70-80	75	4	29.4	7.7	2.4	6.4	73.0	177	43	368	45	412	671	445	848
D3-3	19-Aug-08	80-90	85	-6	23.7	7.6	4.9	6.7	66.0	458	159	655	52	1005	980	403	1140
D3-3	19-Aug-08	90-100	95	-16	18.9	7.4	6.0	8.8	55.0	447	220	920	73	1278	1343	373	1484
D3-3	19-Aug-08	100-110	105	-26	18.8	7.4	6.1	9.2	58.0	453	228	967	86	1312	1466	372	1546
D3-3	19-Aug-08	110-120	115	-36	21.3	7.4	7.2	11.7	58.0	438	259	1247	141	1510	1904	358	1860
D3-3	19-Aug-08	120-130	125	-46	19.9	7.4	9.1	15.6	60.0	427	327	1767	230	1917	3097	332	2793
D3-3	19-Aug-08	130-140	135	-56	18.1	7.5	9.5	17.3	56.0	420	313	1929	273	2000	3371	329	2935
D3-3	19-Aug-08	140-150	145	-66	18.7	7.5	10.2	20.4	68.0	397	281	2176	328	2088	4662	311	3892
D3-4	1-Jun-02	0-10	5	115	48.6	6.5	0.8	0.6	123.1	106	30	29	31	52	55	282	133
D3-4	1-Jun-02	10-20	15	105	19.0	7.0	0.7	0.8	44.9	85	24	30	15	58	51	215	138
D3-4	1-Jun-02	20-30	25	95	18.5	7.0	0.6	0.8	48.5	66	21	28	6	44	49	189	115
D3-4	1-Jun-02	30-40	35	85	18.2	7.3	0.5	0.9	56.9	49	17	28	7	38	55	172	119
D3-4	1-Jun-02	40-50	45	75	20.6	7.5	0.4	1.1	54.0	40	10	29	5	37	52	123	96
D3-4	1-Jun-02	50-60	55	65	18.8	7.6	0.4	1.2	45.1	38	11	32	7	42	54	108	102
D3-4	1-Jun-02	60-70	65	55	19.3	7.5	0.5	1.2	48.0	40	9	33	14	35	58	118	88
D3-4	1-Jun-02	70-80	75	45	17.9	7.3	0.5	1.3	45.9	40	9	34	29	28	60	123	73
D3-4	1-Jun-02	80-90	85	35	17.6	7.4	0.6	1.3	45.4	55	15	43	66	46	76	168	120
D3-4	1-Jun-02	90-100	95	25	24.6	7.2	1.5	3.0	46.0	151	33	155	109	242	236	329	452
D3-4	1-Jun-02	100-110	105	15	21.3	7.4	2.3	5.6	52.3	155	33	296	183	380	531	439	841
D3-4	1-Jun-02	110-120	115	5	16.1	7.5	5.4	10.4	54.1	311	81	796	280	851	1307	415	1177

Sample Location	Sample Date	Sample Depth (cm)	Point Depth (cm)	Above Shale (cm)	M.C. %	pH	EC dS/m	SAR	% Sat	Lab Measured Sat Paste Conc. Ca^{2+} mg/L	Mg^{2+} mg/L	Na^{+} mg/L	Cl^{-} mg/L	SO_4^{2-} mg/L	Phrq-C Calc. Field Conc. Na^{+} mg/L	Ca^{2+} mg/L	SO_4^{2-} mg/L
D3-4	1-Jun-02	120-130	125	-5	18.5	7.2	10.1	16.3	55.5	411	247	1695	362	1669	2850	362	2208
D3-4	1-Jun-02	130-140	135	-15	20.8	7.2	13.1	21.4	57.1	396	321	2366	497	1741	4287	381	2770
D3-4	1-Jun-02	140-150	145	-25	25.9	7.2	13.8	22.9	69.5	376	363	2602	513	1741	5008	368	3274
D3-4	19-Aug-08	0-10	5	115	36.4	7.1	0.7	0.4	86.0	95	28	15	20	33	27	232	79
D3-4	19-Aug-08	10-20	15	105	49.2	7.8	0.5	0.5	52.0	58	14	17	12	24	18	62	25
D3-4	19-Aug-08	20-30	25	95	22.6	7.7	0.6	1.0	53.0	63	16	34	13	48	55	164	111
D3-4	19-Aug-08	30-40	35	85	21.5	7.6	0.6	1.1	65.0	63	16	37	12	50	73	217	151
D3-4	19-Aug-08	40-50	45	75	17.4	7.9	0.6	1.2	60.0	64	15	42	17	67	89	259	229
D3-4	19-Aug-08	50-60	55	65	19.3	7.8	0.8	1.6	55.0	83	20	62	18	103	117	279	292
D3-4	19-Aug-08	60-70	65	55	24.1	7.7	1.1	1.9	60.0	112	28	87	27	156	156	323	387
D3-4	19-Aug-08	70-80	75	45	16.8	7.7	1.1	2.5	73.0	98	25	107	26	155	273	527	636
D3-4	19-Aug-08	80-90	85	35	23.5	7.9	1.3	4.2	60.0	93	25	175	27	178	335	316	455
D3-4	19-Aug-08	90-100	95	25	24.7	7.9	1.3	5.2	68.0	69	18	188	24	160	388	275	442
D3-4	19-Aug-08	100-110	105	15	19.6	7.9	1.6	5.6	56.0	98	26	243	30	223	506	403	638
D3-4	19-Aug-08	110-120	115	5	25.0	8.0	1.9	6.7	58.0	112	34	314	38	286	579	357	667
D3-4	19-Aug-08	120-130	125	-5	25.7	7.6	5.3	8.8	57.0	404	181	844	81	1044	1210	419	1216
D3-4	19-Aug-08	130-140	135	-15	26.9	7.5	7.6	13.5	59.0	437	268	1456	141	1553	2126	380	1842
D3-4	19-Aug-08	140-150	145	-25	25.0	7.5	9.3	17.2	58.0	429	334	1966	210	1897	3092	358	2514
D3-5	1-Jun-02	0-10	5	95	36.3	6.8	0.9	1.3	106.2	90	25	56	16	58	117	295	171
D3-5	1-Jun-02	10-20	15	85	21.8	7.3	0.7	1.5	52.5	68	18	55	9	58	96	190	140
D3-5	1-Jun-02	20-30	25	75	18.2	7.6	0.6	1.4	37.8	53	16	45	7	46	71	126	97
D3-5	1-Jun-02	30-40	35	65	13.5	7.7	0.5	1.1	33.0	40	12	31	8	32	52	113	79
D3-5	1-Jun-02	40-50	45	55	14.2	7.6	0.4	0.7	31.9	44	11	22	8	21	34	110	48

Sample Location	Sample Date	Sample Depth (cm)	Point Depth (cm)	Above Shale (cm)	M.C. %	pH	EC dS/m	SAR	% Sat	Lab Measured Sat Paste Conc. Ca^{2+} mg/L	Mg^{2+} mg/L	Na^{+} mg/L	Cl^{-} mg/L	SO_4^{2-} mg/L	Phrq-C Calc. Field Conc. Na^{+} mg/L	Ca^{2+} mg/L	SO_4^{2-} mg/L
D3-5	1-Jun-02	50-60	55	45	18.0	7.6	0.4	0.7	46.0	43	11	19	10	23	32	120	58
D3-5	1-Jun-02	60-70	65	35	19.2	7.5	0.5	0.7	47.2	53	17	21	20	30	36	143	73
D3-5	1-Jun-02	70-80	75	25	17.3	7.5	0.7	1.0	40.6	68	19	36	31	79	60	180	185
D3-5	1-Jun-02	80-90	85	15	16.6	7.5	1.3	3.1	43.5	86	26	129	31	201	241	297	528
D3-5	1-Jun-02	90-100	95	5	20.6	7.6	3.1	9.2	56.6	135	40	473	40	594	864	361	1296
D3-5	1-Jun-02	100-110	105	-5	22.6	7.3	9.1	16.1	73.2	417	162	1529	42	1767	2563	309	2763
D3-5	1-Jun-02	110-120	115	-15	24.1	7.2	10.6	20.2	84.1	411	174	1936	42	1953	3900	304	3473
D3-5	1-Jun-02	120-130	125	-25	21.8	7.2	9.9	20.3	91.0	345	153	1798	42	1726	4149	307	3512
D3-5	1-Jun-02	130-140	135	-35	21.5	7.3	7.2	21.8	100.9	128	107	1379	56	1185	4015	310	3517
D3-5	1-Jun-02	140-150	145	-45	22.0	7.5	6.1	30.6	110.4	65	30	1188	74	891	3915	316	3067
D3-5	19-Aug-08	0-10	5	103	54.0	7.2	0.6	0.6	124.0	69	21	22	23	38	38	168	86
D3-5	19-Aug-08	10-20	15	93	29.2	7.7	0.5	0.8	63.0	56	15	27	14	32	43	132	70
D3-5	19-Aug-08	20-30	25	83	20.0	8.0	0.4	1.0	40.0	38	10	28	8	28	42	86	56
D3-5	19-Aug-08	30-40	35	73	16.8	7.9	0.7	1.5	35.0	66	17	51	9	76	82	158	157
D3-5	19-Aug-08	40-50	45	63	13.3	7.9	0.8	2.0	39.0	65	18	69	10	89	135	241	264
D3-5	19-Aug-08	50-60	55	53	16.3	7.8	1.1	2.6	38.0	95	27	113	21	145	192	271	341
D3-5	19-Aug-08	60-70	65	43	15.0	7.8	1.7	3.7	44.0	151	43	200	39	266	390	507	695
D3-5	19-Aug-08	70-80	75	33	15.1	7.9	1.9	4.7	49.0	161	47	265	45	320	518	491	752
D3-5	19-Aug-08	80-90	85	23	16.5	8.0	1.9	6.1	48.0	125	36	302	42	296	612	478	793
D3-5	19-Aug-08	90-100	95	13	15.3	8.0	1.3	9.3	58.0	73	22	355	36	271	908	458	920
D3-5	19-Aug-08	100-110	105	3	29.5	7.8	3.0	9.9	53.0	161	48	560	57	502	873	372	899
D3-5	19-Aug-08	110-120	115	-7	28.0	7.6	8.0	15.6	102.0	430	236	1618	36	1637	3557	339	2941
D3-5	19-Aug-08	120-130	125	-17	25.7	7.4	8.3	16.8	129.0	427	233	1752	33	1752	5263	311	4399
D3-5	19-Aug-08	130-140	135	-27	24.0	7.4	8.2	18.1	140.0	408	174	1736	39	1693	5821	301	4735

Sample Location	Sample Date	Sample Depth (cm)	Point Depth (cm)	Above Shale (cm)	M.C. %	pH	EC dS/m	SAR	% Sat	Lab Measured Sat Paste Conc. Ca^{2+} mg/L	Mg^{2+} mg/L	Na^{+} mg/L	Cl^{-} mg/L	SO_4^{2-} mg/L	Phrq-C Calc. Field Conc. Na^{+} mg/L	Ca^{2+} mg/L	SO_4^{2-} mg/L
D3-5	19-Aug-08	140-150	145	-37	18.9	7.5	8.6	19.9	147.0	424	171	1925	48	1769	8595	285	6734
D3-5	21-Oct-05	0-10	5	97		7.2	0.6	0.5	128.0	95	29	22	27	27			
D3-5	21-Oct-05	10-20	15	87		7.4	0.6	0.8	69.0	88	22	35	19	23			
D3-5	21-Oct-05	20-30	26	76		7.7	0.5	1.3	48.0	61	14	44	4	27			
D3-5	21-Oct-05	30-40	36	66		7.8	0.5	1.4	39.0	65	16	46	8	41			
D3-5	21-Oct-05	40-50	45	57		7.8	0.8	1.2	39.0	106	29	54	15	101			
D3-5	21-Oct-05	50-60	55	47		7.7	1.2	1.5	39.0	164	50	87	23	206			
D3-5	21-Oct-05	60-70	65	37		7.5	1.7	2.1	43.0	208	69	135	26	284			
D3-5	21-Oct-05	70-80	75	27		7.5	1.8	3.6	43.0	175	59	214	28	305			
D3-5	21-Oct-05	80-90	85	17		7.8	2.5	6.4	38.0	198	58	395	37	474			
D3-5	21-Oct-05	90-102	96	6		7.8	3.8	10.0	40.0	244	70	725	43	750			
D3-5	21-Oct-05	102-110	106	-4		7.4	8.4	19.8	82.0	466	205	2037	46	1951			
D3-5	21-Oct-05	110-120	115	-13		7.7	6.7	26.0	114.0	181	82	1684	58	1395			
D3-5	21-Oct-05	120-130	125	-23		8.0	4.8	38.0	124.0	44	21	1226	76	887			
D3-5	21-Oct-05	130-140	135	-33		8.1	4.5	40.0	135.0	34	16	1133	81	741			
D3-5	21-Oct-05	140-150	145	-43		8.3	3.5	50.0	166.0	14	6	904	84	542			
D3-5	14-Aug-07	60-70	65	37	15.0	7.3	1.1	1.8	54.0	119	34	85	19	145			
D3-5	14-Aug-07	70-80	75	27	12.4	7.7	1.5	2.9	52.0	161	45	162	27	242			
D3-5	14-Aug-07	80-90	85	17	19.3	7.6	2.7	4.8	56.0	273	76	350	34	518			
D3-5	14-Aug-07	90-100	95	7	15.9	7.6	4.3	8.2	49.0	371	113	704	39	878			
D3-5	14-Aug-07	100-110	105	-3	21.0	7.4	8.5	15.8	86.0	466	271	1733	43	1895			
D3-5	14-Aug-07	110-120	115	-13	22.8	7.2	9.5	17.9	100.0	454	310	2030	48	2100			
D3-5	14-Aug-07	120-130	125	-23	21.0	7.2	9.3	18.9	92.0	442	272	2054	60	2043			

Sample Location	Sample Date	Sample Depth (cm)	Point Depth (cm)	Above Shale (cm)	M.C. %	pH	EC dS/m	SAR	% Sat	Lab Measured Sat Paste Conc. Ca^{2+} mg/L	Mg^{2+} mg/L	Na^{+} mg/L	Cl^{-} mg/L	SO_4^{2-} mg/L	Phrq-C Calc. Field Conc. Na^{+} mg/L	Ca^{2+} mg/L	SO_4^{2-} mg/L
D3-6	1-Jun-02	0-10	5	85	23.3	7.4	0.9	3.3	60.8	52	16	108	23	96	208	183	252
D3-6	1-Jun-02	10-20	15	75	27.6	7.4	1.6	5.6	61.3	93	27	237	17	302	424	282	672
D3-6	1-Jun-02	20-30	25	65	23.4	7.5	2.5	4.3	54.4	197	109	305	18	473	517	446	922
D3-6	1-Jun-02	30-40	35	55	21.3	7.5	2.3	3.3	48.6	215	55	208	20	473	320	410	860
D3-6	1-Jun-02	40-50	45	45	20.1	7.5	1.5	2.3	56.8	147	39	120	17	302	222	432	772
D3-6	1-Jun-02	50-60	55	35	17.8	7.6	1.2	1.3	45.8	122	30	63	15	170	112	359	439
D3-6	1-Jun-02	60-70	65	25	17.5	7.6	0.9	1.1	40.5	101	26	47	17	130	77	260	302
D3-6	1-Jun-02	70-80	75	15	19.4	7.6	1.1	1.9	50.1	105	27	83	14	154	151	321	399
D3-6	1-Jun-02	80-90	85	5	19.2	7.6	2.6	5.3	49.2	188	49	318	20	473	528	410	913
D3-6	1-Jun-02	90-100	95	-5	21.6	7.4	6.3	8.6	57.9	418	167	820	25	1109	1193	385	1313
D3-6	1-Jun-02	100-110	105	-15	23.8	7.4	8.2	11.9	71.3	390	231	1197	24	1480	2015	338	2126
D3-6	1-Jun-02	110-120	115	-25	21.7	7.5	9.2	14.2	71.0	384	255	1457	26	1684	2659	323	2668
D3-6	1-Jun-02	120-130	125	-35	22.5	7.3	10.3	15.8	69.9	384	288	1683	34	1911	3117	312	3165
D3-6	1-Jun-02	130-140	135	-45	21.8	7.2	10.7	16.1	71.5	402	302	1752	38	1870	3428	330	3104
D3-6	1-Jun-02	140-150	145	-55	21.5	7.1	9.9	14.8	78.9	401	274	1569	38	1870	3145	304	3385
D3-6	19-Aug-08	0-10	5	105	22.4	7.6	0.7	1.1	71.0	74	22	44	17	55	91	274	175
D3-6	19-Aug-08	10-20	15	95	28.9	7.7	0.7	1.7	75.0	65	19	60	15	56	112	198	146
D3-6	19-Aug-08	20-30	25	85	19.0	7.5	0.9	3.1	106.0	75	22	118	10	99	360	507	557
D3-6	19-Aug-08	30-40	35	75	17.8	7.7	1.6	4.5	53.0	130	38	228	11	258	467	495	736
D3-6	19-Aug-08	40-50	45	65	18.6	7.7	2.2	3.6	64.0	245	70	253	17	434	457	472	766
D3-6	19-Aug-08	50-60	55	55	17.5	7.8	2.1	3.8	64.0	225	65	252	22	419	474	463	784
D3-6	19-Aug-08	60-70	65	45	20.3	7.7	2.9	3.6	60.0	425	116	325	32	643	516	511	738
D3-6	19-Aug-08	70-80	75	35	21.9	7.8	2.2	4.8	62.0	210	62	308	27	426	552	460	811

Sample Location	Sample Date	Sample Depth (cm)	Point Depth (cm)	Above Shale (cm)	M.C. %	pH	EC dS/m	SAR	% Sat	Lab Measured Sat Paste Conc. Ca^{2+} mg/L	Mg^{2+} mg/L	Na^{+} mg/L	Cl^{-} mg/L	SO_4^{2-} mg/L	Phrq-C Calc. Field Conc. Na^{+} mg/L	Ca^{2+} mg/L	SO_4^{2-} mg/L
D3-6	19-Aug-08	80-90	85	25	18.4	7.8	2.5	5.4	50.0	256	74	386	32	488	643	489	797
D3-6	19-Aug-08	90-100	95	15	19.4	7.8	2.8	7.0	46.0	237	74	480	37	541	773	456	892
D3-6	19-Aug-08	100-110	105	5	25.6	7.7	3.2	6.6	53.0	326	102	532	38	670	769	459	891
D3-6	19-Aug-08	110-120	115	-5	23.5	7.6	4.9	7.2	79.0	529	180	749	32	1058	1263	439	1170
D3-6	19-Aug-08	120-130	125	-15	25.6	7.6	6.7	10.6	79.0	492	296	1216	34	1519	2128	373	1986
D3-6	19-Aug-08	130-140	135	-25	22.4	7.6	8.0	14.4	85.0	487	319	1671	40	1835	3564	337	3128
D3-6	19-Aug-08	140-150	145	-35	26.8	7.6	8.4	16.2	90.0	480	289	1822	49	1911	3768	332	3193
D3-7	1-Jun-02	0-10	5	95	15.5	7.3	0.6	0.9	51.1	66	15	32	14	49	65	249	161
D3-7	1-Jun-02	10-20	15	85	19.6	7.2	0.8	1.2	56.3	82	21	47	24	69	90	269	198
D3-7	1-Jun-02	20-30	25	75	15.0	7.5	0.7	1.5	46.6	65	15	50	24	82	99	244	256
D3-7	1-Jun-02	30-40	35	65	18.0	7.5	0.7	1.5	47.6	64	15	52	17	82	94	202	218
D3-7	1-Jun-02	40-50	45	55	15.8	7.3	0.6	1.5	52.1	51	12	46	11	64	96	209	213
D3-7	1-Jun-02	50-60	55	45	16.3	7.4	0.6	1.4	49.8	51	14	45	9	71	88	191	215
D3-7	1-Jun-02	60-70	65	35	16.8	7.3	0.6	1.2	59.2	53	16	40	8	71	85	227	249
D3-7	1-Jun-02	70-80	75	25	17.8	7.3	0.8	1.2	64.1	71	25	47	12	98	103	302	353
D3-7	1-Jun-02	80-90	85	15	20.5	7.2	1.3	2.0	69.9	104	35	92	16	175	203	432	598
D3-7	1-Jun-02	90-100	95	5	21.6	7.2	2.1	4.9	72.6	127	43	251	25	444	496	367	1154
D3-7	1-Jun-02	100-110	105	-5	24.1	7.1	6.7	8.3	74.7	408	210	824	54	1320	1304	334	1903
D3-7	1-Jun-02	110-120	115	-15	23.1	7.1	9.2	12.0	75.9	376	299	1289	75	1829	2370	301	3240
D3-7	1-Jun-02	120-130	125	-25	23.6	7.2	10.7	15.0	78.1	390	309	1634	98	1953	3249	305	3516
D3-7	1-Jun-02	130-140	135	-35	17.8	7.3	10.7	17.3	69.1	384	231	1732	121	1932	3434	301	3549
D3-7	1-Jun-02	140-150	145	-45	12.7	6.9	8.4	15.8	46.8	297	164	1367	166	1460	2282	331	2317
D3-7	19-Aug-08	0-10	5	113	22.4	7.7	0.6	0.3	71.0	84	20	13	11	34	25	277	108

Sample Location	Sample Date	Sample Depth (cm)	Point Depth (cm)	Above Shale (cm)	M.C. %	pH	EC dS/m	SAR	% Sat	Lab Measured Sat Paste Conc. Ca^{2+} mg/L	Mg^{2+} mg/L	Na^{+} mg/L	Cl^{-} mg/L	SO_4^{2-} mg/L	Phrq-C Calc. Field Conc. Na^{+} mg/L	Ca^{2+} mg/L	SO_4^{2-} mg/L
D3-7	19-Aug-08	10-20	15	103	22.1	7.7	0.4	0.4	64.0	63	14	13	9	24	23	191	70
D3-7	19-Aug-08	20-30	25	93	20.3	7.7	0.5	0.6	58.0	57	13	19	9	21	36	175	60
D3-7	19-Aug-08	30-40	35	83	19.3	7.7	0.6	1.2	55.0	63	14	42	7	54	80	211	155
D3-7	19-Aug-08	40-50	45	73	16.8	7.9	0.6	1.9	51.0	50	11	57	8	58	115	192	176
D3-7	19-Aug-08	50-60	55	63	17.5	7.8	1.1	2.4	53.0	101	22	102	17	148	208	385	454
D3-7	19-Aug-08	60-70	65	53	19.8	7.8	1.6	2.8	54.0	155	36	148	22	241	282	505	647
D3-7	19-Aug-08	70-80	75	43	21.3	7.8	1.5	3.5	56.0	119	28	164	20	213	314	398	561
D3-7	19-Aug-08	80-90	85	33	19.9	7.8	1.8	4.2	60.0	140	36	217	23	278	438	474	735
D3-7	19-Aug-08	90-100	95	23	23.4	7.8	1.7	3.8	61.0	142	35	193	21	262	375	470	691
D3-7	19-Aug-08	100-110	105	13	24.0	7.8	1.9	5.0	66.0	128	36	252	23	291	512	463	783
D3-7	19-Aug-08	110-120	115	3	22.8	7.5	4.9	6.1	76.0	459	176	608	30	1000	990	402	1180
D3-7	19-Aug-08	120-130	125	-7	25.1	7.4	6.4	9.1	87.0	447	261	980	41	1356	1797	357	1908
D3-7	19-Aug-08	130-140	135	-17	26.2	7.5	7.1	10.8	96.0	438	271	1167	56	1500	2371	341	2378
D3-7	19-Aug-08	140-150	145	-27	23.7	7.5	7.9	13.0	87.0	436	285	1425	78	1678	2900	329	2794
D3-8	1-Jun-02	0-10	5	135	41.7	5.3	0.6	0.6	218.2	65	21	23	32	71	76	380	370
D3-8	1-Jun-02	10-20	15	125	85.0	5.3	0.6	0.7	220.0	71	23	26	30	84	54	197	218
D3-8	1-Jun-02	20-30	25	115	66.6	5.4	0.7	0.7	202.1	86	26	29	20	103	66	281	314
D3-8	1-Jun-02	30-40	35	105	60.7	5.5	0.6	0.7	188.2	73	22	27	15	86	62	244	266
D3-8	1-Jun-02	40-50	45	95	65.6	6.2	0.8	0.9	123.6	93	28	40	10	63	62	184	118
D3-8	1-Jun-02	50-60	55	85	24.1	7.2	0.6	1.3	64.0	57	13	42	5	44	77	175	118
D3-8	1-Jun-02	60-70	65	75	20.4	7.4	0.5	1.5	55.4	45	9	43	5	39	80	149	105
D3-8	1-Jun-02	70-80	75	65	28.5	7.3	0.5	1.7	64.8	41	9	46	6	39	79	113	88
D3-8	1-Jun-02	80-90	85	55	21.4	7.2	0.5	1.7	62.4	39	9	46	6	36	91	143	105
D3-8	1-Jun-02	90-100	95	45	21.8	7.4	0.6	1.7	57.6	43	11	48	12	41	89	140	110

Sample Location	Sample Date	Sample Depth (cm)	Point Depth (cm)	Above Shale (cm)	M.C. %	pH	EC dS/m	SAR	% Sat	Lab Measured Sat Paste Conc. Ca^{2+} mg/L	Mg^{2+} mg/L	Na^{+} mg/L	Cl^{-} mg/L	SO_4^{2-} mg/L	Phrq-C Calc. Field Conc. Na^{+} mg/L	Ca^{2+} mg/L	SO_4^{2-} mg/L
D3-8	1-Jun-02	100-110	105	35	23.1	7.4	0.7	1.9	57.1	64	15	64	17	75	115	191	187
D3-8	1-Jun-02	110-120	115	25	24.1	7.3	1.4	3.1	60.6	114	25	138	17	179	257	354	450
D3-8	1-Jun-02	120-130	125	15	18.2	7.4	2.3	6.3	50.8	152	33	329	21	344	627	469	791
D3-8	1-Jun-02	130-140	135	5	24.8	7.2	4.5	8.9	57.7	276	74	647	23	755	977	397	1097
D3-8	1-Jun-02	140-150	145	-5	27.4	7.1	9.9	15.1	82.6	412	268	1598	33	1788	3003	325	2857
D3-8	1-Jun-02	150-160	155	-15	24.3	7.1	10.7	15.1	79.1	423	369	1762	38	1891	3640	335	3333
D3-8	1-Jun-02	160-170	165	-25	17.9	7.4	9.8	15.1	46.5	469	247	1623	53	1746	2320	360	2012
D3-8	19-Aug-08	0-10	5	144	79.0	6.0	0.6	0.6	216.0	68	23	22	20	55	48	200	151
D3-8	19-Aug-08	10-20	15	134	70.9	6.1	0.3	0.7	193.0	38	11	19	13	25	39	112	68
D3-8	19-Aug-08	20-30	25	124	82.2	5.9	0.7	1.2	166.0	69	20	43	17	80	72	150	163
D3-8	19-Aug-08	30-40	35	114	83.9	5.6	1.0	1.2	235.0	110	33	56	23	132	126	335	371
D3-8	19-Aug-08	40-50	45	104	16.4	7.3	1.1	1.5	62.0	110	29	68	18	122	154	487	458
D3-8	19-Aug-08	50-60	55	94	20.2	7.6	1.1	1.6	61.0	110	27	75	21	128	149	386	386
D3-8	19-Aug-08	60-70	65	84	21.9	7.7	1.1	1.8	67.0	112	27	84	24	140	172	403	428
D3-8	19-Aug-08	70-80	75	74	22.0	7.6	1.2	2.0	70.0	123	29	96	24	166	206	472	531
D3-8	19-Aug-08	80-90	85	64	22.7	7.7	1.1	2.0	71.0	110	25	87	25	141	185	411	441
D3-8	19-Aug-08	90-100	95	54	20.2	7.9	1.0	2.2	57.0	86	19	88	23	126	170	301	356
D3-8	19-Aug-08	100-110	105	44	15.5	7.9	1.2	3.1	52.0	91	20	127	29	155	279	415	525
D3-8	19-Aug-08	110-120	115	34	19.9	7.9	1.6	4.3	62.0	115	25	194	29	221	424	492	694
D3-8	19-Aug-08	120-130	125	24	26.6	7.8	1.9	5.2	64.0	127	28	247	31	269	460	401	649
D3-8	19-Aug-08	130-140	135	14	22.6	7.9	2.0	6.4	56.0	114	26	291	30	284	558	395	704
D3-8	19-Aug-08	140-150	145	4	25.6	7.9	2.7	9.1	65.0	144	44	488	28	483	915	409	1040
D3-8	19-Aug-08	150-160	155	-6	28.2	7.5	6.9	11.4	110.0	459	270	1245	17	1582	2750	328	2755
D3-8	19-Aug-08	160-170	165	-16	30.6	7.4	8.8	15.8	107.0	464	330	1822	24	2056	4192	305	4040

Sample Location	Sample Date	Sample Depth (cm)	Point Depth (cm)	Above Shale (cm)	M.C. %	pH	EC dS/m	SAR	% Sat	Lab Measured Sat Paste Conc. Ca^{2+} mg/L	Mg^{2+} mg/L	Na^{+} mg/L	Cl^{-} mg/L	SO_4^{2-} mg/L	Phrq-C Calc. Field Conc. Na^{+} mg/L	Ca^{2+} mg/L	SO_4^{2-} mg/L
D3-8	19-Aug-08	170-180	175	-26	26.9	7.6	8.3	16.5	100.0	458	239	1750	24	1890	3847	313	3437
D3-9	1-Jun-02	0-10	5	155	41.1	5.9	0.8	0.8	102.0	99	33	35	36	84	65	264	209
D3-9	1-Jun-02	10-20	15	145	35.0	6.5	1.3	0.8	80.5	153	51	48	15	82	83	358	189
D3-9	1-Jun-02	20-30	25	135	18.5	6.9	1.0	1.1	53.1	119	31	53	21	72	101	369	207
D3-9	1-Jun-02	30-40	35	125	19.8	7.4	0.6	1.4	46.0	62	15	47	18	47	78	164	110
D3-9	1-Jun-02	40-50	45	115	19.4	7.4	0.5	1.2	47.3	53	14	38	11	44	65	148	108
D3-9	1-Jun-02	50-60	55	105	17.2	7.4	0.5	1.1	45.6	49	14	33	10	32	59	148	84
D3-9	1-Jun-02	60-70	65	95	17.4	7.5	0.6	1.1	42.1	60	14	36	8	41	61	163	100
D3-9	1-Jun-02	70-80	75	85	22.7	7.5	0.5	1.3	50.0	48	13	38	7	36	62	121	79
D3-9	1-Jun-02	80-90	85	75	20.9	7.5	0.5	1.4	56.0	50	12	41	5	41	76	159	111
D3-9	1-Jun-02	90-100	95	65	17.6	7.5	0.6	1.4	43.1	51	14	43	10	41	75	146	102
D3-9	1-Jun-02	100-110	105	55	22.8	7.5	0.6	1.3	55.5	51	15	41	10	41	72	144	101
D3-9	1-Jun-02	110-120	115	45	20.7	7.3	0.6	1.2	54.7	60	16	39	13	46	70	180	121
D3-9	1-Jun-02	120-130	125	35	20.2	7.3	0.7	1.2	50.6	75	19	44	26	58	77	212	145
D3-9	1-Jun-02	130-140	135	25	20.3	7.3	0.9	1.5	59.2	84	22	59	25	82	114	285	240
D3-9	1-Jun-02	140-150	145	15	18.9	7.3	1.7	3.8	55.0	131	33	188	52	195	387	496	569
D3-9	1-Jun-02	150-160	155	5	17.4	7.5	4.0	10.2	46.3	182	48	598	96	563	1041	422	1029
D3-9	1-Jun-02	160-170	165	-5	30.4	7.1	9.7	18.7	96.9		164	1719	94	1541	3508	353	2604
D3-9	1-Jun-02	170-180	175	-15	26.6	7.2	10.9	21.5	97.1		180	2007	96	1746	4692	331	3501
D3-9	1-Jun-02	180-190	185	-25	25.1	7.1	13.4	25.6	100.6		230	2602	109	1684	6828	332	4441
D3-9	1-Jun-02	190-200	195	-35	21.4	7.1	13.8	28.1	107.0		212	2756	127	1947	9262	300	6379
D3-9	19-Aug-08	0-10	5	175	50.7	6.3	0.4	0.5	161.0	53	17	16	34	20	37	182	63
D3-9	19-Aug-08	10-20	15	165	55.4	6.2	0.4	0.6	160.0	51	16	19	19	32	40	157	93

Sample Location	Sample Date	Sample Depth (cm)	Point Depth (cm)	Above Shale (cm)	M.C. %	pH	EC dS/m	SAR	% Sat	Lab Measured Sat Paste Conc. Ca^{2+} mg/L	Mg^{2+} mg/L	Na^{+} mg/L	Cl^{-} mg/L	SO_4^{2-} mg/L	Phrq-C Calc. Field Conc. Na^{+} mg/L	Ca^{2+} mg/L	SO_4^{2-} mg/L
D3-9	19-Aug-08	20-30	25	155	43.2	6.4	0.4	0.8	119.0	45	12	23	25	27	44	135	75
D3-9	19-Aug-08	30-40	35	145	29.0	7.4	0.7	1.0	71.0	79	22	38	37	41	69	211	101
D3-9	19-Aug-08	40-50	45	135	15.2	7.8	0.5	1.2	51.0	51	13	37	18	36	77	204	121
D3-9	19-Aug-08	50-60	55	125	14.2	7.8	0.5	1.3	53.0	52	13	40	15	37	89	234	136
D3-9	19-Aug-08	60-70	65	115	15.0	7.8	0.5	1.4	52.0	52	13	44	13	47	92	219	163
D3-9	19-Aug-08	70-80	75	105	14.8	7.8	0.5	1.3	56.0	56	14	41	11	46	92	254	174
D3-9	19-Aug-08	80-90	85	95	16.8	7.8	0.6	1.3	55.0	68	16	45	13	60	93	261	197
D3-9	19-Aug-08	90-100	95	85	20.2	8.0	0.6	1.3	74.0	63	15	45	12	56	103	279	208
D3-9	19-Aug-08	100-110	105	75	16.7	7.9	1.0	1.4	55.0	120	28	65	33	130	137	456	427
D3-9	19-Aug-08	110-120	115	65	16.1	7.9	1.1	1.7	54.0	130	31	81	39	159	174	515	532
D3-9	19-Aug-08	120-130	125	55	17.4	7.8	1.4	2.1	54.0	158	40	117	48	213	234	541	612
D3-9	19-Aug-08	130-140	135	45	15.0	7.8	1.7	3.0	58.0	178	48	176	55	272	364	539	653
D3-9	19-Aug-08	140-150	145	35	21.0	7.8	1.9	3.6	59.0	198	54	220	66	337	405	493	710
D3-9	19-Aug-08	150-160	155	25	20.5	7.8	2.1	4.6	60.0	183	51	272	72	350	515	484	752
D3-9	19-Aug-08	160-170	165	15	24.2	7.9	2.2	7.3	63.0	135	38	373	76	367	723	444	877
D3-9	19-Aug-08	170-180	175	5	22.2	8.0	2.8	11.2	66.0	123	38	555	77	479	1139	411	1109
D3-9	19-Aug-08	180-190	185	-5	26.6	7.7	9.4	18.9	96.0	457	268	2063	83	2094	4724	305	4087
D3-9	19-Aug-08	190-200	195	-15	27.6	7.5	10.2	21.7	116.0	445	286	2388	78	2276	6994	288	5933
D3-9	19-Aug-08	200-210	205	-25	27.3	7.7	11.2	24.4	115.0	446	291	2696	96	2530	8225	275	7008
D3-9	21-Oct-05	0-10	5	165		6.1	0.4	0.6	88.0	56	18	22	36	28			
D3-9	21-Oct-05	10-20	15	155		6.0	0.2	0.8	150.0	33	9	21	7	18			
D3-9	21-Oct-05	20-30	25	145		7.2	0.7	1.2	77.0	103	30	52	6	52			
D3-9	21-Oct-05	30-40	35	135		7.5	0.9	1.4	40.0	117	30	68	13	107			
D3-9	21-Oct-05	40-50	45	125		7.7	0.8	1.5	39.0	100	25	67	15	106			

Sample Location	Sample Date	Sample Depth (cm)	Point Depth (cm)	Above Shale (cm)	M.C. %	pH	EC dS/m	SAR	% Sat	Lab Measured Sat Paste Conc. Ca^{2+} mg/L	Mg^{2+} mg/L	Na^{+} mg/L	Cl^{-} mg/L	SO_4^{2-} mg/L	Phrq-C Calc. Field Conc. Na^{+} mg/L	Ca^{2+} mg/L	SO_4^{2-} mg/L
D3-9	21-Oct-05	50-60	55	115		7.8	0.7	1.5	39.0	87	22	62	15	90			
D3-9	21-Oct-05	60-70	65	105		7.7	0.6	1.3	45.0	69	17	47	11	56			
D3-9	21-Oct-05	70-80	75	95		7.6	0.5	1.3	49.0	54	14	43	10	37			
D3-9	21-Oct-05	80-90	85	85		7.8	0.4	1.3	64.0	47	13	41	11	31			
D3-9	21-Oct-05	90-100	95	75		7.7	0.5	1.4	61.0	60	16	46	16	49			
D3-9	21-Oct-05	100-110	105	65		7.5	0.8	1.4	58.0	97	26	62	24	84			
D3-9	21-Oct-05	110-120	115	55		7.8	0.9	1.7	33.0	106	29	76	39	123			
D3-9	21-Oct-05	120-130	125	45		7.6	1.0	2.0	38.0	119	35	97	42	155			
D3-9	21-Oct-05	130-140	135	35		7.7	1.5	2.9	50.0	145	43	156	46	216			
D3-9	21-Oct-05	140-150	145	25		7.8	2.1	5.2	43.0	170	47	298	65	333			
D3-9	21-Oct-05	150-160	155	15		7.8	2.9	11.0	52.0	135	38	577	81	500			
D3-9	21-Oct-05	160-170	165	5		7.8	4.2	17.0	56.0	144	48	929	100	768			
D3-9	21-Oct-05	170-180	175	-5		7.4	9.0	21.4	104.0	446	211	2192	91	2115			
D3-9	21-Oct-05	180-190	185	-15		7.4	9.8	29.1	118.0	324	177	2619	102	2263			
D3-9	21-Oct-05	190-200	195	-25		7.5	10.1	33.6	128.0	255	155	2773	114	2328			
D3-9	21-Oct-05	200-210	205	-35		7.5	10.1	38.1	139.0	217	135	2906	129	2353			
D3-10	1-Jun-02	0-10	5	135	40.1	5.3	1.1	0.8	187.7	135	43	41	26	144	125	603	581
D3-10	1-Jun-02	10-20	15	125	70.4	5.5	0.7	0.7	199.0	100	28	32	21	82	69	299	233
D3-10	1-Jun-02	20-30	25	115	46.1	6.4	1.1	0.7	117.7	163	39	37	13	59	70	382	152
D3-10	1-Jun-02	30-40	35	105	19.1	7.2	0.7	1.0	46.7	77	18	37	7	44	64	209	109
D3-10	1-Jun-02	40-50	45	95	18.7	7.2	0.6	0.9	45.0	66	16	32	6	34	54	175	83
D3-10	1-Jun-02	50-60	55	85	19.0	7.2	0.6	0.8	54.3	74	16	31	5	30	58	231	87
D3-10	1-Jun-02	60-70	65	75	19.1	7.3	0.6	1.0	44.5	70	14	37	6	39	61	181	90
D3-10	1-Jun-02	70-80	75	65	18.2	7.4	0.6	1.2	45.3	65	11	39	7	32	68	185	79

Sample Location	Sample Date	Sample Depth (cm)	Point Depth (cm)	Above Shale (cm)	M.C. %	pH	EC dS/m	SAR	% Sat	Lab Measured Sat Paste Conc. Ca^{2+} mg/L	Mg^{2+} mg/L	Na^{+} mg/L	Cl^{-} mg/L	SO_4^{2-} mg/L	Phrq-C Calc. Field Conc. Na^{+} mg/L	Ca^{2+} mg/L	SO_4^{2-} mg/L
D3-10	1-Jun-02	80-90	85	55	17.0	7.5	0.5	1.2	46.9	54	9	37	8	30	68	175	83
D3-10	1-Jun-02	90-100	95	45	18.6	7.5	0.6	1.2	49.5	56	9	38	14	33	69	175	88
D3-10	1-Jun-02	100-110	105	35	19.5	7.5	0.7	1.4	50.4	65	10	45	30	43	81	196	111
D3-10	1-Jun-02	110-120	115	25	20.1	7.4	1.2	2.1	47.5	118	18	92	55	105	160	325	249
D3-10	1-Jun-02	120-130	125	15	19.0	7.5	2.1	5.7	54.8	156	21	286	76	195	569	532	563
D3-10	1-Jun-02	130-140	135	5	16.8	7.5	4.9	11.4	53.5	251	43	740	99	594	1321	482	955
D3-10	1-Jun-02	140-150	145	-5	19.2	7.1	10.4	19.2	82.3	410	212	1925	83	1767	4518	339	3376
D3-10	1-Jun-02	150-160	155	-15	21.8	7.0	11.9	22.4	100.6	400	243	2299	93	2035	6804	305	5321
D3-10	1-Jun-02	160-170	165	-25	21.7	6.8	13.0	24.5	105.7	381	261	2535	134	2480	8523	260	7916
D3-10	19-Aug-08	0-10	5	145	54.4	6.2	0.4	0.2	167.0	68	22	8	17	25	17	218	76
D3-10	19-Aug-08	10-20	15	135	66.7	6.2	0.6	0.7	124.0	70	23	27	11	55	42	137	102
D3-10	19-Aug-08	20-30	25	125	50.4	6.8	0.8	0.4	154.0	112	28	19	16	41	41	306	125
D3-10	19-Aug-08	30-40	35	115	20.8	7.6	0.5	0.6	54.0	58	13	19	9	28	34	163	73
D3-10	19-Aug-08	40-50	45	105	17.4	7.8	0.4	0.8	49.0	42	9	22	8	23	42	136	65
D3-10	19-Aug-08	50-60	55	95	14.1	7.8	0.4	1.0	45.0	41	8	27	7	24	52	155	77
D3-10	19-Aug-08	60-70	65	85	15.8	8.0	0.4	1.0	50.0	39	7	26	8	25	53	145	78
D3-10	19-Aug-08	70-80	75	75	15.6	7.9	0.4	1.3	46.0	39	7	35	9	27	65	138	78
D3-10	19-Aug-08	80-90	85	65	19.1	7.8	0.4	1.3	54.0	35	7	33	7	24	63	122	69
D3-10	19-Aug-08	90-100	95	55	18.6	7.8	0.6	1.5	55.0	52	10	45	13	48	88	184	142
D3-10	19-Aug-08	100-110	105	45	20.9	7.8	0.6	1.7	66.0	58	11	55	12	56	115	228	177
D3-10	19-Aug-08	110-120	115	35	22.4	7.9	1.0	3.4	66.0	67	12	115	18	108	238	270	317
D3-10	19-Aug-08	120-130	125	25	18.5	8.1	1.6	7.2	50.0	68	12	246	32	186	517	297	508
D3-10	19-Aug-08	130-140	135	15	19.8	8.1	2.0	11.4	50.0	58	11	358	42	250	753	263	640
D3-10	19-Aug-08	140-150	145	5	19.7	8.2	2.8	12.8	48.0	102	22	546	54	442	1100	407	1077

Sample Location	Sample Date	Sample Depth (cm)	Point Depth (cm)	Above Shale (cm)	M.C. %	pH	EC dS/m	SAR	% Sat	Lab Measured Sat Paste Conc. Ca^{2+} mg/L	Mg^{2+} mg/L	Na^{+} mg/L	Cl^{-} mg/L	SO_4^{2-} mg/L	Phrq-C Calc. Field Conc. Na^{+} mg/L	Ca^{2+} mg/L	SO_4^{2-} mg/L
D3-10	19-Aug-08	150-160	155	-5	29.4	7.6	8.2	15.7	108.0	432	206	1583	58	1722	3433	313	3149
D3-10	19-Aug-08	160-170	165	-15	25.4	7.7	9.5	18.3	102.0	426	255	1931	69	2000	4818	297	4338
D3-10	19-Aug-08	170-180	175	-25	26.8	7.6	12.2	24.2	112.0	412	327	2714	92	2679	8373	263	7733

Table B4: Laboratory and Phreeq-C soil salinity data for Plateau locations.

Sample Location	Sample Date	Sample Depth (cm)	Point Depth (cm)	Above Shale (cm)	M.C. %	pH	EC dS/m	SAR	% Sat	Lab Measured Sat Paste Conc. Ca^{2+} mg/L	Mg^{2+} mg/L	Na^{+} mg/L	Cl^{-} mg/L	SO_4^{2-} mg/L	Phrq-C Calc. Field Conc. Na^{+} mg/L	Ca^{2+} mg/L	SO_4^{2-} mg/L
Pro 33	26-May-09	0-6	3	89	62.6	6.3	0.7	1.5	149.0	67	21	54	32	72	102	181	173
Pro 33	26-May-09	6-20	13	79	30.9	7.3	0.7	1.4	72.0	75	22	54	25	49	93	195	114
Pro 33	26-May-09	20-30	25	67	25.6	7.4	0.8	2.6	70.0	57	20	91	14	96	177	201	263
Pro 33	26-May-09	30-40	35	57	25.5	7.3	0.9	3.2	76.0	58	22	112	14	126	234	233	376
Pro 33	26-May-09	40-50	45	47	21.9	7.6	1.1	3.6	64.0	70	25	139	19	138	287	277	404
Pro 33	26-May-09	50-60	55	37	21.3	7.7	1.5	4.8	70.0	86	34	209	21	219	478	409	718
Pro 33	26-May-09	60-70	65	27	26.8	7.9	1.7	7.2	84.0	68	30	283	25	254	664	344	800
Pro 33	26-May-09	70-80	75	17	26.2	7.8	2.3	9.2	62.0	93	43	429	37	360	835	328	858
Pro 33	26-May-09	80-90	85	7	27.2	7.8	2.4	9.8	63.0	95	45	465	35	390	884	326	903
Pro 33	26-May-09	90-100	95	-3	28.0	7.4	4.7	7.4	70.0	401	174	711	33	966	1099	421	1179
Pro 33	26-May-09	100-110	105	-13	26.6	7.4	4.5	8.6	55.0	340	135	747	45	873	1068	425	1110
Pro 33	26-May-09	110-120	115	-23	21.2	7.7	2.9	9.6	40.0	163	59	565	45	503	906	404	945
Pro 33	26-May-09	120-130	125	-33	16.6	7.6	2.7	7.7	44.0	170	63	466	48	448	843	463	920
Pro 33	26-May-09	130-140	135	-43	21.0	7.5	2.1	5.2	48.0	145	56	292	38	344	520	430	792
Pro 33	26-May-09	140-150	145	-53	22.1	7.3	1.7	3.6	48.0	142	59	202	46	285	341	373	620
Pro 33	26-May-09	150-160	155	-63	19.5	7.3	1.3	2.6	52.0	109	48	131	40	196	245	356	522
Pro 33	26-May-09	160-170	165	-73	21.6	7.4	1.1	2.0	55.0	98	43	95	38	155	172	298	399
Pro 33	26-May-09	170-180	175	-83	16.1	7.3	1.1	1.8	44.0	93	42	86	32	147	159	299	399
Pro 33	26-May-09	180-190	185	-93	15.7	7.3	1.0	1.8	42.0	91	41	83	36	142	151	291	384
Pro 33	26-May-09	190-200	195	-103	19.1	7.3	1.0	1.9	48.0	87	36	83	27	134	147	258	334
Pro 33	26-May-09	200-210	205	-113	22.1	7.5	1.0	2.0	54.0	86	37	87	30	138	156	249	340
Pro 33	26-May-09	210-220	215	-123	22.0	7.5	1.2	2.4	50.0	102	41	112	38	169	191	274	387
Pro 33	26-May-09	220-230	225	-133	21.1	7.5	1.4	3.0	53.0	108	44	149	43	204	275	339	516
Pro 33	26-May-09	230-240	235	-143	21.5	7.5	1.9	5.1	53.0	116	46	258	45	294	484	382	724

Sample Location	Sample Date	Sample Depth (cm)	Point Depth (cm)	Above Shale (cm)	M.C. %	pH	EC dS/m	SAR	% Sat	Lab Measured Sat Paste Conc. Ca^{2+} mg/L	Mg^{2+} mg/L	Na^{+} mg/L	Cl^{-} mg/L	SO_4^{2-} mg/L	Phrq-C Calc. Field Conc. Na^{+} mg/L	Ca^{2+} mg/L	SO_4^{2-} mg/L
Pro 33	26-May-09	240-250	245	-153	24.8	7.4	2.3	6.4	61.0	134	50	344	57	362	660	446	890
Pro 50	1-Oct-04	0-15	7	105		5.0	2.2	2.4	109.0	179	84	146	33	513	115	259	500
Pro 50	1-Oct-04	15-30	22	88		7.2	1.0	2.2	43.5	232	97	195	18	262	201	451	457
Pro 50	1-Oct-04	30-50	40	70		7.4	0.9	2.5	45.5	193	75	175	31	269	201	396	504
Pro 50	1-Oct-04	50-70	60	50		7.4	1.1	3.0	59.0	164	66	187	26	268	277	534	716
Pro 50	1-Oct-04	70-90	80	30		7.2	1.4	3.9	62.0	175	69	255	30	302	379	565	714
Pro 50	1-Oct-04	90-110	100	10		6.9	4.1	10.2	60.0	345	206	1268	140	1366	872	401	1110
Pro 50	1-Oct-04	110-130	120	-10		7.2	5.5	16.0	71.0	265	195	1650	42	1605	2061	322	2387
Pro 50	1-Oct-04	130-150	140	-30		7.3	8.5	23.1	46.5	515	441	4402	227	3656	4678	299	4212
Pro 50	1-Oct-04	150-160	155	-45		7.5	5.4	25.4	56.8	204	145	2315	161	1816	3151	304	3341
Pro 50	26-May-09	0-10	5	92	42.1	7.1	0.7	0.6	109.0	106	25	26	28	54	49	282	140
Pro 50	26-May-09	10-20	15	82	18.8	7.8	0.5	1.2	44.0	64	15	41	16	41	66	167	95
Pro 50	26-May-09	20-30	25	72	9.4	7.8	0.8	1.8	43.0	80	20	72	23	92	176	477	422
Pro 50	26-May-09	30-40	35	62	14.2	7.8	1.2	2.4	42.0	121	31	112	31	168	223	444	503
Pro 50	26-May-09	40-50	45	52	23.0	7.6	1.8	3.1	49.0	178	50	184	55	273	300	440	578
Pro 50	26-May-09	50-60	55	42	24.1	7.6	1.9	3.7	56.0	176	51	218	54	296	387	491	686
Pro 50	26-May-09	60-70	65	32	26.1	7.6	2.0	4.3	62.0	174	50	252	48	308	453	498	720
Pro 50	26-May-09	70-80	75	22	19.2	7.6	2.1	5.3	62.0	165	47	300	52	342	594	483	780
Pro 50	26-May-09	80-90	85	12	30.2	7.7	2.3	6.2	58.0	157	42	340	62	353	546	376	678
Pro 50	26-May-09	90-100	95	2	34.5	7.8	2.7	8.2	60.0	173	52	482	67	447	738	373	781
Pro 50	26-May-09	100-110	105	-8	25.7	7.5	5.7	8.3	71.0	489	187	858	55	1190	1298	393	1338
Pro 50	26-May-09	110-120	115	-18	21.7	7.8	6.6	12.7	88.0	348	191	1193	47	1307	2493	355	2213
Pro 50	26-May-09	120-130	125	-28	19.9	7.7	7.7	14.5	42.0	405	234	1486	93	1667	1939	346	1939

Sample Location	Sample Date	Sample Depth (cm)	Point Depth (cm)	Above Shale (cm)	M.C. %	pH	EC dS/m	SAR	% Sat	Lab Measured Sat Paste Conc. Ca^{2+} mg/L	Mg^{2+} mg/L	Na^{+} mg/L	Cl^{-} mg/L	SO_4^{2-} mg/L	Phrq-C Calc. Field Conc. Na^{+} mg/L	Ca^{2+} mg/L	SO_4^{2-} mg/L
Pro 50	26-May-09	130-140	135	-38	24.1	7.8	9.2	17.2	51.0	425	276	1869	98	2020	2596	327	2499
Pro 50	26-May-09	140-150	145	-48	25.0	7.8	9.4	18.2	94.0	423	266	1936	84	2021	4500	302	4050
Pro 50	26-May-09	150-160	155	-58	25.7	7.8	11.4	22.2	56.0	425	325	2518	146	2482	3879	310	3434
Pro 50	26-May-09	160-170	165	-68	27.3	7.9	11.4	23.4	41.0	388	312	2561	200	2463	3119	322	2779
Pro 50	26-May-09	170-180	175	-78	21.0	7.7	11.3	23.5	52.0	394	304	2577	202	2423	4241	311	3596
Pro 50	26-May-09	180-190	185	-88	22.5	8.0	8.5	33.0	108.0	120	95	2000	183	1556	6845	284	5416
Pro 50	26-May-09	190-200	195	-98	25.4	7.4	12.0	25.9	52.0	396	292	2808	221	2538	4212	314	3468
Pro 51	1-Oct-04	0-10	5	120		4.4	1.8	3.5	195.0	91	50	115	31	298	161	223	515
Pro 51	1-Oct-04	10-30	20	105		7.2	1.1	1.9	51.0	262	94	175	19	523	166	466	709
Pro 51	1-Oct-04	30-50	40	85		7.3	1.1	1.9	50.0	257	90	168	20	492	166	477	692
Pro 51	1-Oct-04	50-70	60	65		7.2	1.3	1.8	56.5	271	110	168	16	494	181	544	639
Pro 51	1-Oct-04	70-90	80	45		7.4	1.2	2.1	49.0	279	113	207	21	502	203	547	652
Pro 51	1-Oct-04	90-110	100	25		7.6	1.0	3.9	59.0	167	51	234	27	311	330	511	729
Pro 51	1-Oct-04	110-125	117	8		7.5	1.8	9.5	64.5	190	68	677	63	684	873	392	1154
Pro 51	1-Oct-04	125-135	130	-5		7.5	4.5	17.8	89.0	255	172	1621	61	1569	2526	310	2828
Pro 51	1-Oct-04	135-145	140	-15		7.5	5.2	17.7	85.0	324	235	1933	87	1820	3348	315	3154
Pro 51	1-Oct-04	145-155	150	-25		7.6	5.5	19.4	83.0	329	251	2182	82	1955	3545	316	3197
Pro 51	1-Oct-04	155-165	160	-35		7.7	5.3	25.4	93.0	202	152	2020	79	1501	3976	326	3236
Pro 51	26-May-09	0-10	5	115	60.1	5.0	1.4	1.2	195.0	169	54	70	37	222	171	528	641
Pro 51	26-May-09	10-20	15	105	18.7	7.6	1.0	1.4	56.0	122	31	68	20	138	134	416	411
Pro 51	26-May-09	20-30	25	95	18.5	7.4	1.4	1.7	46.0	172	46	98	28	210	173	482	519
Pro 51	26-May-09	30-40	35	85	12.5	7.2	1.6	1.9	50.0	204	56	120	30	262	243	585	598
Pro 51	26-May-09	40-50	45	75	24.5	7.7	2.0	2.0	50.0	256	72	142	46	344	222	520	638

Sample Location	Sample Date	Sample Depth (cm)	Point Depth (cm)	Above Shale (cm)	M.C. %	pH	EC dS/m	SAR	% Sat	Lab Measured Sat Paste Conc. Ca^{2+} mg/L	Mg^{2+} mg/L	Na^{+} mg/L	Cl^{-} mg/L	SO_4^{2-} mg/L	Phrq-C Calc. Field Conc. Na^{+} mg/L	Ca^{2+} mg/L	SO_4^{2-} mg/L
Pro 51	26-May-09	50-60	55	65	21.5	7.6	3.0	1.6	54.0	587	136	169	46	698	237	550	613
Pro 51	26-May-09	60-70	65	55	16.7	7.4	2.5	2.3	59.0	381	107	198	71	492	354	598	623
Pro 51	26-May-09	70-80	75	45	29.2	7.7	2.6	2.6	49.0	373	104	224	78	500	301	523	656
Pro 51	26-May-09	80-90	85	35	23.7	7.8	2.7	4.2	51.0	306	95	327	98	488	499	515	727
Pro 51	26-May-09	90-100	95	25	23.3	7.8	3.1	7.1	59.0	229	86	493	108	536	852	464	922
Pro 51	26-May-09	100-110	105	15	24.4	7.8	3.8	11.0	66.0	180	68	683	94	617	1263	418	1167
Pro 51	26-May-09	110-120	115	5	28.8	7.5	5.7	12.9	63.0	313	122	1067	113	1060	1597	385	1434
Pro 51	26-May-09	120-130	125	-5	24.0	7.6	7.9	14.0	89.0	452	236	1483	107	1652	2980	334	2638
Pro 51	26-May-09	130-140	135	-15	24.5	7.6	9.3	17.1	85.0	446	266	1847	114	1988	3800	309	3494
Pro 51	26-May-09	140-150	145	-25	23.6	7.8	10.0	20.1	83.0	447	273	2193	120	2241	4799	297	4298
Pro 51	26-May-09	150-160	155	-35	24.7	7.8	10.0	21.0	93.0	429	237	2183	118	2161	5181	294	4498
Pro 51	26-May-09	160-170	165	-45	26.5	7.7	9.1	21.7	99.0	343	179	1990	101	1879	4715	299	4027
Pro 51	26-May-09	170-180	175	-55	22.7	7.8	7.7	26.2	99.0	169	105	1758	110	1455	4929	303	3985
Pro 51	26-May-09	180-190	185	-65	21.8	7.9	7.7	27.1	87.0	156	95	1747	149	1391	4533	314	3531
Pro 51	26-May-09	190-200	195	-75	23.7	7.7	6.5	27.2	87.0	113	67	1471	132	1149	3730	322	2955
Pro 52	1-Oct-04	0-20	10	80		7.1	1.6	3.5	103.0	123	43	154	17	280	262	457	743
Pro 52	1-Oct-04	20-40	30	60		7.0	1.3	2.6	58.7	189	59	172	77	313	216	536	647
Pro 52	1-Oct-04	40-60	50	40		7.4	1.4	3.4	58.7	191	62	233	43	288	294	551	609
Pro 52	1-Oct-04	60-80	70	20		7.5	1.9	8.0	58.7	173	54	508	57	405	692	512	821
Pro 52	1-Oct-04	80-90	85	5		7.4	3.9	16.5	81.0	159	82	1056	69	882	1612	353	1718
Pro 52	1-Oct-04	90-100	95	-5		7.5	7.4	16.2	76.0	354	266	1968	86	1788	2837	361	2344
Pro 52	1-Oct-04	100-110	105	-15		7.4	10.2	18.0	74.0	542	466	2907	107	2727	4477	328	3772
Pro 52	1-Oct-04	110-120	115	-25		7.3	11.1	18.8	63.0	693	612	3760	130	3465	5034	323	4216
Pro 52	1-Oct-04	120-130	125	-35		7.2	10.2	19.5	68.0	552	437	3234	135	2731	4732	342	3595

Sample Location	Sample Date	Sample Depth (cm)	Point Depth (cm)	Above Shale (cm)	M.C. %	pH	EC dS/m	SAR	% Sat	Lab Measured Sat Paste Conc. Ca^{2+} mg/L	Mg^{2+} mg/L	Na^{+} mg/L	Cl^{-} mg/L	SO_4^{2-} mg/L	Phrq-C Calc. Field Conc. Na^{+} mg/L	Ca^{2+} mg/L	SO_4^{2-} mg/L
Pro 52	26-May-09	0-10	5	75	53.1	7.2	2.2	3.1	103.0	220	79	210	87	308	343	469	594
Pro 52	26-May-09	10-20	15	65	20.8	7.6	1.5	3.6	55.0	116	38	176	36	213	339	391	560
Pro 52	26-May-09	20-30	25	55	19.5	7.7	2.1	4.2	57.0	186	60	260	44	360	487	481	768
Pro 52	26-May-09	30-40	35	45	27.2	7.5	2.9	5.3	64.0	272	89	394	80	511	647	485	816
Pro 52	26-May-09	40-50	45	35	358.0	6.3	3.9	7.0	130.0	305	115	564	95	690	243	92	251
Pro 52	26-May-09	50-60	55	25	226.0	6.0	3.6	8.2	274.0	245	103	606	88	657	722	311	799
Pro 52	26-May-09	60-70	65	15	101.0	6.0	4.2	10.9	173.0	214	95	763	86	734	1200	401	1219
Pro 52	26-May-09	70-80	75	5	33.4	7.9	3.0	13.2	81.0	96	41	615	64	459	1258	369	1113
Pro 52	26-May-09	80-90	85	-5	30.7	7.4	8.0	13.2	76.0	447	289	1461	72	1697	2367	347	2255
Pro 52	26-May-09	90-100	95	-15	17.2	7.4	9.3	16.1	74.0	438	346	1865	103	2054	4334	309	4053
Pro 52	26-May-09	100-110	105	-25	17.4	7.6	10.2	18.3	63.0	427	368	2143	113	2254	4502	305	4178
Pro 52	26-May-09	110-120	115	-35	21.4	7.7	10.6	19.8	68.0	441	347	2294	134	2324	4630	307	4110
Pro 52	26-May-09	120-130	125	-45	22.0	7.9	11.4	22.0	82.0	437	337	2512	129	2439	6279	294	5422
Pro 52	26-May-09	130-140	135	-55	31.3	7.9	10.0	23.1	120.0	348	214	2225	140	2067	6040	288	5125
Pro 52	26-May-09	140-150	145	-65	28.8	7.6	10.0	24.6	128.0	330	186	2250	159	2063	7044	277	5964
Pro 52	26-May-09	150-160	155	-75	28.9	7.7	9.5	24.1	147.0	324	155	2116	127	1898	7413	277	6092
Pro 52	26-May-09	160-170	165	-85	34.3	7.6	8.5	29.1	144.0	170	103	1951	148	1611	6141	286	5005
Pro 52	26-May-09	170-180	175	-95	33.0	7.9	7.8	32.0	148.0	120	75	1811	135	1412	6146	289	4835
Pro 52	26-May-09	180-190	185	-105	29.5	7.8	8.0	31.3	152.0	138	77	1849	122	1480	6922	280	5529
Pro 52	26-May-09	190-200	195	-115	29.9	7.8	9.0	28.6	142.0	232	105	2092	141	1725	7025	283	5465
Pro 53	1-Oct-04	0-15	7	103		6.0	1.3	2.2	191.0	60	22	48	18	96	120	259	316
Pro 53	1-Oct-04	15-30	22	88		5.2	1.1	2.2	191.0	50	13	37	8	81	159	425	604
Pro 53	1-Oct-04	30-50	40	70		6.7	1.4	2.7	61.0	180	66	178	22	332	212	464	657

Sample Location	Sample Date	Sample Depth (cm)	Point Depth (cm)	Above Shale (cm)	M.C. %	pH	EC dS/m	SAR	% Sat	Lab Measured Sat Paste Conc. Ca^{2+} mg/L	Mg^{2+} mg/L	Na^{+} mg/L	Cl^{-} mg/L	SO_4^{2-} mg/L	Phrq-C Calc. Field Conc. Na^{+} mg/L	Ca^{2+} mg/L	SO_4^{2-} mg/L
Pro 53	1-Oct-04	50-70	60	50		6.9	1.4	3.6	64.0	155	50	204	19	310	278	452	730
Pro 53	1-Oct-04	70-90	80	30		7.6	1.5	4.5	68.0	148	41	234	28	238	359	498	601
Pro 53	1-Oct-04	90-110	100	10		7.7	2.4	10.1	52.0	205	68	774	54	709	835	408	1058
Pro 53	1-Oct-04	110-120	115	-5		7.5	6.0	12.7	77.0	328	210	1409	52	1799	1686	295	2846
Pro 53	1-Oct-04	120-130	125	-15		7.4	8.3	13.4	77.0	507	354	1956	78	2251	2650	326	2646
Pro 53	1-Oct-04	130-150	140	-30		7.5	7.5	14.3	78.0	392	277	1790	65	1519	2538	410	1850
Pro 53	1-Oct-04	150-160	155	-45		7.4	6.9	13.5	87.0	323	223	1441	78	1286	2252	410	1735
Pro 53	26-May-09	0-10	5	93	108.0	5.4	0.5	1.1	164.0	47	15	34	28	50	47	76	77
Pro 53	26-May-09	10-20	15	83	105.0	5.0	0.6	1.1	218.0	59	20	39	21	72	68	131	152
Pro 53	26-May-09	20-30	25	73	24.5	7.2	1.6	1.3	61.0	215	68	89	11	277	156	535	626
Pro 53	26-May-09	30-40	35	63	19.8	6.7	1.8	1.5	78.0	223	75	104	17	338	208	483	698
Pro 53	26-May-09	40-50	45	53	19.8	6.9	1.8	1.8	64.0	225	74	120	25	344	223	487	692
Pro 53	26-May-09	50-60	55	43	23.0	7.2	2.1	2.4	77.0	249	79	169	44	396	320	483	721
Pro 53	26-May-09	60-70	65	33	25.6	7.5	2.4	3.3	68.0	269	85	247	56	429	426	507	723
Pro 53	26-May-09	70-80	75	23	21.5	7.6	2.9	4.9	51.0	298	90	376	51	539	584	483	791
Pro 53	26-May-09	80-90	85	13	21.4	7.7	3.2	8.8	52.0	198	69	563	79	544	968	445	985
Pro 53	26-May-09	90-100	95	3	21.4	7.8	4.8	11.5	64.0	238	112	858	69	845	1532	400	1390
Pro 53	26-May-09	100-110	105	-7	23.2	7.5	7.4	11.9	77.0	453	291	1325	65	1623	2414	345	2337
Pro 53	26-May-09	110-120	115	-17	23.1	7.5	8.5	13.8	77.0	444	338	1584	81	1844	3100	331	2963
Pro 53	26-May-09	120-130	125	-27	24.9	7.3	9.8	17.4	78.0	449	342	2026	103	2179	4020	310	3738
Pro 53	26-May-09	130-140	135	-37	25.0	7.4	10.1	19.7	81.0	431	291	2160	117	2198	4504	303	4007
Pro 53	26-May-09	140-150	145	-47	28.5	7.5	10.2	21.5	87.0	448	259	2310	103	2253	4707	303	4026
Pro 53	26-May-09	150-160	155	-57	28.4	7.7	10.2	21.6	87.0	438	237	2264	124	2184	4598	307	3842
Pro 53	26-May-09	160-170	165	-67	27.3	7.6	10.2	21.7	83.0	437	239	2289	129	2217	4538	303	3860

Sample Location	Sample Date	Sample Depth (cm)	Point Depth (cm)	Above Shale (cm)	M.C. %	pH	EC dS/m	SAR	% Sat	Lab Measured Sat Paste Conc. Ca^{2+} mg/L	Mg^{2+} mg/L	Na^{+} mg/L	Cl^{-} mg/L	SO_4^{2-} mg/L	Phrq-C Calc. Field Conc. Na^{+} mg/L	Ca^{2+} mg/L	SO_4^{2-} mg/L
Pro 53	26-May-09	170-180	175	-77	26.4	7.6	10.6	23.3	88.0	431	233	2420	126	2295	5341	295	4478
Pro 53	26-May-09	180-190	185	-87	30.1	7.6	10.1	22.9	98.0	397	206	2265	131	2133	5021	299	4184
Pro 53	26-May-09	190-200	195	-97	29.8	7.8	9.1	25.1	120.0	295	141	2092	113	1833	5751	293	4630